INTERNATIONAL COLLOQUIUM

STABILITY OF STEEL STRUCTURES

HUNGARY, BUDAPEST 1990

PRELIMINARY REPORT

VOLUME III.

TECHNICAL UNIVERSITY OF BUDAPEST

HUNGARIAN ACADEMY OF SCIENCES

STRUCTURAL STABILITY RESEARCH COUNCIL

INTERNATIONAL ASSOCIATION FOR BRIDGE
AND STRUCTURAL ENGINEERING

INTERNATIONAL COLLOQUIUM
EAST-EUROPEAN SESSION

STABILITY OF STEEL STRUCTURES

PRELIMINARY REPORT

VOLUME III.

EDITED BY
M. IVÁNYI
B. VERŐCI

HUNGARY, BUDAPEST
APRIL 25-27, 1990

Címlap
részlet Somogyi Győző
rajzából

Cover
a piece of Győző Somogyi's
drawing

ISBN 963-421-487-8 Ó

ISBN. 963. 420. 220. 9. III

Felelős szerkesztők: Dr. Iványi Miklós
Dr. Verőci Béla
Kiadja: a Budapesti Műszaki Egyetem
Acélszerkezetek Tanszék
A kiadásért felelős: az Acélszerkezetek
Tanszék vezetője
Készült: a Budapesti Műszaki Egyetem
Sokszorosító Üzemében
Felelős vezető: Miszori Sándor
Példányszám: 350, Méret: B/5

SESSION 8

ARCHES

(1)

AIRUMYAN, E.L. (1)
EMELIN, E.I. (2)
HADIDANE, Yazid (3)

BUCKLING OF COLD-FORMED CORRUGATED SHELLS

INTERNATIONAL COLLOQUIUM
STABILITY OF STEEL STRUCTURES
BUDAPEST, HUNGARY, 1990
PRELIMINARY REPORT

Summary: This paper presentsthe experimental and analysis research results of the behaviour of half-barrel shells consisted of cold-formed thin profiles or corrugated shells under asymmetrical distribution loads. The rational method for determining the buckling load and deformations of these shells with geometrical nonlinearity is presented.

1. Introduction

Overall and local stability are major operating characteristics of frameless cylindrical shells consisting of cold-formed steel profiles or corrugated sheets. Such structures include shells with cold rolled profiles of trough-shaped section, produces on site using a Knudson K-SPAN movable profile bending unit (USA). Recently, several such units have been employed for building vegetable and fruit storages, refrigirators and warehouses in various regions of the Soviet Union.

Carrying capacity of those shell types has been studied with the aim of determining their maximum spans depending on profile dimensions and taking into account symmetrical snow load (Benussi, Mauro, 1986).

CNIIproyektstalkonstruktsiya Institute has carried out a research into characteristics of such shells, as well as of other shell structures made of corrugated sheets under different load combinations, including snow load distributed nonuniformly and asymmetrically across the shell, in accordance with

(1) Head of laboratory, CNIIproyektstalkonstruktsia, Moscow
(2) Senior Researcher, CNIIPSK, Moscow, USSR
(3) Research Assistent, University of Annaba, Algeria

with the construction norms accepted in the USSR and International Load Standard /2/.

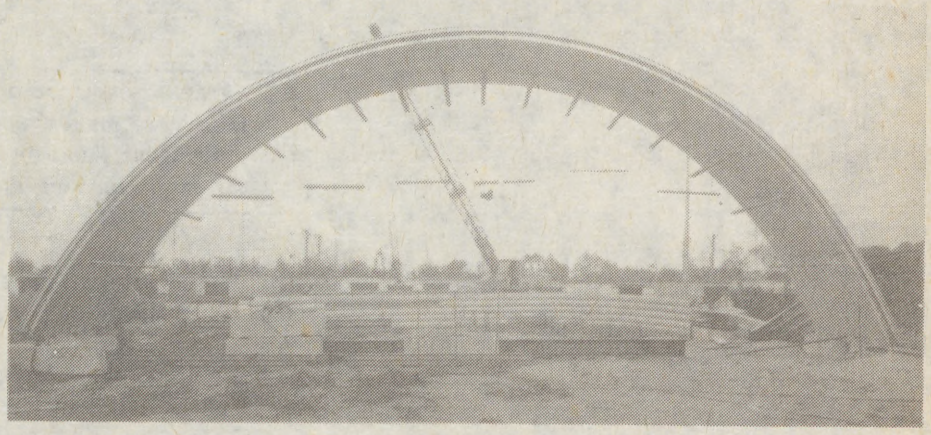

Fig.1. Test of cold-formed sections shell

2. Test of K-SPAN shells

Test specimens were represented by arch fragments of K-SPAN single- and three-layer shells of span L=18 m and 21 m respectively and 3 m in length, composed of 10 profiles (Fig. 1). The profiles were made of rolled zink-coated steel, of width of 600 mm, yield limit of 260-270 MPa, elongation of about 22% and thickness of 0.8 mm and 1.0 mm for single- and three-layer specimens respectively. In the later case bottom profiles were coated with foam polyurethane layer, 90-130 mm thick, using a movable sprayer. Outer profiles had a clearance of 60-100 mm to the urethane surface (Fig.2).

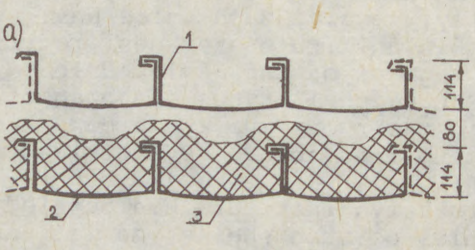

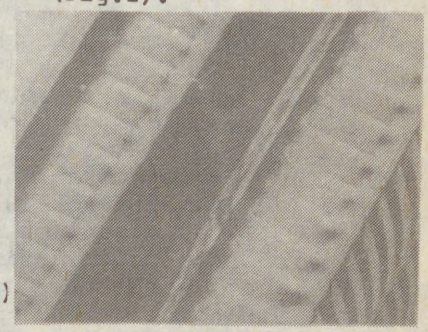

Fig.2. Section (a) and fragment (b) of three-layer shell
1 - outside layer, 2 - inside layer, 3 - polyurethane foam

The specimens were put under load using a suspended beam system, which enabled a uniform distribution of concentrated load P of a hydraulic jack both in symmetrical and asymmetrical loading (Fig.3). Load at the jack was increased in steps

(3)

of 1-2 kN with subsequent off-loading.

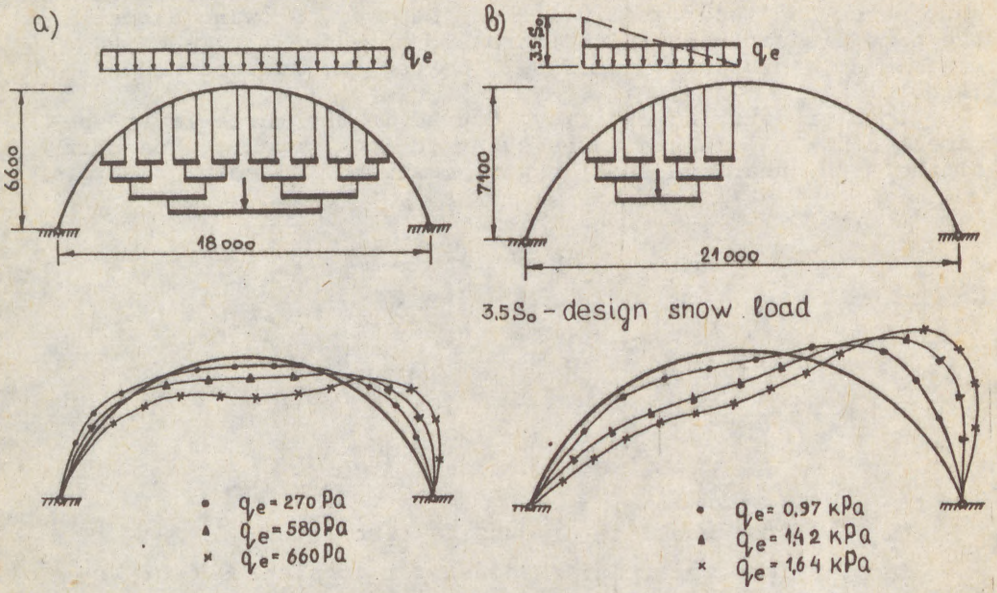

Fig.3. Load and test shells results under symmetrical (a) and asymmetrical (b) loading.

Changes in the specimens' geometry were recorded using analytical photogrammetry including photography stereography with a UMK 10/1318 universal camera (Karl Zeiss, GDR), camera print processing with a Stecometer precision stereocomparator and automatic print-out. After the prints had been processed by the coordinate method and a FOTO computer program in BASIC, the following data was obtained: displacement of marked structure points, displacement vector length, displacement vector angles, structures' linear dimensions, and displacement diagrams. Average square error in determining the coordinates of marked points was 0.4 mm.

In the single-layer arch under symmetrical vertical load (snow), displacement increased non-linearly, but almost symmetrically about midspan, to q_e = 0.4 kPa. Under greater loads, the arch became asymmetrical and there was a sharp decrease of rigidity, but the structure maintained a new stable position, as at bifurcation (Fig.3a). Loss of carrying capacity occurred at q_e = 0.71 kPa, subsequent to local buckling on broad flanges and walls of profiles at a distance of about 0.15 L from the nearest support.

In the three-layer arch under asymmetrical load, displacement rapidly increased at q_e = 0.7 kPa, that is at about 40%

of collapse load, reaching clearance of the top shell to the foam plastic coating of the bottom profiles. As load increased, outer and inner shells worked together, showing almost the same displacement which increased non-linearly reaching a maximum at a distance of 0.2-0.25 L from the nearest support (Fig.3b).

Loss of carrying capacity occured in the three-layer speciment at q_e = 1.65 kPa, subsequent to local buckling on part of the arch, near the section with maximum displacement (Fig.4)

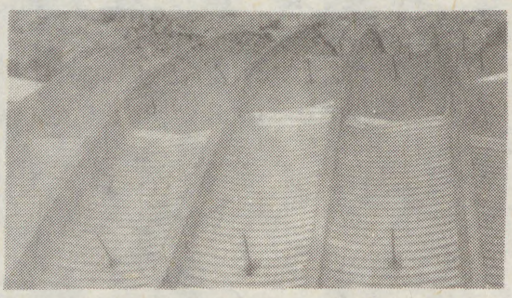

Fig.4. Local buckling of outside test arch

Computations were performed using a complete set of linear equations for geometrically non-linear problems:

$$\vec{A}(\vec{Z})\vec{S} = \vec{P}$$

$$\vec{A}^{T}(\vec{Z})d\vec{Z} = d\vec{\Delta}$$

$$\vec{\Delta} = B\vec{S}$$

where A - balance equation matrix;
S,P - internal and external force vectors;
Z - displacement vector.

The equations were solved using Newton-Raphson iteration method, assuming rigidity tangent matrix (Yacoby matrix) to be

$$\frac{d\vec{\Psi}(\vec{Z})}{d\vec{Z}} = K_1(\vec{Z}) + K_2(\vec{S}) + K_T$$

where

$$\vec{\Psi}(\vec{Z}) = A(\vec{Z})\vec{S} - \vec{P}$$

$$K_1(\vec{Z}) = A(\vec{Z})B^{-1}A^{T}(\vec{Z})$$

$$K_2(\vec{S})d\vec{Z} = dA(\vec{Z})\vec{S}$$

Stability is maintained if matrix K_t is positive defined (positive principal minors). A critical state occurs if $K_t dZ = 0$.

Comparatively low carrying capacity of the structure was due to buckles on broad flanges of K-SPAN-type profiles, which

(5)

led to a considerable decrease in critical force within compression zones (Fig.4).

3. Test of corrugated shells

To investigate properties of flexible semi-cylindrical shells without local buckling a single-layer arch structure of span of 12 m was tested, composed of sheets with corrugations of 35 mm in height (Fig.5a). The profiles were made of 2 mm-gage steel of yield limit of 310 MPa and elongation of 22%.

The profiles were connected to each other with bolts, 16 mm in diameter, positioned in longitudinal and transverse joints of the circular shell.

Test specimens were represented by arch structures, 12.2 m in span, 2.7 m wide and of 6.2 m radius, both braced and braceless (Fig.5). Braces of 8 mm in diameter were hinged to angles at the specimen's joints.

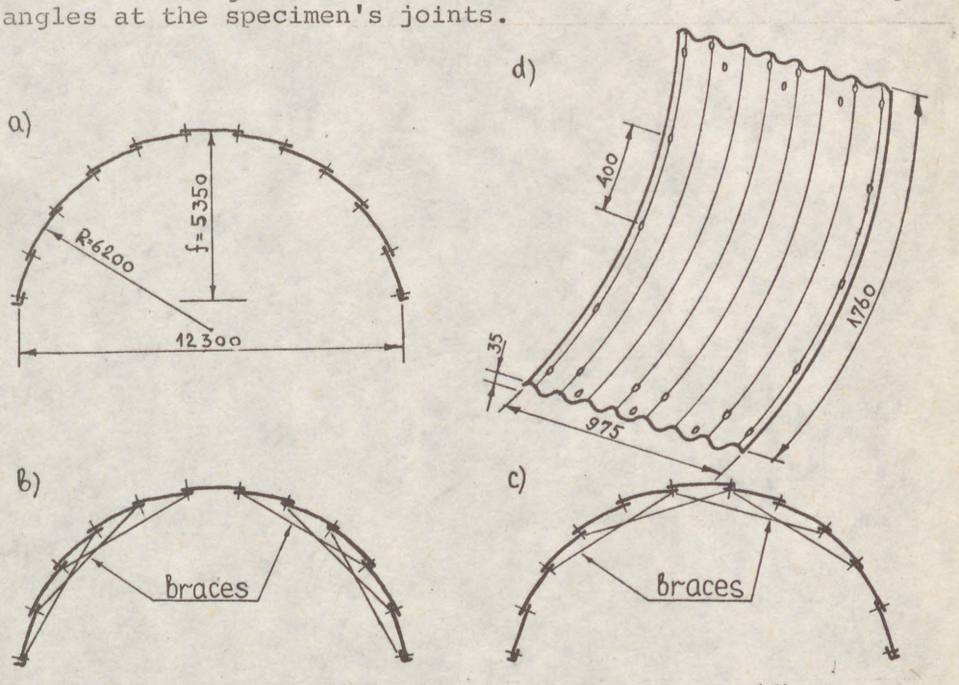

Fig.5. Cross-sections of shells and sheet element (d).

Static tests were carried out for vertical (snow) and horizontal (wind) load. Non-uniform vertical load, approximated, to triangular design load, was produced by suspended beams, a lever system and weights. Horizontal load was simulated by resultant concentrated force P applied at a height of about 4 m using a tie-rod and a counterweight (Fig.6).

Displacement in the test specimens under load were measured by the photogrammetry technique described above.

The tests showed low carrying capacity in the braceless arch, which was practically lost after overall stability loss had occurred due to vertical non-uniform load of maximum intensity of 2.4 kPa. After bracing, as shown in Fig.5b, the structure's rigidity and carrying capacity increased by a factor of 1.5.

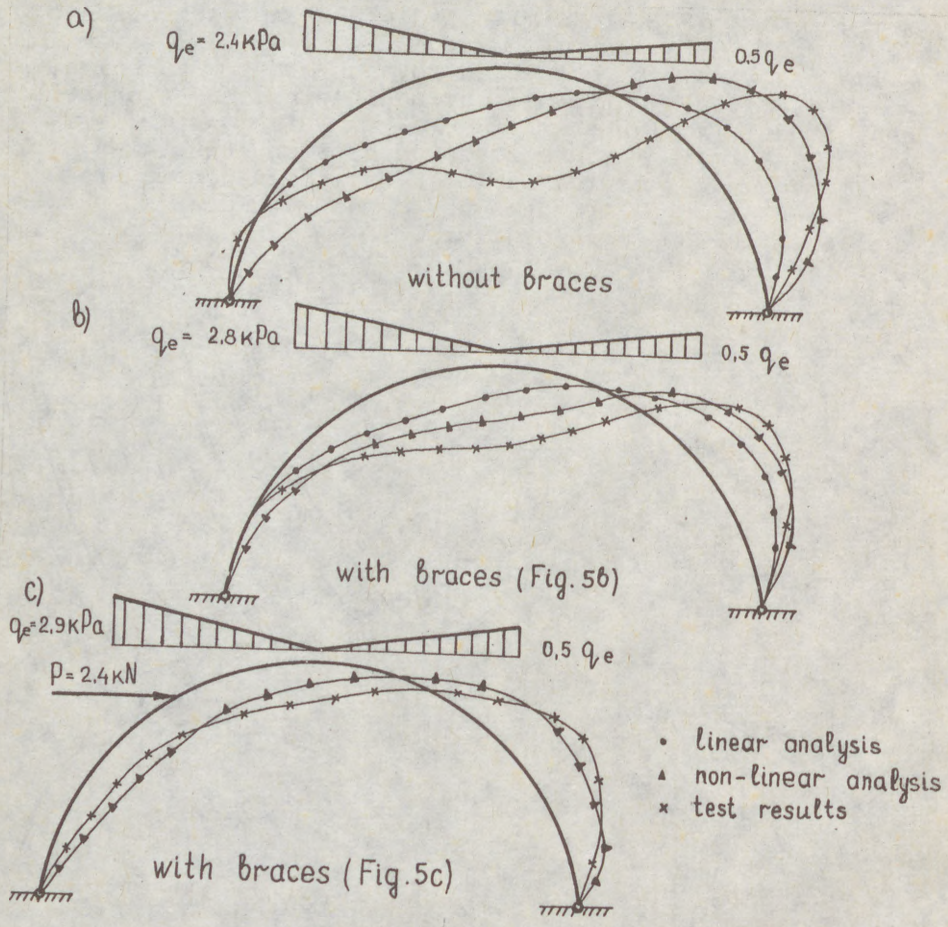

Fig.6.

4. Computation

Computations for both braced and braceless specimens were performed using a BIPLAN program on an EC computer, allowing to take into consideration the structure's geometrical non-linearity. The following assumptions were made: the structure's elasticity in operation; zero eccentricity at joints; the

(7)

structure was presented as a bar model of a polygonal contour, of the same width as corrugation; the effect of end-face walls was not considered; design loads were applied at design model nodes; the structure was hinged at the abutments. Block diagram for the computations is shown in Fig.7.

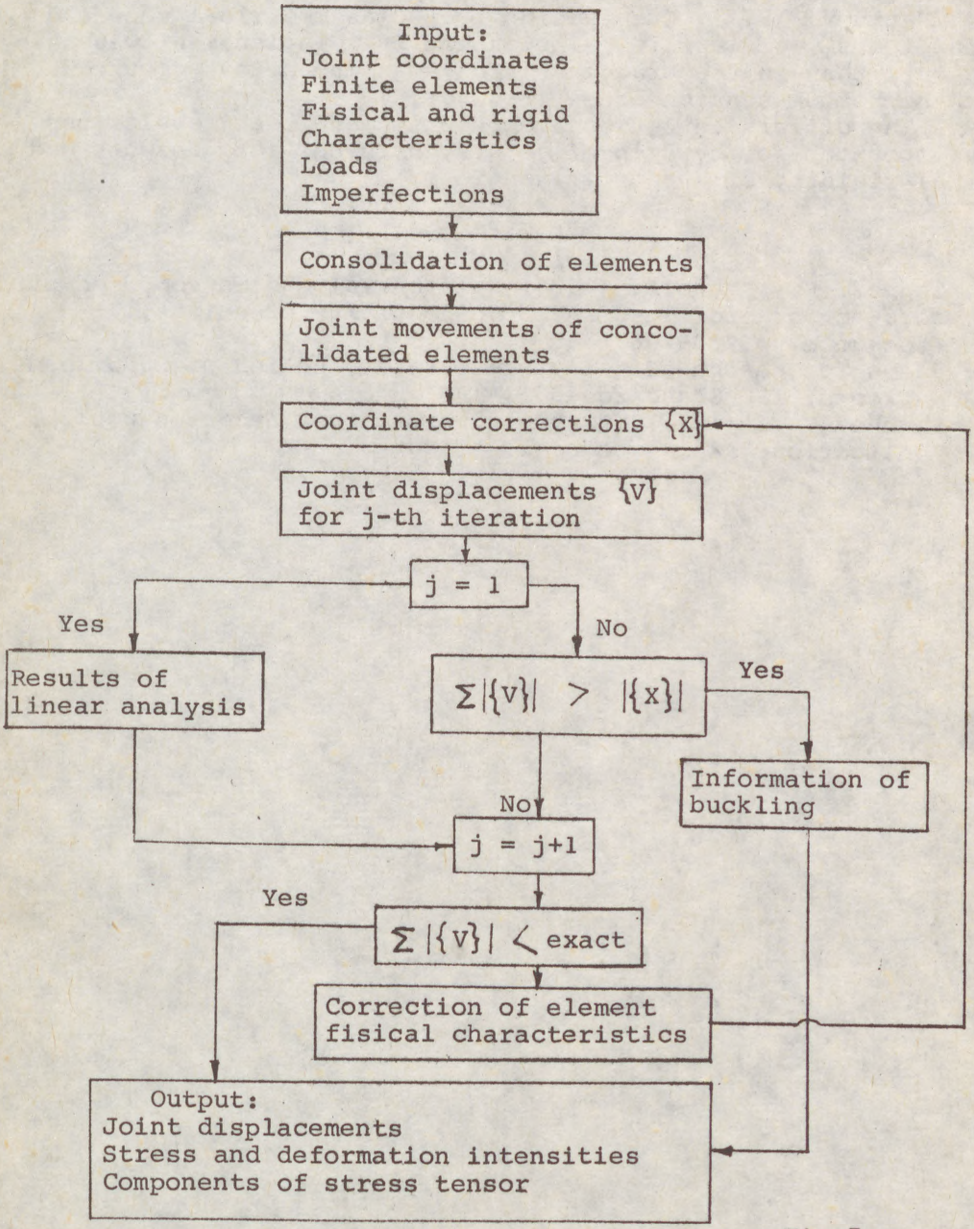

Fig.7

5. Conclusion

According to the computation results, maximum displacement and stress were considerably greater if non-linearity was taken into account, in which case they approximated the experimental data (Fig.6).

The most rigid arch was that braced on Shukhov's principle /Shukhov, 1977/. When design loads (asymmetrical snow and wind loads) were applied simultaneously, displacement was less by half than in the braceless arch; maximum stress occurred at the bottom tension brace (Fig.5c).

The difference between computation and test results can be accounted for by slip of joints, original form defects and final rigidity of support fixing.

References

1. Benussi F., Mauro A. (1986) Half-barrel shells composed of cold-formed profiles. IABSE Colloquium Proceedings, Stockholm, p.263-268
2. Bases for design of structures. Determination of Snow loads on roofs. ISO Standard 4355, 1981.
3. Shukhov V.G. (1977) Structural mechanics. Selected works. Publication "Nauka", Moscow, p.193.

(1)
KURANISHI shigeru(1)
MAALLA Khaled(2)

ESTIMATION OF ELASTIC LATERAL BUCKLING OF CURVED BEAM BY FEM USING STRAIGHT BEAM ELEMENTS and EXPERIMENT

INTERNATIONAL COLLOQUIUM
STABILITY OF STEEL STRUCTURES
BUDAPEST, HUNGARY, 1990
PRELIMINARY REPORT

Summary: In spite of that the curved member is assumed to be an assemblage of straight members, analyses by FEM using straight beam element do not give consistent results with analytical ones. Modification of currently used stiffness matrix by taking into consideration of the effect of quadratic terms of displacements and the out-of-plane balance of the internal forces at the joint of two adjacent elements meeting at an angle (introducing semitangential moment) can yield consistent results with analytical ones. The validity is also proved by experiment.

1. INTRODUCTION

Lateral buckling of compressed circular arches with solid cross sections or open cross section has been successfully analyzed already by Timoshenko[1], Vlasov[2], Fukazawa[3] and others for a certain type of supporting conditions and closed form solutions are given by them.

But, as discussed by Bazant and El Nimeir[4] in 1972, the results of the same problem analyzed numerically by FEM using straight beam elements shows disconsistency with the works mentioned above. They concluded that the straight beam elements cannot model curved beams, especially when the curvature is large or the arch is slender. Recently, Yoo[5] carried out a numerical analysis of this problem also using the FEM with 16 straight beam elements and drewn the same conclusion as Bazant et al. This disconsistency with the analytical results is also reported by Hasegawa[6] et al.

---

(1) Professor of Civil Engrg. Tohoku University
(2) Former graduate student of Civil Engrg. Tohoku University

Hayashi and Iwasaki[7] also discussed this problem and concluded that the use of the curved beam element model should not be recommended for the analysis of the lateral buckling problem of curved members. And they showed that the result obtained by using the curved beam elements agrees well with those of Vlasov and the results obtained by using the straight beam reaches to almost the same results by Yoo. This problem is also discussed by Papangelis and Trahair[8], and Yang and Kuo[9]. They arrived also the same conclusion.

This paper shows that the incorporation of the quadratic terms of displacements of beam elements into the formulation of the stiffness matrix of a straight element and the adoption of the semi-tangential end moment instead of the quasitangential end moment can lead to the consistent results obtained by the analytical and experimental approach.

2. BASIC EQUATION

In the formulation of the stiffness matrix, the virtual work principle is generally applied as follows:

$$\int_V(\sigma^0 + \sigma_{ij})\delta e_{ij}\, dV - \int_S(T^0_i + T_i)\delta u_i dS = 0 \qquad (1)$$

in which σ_{ij} and e_{ij} are the incremental components of the second Piola-Kirchhoff stress tensor and the Green strain tensor, respectively; T_i and u_i denote the external load components applied at the surface S and their corresponding displacements. All these quantity are measured from the reference state where σ^0_{ij} and T^0_i are acting. The displacements of the reference axis of a beam as shown in Fig. 1 can be expressed conventionally being separated into their linear and quadratic parts with the superscripts l and q as follows:

$$e_{ij} = e^l_{ij} + e^q_{ij} \quad \text{and} \quad u_i = u^l_i + u^q_i. \qquad (2)$$

Substituting Eqs.2 into Eq.1 and taking into account that the system is in equilibrium with respect to the small displacements near the reference state, Eq.1 can be written as

$$\int_V(\sigma_{ij}\delta e^l_{ij} + \sigma^0_{ij}\delta e^q_{ij})dV - \int_S(T_i\delta u^l_i + T^0_i\delta u^q_i)dS = 0. \qquad (3)$$

It should be noted that the last term $T^0\delta u^q_i$ has been usually neglected, and will play an important role.

Substituting the relationship between strain and displacement with respect to the quadratic terms and stress at the current stress state into Eq.3, Eq.3 is reduced to

$$\delta r^T[\, K_e + K_{gq}\,]r = 0 \qquad (4)$$

$$\text{where } K_{gq} = K_g - K_q \qquad (5)$$

The matrix presented by Eq.5 is so-called the geometrical stiffness matrix and the last matrix K_q which stems from the compo-

nents of the kinematics has never been introduced by any researcher. The explicit expressions of the other matrices are referred to the literature (12).

3) CORRECTION OF THE GEOMETRIC STIFFNESS MATRIX

Curved beams will be modeled as an assemblage of straight elements which are connected to each other at the nodal points on the curved line. But, as mentioned by Argyris et al.[10], the rotation of the cross sections of the two members meeting at an angel will cause imbalance at the joint because the bending moment resulted from the stress distribution behaves quasitangentially. Consider the two-member planar frame and let it be subjected to a constant bending moment applied at the free end as shown in Fig.2, the cross sections of element 1 and 2 meeting at an angle $(\pi-\alpha)$. The internal bending moment on these cross sections being

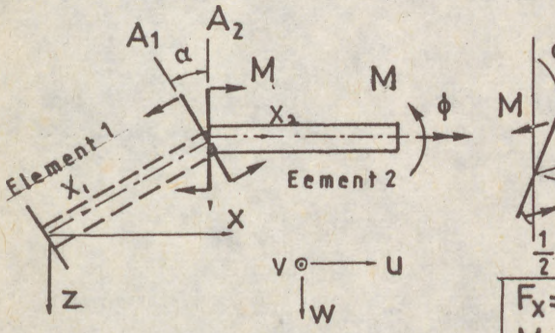

Fig.1 Planar Frame under Quasi-tangential Bending Moment

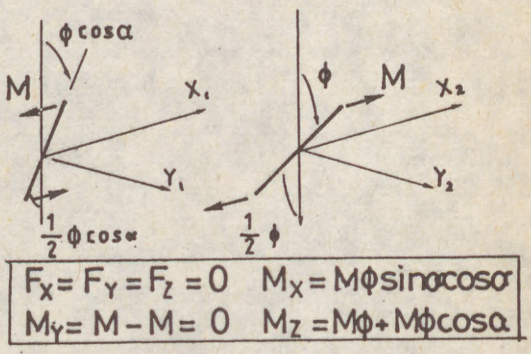

Fig.2 Imbalance at the Joint

quasitangential can be replaced by a couple force acting on a rigid lever which is orthogonal to the axis of the beam as well as to the axis of the moment. When the joint undergoes a rotation Φ applied with respect to the longitudinal axis of element 2, it can be seen from the table in Fig.2 that as long as the meeting angle is different from π, there will be always an imbalance of moment at the joint. However, if the bending moment is not quasitangetial but semitangential, it can be proven that the joint retains its equilibrium even in the presence of the rotation. This is demonstrated in Fig.3, where two members under the uniform bending are connected by the right angle. Therefore, it seems necessary to make modification on the nodal force vector by replacing the conventional quasitangential bending moment by a semitangential one as Argyris et all have shown.

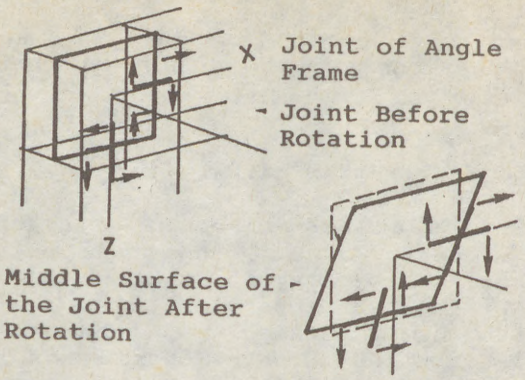

Fig.3 Equilibrium of the joint in case of Semitangential moment

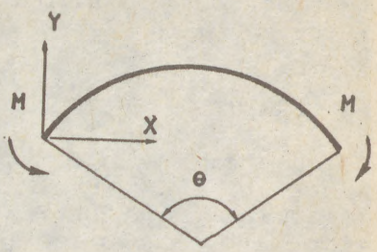

Fig.4 Circular arch in uniform bending

The presence of an in-plane semitangential bending moment M^0_z results in two out-of-plane moments M_x and M_y due to the out-of-plane rotations, given by

$$M_x = \tfrac{1}{2} M^0_z \theta_z , \quad M_y = \tfrac{1}{2} M^0_z \Phi . \qquad (5)$$

Consequently, the modification for M^0_z in the quasitangential expression can be done by replacing M^0_z by $M^0_z/2$. Then the corrected stiffness matrix is given as

$$\delta r^T [K_e + K_{gs}] r = 0$$

where $K_{gs} = K_g - \tfrac{1}{2} K_q$.

4. LATERAL TORSIONAL BUCKLING OF CIRCULAR ARCHES

Using Eq.6, the critical moment for the arch shown in Fig.4 is computed for certain subtended angles α. The applied moment in this figure is reckoned positive. the ordinary procedure of FEM using an appropriate number of straight elements leads to the eignevalue problem in this special case, because M^0_z is constant along the arch.

For comparison with the results in other references, the following material and sectional properties are adopted: $E=2.0\times10^8$ kN/m^2, $G= 7.72\times10^7$ kN/m^2, $A= 92.9$ cm^2, $I_{yy} =11,360$ cm^4, $I_{zz} =3,870$, $I_\omega = 5.559\times10^5$ cm^6, $J_T= 58.9$ cm^4 and the length of the arch is 10.24m. The computed positive and negative critical moments for several subtended angles are shown in Table 1 and 2, respectively. Here the case with the small subtended angle, i.e. $\alpha =0.05$ is examined in order to show that the presented new geometric stiffness matrix leads to the well-known, already established and confirmed results for the straight beams, and thus the new terms in this matrix play a significant role when there exists a very small but non-zero angle between elements, the rate of convergence of solutions has been found very rapid

and all the results in the table have been obtained using 16 elements.

Researcher	Subtended angle in degree				
	0.05	10.0	30.0	50.0	90.0
Vlasov	346.8	590.2	1257.1	1996.3	3519.2
Timoshenko	312.8	561.0	1241.0	1986.0	3513.0
Yoo	345.8	345.9	339.3	323.8	266.1
Yang	347.8	905.7	2343.0	3756.2	6121.5
Bazant	347.8	909.5	2438.5	4101.9	6820.1
Hasegawa	345.8	345.9	339.4	324.8	261.1
Present 1	346.8	589.8	1257.3	1998.1	3529.8
" 2	312.9	561.2	1242.2	1988.1	3520.5

Table 1 Comparison of The Positive Critical Moment in kN m
Present 1 Warping considered, Present 2 Warping not considered

Researcher	Subtended angle in degree				
	0.05	10.0	30.0	50.0	90.0
Vlasov	344.9	202.0	92.5	55.3	25.5
Timoshenko	310.9	173.1	76.2	45.2	20.8
Yoo	345.8	343.8	333.6	315.0	253.0
Yang	343.9	131.2	48.3	27.1	10.9
Bazant	343.9	132.3	51.8	33.1	22.2
Hasegawa	345.8	343.6	333.0	315.5	244.1
Present 1	344.9	203.0	95.0	58.3	35.0
" 2	311.0	174.0	78.5	49.1	30.2

Table 2 Comparison of The Negative Critical Moment in kN m

4. COMPARISON WITH EXPERIMENTAL RESULTS

To examine the validity of this analysis, an experimental study is carried out. The cantilever type of curved I beam tested is made of polyester and has the following mechanical properties and dimensions: $E=0.324\text{MPa}$, $G=0.120\text{MPa}$, $A=54.4\text{mm}^2$, $I_y=2.25\times10^2\,\text{mm}^4$, $I_z=8.98\times10^3\,\text{mm}^4$, $I_\omega=6.04\times10^4\,\text{mm}^6$ and $J_T=18.3\text{mm}^4$. The configuration of the test piece is shown in Fig.5 and their curvature is kept constant and the subtended angle is taken as 30, 35, 40 or 45 degree. The dimensions are chosen by considering that buckling should occur in the elastic range and laterally.

The results obtained by the experiment are shown in the Fig.6 by solid circles. In the figure, the doted line shows the results analyzed by FEM in which quadratic terms of the displacements in the derivation of the virtual work equation are neglected and corresponds the analysis by Yoo and Hasegawa et al. The broken line indicates the results which are got by considering the quadratic terms and the quasitangential bending moments at the nodal points and corresponds those by Mrray and Rajasekaran'

method. The solid line is the result obtained by the method presented here in which the quadratic terms and the semitangential bending moments at the nodal points are considered.

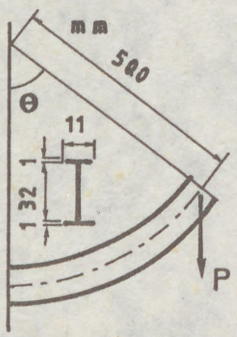

Fig.5 Test piece

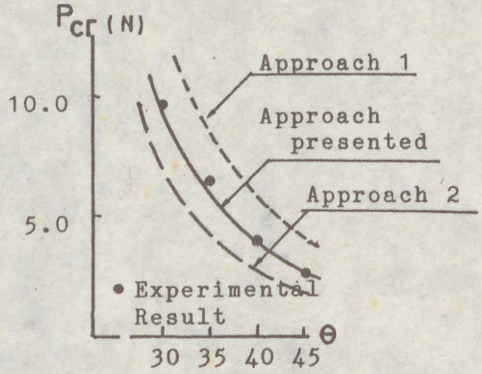

Fig.6 Comparison of test results with analytical ones

5. CONCLUSION

A geometric stiffness matrix for analyzing out-of-plane buckling of thin-walled members with open and doubly symmetric cross sections has been derived through the use of the virtual work equation of an initially stressed and equilibrated state. The geometric stiffness matrix considered the quadratic terms of the displacements in the derivation the virtual work equation and modified by considering the semitangential moment transfer between elements are presented.

Analysis of lateral buckling of circular arch under a certain type of loading and supporting conditions shows that the results given by this approach presented here has significant consistency with the analytical results given by Timoshenko and Vlasov and the experimental results conducted by the authors.

REFERENCES

1) Vlaxov, V.Z.:Thin-Waslled Elastic Beams, 2nd ed., Israel Program for Scientific Translations, Jerusalem, 1961
2) Timoshenko, S.P. and J.M. Gere: Theory of Elastic Stability, McGraw-Hill, 1961
3) Fukasawa, Y.: The Buckling of Circular Arches by Lateral Flexure and Torsion under Axial Thrust, Trans.JSCE, No.96,pp. 29-47,1963(in Japanese)
4) Bazant, Z.P. and El Nimeiri,M.: Large-Deflection Buckling of Thin-Walled Beams and Frames, Jour. of Engrg. Mech. ASCE, Vol.99,No.EM6, pp.1259-1281, 1972
5) Yoo,C.H.: Flexural-Torsional Stability of Curved Thin -Walled Beams, Jour. of Engrg. Mech.,ASCE Vol.108, No.EM6, pp 1351-1368, 1982
6) Rajesekaran, S, and Ramm,E.: Discussion of "Flexural-

Torsional Stability of Curved Beams"by C.H. Yoo, Jour. of Engrg.Mech.,ASCE Vol.110, No.1, 1984

7) Hasegawa,A. Liyanage,K. Ikeda,T. and Nishino,F.: A Concise and Explicit Formulation of Out-Of-Plane Instability of Thin-Walled Members, Proc. of Struct. Engrg./ Earthquake Engrg.,JSCE, I-3,1985

8) Hayashi M. and Iwasaki,E.: Validity of Approximations for Curved Thin-Walled Members on Geometrical Nonlinear Analysis, Proc. of Struct. Engrg./Earthquake Engrg.,JSCE, 392, 1988(in Japanese)

9) Papanelis, J.P. and Trahair,N.S.: Flexural-Torsional Buckling of Arches, Jour. of Struct. Engrg, ASCE, Vol.113,No.4,1987

10) Argyris, J.H., Hilbert,O. Malejannakis,G.A. and Scharpf,D.W.: On the Geometrical Stiffness of a Beam in the Space - a Consitent V.W. Approach, Computer Methods in Applied Mech. and Engrg.,Vol.20,pp.105-131, 1979

11) Yang Y.B. and McGuire,W.F.: Joint Rotation and Geometric Nonlinear Analysis, Jour. of Struct. Engrg., ASCE, Vol. 112, No.4,pp.879-905,

12) Maala K., Kuranishi,S. and Iwakuma,T.: Geometric Stiffness Matrix to Analyze the Lateral-Torsional Buckling of Curved Members, Proc. of Struct.Engrg./Earthquake Engrg.,JSCE, No. I-11,1989 (in print)

(1)
NEY, Laurent (1)
de VILLE de GOYET, Vincent (2)
MAQUOI, René (3)

OPTIMUM BRACING OF THE ARCHES OF TIED-ARCH BRIDGES.

INTERNATIONAL COLLOQUIUM
STABILITY OF STEEL STRUCTURES
BUDAPEST, HUNGARY, 1990
PRELIMINARY REPORT

Summary : Based on a parametric analysis of the arch bracing in tied-arch bridges, recommendations are drawn concerning the optimum location of cross beam bracings. A simple design method is also suggested which allows a satisfactory accurate assessment of the critical out-of-plane buckling load of the arches.

1. INTRODUCTION

The widening of the Albert Canal in Belgium has resulted in the erection of several new tied-arch bridges (Hermalle, Haccourt, Marexhe and Milsaucy), the clear span of which is about 130 meters. Their deck has ends fixed to two parabolic arches and is suspended to these latter by a lattice of hangers. (fig. 1).

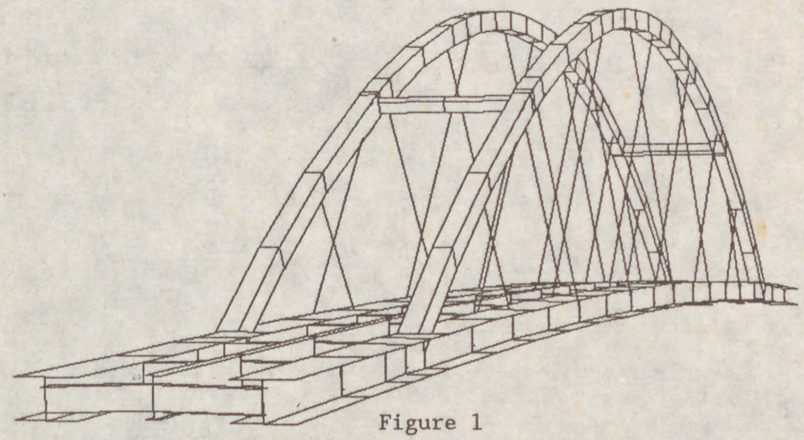

Figure 1

(1) Design Engineer, Bureau d'Etudes R. GREISCH, Liège, Belgium.
(2) Senior Research Engineer, Université de Liège, Liège, Belgium.
(3) Professor of Steel Construction, Université de Liège, Liège, Belgium.

(2)
While the arches of such bridges are usually braced by a truss extending over most of the span, the bracing of the new bridges either is not present or is composed only of one or two cross-beams. As the arches and the floor are connected by lattice hangers, the in-plane buckling of arches is not of concern [1, 2]. The out-of-plane buckling is much more complex; it is indeed intimately depending on the forces in the hangers and on the elastic support provided by the arch bracings. The optimum location and rigidity of this bracing as well as the assessment of the actual safety against ultimate load are problems, with which the authors have been concerned and to which several research works [3, 4, 5, 6, 7] have been devoted in the very last years. Present paper is aimed at presenting the main conclusions of the last work [7], with a peculiar attention paid to practice design considerations. Its scope is restricted to parallel arches, i.e. arches located in two vertical planes which are either unbraced or braced either by one beam at the crown of the arches, or by two beams located symmetrically with respect to the mid-span. The bracing beams are made with circular hollow sections rigidly connected to the arches. The main symbols used in the following are (fig. 2.a) :

L_p : span of the arches, measured between the springings ;
L_a : developped length of the arches ;
l : distance between the arch springings and the bracing ($l = \alpha L_a$)
b : the width of the deck, measured between arch axis ;
$h(x)$: current height of the arches ;
f : height of the arches of the crown ;
I : transverse moment of inertia of the arches ;
I_b : moment of inertia of the bracings ;
λ : load factor ;
N : design axial force in the arches.

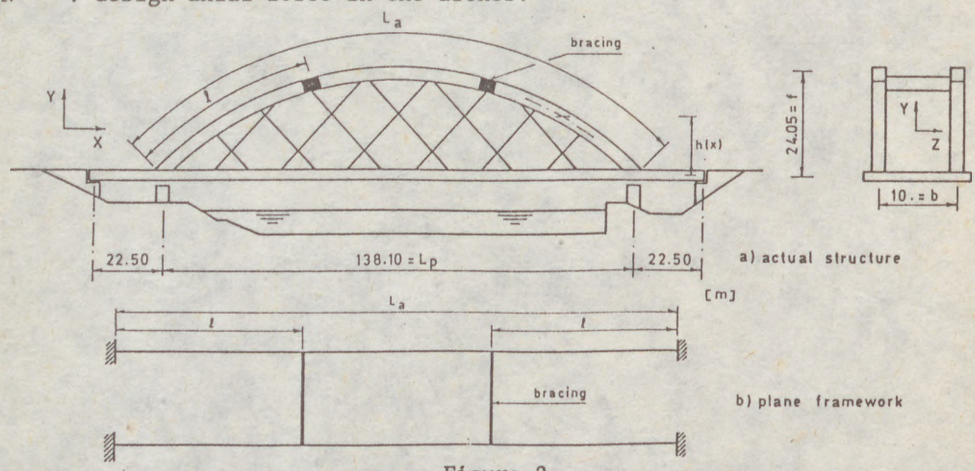

Figure 2

2. OPTIMUM LOCATION OF THE BRACINGS.

Ideally the bracings should be located so that to maximize the ultimate (or collapse) load of the arches. This load can be evaluated according to generalized beam-column formula (see § 2.3.) that accounts for the out-of-plane buckling of the arches, on the one hand, and the transverse bending due to wind load, on the other hand. It is thus appropriate, in a first step, to determine the optimum location of the bracings with a view to:

1. either maximize the eulerian elastic critical buckling load ;
2. or minimize the transverse bending.

(3)

2.1. EULERIAN CRITICAL BUCKLING LOAD.

2.1.1. Computer results of the analysis of the actual spatial structure.

Computer results have been obtained by using a non-linear finite element programme, developed at MSM Department of Liège University [8, 6]. This programme, so called FINELG, enables the calculation of critical loads, or the non linear behavior of any actual structure.

The results dealing with the Hermalle bridge are plotted in figure 3, in the form of the critical load factor versus the location of the bracings. Several curves are drawn which correspond to different values of the relative bracing stiffness.

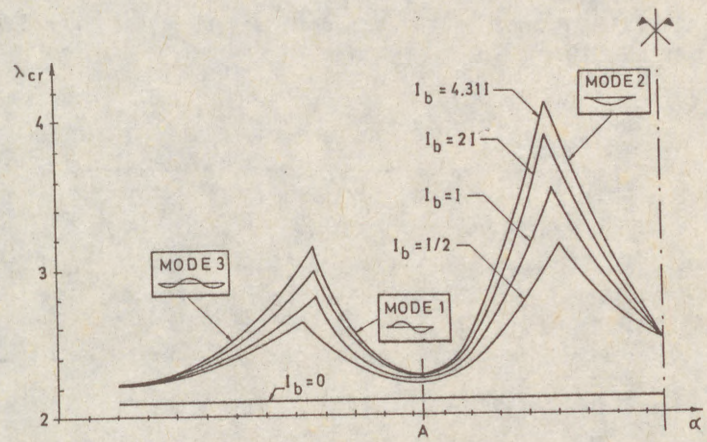

Figure 3

Each curve is a succession of three festoons; these are associated to three instability modes involving respectively one, two or three half buckling waves. There are thus two peak values, corresponding to the transition from one instability mode to another. A primary maximum is got for bracings located at roughly 4/10 L_a, while a secundary maximum corresponds to bracings at approximately 2/10 L_a.

2.1.2. Simplified approach based on the plane framework idealisation.

Though the critical buckling load is obviously not a proper measure of the collapse load, its knowledge may be a useful reference for a preliminary design. In addition its determination is possible by using a by hand method, and stresses the role played by the governing parameters in the design process. Therefore the need for a simple but sufficiently accurate assessment method in this respect. The basic idea, developed in [3], successively consists in :

- reducing the arches with their bracings to a substitute plane framework to straight plane beams, the length of which is the developed length, L_a, and fully restrained at their ends because of the firm connection existing between the arches and the deck ;
- idealizing the action of hangers in the actual structure by means of non-linear elastic translational springs acting in the plane of the substitute framework (indeed, when the arch tends to go out-of-plane, the axial forces in the hangers have a horizontal component which has a stabilizing effect on the arches, [3]) ;

(4)
- experiencing the beams with end axial forces, equal to the mean compressive loads N, in the arches.

A similar approach was used by SAKIMOTO [9] but restricted to arches with X braces distributed over most of the arch span, the bracing members being assumed pin-ended at their connections with the arches.

The values of the critical load factor λ_{cr}, are deduced from an energy approach combined with RAYLEIGH principle. In accordance with computer results (§ 2.1.1.), three instability modes are liable to occur. The three associated buckling deflections v are choosen as polynoms - of the fourth degree with respect to the abscissa s - that comply with the kinematic boundary conditions.

Applying the RAYLEIGH principle to each deformed shape and considering only the bending energy yields the critical load factor as the lowest value of the quotient :

$$\frac{N_{cr}}{N} = \frac{(EI/2)\int_{L_a} v''^2\,ds + (EI_b/2)\int_{b} v''^2\,ds}{N\,[1/2\int_{L_a} v'^2\,ds - C/(2L_p)\int_{L_p}(v^2/h)dx]} = \frac{E_{fl}}{T - T_s} \qquad (1)$$

where v', v" are respectively the first and second derivatives of v, C, the ratio (almost close to unity) between the vertical load transmitted by the hangers to one arch and N, E_{fl}, the internal deformation energy, T, the external deformation energy of the arch and T_s the external deformation energy due to hangers.
The critical buckling load N_{cr} may also be written :

$$N_{cr} = \lambda_{cr}\, N = \pi^2\, EI\, /\, (kL_a)^2 \qquad (2)$$

where k is the buckling length coefficient. The latter depends on the location of the bracings, $\alpha = 1/L_a$, on the relative arch-to-bracing stiffness ratio, $\tau = 6I_bL_a/Ib)$, and on the curvature of the arch, f/L_p.

It should be convenient to make easier the computation effort to be produced by the designer in a preliminary design. Therefore, the main results of the energy approach have been presented in the form of charts reflecting the influence of the governing parameters [7].
First, expression (1) is written :

$$N/N_{cr} = T/E_{fl} - T_s/E_{fl} \qquad (3)$$

wherefrom :

$$k^2 = k_e^2 - k_s^2 \qquad (4)$$

$k_e(\alpha, \tau)$ is the buckling length factor when the hanger restraining effect is disregarded while $k_s(\alpha,\tau, f/L_p)$ is the correction to be brought due to this effect.

It is rather easy to demonstrate that k_s^2 factor is proportional to a constant C and can be written :

$$k_s^2 = C\, \chi_1(\alpha,\tau)\, \chi_2(f/L_p) \qquad (5)$$

(5)
For each of the three buckling patterns, three charts are computed once for all : two double entry tables giving respectively k_e^2 and χ_1 versus τ and α, and a single table providing χ_2 versus f/L_p.

Assuming the dead weight contributes the axial load in the arches in an average proportion of 10 % of the superimposed load, the ratio C writes :

$$C = 1/1.1 \sqrt{(L_p/8f)^2 + 0.25} \qquad (6)$$

Let us remind that C is usually close to 1.

2.1.3. Simplified account for the actual spatial behaviour of arches.

Up to now, any point of the arches has been presumably moving only perpendicular to the arch plane. The actual behaviour is somewhat else.

When, in actual structure, the arches buckle out-of-plane, that results in a torque of the cross-section of both arches and in bending of the bracings about x axis (fig. 2). This effect is not accounted for in (1); it can however become of appreciable importance for one half wave symmetrical buckling mode (so called Mode 2). Indeed torque of the arches is rather limited when the buckling pattern is antimetrical, as there are three sections of zero torque: at mid-length and at the ends of the arches ; for a symmetrical buckling pattern, only the ends have a zero torque while the maximum torque occurs at mid-length.

It is acceptable to assume that the out-of-plane behaviour of the bracings does not change the work produced by the axial loads N and results in an additional strain energy only. Compared to (1), there will be an additional term at the numerator, the denominator remaining unchanged; consequently the critical buckling load is increased.

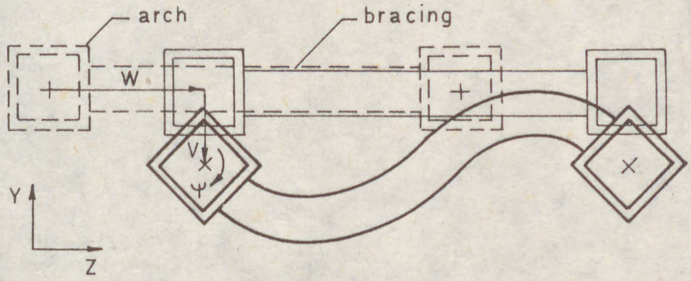

plane behavior: W spatial behavior: V, ψ
=> bending in arch plane, torsion of arch, bending of bracing

Figure 4

Let us remind that for buckling mode 2, account must be taken of the out-of-plane behaviour. Either a discretionary reduction by 0.9 of the k^2 value is used, or a more refined assessment is made ; in the latter case, the square of the actual buckling coefficient writes :

$$k_{act}^2 = k^2/[1 + (Kb^2L_a^3/8\pi^4 EI\ R^2)] \qquad (7)$$

with :

$$1/K = 1/K_a + b^2/4C_a + 1/K_e \qquad (8)$$

(6)

$$R = L_p^2/8f \; ; \quad K_a = 48\, EI/L_{AB}^3 \; ; \quad C_a = 12GC_t/L_a \; ; \quad K_e = 24EI_b/b^3 \qquad (9)$$

Expression (8) is got by modelling the out-of-plane behaviour ; L_{AB} is taken as twice the hanger spacing and C_t is the torsional inertia of the arch. For more details concerning this model see [7].

2.1.4. Design procedure in practice conditions.

In practice, for a specified location of the bracings, values of k^2 corresponding to buckling modes 1 and 3, (§ 2.1.2.), and value of k^2_{act} for buckling mode 2, (§ 2.1.3.), are computed. The maximum k^2 or k^2_{act} value is kept and provides the designer with the smaller out-of-plane buckling load.

When the properties of the arch are not constant over the span, average properties can be used without a loss of significative accuracy. The energy approach applied to the substitution plane framework gives results in very good agreement with those get from numerical simulations of the actual structure (fig. 5). The discrepancy reaches indeed an average of 5 % either on the safe or on the unsafe side. The location of the two maxima is obtained with a great accuracy. Both locations are changing in a very narrow range with respect to the value of factor τ, similarly as the computer results have shown.

The optimum locations for bracings correspond to the transition from one buckling mode to the adjacent one. By using the by hand computation procedure, optimum locations are found respectively close to $\alpha = 0.400$ for the primary optimum and to $\alpha = 0.210$ for the secundary optimum. These values are in complete agreement with the refined analysis of the actual structure conducted by means FINELG programme (§ 2.1.1.).

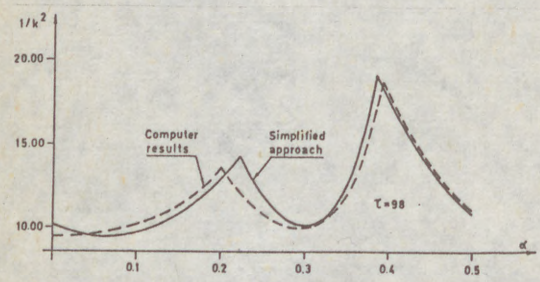

Figure 5

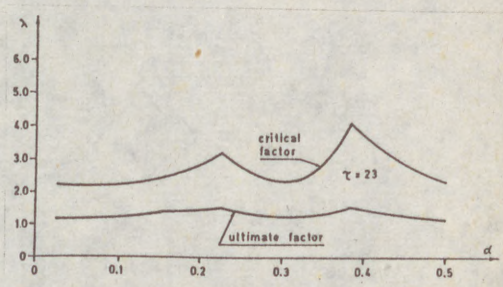

Figure 6

2.2. BENDING DUE TO TRANSVERSE LOADS.

Another way to analyse the influence of the inertia and location of the bracings is to consider the resistance to transverse loads, i.e. wind loads acting perpendicular to the plane of the arch.

The optimum location of the bracings in this respect would correspond to the least first order bending moments in the arch under the action of uniformly distributed transverse loads. Again the substitution plane framework is used for this purpose ; the favourable effect due to the hangers is fully disregarded.

(7)
Following conclusions can be drawn :

- the optimum location for the bracings is significantly depending on the parameter τ defined above ; it is found approximatively close to α=0.150
- for the optimum location of the bracings, the governing transverse bending moment is rapidly decreasing when τ increases.

2.3. OPTIMUM DESIGN WITH REGARD TO THE ULTIMATE STRENGTH.

Rigourously the optimum location of the bracings should maximize the collapse load of the structure. Contrary to the critical buckling load, the collapse load must account for the detrimental effects due to structural and geometrical imperfections and to elasto-plastic constitutive laws, and for large displacements resulting from the action of transverse loads and buckling. The question arises obviously whether the use of the collapse load maximization as criterion is liable to change the results obtained in the previous section.

To answer this question in a very simple way, it has been referred to the beam-column formula, because it is liable to yield the collapse axial load when the formula is written with the equality sign. This load is termed as λ N.

For a preliminary design, the ultimate out-of-plane buckling load of the tied-arch bridge, measured by the ultimate axial force in the arches, could be assessed by applying a beam-column formula to the substitute plane framework. This formula is composed of two normalized terms, dealing respectively with axial load and bending. All the effects described hereabove - i.e. spatial behavior, influence of hangers, ... - are accounted for in the first term. In the second term, the equivalent bending moment is taken, for sake of conservatism, as the maximum bending moment due to wind loads only so that the beneficial effect provided by the hangers is disregarded. These simplifications shall obviously yield a conservative value of the axial load factor but it is reminded that the attention is focused on the optimum location of the bracings.

Many computations have been carried out based on the beam-column formula and the load factor plotted against the relative abscissa α of the bracings. The corresponding curves (fig.6) are similar to though lower and more smooth than those obtained on base of the bifurcation approach (§2.1.); the drop reflects the detrimental effects due to material plasticity and to geometrical imperfections and residual stresses, which are implicitely accounted for in the beam-column formula. Such a curve shows three peaks : two of them are found to be mainly associated to the changes in buckling modes and thus to the optimization of the axial load term of the formula while the third one represents the contribution of the bending term. Because of the interaction between bending and axial load, the location of these peaks should move with respect to that obtained when considering these effects independently (§ 2.1. and 2.2.). This move is however barely observable. The two peaks corresponding to the transition of buckling modes are determinative compared to the third peak; they provide maximum and near equal values of the axial load factor.

The conclusions regarding the optimum location of the bracings, as drawn from the use of the beam-column formula to the substitute plane framework, have been confirmed by non linear F.E. computations of the behaviour, up to collapse, of the actual spatial structure. The simplified approach is thus subsequently validated.

(8)
Because of the simplifications introduced when using the beam-column formula, the ultimate values of the axial load factors obtained accordingly are smaller - by 5 to 15 % - than these get from the F.E. analysis. (The beam-column formula could be improved in order to account for the hangers effect and some efforts in this way are in progress). The magnitude of such a discrepancy is quite acceptable for a preliminary design, keeping in mind that the simplified approach provides anyway a conservative result.

3. CONCLUSIONS

For practice purposes, it may be concluded as follows :

a) Bracing with a single cross-beam at mid-span will ever yield a lower ultimate load than bracing with a pair of cross-beams, each of them having half the inertia of the single one;
b) The location of the cross-beams (bracings) which maximize the ultimate carrying capacity is mainly governed by the changes in buckling modes;
c) Both cross-beams shall be located roughly at either 0.21 or 0.4 times the developped length of the arches from their springings;
d) None of these locations predominates over each other regarding the ultimate load;
e) Only, aesthetics or considerations regarding dynamic behaviour (eigen mode frequency) may govern the choice amongst the two optimum locations : bracings located at $\alpha = 0.4$ cause a drop in frequency of ± 50 % compared to bracings at $\alpha = 0.21$.

REFERENCES

[1] PALKOWSKI S. - 1987
Stabilität von Zweigelenkbögen mit Hängern und Zugband, Stahlbau, Nr. 56.

[2] PALKOWSKI S. - 1987
Statik und Stabilität von Zweigelenkbögen mit schrägen Hängern und Zugband, Stahlbau, Nr. 56.

[3] de VILLE de GOYET V., FONDER Gh., LOTHAIRE A. - 1982
Stability of a Bowstring Bridge with Twin Inclined Arches,
Proceedings of IABSE Workshop "Informatics in Structural Engineering", Bergamo.

[4] CHAIB A. - 1987
Stabilité des ponts bowstring - Etude paramétrique,
Master Degree, Department MSM, University of Liège, Belgium.

[5] de VILLE de GOYET V., MASSONNET, C.E. - 1988
Comparative Study of the Stability of Various Dispositions of Tied-Arch Bridges, Der Metallbau in Konstruktiven - Ingenieurbau Festive Publication for Professor BAEHRE, Karlsruhe.

[6] de VILLE de GOYET V. - 1988
L'analyse statique non linéaire par la méthode des éléments finis des structures spatiales formées de poutres à section non symétrique.
Ph.D., Department MSM, University of Liège, Belgium.

[7] NEY L. - 1989
Etude paramétrique du contreventement de ponts en arcs,
Master Degree, Department MSM, University of Liège, Belgium.

[8] FREY F. - 1977
L'analyse statique non linéaire des structures par la méthode des éléments finis et son application à la construction métallique.
Ph. D., Department MSM, University of Liège, Belgium.

[9] SAKIMOTO - 1978
Elasto-plastic Finite Displacement Analysis of Three Dimensional Structures and its Application to Design of Steel Arch Bridges.
Kumato University, Japan.

(1)

SAKIMOTO, Tatsuro [1]
SAKATA, Tsutomu [2]

OUT-OF-PLANE BUCKLING STRENGTH OF THROUGH-TYPE ARCH BRIDGES

INTERNATIONAL COLLOQUIUM
STABILITY OF STEEL STRUCTURES
BUDAPEST, HUNGARY, 1990
PRELIMINARY REPORT

Summary : Numerical results for out-of-plane buckling strength of theoretical models of through-type arch bridges are evaluated by the provisions of DIN4114, Japanese Specifications (JSHB), DIN18800(draft) and by the proposed formula. It was shown that DIN4114 and JSHB provide a quite unsafe side predictions for all of the numerical results, but DIN18800 and the proposed formula can give good predictions for the buckling strength of all the theoretical models. Further improvement considered in the proposed formula but not in DIN18800 is pointed out for further revision of DIN18800.

1. INTRODUCTION

At present, only the German specifications DIN and the Japanese Specifications for Highway Bridges (JSHB) have provisions for out-of-plane buckling strength of arch bridges. Since current provisions for arch bridges of JSHB were originally transferred from DIN4114(1952 edition) and were modified a little, the provisions of JSHB and DIN4114 are basically the same.

DIN4114 and JSHB recommend to determine the compressive allowable stress for arch members by substituting an effective length for the arch into a column strength formula. But, since the effective length factors are determined by using buckling coefficients obtained as an eigenvalue for elastic buckling of a single solid arch member, it is questionable to apply it to through-type arch bridges which have an opening portion with no lateral bracings in order to provide traffic access.

The writers pointed out this in 1982 (Sakimoto et al.) and suggested that the application of the provisions to through-type arch bridges might lead the design to the unsafe side. Later in 1983, the writers proposed a simple but comprehensive formula which can determine the

[1] Professor of Civil & Environmental Eng., Kumamoto University, Japan
[2] Doctor Candidate of Civil & Environmental Eng., Kumamoto University, Japan

(2)
out-of-plane buckling strength of through-type arch bridges with end portal frames (Sakimoto et al. 1983, 1988).

By the way, now DIN4114 is going to be revised to DIN18800 and the draft has been circulated in Oct., 1986 and May, 1988. The main change in the arch provisions in the current draft of DIN18800 is that the provisions for out-of-plane buckling strength of through-type arch bridges with end portal frames are newly prescribed and added to the former ones (Dec. 1980 edition). There is no way to know whether our former papers could give some suggestion to this revision of DIN18800, but the writers are surprised and pleased to find the revision in the current draft of DIN18800, and have a respectful feeling to the German engineers.

In this paper, the applicability of the provisions of DIN4114, JSHB, DIN18800 (draft May, 1988 edition) and the proposed formula is studied by comparing the accuracy of the evaluations for the numerical results for out-of-plane buckling strength of arch bridges by these four methods. For this purpose, the ultimate strength of realistic theoretical models for through-type arch bridges are computed by a finite element method, which is capable of considering finite displacements and material plasticity (Komatsu, Sakimoto, 1976).

2. SUMMARY OF PROVISIONS AND PROPOSED FORMULA

All of the four methods are same in procedure to determine the buckling strength of arch bridges by substituting an effective length for the arch into a column strength formula. But, the ways to determine the effective length for the arch and the force terms, which are used in place of the axial force term in the column formula, are different in the respective methods.

The following are brief explanation of three provisions and the proposed formula. The allowable stress expressions in DIN4114 and JSHB are changed into the ultimate strength expressions to make the comparison among the four methods easier. The symbols also changed from their original ones for the same reason.

1) DIN4114

The requirement in the allowable stress form $\omega_y N_v/F \leq \sigma_{zul}$ in DIN4114 can be rewritten in the ultimate strength form as follows;

$$\frac{N_q}{(1/\omega_y)N_{pl}} \leq 1 \tag{1}$$

in which

N_q = axial force of the arch at the quarter point of the span computed by a linear theory under the factored design load

N_{pl} = fully plastic axial force of the arch

$1/\omega_y$ = reduction factor, Knickzahr ω_y is given as a table of numerals with the variation of the slenderness ratios λ, according to the column strength curve used.

The slenderness ratio to determine the value ω_y is defined as

$$\lambda = K_1 K_2 (\ell/i) \tag{2}$$

in which

K_1 = effective length factor determined as $K_1 = \pi/\sqrt{\gamma}$ by using the buckling coefficient γ obtained for elastic buckling of a single arch member, and given by a table as

f/ℓ	0.05	0.1	0.2	0.3	0.4
K_1	0.5	0.54	0.65	0.82	1.07

(3)

K_2 = effective length factor to account for the direction of the load applied to the arch rib, and given as

$K_2 = 1.0$ for vertical loading

$K_2 = 1 - 0.35\,\alpha$ for tilting hanger load in through-type arches, in which α denotes a ratio of the load intensity sustained by a hanger to the load intensity applied.

ℓ = span length of the arch

i = radius of gyration of the whole cross section of the twin arch ribs with respect to the out-of-plane bending.

2)JSHB

The requirement in the allowable stress form $H/A_g \leq \sigma_{ca}$ in JSHB can be rewritten in the ultimate strength form as follows,

$$\frac{H}{\overline{\sigma} N_{p\ell}} \leq 1 \tag{3}$$

in which

H = horizontal thrust of the arch, computed by a linear theory under the factored design load

$N_{p\ell}$ = fully plastic axial force of the arch

$\overline{\sigma}$ = reduction factor computed from the Japanese column curve as a function of slenderness parameter $\overline{\lambda}$, that is

$\overline{\sigma} = 1.0$ for $\overline{\lambda} \leq 0.2$

$\overline{\sigma} = 1.109 - 0.545\overline{\lambda}$ for $0.2 < \overline{\lambda} \leq 1.0$

$\overline{\sigma} = 1.0/(0.773+\overline{\lambda}^2)$ for $1.0 < \overline{\lambda}$

The determination of the slenderness is basically same with DIN4114, but $\overline{\lambda}$ is defined as the ratio to the yield point slenderness $\pi\sqrt{E/\sigma_y}$ as follows;

$$\overline{\lambda} = \frac{1}{\pi}\sqrt{\frac{\sigma_y}{E}}\frac{K_1 K_2 \ell}{i} = \frac{1}{\pi}\sqrt{\frac{\sigma_y}{E}}\lambda \tag{4}$$

in which σ_y and E denote the yield point stress and Young's modulus, respectively. In design practice, the value 1.7/2.0 = 0.85 is multiplied to the right hand term of Eq.3 to increase the safety factor from 1.7 to 2.0, but this is not considered herein to make direct comparison possible.

3) DIN18800

The requirement is

$$\frac{N_s}{\kappa N_{p\ell}} \leq 1 \tag{5}$$

(4)

in which

N_s = the maximum axial force computed by a linear theory under the factored design load (equivalent to the axial force at the springings for a parabolic arch under the fully distributed uniform load, which is the case considered herein.)

Though in the 1988-draft, the word 'maximum' is not quoted, it is thought to be 'maximum', because the word 'maximum' was used in the 1986-draft.

N_{pl} = fully plastic axial force of the arch rib

κ = reduction factor computed by *EC* multiple column curves as the function of the slenderness parameter $\overline{\lambda}$ or λ_k.

The slenderness parameter $\overline{\lambda}$ is for arch bridges without end portal frames and same with Eq. 4. The slenderness parameter λ_k is for arch bridges with lateral bracings and end portal frames, and defined as

$$\lambda_k = \frac{1}{\pi}\sqrt{\frac{\sigma_y}{E}}\frac{K_3 h}{r_c} \tag{6}$$

in which

K_3 = effective length factor for the column of an end portal frame subjected to tilting load. This value is given by diagrams as a result of an elastic bifurcation analysis.

h = the length of the column of the end portal frame

r_c = radius of gyration of the column cross section of the end portal frame.

4) Proposed formula

The requirement is

$$\frac{N_s}{\overline{\sigma} N_{pl}} \leq 1 \tag{7}$$

in which

N_s = axial force at the springings computed by a linear theory under the factored design load

$\overline{\sigma}$ = reduction factor computed from the JSHB column strength curve or equivalent column curves as a function of the slenderness paremeter λ_y.

The slenderness parameter λ_y is determined from an analogy between a column and an arch, which is based on the numerical results of ultimate strength analysis of typical arch bridge models, and defined as

$$\lambda_y = \frac{1}{\pi}\sqrt{\frac{\sigma_y}{E}}\frac{K_e K_\beta K_\ell L}{r} \tag{8}$$

in which

K_e = effective length factor related to end conditions, which equals 0.5 for the arch with laterally clamped ends

K_β = effective length factor to account for the effect of the lateral bracing or end portal frame, given as a function of the laterally braced length of the arch rib (βL), shear flexibility parameter μ of the bracing members (Sakimoto et al. 1988) and the distance between the two arch ribs a as follows;

$$K_\beta = 1 - \beta + \{2r(0.5 + 0.94\sqrt{\mu})/(aK_e)\}\beta$$

(5)

K_ℓ = effective length factor to account for the direction of the applied load, which is similar to K_2, but given as a function of the ratio I_{gy}/I_{ay} representing the lateral bending stiffness of the floor system. That is,

$$K_\ell = 1\text{-}0.35(I_{gy}/I_{ay})^{1/4} \quad \text{for } I_{gy}/I_{ay} \leq 1.0$$
$$K_\ell = 0.65 \quad \text{for } I_{gy}/I_{ay} > 1.0$$

L = curved length of the arch rib

r = radius of gyration of the single arch rib with respect to out-of-plane bending.

The main differences between DIN18800 and the proposed formula are the following;

a) The effective length factors in DIN18800 are still determined from the results of elastic bifurcation analysis, but these in the proposed formula are determined from an analogy between a column and an arch derived from the numerical results of ultimate strength analysis of typical arch bridge models.

b) On the determination of the effective length factor K_3 in DIN18800, specified tilting load(stabilizing effect) is always assumed regardless to the variation of the lateral stiffness of the floor system. But, in the proposed formula, the stabilizing effect, that is, the direction of the applied load is evaluated as a function of lateral stiffness of the floor system in determining the effective length factor K_ℓ.

3. THEORETICAL MODELS FOR NUMERICAL COMPUTATIONS

Theoretical models studied are 2-hinged parabolic arches shown in Fig. 1. The rise to span ratio f/l is changed as 0.1 and 0.2 with constant span length of $l = 150m$ and the arch rib distance $a = 10m$. Braced length ratio β is varied as 0.875 and 0.750. The braced length ratio β is defined as the ratio of the partial length of arch rib, where lateral bracing members are located, to the total length of the arch rib.

The ratio of the lateral bending stiffness of the floor system as a whole, EI_{gy}, to the lateral bending stiffness of the connected twin arch ribs as a whole, EI_{ay}, is also varied as $\overline{I} = I_{gy}/I_{ay} = 0.1$, 1.0 and 3.0, to cover its possible range in actual bridges. A uniform load fully distributed on the bridge deck is considered to be the severest one possible and is applied to the floor system as equivalent concentrated nodal forces in the analysis. The material is assumed to be a mild steel of which yield point stress is $235MN/m^2(24kgf/mm^2)$. Dimension of the cross section of each member and the residual stress distribution assumed are shown in Fig. 2.

4. EVALUATION OF NUMERICAL RESULTS BY EXISTING PROVISIONS AND PROPOSED FORMULA

The slenderness parameters and the ultimate strength of the theoretical models are evaluated by the four mothods and summarized in Table 1. The ultimate strength of the theoretical models are expressed by N_{qu}, H_u, N_{su} which are computed as the ultimate values of H_q, H, N_s by an ordinary linear theory against the ultimate load at which the theoretical model fails in the computer analysis. The values of predictions of the four methods can be calculated by substituting the respective slenderness parameters into the respective column strength formula used, but are not shown in the Table. The comparison between the respective predictions (=respective column curves) and the respecetive evaluations for the ultimate strength of the theoretical models are shown in Fig. 3 ~ Fig. 6, respectively.

(6)

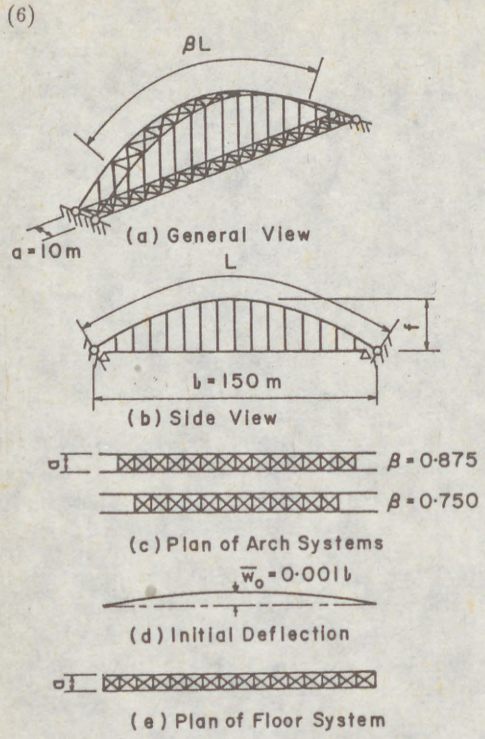

Fig.1 Theoretical models for numerical computations

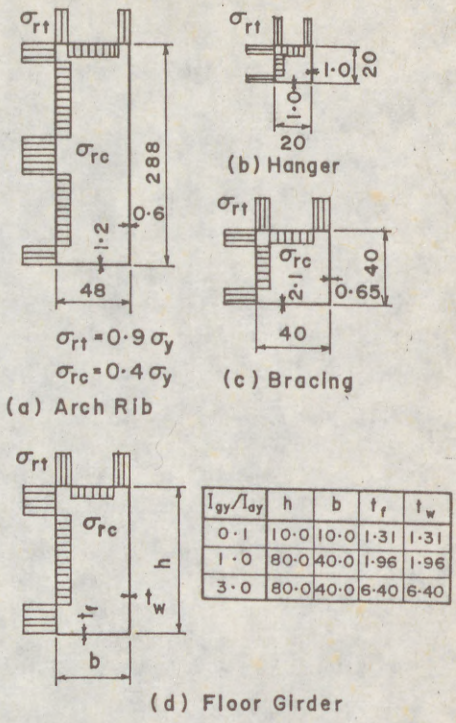

I_{gy}/I_{ay}	h	b	t_f	t_w
0·1	10·0	10·0	1·31	1·31
1·0	80·0	40·0	1·96	1·96
3·0	80·0	40·0	6·40	6·40

Fig.2 Cross-sections of theoretical models

Table 1 Slenderness parameters and ultimate strength of theoretical models evaluated by respective methods

β	f/l	I_{gy}/I_{ay}	DIN 4114		JSHB		DIN 18800		Proposed Formula	
(1)	(2)	(3)	λ (4)	N_{qu}/N_{pl} (5)	$\bar{\lambda}$ (6)	H_u/N_{pl} (7)	λ_k (8)	N_{su}/N_{pl} (9)	λ_y (10)	N_{su}/N_{pl} (11)
0·875 (14/16)	0·1	0·1	10·5	0·843	0·113	0·826	0·598	0·890	0·662	0·890
		1·0		0·881		0·863		0·930	0·536	0·930
		3·0		0·900		0·882		0·950	0·536	0·950
	0·2	0·1	12·7	0·747	0·137	0·694	0·664	0·888	0·754	0·888
		1·0		0·786		0·730		0·935	0·610	0·935
		3·0		0·795		0·738		0·945	0·610	0·945
0·750 (12/16)	0·1	0·1	10·5	0·597	0·113	0·585	0·839	0·630	0·918	0·630
		1·0		0·672		0·659		0·710	0·743	0·710
		3·0		0·706		0·691		0·745	0·743	0·745
	0·2	0·1	12·7	0·496	0·137	0·461	0·944	0·590	1·043	0·590
		1·0		0·563		0·523		0·670	0·844	0·670
		3·0		0·563		0·523		0·670	0·844	0·670

(7)

As can been seen from Fig. 3 and 4, DIN4114 and JSHB can not evaluate the theoretical results properly and their predictions (=column curves) give fairly unsafe side value especially for the models with a small β value (=large portal opening) and with a large f/l value. The discrepancy is apparently caused by the fact that DIN4114 and JSHB do not consider the phenomenon that the portal opening without lateral bracing weaken the buckling strength of the total arch bridge significantly.

On the contrary, DIN18800 and the proposed formula can give good predictions for strength of the models. But, DIN18800 still give a little unsafe predictions for models with a small β value and a small I_{gy}/I_{ay} value. This is so, because DIN18800 does not consider the effect of the fact that the stabilizing effect due to the tilting hanger load depends on the lateral bending stiffness ratio (I_{gy}/I_{ay}). The proposed formula can provide good and safe side predictions for all the theoretical results.

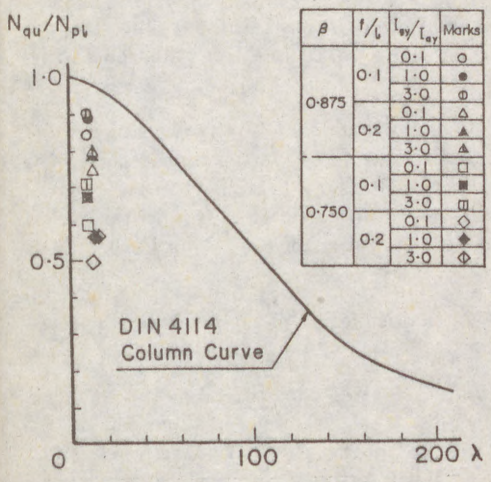

Fig.3 Evaluation of numerical results by DIN4114

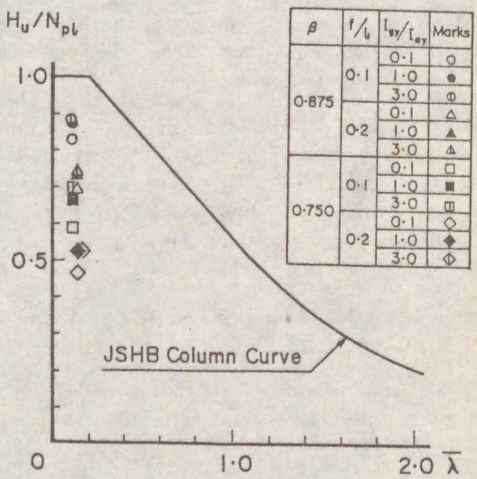

Fig.4 Evaluation of numerical results by JSHB

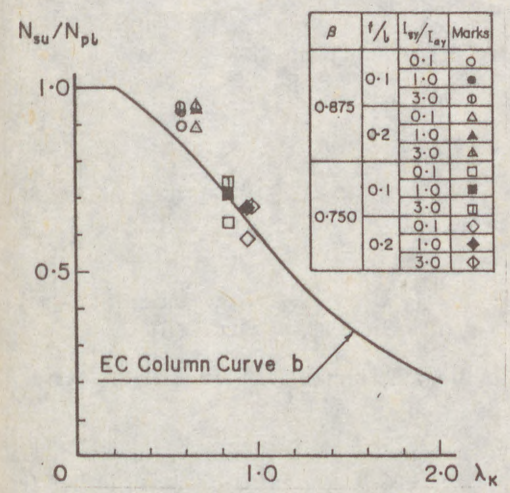

Fig.5 Evaluation of numerical results by DIN18800

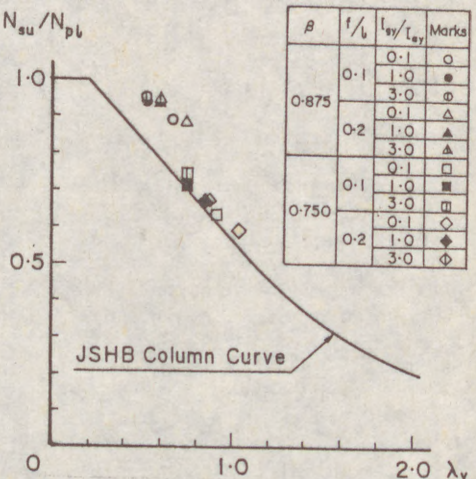

Fig.6 Evaluation of numerical results by the proposed formula

(8)

5. CONCLUSIONS

The following conclusions can be drawn from this numerical study;

1) Numerical results for out-of-plane buckling strength of theoretical models are evaluated by the provisions of DIN4114, JSHB, DIN18800 and by the proposed formula. The theoretical models are proportioned so as to be the representative of actual arch bridges of through-type with end portal frames.

2) It was shown that the provisions of DIN4114 and JSHB provide a quite unsafe side predicdtions for all of the numerical results. The overestimation of the buckling strength by these provisions are caused by the fact that both provisions do not take the effect of the portal opening into account.

3) DIN18800 and the proposed formula can give good predictions for the buckling strength of all the theoretical models. The revision in the current draft of DIN18800 seems to be acceptable in general.

4) But, since DIN18800 still give a little unsafe predictions for models with a small β value and a small I_{gy}/I_{ay} value, it is advisable for the designer to be cautious for applying the provision to the arch bridges with a floor system of small lateral bending stiffness, because for those arch bridges, the floor system has a possibility to move laterally with the lateral buckling movement of the arch ribs and the stabilizing effect of the tilting hanger loads can not be expected.

5) The proposed formula can give good and safe predictions for all of the theoretical models.

ACKNOWLEDGEMENTS

The writers express their thanks to Mr. C. Iiboshi, graduate student of Kumamoto University for his valuable assistance in numerical computations. Numerical computations are carried out by using a digital computer FACOM M-380 of the computer center in Kyushu University.

REFERENCES

DEUTSCHE NORMEN, 1952 : DIN4114 Blatt 1, Seite 13.

DEUTSCHE NORMEN, 1986 : Entwurf DIN18800 Teil 2, Seite 49, 6.1.4.

DEUTSCHE NORM, 1988 : Entwurf DIN18800 Teil 2, Seite 45, 6.1.2.

Japan Road Association, 1980 : Specifications for Highway Bridges.

Komatsu, S. and T. Sakimoto, 1976 : Nonlinear Analysis of Spatial Frames Consisting of Members with Closed Cross Sections, Proceeding of Japan Society of Civil Engineers, No. 252, pp. 143-157.

Sakimoto, T. and S. Komatsu, 1982 : Ultimate Strength of Arches with Bracing Systems, Journal of the Structural Divisions, ASCE, Vol. 108, No. ST5, pp. 1064-1076.

Sakimoto, T. and S. Komatsu, 1983 : Ultimate Strength Formula for Steel Arches, Journal of Structural engineering, ASCE, Vol. 109, No. 3, pp. 613-627.

Sakimoto, T., T. Sakata and E. Tsuruta, 1988 : Elasto-plastic Out-of-plane Buckling Strength of Through Type or Half-tyrough Type Arch Bridges, Proceedings of Annual Technical session of SSRC, pp. 141-152.

(1)
SCHOLZ, Hans (1)

CODE PROVISIONS FOR THE IN-PLANE STABILITY OF STEEL ARCHES

INTERNATIONAL COLLOQUIUM
STABILITY OF STEEL STRUCTURES
BUDAPEST, HUNGARY, 1990
PRELIMINARY REPORT

SUMMARY

This paper provides simple guidelines for the plastic analysis and design of steel arches. In-plane sway and snap-through buckling are considered; but the aspects of localised buckling and lateral buckling are excluded from this study. A number of comparisons with experiments and rigorous analysis have confirmed the feasibility of the proposed rules. A similar approach has already been suggested for pitched-roof steel frames.

INTRODUCTION

The second edition of "Stability of Metal Structures-A World View" (SSRC,1989), summarises in Chapter 7 present code approaches to the design of arches. It is apparent that typically service load or load factor methods are used in conjunction with elastic analysis. Regarding the in-plane arch stability, effective buckling lengths and moment magnification factors are employed in a stress analysis. In his address to the Fourth International Colloquium on Metal Structures in New York, Vinnakota (1989) identified the need for more guidance in regard to methods of arch analysis viz à viz the magnitude of the buckling effects and, in particular, with respect to snap-through buckling. These aspects are addressed in this paper. The elastic sway and snap-through buckling loads are used in conjunction with an approximate elastic-plastic method of analysis.

1) Associate Professor of Civil Engineering, University of the Witwatersrand, Johannesburg

(2)

HYPOTHESIS

It is argued that a recently developed approximate elastic-plastic method of analysis by Scholz (1984a,1984b,1989a) can be utilized to formulate a ratio of elastic buckling load, P_c, to rigid-plastic load, P_p, beyond which the instability loss is small enough to be neglected, so that simple first-order plastic analysis and design is sufficient.

The approximate method of analysis by Scholz has been fully documented in the abovementioned publications; only a few salient details are repeated here. The method presents itself in the form of the multi-curve diagram of Fig 1. These curves are similar to the more familiar single column curves.

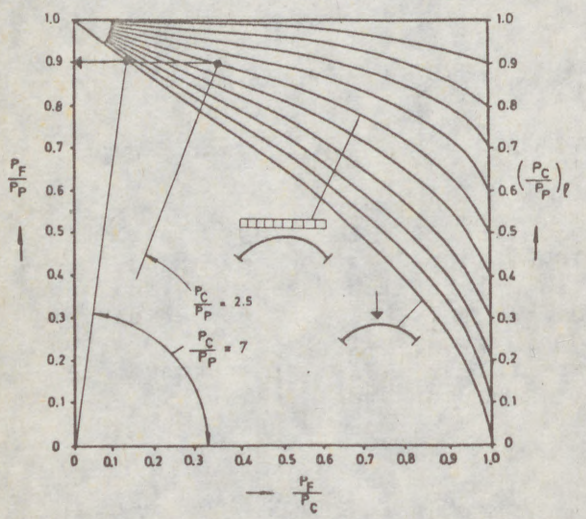

FIG 1: MULTI-CURVE DIAGRAM

In Fig 1, P_C/P_P, is the ratio of elastic buckling load to fully-plastic load of the actual structure, in the presence or absence of bending moments. The ratio $(P_C/P_P)_\ell$ in Fig 1 identifies a so-called limiting structure for which inelastic action just occurs under the application of the elastic buckling load. To define the geometry and ratio $(P_C/P_P)_\ell$ of the limiting arch, the stress due to axial forces and bending (if any) under the elastic buckling load, at the most critical arch section, must not exceed the stress at first yield, f.

$$\frac{P}{Af_y} + \frac{M_{II}}{Zf_y} = \frac{f}{f_y} \qquad (1)$$

The axial and moment stress terms are both a function of the elastic buckling load. Using the analogy of a column bent in single curvature, the second-order elastic bending moment, M_{II}, can be related to first-order moments, M_I, by way of the well known magnification factor, $1/(1-P/P_C)$.

Eq 1 can be solved to give a relationship between the ratio

(3)

$(P_C/P_P)_\ell$ of the limiting structure and P_C/P_P of the actual structure. If bending action dominates, e.g. for arches subjected to a central point load, $(P_C/P_P)_\ell=0$ is approached. At the other end of the spectrum, for arches subjected to pure axial forces, when evaluated on a first-order basis, $(P_C/P_P)_\ell=f/f_y$ is reached. The stress at first yield, f, is here taken as half the yield stress, f_y. This is in line with the CRC column strength curve of the SSRC Guide (1976) and has been entered in Fig 1.

P_C/P_P AND P_F/P_P LIMITS

It has been argued by Anderson (1986) and Scholz (1988) that analysis and design of a so-called bare structure could aim for a failure load, P_F, equal to 90% of the first-order rigid-plastic load. The shortfall of 10% would be found from strain-hardening and sundry composite action.

If a level of $P_F=0.90P_P$ is entered in Fig 1, it intersects a ratio of elastic buckling load to rigid-plastic load near 7 for arches subjected to a point load at the crown and near 2.5 for arches subjected to axial forces. A measure whether axial forces or bending moments dominate is the ratio of the applied first-order moment M_I to fully-plastic moment M_P, at the critical section as the actual loads are applied. Interpolating linearly between $P_C/P_P=7$ and 2.5 gives

$$\frac{P_C}{P_P} = 2.5 + 4.5\,\frac{M_I}{M_P} \qquad (2)$$

As axial forces dominate M_I approaches zero, giving $P_C/P_P=2.5$. As M_I reaches M_P, $P_C/P_P=7$ is obtained.

ELASTIC BUCKLING LOADS - SHALLOW ARCHES

The following elastic buckling loads are used in the expression $P_C/P_P=2.5+4.5M_I/M_P$:

For shallow pinned arches with sinosoidal, circular or parabolic shape subjected to uniformly distributed symmetrical load over the full arch length Fung and Kaplan (1952) derived and confirmed by experiments for symmetrical buckling

$$P_C = \frac{\pi^5 EIH}{4L^3}\left\{1 + \frac{1}{6H/r}\sqrt{\frac{1}{3}\left[\left(\frac{H}{r}\right)^2 - 4\right]^3}\right\} \qquad (3)$$

and for sway buckling for the same arch shapes and loading

$$P_C = \frac{\pi^5 EIH}{4L^3}\left[1 + 3\sqrt{1 - \frac{16}{(H/r)^2}}\right] \qquad (4)$$

(4)

For fixed arches and symmetrical snap-through buckling under uniform load, Uemura (1964) derived

$$P_c = \frac{112EIH}{L^3} \{3 + 0.0008(\frac{H}{r})^2[16 - \frac{360}{(H/r)^2}]^{1.5}\} \quad (5)$$

For fixed arches and sway buckling under uniform load Schreyer and Masur (1966) proposed

$$P_c = \frac{129.2EIH}{L^3} [3 + 2\sqrt{1 - \frac{75}{(H/r)^2}}] \quad (6)$$

For a point load applied at the crown, a factor of 0.64 is applied to Eqs 3-6.

The parameters in Eqs 3-6 are the modulus of elasticity, E, the second moment of area, I, the arch rise, H, the radius of gyration, r, of the arch member and the arch span, L.

ELASTIC BUCKLING LOADS - DEEP ARCHES

The SSRC Guide to Stability of Metal Structures (1976) conveniently presents elastic buckling loads for deep arches as

$$P_c = \frac{EI\pi^2}{k^2S^2} \quad (7)$$

where k is the effective length factor, S is half the arch length and P_c is the axial force at elastic buckling in the quarter span point of the arch. For the formation of the ratio P_c/P_p in Eq 2, the two forces must refer to the same reference point. For instance, since P_c of Eq 7 refers to the quarter span, then P_p must also be the axial thrust due to first-order plastic analysis at the quarter span point.

RIGID-PLASTIC LOAD

The computation of the first-order rigid-plastic load of an arch is elementary. The moment capacity reducing effect of the axial arch thrust needs to be considered. If no first-order bending moments are present,e.g. circular arch subjected to radial pressures or parabolic arch subjected to uniform load along the span, the rigid-plastic load amounts to section area times yield stress. In this paper, the rigid-plastic load is expressed as

$$P_p = \frac{16M_p}{L} R \quad (8)$$

with M_p the fully-plastic moment capacity of the section in the absence of axial forces and a reference factor, R.

(5)

ALLOWABLE SLENDERNESSES

The stipulated ratios P_c/P_p of Eq 2 can now be solved for an allowable slenderness ratio, span to section depth, i.e. L/d or S/d, corresponding to an expected failure load equal to 90% of the rigid-plastic load. For I-sections or box-sections and uniform loading causing predominant axial thrust, the curves of Figs 2 and 3 are obtained for pinned and fixed arches respectively.

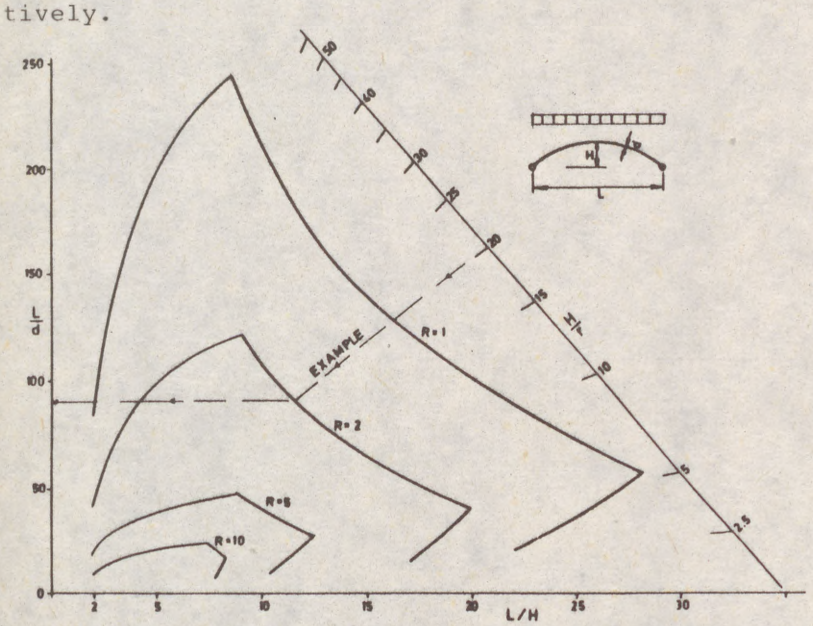

FIG 2: PINNED ARCHES UDL

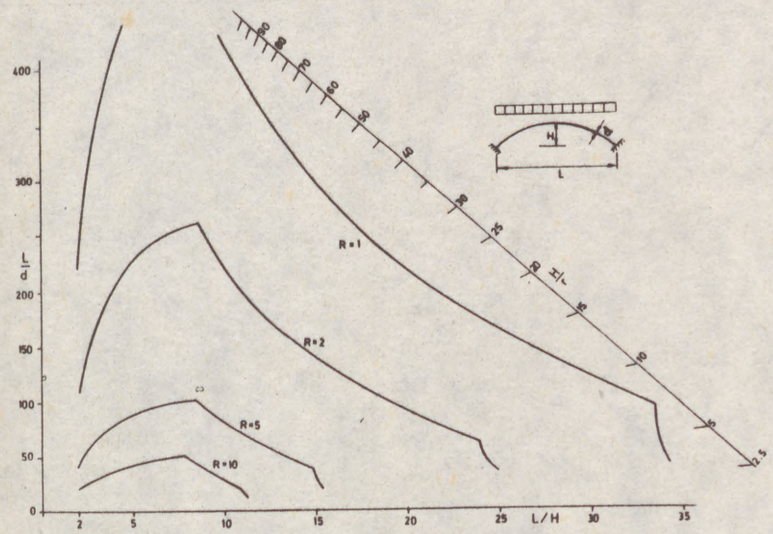

FIG 3: FIXED ARCHES UDL

(6)

For arches subjected to a concentrated load at the crown Figs 4 and 5 are obtained for pinned and fixed arches respectively.

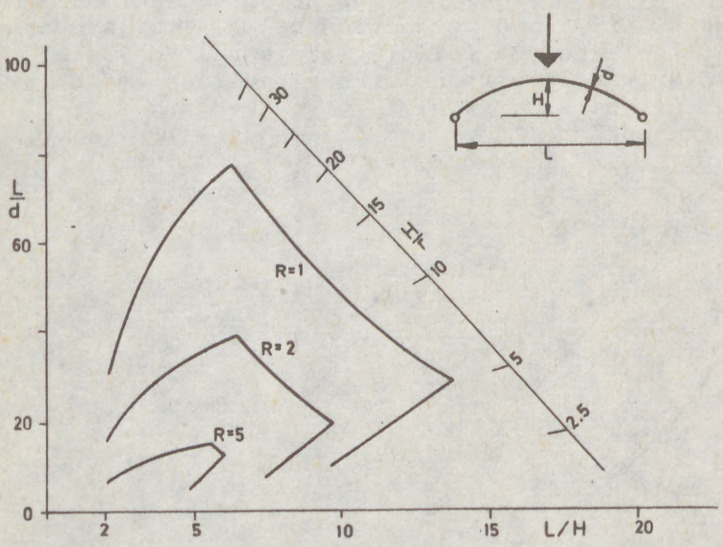

FIG 4: PINNED ARCHES POINT LOAD

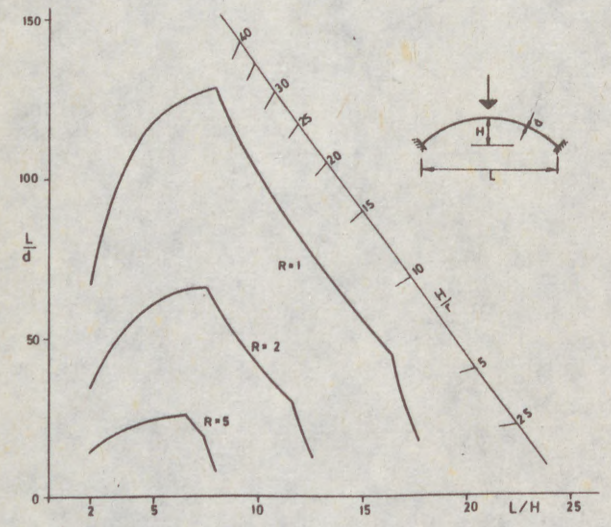

FIG 5: FIXED ARCHES POINT LOAD

The yield stress incorporated in Figs 2 to 5 is 300MPa. For a different yield stress, the curve values need to be factored by $\sqrt{300/f_y}$. Load conditions different from the uniform case or the central point load can be recognized by employing the relationship given in Eq 2.

(7)

DESIGN

An arch would initially be designed on a first-order plastic basis, ignoring the in-plane instability effects. The slenderness L/d of the resulting structure would then be compared with the allowable slenderness value of Figs 2 to 5 respectively. If found inadequate the section depth should be increased without increasing the plastic capacity of the section.

COMPARISONS

A number of experiments by Scholz (1989b) and Tin Loi and Pulmano (1988) on small-scale model arches of rectangular cross section are compared with the design rules of this study. They are entered in Fig 6. Good agreement can be observed. All test arches were subjected to a central point load at the crown and were forced to fail in a symmetrical mode. The required symmetrical elastic buckling loads were taken from the research by Harrison (1983). The given loads of Eqs 3 and 5 are only accurate as long as their results are below those of Eqs 4 and 6. Some of the test results were also confirmed with a finite element program.

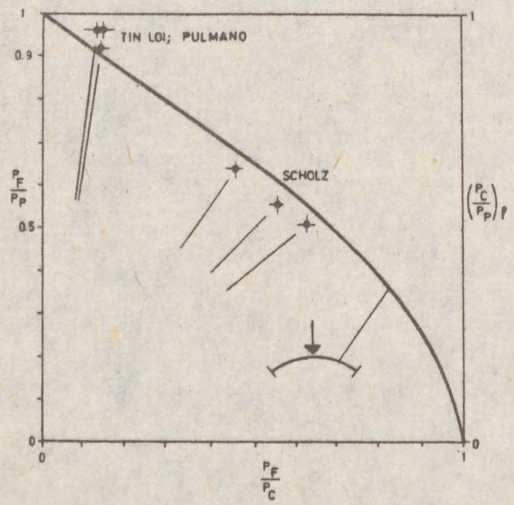

FIG 6: COMPARISONS

EXTENSION TO OTHER ARCHES

It is hypothesized that arches of other configuration, other cross-sections, with different support conditions and loadings compared with the here investigated arches can also be designed in line with the described approach, provided the correct elastic buckling load is used in the expression $P_C/P_P=2.5+4.5M_I/M_P$.

(8)

CONCLUSION

A rational and simple method to safeguard arches against in-plane snap-through and sway failure has been proposed. First experimental and rigorous analytical comparisons have confirmed the feasibility of the approach. A wider study of other arches is presently in progress.

REFERENCES

Anderson, D.1986. "First-Order Plastic Design of Single Storey Pinned-Base Frames", Document 86/3 of ECCS Working Group TWG8.2

Fung, YC and Kaplan, A.1952. "Buckling of Low Arches or Curved Beams of Small Curvature", NACA T.N. 2840, Washington D.C.

Harrison, HB.1983. "Elastic Post-Buckling Response of Plane Frames", Instability and Plastic Collapse of Steel Structures, Ed. LJ Morris, London, 56-65

Scholz, H.1984a. "Evolution of an Approximate Analysis Technique for Unbraced Steel Frames", The Civil Engineer in South Africa, 26, 12, 587-594

Scholz, H.1984b. "Simplified Interaction Method for Sway Frames", ASCE, 110, 5, 992-1007

Scholz, H.1989a. "Towards a Unified Stability Approach", 2nd East Asia Pacific Conf., Thailand, Vol 2, 1354-1359

Scholz, H.1988. "A New Solution to the Snap-Through Strength of Pitched-Roof Steel Frames", J. of Constr. Steel Res, No 9, 265-285

Scholz, H.1989b. "A Contribution to the In-Plane Stability of Shallow Arches", unpublished

Schreyer, HL and Masur, EG.1966. "Buckling of Shallow Arches", ASCE, 92, 4, 1-19

SSRC.1989. "Stability of Metal Structures-A World View", Introductory Document, Chapter 7-Arches, New York, 361-392

SSRC.1976. "Guide to Stability Design Criteria for Metal Structures", J Wiley & Sons, New York, 3rd Ed.

Tin Loi, F and Pulmano, VA.1989. "Collapse Load of Two-Hinged Steel Arches", 2nd East Asia Pacific Conf., Thailand, Vol 2, 1247-1253

Uemura, M.1964. "On the Finite Deformation Mode in the Non-Linear Snap-Buckling", Report of Aeron. Res. Inst., Univ. of Tokyo, No 382, 39-53

Vinnakota, S.1989. "Stability of Steel Arches: Need for more Specification Guidance", 4th Intern. Colloquium on Stability of Metal Structures, SSRC, New York

SESSION 9

TRIANGULATED STRUCTURES

(1)

CHLADNÝ, Eugen (1)
ÁROCH, Rudolf (2)
MACHÁČ, Peter (3)

GEOMETRICAL IMPERFECTIONS OF COMPRESSED CHORDS OF PONY TRUSS BRIDGES

INTERNATIONAL COLLOQUIUM
STABILITY OF STEEL STRUCTURES
BUDAPEST, HUNGARY, 1990
PRELIMINARY REPORT

Summary:

Measurements of initial geometrical imperfections on eight top chords of pony truss bridges were carried out. Elastic-plastic computer procedures were used to analyze the influence of real imperfections on the limit load of top chords and stressing of transverse frames. Good agreement with Czechoslovak standards which are based on an elastic analysis was found.

---

(1) Associate Professor
(2) Senior Lecturer
(3) Ph.D. Student
Department of Steel and Timber Structures
Slovak Technical University, Bratislava, Czechoslovakia

1. INTRODUCTION

In Proceedings of the Second Regional Colloquium on Stability of Steel Structures, Hungary 1986, a paper describing the elastic-plastic analysis of elastically supported bars with geometrical and structural imperfections loaded in compression was published [3]. Such bars are used for modelling the upper compressed chords of pony truss bridges, which buckle from the plane of the truss due to unavoidable imperfections and because of live load acting on the bridge. Lateral displacements of the panel points of the top chord cause an additional stressing in transverse frames. It can be calculated as the response to the action of two fictitious horizontal forces V acting in the plane of the transverse frames in the top chord centroids. An empirical value of these forces has been introduced in most of the current codes.

The magnitude of the force V can be expressed as a product of the transverse frame stiffness H and the displacement w_{max}

$$V = H \cdot w_{max} \qquad (1)$$

The value of w_{max} based on an elastic analysis is used in the Czechoslovak code CSN 736205 "The Design of Steel Bridge Structures" [2]. An elastic-plastic analysis [3] was used to check the code's procedure. A good agreement in results of both analyses was found. Because of lack of information about real geometrical imperfections of compressed top chords of pony truss bridges the first eigen-function with a maximum amplitude determined with the help of analogy with simple pin-ended columns was used in these analyses [3]. In order to check this assumption a series of measurements of initial crookedness of top chords of realized pony truss bridges was started. The results of measurements and the analysis of four bridges are presented in this paper.

2. MEASUREMENTS OF INITIAL CROOKEDNESS OF TOP CHORDS OF PONY TRUSS BRIDGES

In panel points and in the points in the middle of them the centroids of cross sections were found. Measuring bars were used to transfer these points into a vertical plane of a theodolite used for measuring. Simple calculation enabled us to find the initial displacements of measured points.

Measurements were carried out on bridges with truss shapes shown in Fig.1. Two of them have the shape a), the

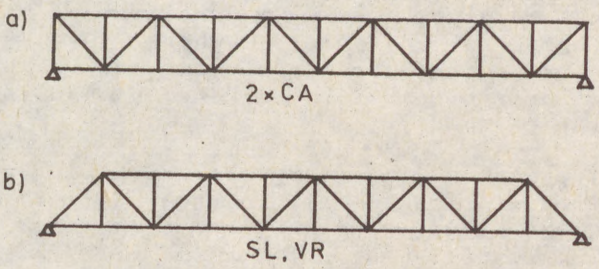

Fig.1

other two the shape b). One of the bridges (indicated as SL) has welded box cross sections of the top chord, the others have riveted T cross sections (Fig.2). Altogether

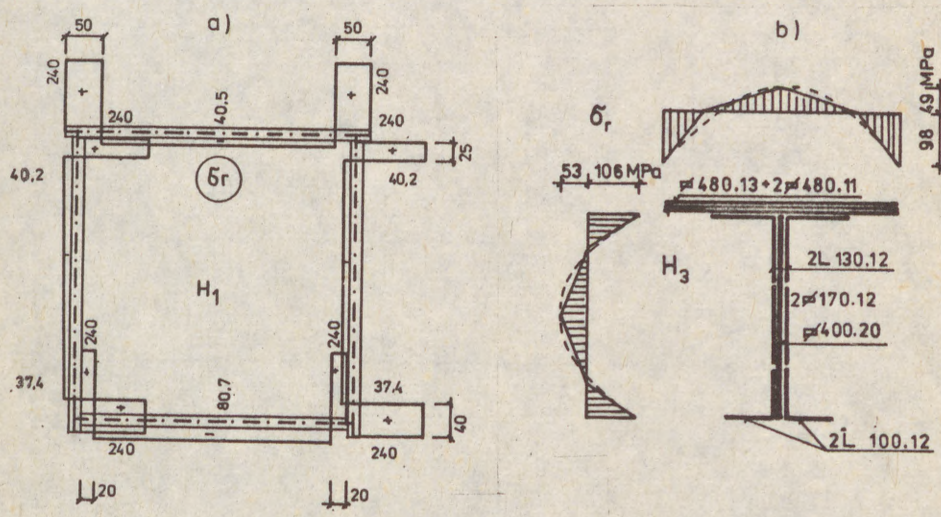

Fig.2

eight top chords, indicated as SLA, SLB, VRA, VRB, CAA, CAB, CAC, CAD, were measured until now.

(4)

3. ANALYTICAL EVALUATION OF MEASURED INITIAL CROOKEDNESSES

Two computer procedures, one based on the finite element method [1] the other on the transfer matrix method [4], were developed at the Department of Steel and Timber Structures of Slovak Technical University in order to evaluate the results of measurements. A bar, elastically supported in points where the stiffening transverse frames of the bridge are located, with various cross sections and normal forces between supports, was used as a statical model.

The end posts of b) shape trusses in Fig.1 were included in the statical model, so the ends of the bar are supported rigidly (Fig.3). In a) shaped trusses the ends are elastically supported.

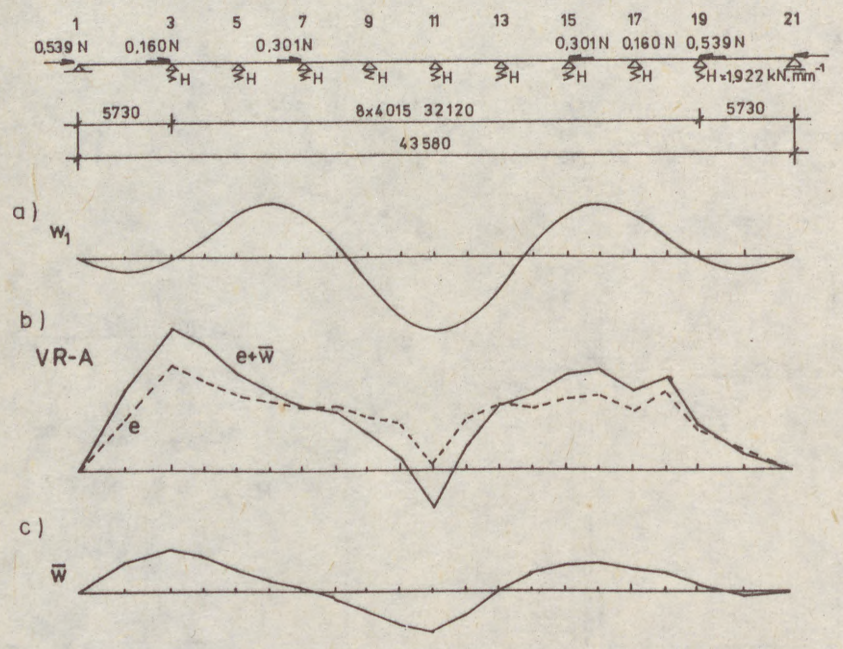

Fig.3

The two computer procedures give the possibility of:

1. determining the eigenvalues and eigenfunctions of the compressed chord without imperfections (Fig.3a). The first eigenvalue gives the critical load, effective length and the slenderness of the top chord. That enables the computation of the design limit load $\bar{N}$ with the help of an appropriate column strength curve from the codes.

(5)

2. simulating the development of the initial crookedness under increasing load from zero to the critical load. Materially elastic model is used for this purpose.

3. calculating the ultimate load when residual stresses are taken into account and materially elastic -plastic model is used. The shape and the magnitude of residual stresses in welded box cross sections of the SL bridge were computed using Okerblom's method (Fig.2a). For riveted sections (Fig.2b) empirical formulae were used [5].

The statical model of the VR bridge top chord is shown in Fig.3. The first eigenfunction w_1 and initial displacements measured on the VRA top chord are presented there as well. The maximum displacement was 23.5mm in point 3. The shape of the increment of initial displacements $\overline{w}$ under the design limit load $\overline{N}$ is shown in Fig.3c. The load-displacement relationship for points 3, 11 and 15 of the top chord VRA are presented in Fig.4. The solid lines indicate

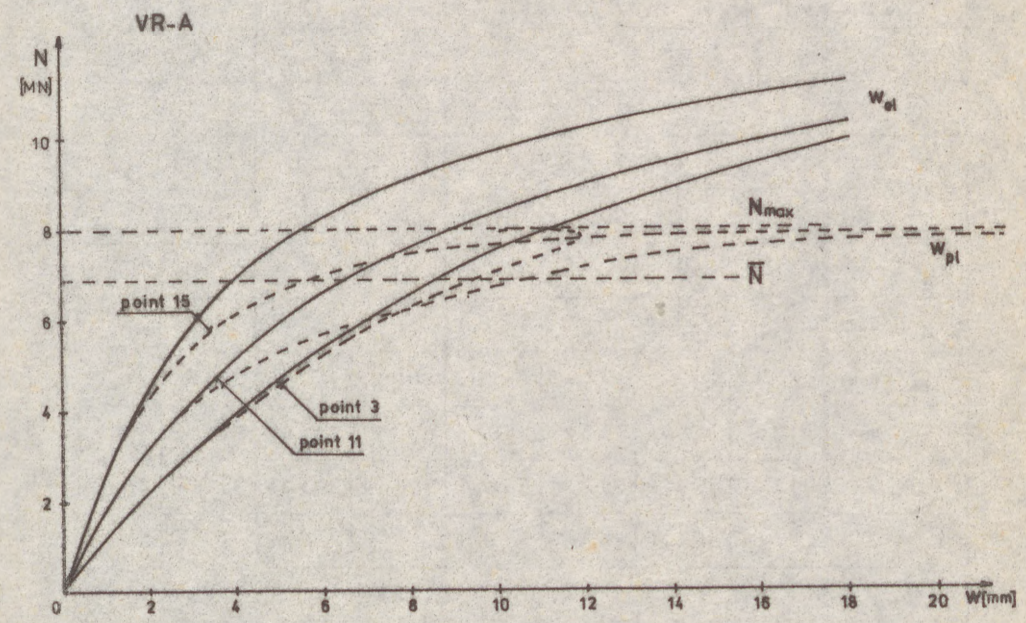

Fig.4

the elastic increment and the dashed lines the elastic-plastic one. Fig.4 shows that the ultimate load of the top chord N_{max} is about 16% higher than the design limit load $\bar{N}$. The ultimate load is reached at large increments of displacements. That is the reason why the design limit load was adopted as the real limit load. The increments $\bar{w}$ reached at this state were used in order to compute the horizontal force V (Eq.1).

4. CONCLUSION

The results of evaluation of all top chord measurements and analyses are presented in Table 1.

Table 1.

Bridge	CA				SL		VR	
Chord	A	B	C	D	A	B	A	B
L m	31.4				39.4		40.15	
β	1.2756				1.825		1.857	
λ	63.9				52.1		78.3	
N_{cr} MN	14.678				25.732		13.321	
$\bar{N}$ MN	5.772				7.279		6.877	
$\varkappa_d$	0.17				0.26		0.17	
w_d mm	2.97				7.46		12.44	
e_{max} mm	8.3	19.0	7.7	16.0	10.0	40.6	23.5	11.3
$\bar{w}_{max}$ mm	1.25	1.65	1.247	2.024	6.96	11.66	9.502	6.452
$\bar{N}/V_m$	911.1	690.2	913.3	562.7	337.4	201.4	376.6	554.6
$\bar{N}/V_k$	781.6	474.9	440.2	577.1				
$\bar{N}/V_{m,d}$	383.4				314.8		287.7	
$\bar{N}/V_{k,d}$	176.8							

L - length of the compressed chord
β - effective length coefficient relative to the panel length
λ - slenderness of the most stressed bar of the compressed chord
N_{cr} - critical force

$\overline{N}$ - design limit load calculated according to the Czechoslovak code

α_d - imperfection's standard belonging to the column strength curve A or B according to CSN 731401

w_d - increment of displacement calculated with the formula in CSN 736205

$\overline{w}_{max}$ - maximum displacement of the panel point under load $\overline{N}$

The ratio of the design limit load and the force V, which the majority of codes recommend as 100, is calculated according to CSN 736205 in the last rows of Table 1. Above them there are values calculated on the basis of measured geometrical imperfections. It is evident that these values as well as the values according to CSN are much greater than 100. It means that the force V determined as $\overline{N}/100$ is too large and with probability it will be possible to reduce the CSN values too.

The ultimate load of the compressed chords was always greater than the design limit load also when large initial geometrical imperfections were present. Besides, the analyses also confirmed that not only the absolute magnitude of the geometrical imperfections but also their shape, the similarity or the dissimilarity with the first eigenfunction is of great importantance.

REFERENCES

[1] Ároch, R. (1988) Medzná únosnosť tlačených prútov s imperfekciami (Load-Bearing Capacity of Compressed Bars with Imperfections), Report, Slovak Technical University, Bratislava

[2] Chladný, E. (1974) Vzper pružne podopretých prútov (The Buckling of Elastically Supported Bars), Habilitation, Slovak Technical University, Bratislava

[3] Chladný, E. Šoltész, J. (1986) The Elastic -Plastic Analysis of Elastically Supported Bars with Geometrical and Structural Imperfections Loaded in Compression, Proceedings of the Second Regional Colloquium on Stability of Steel Structures, Hungary, Vol.I/1, pp.43-50

[4] Macháč, P. (1989) Vzper prútov na pružných podperách (Buckling of Elastically Supported Bars), Diploma thesis, Slovak Technical University, Bratislava

[5] ECCS (1976) Second International Colloquium on Stability, Introductory Report, Liege, pp.31-46

DIAC

A N

Summa
in l
for
On t
luate
inte
defo
force

1. In
confi

table
puter
this

propo

estab
resea

nates

intro

2. H
known
valed
suppo
ion/t

---

(1)

DIACU, Ioan (1)

A NONLINEAR ANALYSIS PROGRAM FOR HINGED IMPERFECT MEMBERS SPACE STRUCTURES.

INTERNATIONAL COLLOQUIUM
STABILITY OF STEEL STRUCTURES
BUDAPEST, HUNGARY, 1990
PRELIMINARY REPORT

Summary: The finite element rigidity for imperfect hinged member in local coordinates is determined. The tangent rigidity matrix for the finite element having high displacements is established. On this basis there is proposed an analysis algorithm able to evaluate the general (snap through) and local (member) instability interaction. Using a Newton-Raphston iterative technique, on the deformed position, the procesus is stopped when the unbalanced forces become small enough.

1. Introduction. Space structures having hinged members are often confronted with essential instability phenomena.

For real complex structures the only chance to get an acceptable accurate analysis resides in the use of an appropriate computer program. A tentative for such a program is presented in this paper.

The finite element technique was found suitable for the proposed aim.

The imperfect hinged member axial rigidity was analysed, establishing formulas compatible with well-known european column research results /1,2/.

The imperfect member tangent stiffeness in global coordinates, having great displacements, is obtained.

The analysis program algorithm and some of its results are introduced.

2. Hinged imperfect member axial rigidity. There is used the known hypothesis /1/ that all kinds of imperfections can be equivaled with an initial geometrical deflected shape. So it is supposed that the member acts from the very begining in compression/tension and bending, the axial rigidity being nonlinear.

---

(1) C.Eng.,Ph.D., Assistant Professor of Steel Structures, Civil Engineering Institute, Bucharest, Romania.

(2)

* The initial equivalent deflection can be accepted that resulting from the appropriate column resistance curve or in an agreedment with it.

$$\sigma_{max} = \frac{N_u}{A} + \frac{N_u \cdot w_o}{(1 - N/N_E)W} = \sigma_y \qquad (1)$$

Taking $N_u/N_p = \chi$ $(N_p = A\sigma_y)$ it results:

$$w_{oeq} = \left(\frac{1}{\chi} - 1\right)\cdot(1 - \chi\cdot\bar{\lambda}^2)\cdot\frac{W}{A} \qquad (2)$$

In the EUROCODE 3 /1/ a forfetary value for equivalent geometrical imperfection is recommended, tab.1, although from eq.(2) results a value dependent on the slenderness $\bar{\lambda}$.

Table 1.

Column curve:	a_0	a	b	c	d
w_o equivalent:	1/750	1/500	1/250	1/200	1/150
$\alpha = \frac{w_o}{\bar{\lambda} - 0.2}\cdot\frac{A}{W}$:	0.13	0.21	0.34	0.49	0.76

* The axial deformation of a member, fig.1, has two components/4/:

$$u_\varepsilon = \frac{N l_o}{EA} \qquad (3)$$

$$u_w = \frac{1}{2}\int_0^{l_o}\left(\frac{dw}{dx}\right)^2 dx = \frac{1}{2}\int_0^{l_o}\left[(w_o + w_1)\frac{\pi}{l_o}\cdot\cos\frac{\pi x}{l_o}\right]^2 dx$$

$$-\frac{1}{2}\int_0^{l_o}\left[w_o\frac{\pi}{l_o}\cos\frac{\pi x}{l_o}\right]^2 dx = \frac{\pi^2}{4 l_o^2}\left[(w_o + w_1)^2 - (w_o)^2\right] \qquad (4)$$

According to Ayrton-Perry concept:

$$w = w_o + w_1 = \frac{1}{1 - N/N_E}\cdot w_o \qquad (5)$$

So u_w becomes:

$$u_w = \frac{\pi^2}{4 l_o^2}\left[\frac{1}{(1 - N/N_E)^2} - 1\right](w_o)^2 \qquad (6)$$

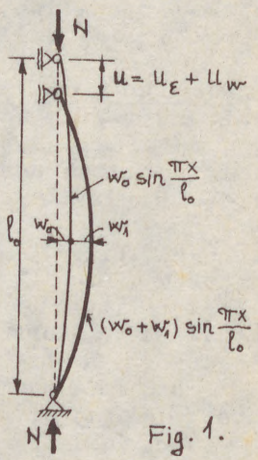

Fig. 1.

and:

$$u = u_\varepsilon + u_w = \left[1 + \frac{2 - N/N_E}{(1 - N/N_E)^2}\cdot\left(\frac{w_o}{2\cdot i}\right)^2\right]\cdot\frac{N\cdot l_o}{E\cdot A} \qquad (7)$$

For tension member the above formula coresponds to:

$$u = \left[1 + \frac{2 + N/N_E}{(1 + N/N_E)^2}\cdot\left(\frac{w_o}{2\cdot i}\right)^2\right]\cdot\frac{N\cdot l_o}{E\cdot A} \qquad (8)$$

(3)

* Formula (7) is valid until the yield stress is reached in the extreme fiber of the central section. When $N=N_u$ (fig.3):

$$u_u = \left[1 + \frac{2-\chi\bar{\lambda}^2}{(1-\chi\bar{\lambda}^2)^2}\left(\frac{w_o}{2.i}\right)^2\right]\cdot\chi\cdot u_y \qquad (9)$$

where:

$$u_y = l_o\cdot\sigma_y/E\ ;\quad \bar{\lambda} = \lambda/\lambda_E\ ;\quad \lambda_E = \pi\sqrt{E/\sigma_y}$$

* After reaching the yield stress a plastic mechanism is expected, fig.2. This plastic mechanism leads to:

$$N\cdot u = M\cdot\theta \qquad (10)$$

$$\theta = \frac{2\cdot w}{l_o/2} = \frac{4w}{l_o} \qquad (11)$$

$$M = N\cdot w\ ;\quad u = \frac{4w^2}{l_o} \qquad (12)$$

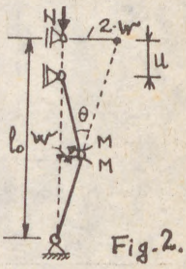

Fig.2.

For tubes an acceptable interaction plastic formula can be /3/:

$$\left(\frac{N}{N_P}\right)^{1.7} + \frac{M}{M_P} = 1 \qquad (13)$$

When $N = N_u$ the above formulas lead to (fig.3):

$$u_p = \frac{4}{l_o}\left[1 - \left(\frac{N_u}{N_P}\right)^{1.7}\right]^2\cdot\left(\frac{M_P}{N_u}\right)^2 \qquad (14)$$

or:

$$u_p = \frac{4}{l_o}\left[\frac{1-\chi^{1.7}}{\chi}\right]^2\cdot\left(\frac{W_P}{A}\right)^2 \qquad (15)$$

* The above ideas are represented in an unitary diagram, fig.3. From the plastic mechanism a simplified practical model is deducted, fig.3.

In tension the diagram is limited at N_p.

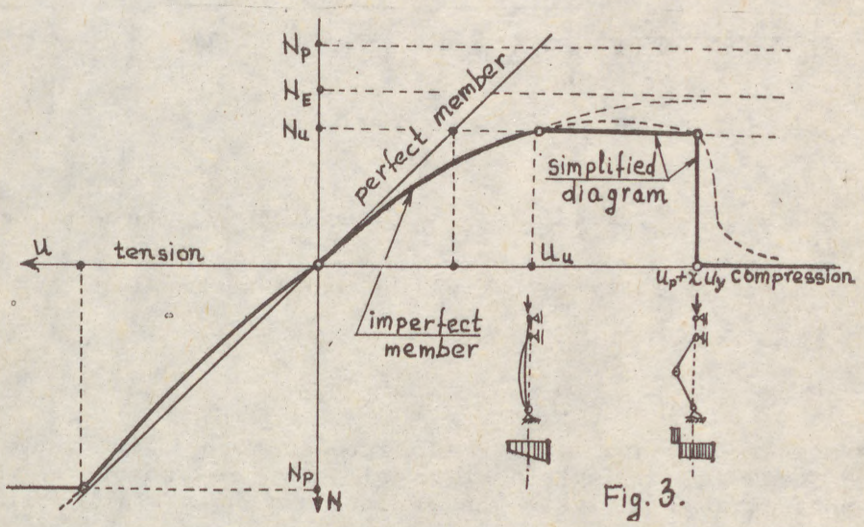

Fig.3.

(4)

3. Tangent rigidity matrix for hinged imperfect member. In the global coordinates system a member with initial length l_o (l_{ox}; l_{oy}; l_{oz}) has the end displacement u (u_x; u_y; u_z) and the axial force N (N_x; N_y; N_z).

The tangent member rigidity matrix for one end is:

$$k_{ot} = \begin{bmatrix} \frac{\partial N_x}{\partial u_x} & \frac{\partial N_x}{\partial u_y} & \frac{\partial N_x}{\partial u_z} \\ \frac{\partial N_y}{\partial u_x} & \frac{\partial N_y}{\partial u_y} & \frac{\partial N_y}{\partial u_z} \\ \frac{\partial N_z}{\partial u_x} & \frac{\partial N_z}{\partial u_y} & \frac{\partial N_z}{\partial u_z} \end{bmatrix} \qquad (16)$$

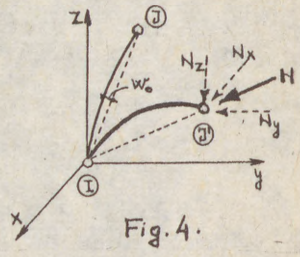

Fig. 4.

Having:

$$u = \sqrt{(l_{ox}+u_x)^2+(l_{oy}+u_y)^2+(l_{oz}+u_z)^2} - l_o ;$$

$$N_x = N\cdot\frac{l_{ox}+u_x}{l_o+u} ; \quad N_y = N\cdot\frac{l_{oy}+u_y}{l_o+u} ; \quad N_z = N\cdot\frac{l_{oz}+u_z}{l_o+u} ,$$

the matrix terms are deducted by simple diferential operations as by instance:

$$\frac{\partial N_x}{\partial u_x} = \frac{\partial N}{\partial u_x}\frac{l_{ox}+u_x}{l_o+u} + N\frac{\partial}{\partial u_x}\left(\frac{l_{ox}+u_x}{l_o+u}\right) ; \quad \frac{\partial}{\partial u_x}\left(\frac{l_{ox}+u_x}{l_o+u}\right) = \frac{(l_o+u)^2-(l_{ox}+u_x)^2}{(l_o+u)^3} ;$$

$$\frac{\partial N}{\partial u_x} = \frac{dN}{du}\frac{\partial u}{\partial u_x} ; \quad \frac{\partial u}{\partial u_x} = \frac{l_{ox}+u_x}{l_o+u} ;$$

$$\frac{dN}{du} = \frac{1}{\frac{du}{dN}} = \frac{E\cdot A}{l_o}\cdot\frac{(1+N/N_E)^3}{(1+N/N_E)^3+\frac{1}{2}\left(\frac{w_o}{i}\right)^2} .$$

So:

$$k_{ot} = \left[\frac{EA}{l_o}\cdot\frac{(1+\frac{N}{N_E})^3}{(1+\frac{N}{N_E})^3+\frac{1}{2}(\frac{w_o}{i})^2} - \frac{N}{l_o+u}\right]\cdot\begin{bmatrix} l^2 & lm & ln \\ ml & m^2 & mn \\ nl & nm & n^2 \end{bmatrix} + \frac{N}{l_o+u}\cdot\begin{bmatrix} 1 & 0 & 0 \\ 0 & 1 & 0 \\ 0 & 0 & 1 \end{bmatrix} \qquad (17)$$

where:

$$l = \frac{l_{ox}+u_x}{l_o+u} ; \quad m = \frac{l_{oy}+u_y}{l_o+u} ; \quad n = \frac{l_{oz}+u_z}{l_o+u} ;$$

N and u are positive in tension.

The tangent rigidity matrix of the whole member is:

$$k_t = \begin{bmatrix} k_{ot} & -k_{ot} \\ -k_{ot} & k_{ot} \end{bmatrix} \qquad (18)$$

The member tangent rigidity is deppendent on its load level and varies between linear classical rigidity and zero. On this basis a postcritical analysis can be done for hyperstatic structures.

(5)

As a special case the perfect member tangent rigidity matrix is:

$$k_{ot} = \frac{E\cdot A}{l_o}\begin{bmatrix} l^2 & lm & ln \\ ml & m^2 & mn \\ nl & nm & n^2 \end{bmatrix} + \frac{EA}{l_o}\frac{u}{l_o+u}\begin{bmatrix} 1 & 0 & 0 \\ 0 & 1 & 0 \\ 0 & 0 & 1 \end{bmatrix} \qquad (19)$$

4. Computer program analysis algorithm. The algorithm consists in three main iterative steps.

* Step 1. Structure rigidity matrix is assembled from everyone member rigidity, according with eq.(17), so taking into account the previous step member deformed position.

* Step 2. From and on the previous deformed position (initial undeformed) the internal forces are evaluated and nodal unbalanced forces are calculated. The iterative procesus is stopped when resides become negligible. For an instable situation the iterative procesus becomes divergent.

* Step 3. Equations system:

$$K\cdot\Delta = F \qquad (20)$$

is solved by a Crout algorithm. When K is not positive definite an instable equillibrium is announced. This situation is simply analysed controlling the diagonal matrix term sign in the Crout reduction process.

Member forces and stresses are finaly calculated:

$$\sigma_{max} = \sigma_N + \sigma_M = \frac{N}{A} + \frac{N\cdot w_o}{\left(1-\frac{N}{N_E}\right)W} = \frac{N}{\chi_1 A} \qquad (21)$$

where:

$$\chi_1 = \frac{1}{1+\frac{w_o}{1-N/N_E}\frac{A}{W}} \qquad (22)$$

It can be seen that $\chi_1 \geq \chi$. The "equal" relation is valid when $N = N_u$, that is when $\sigma_{max}=\sigma_y$. Eq. (1) may be writen (Rondal-Maquoi formulation /1/):

$$(N_E - N_u)(N_P - N_E) = \frac{w_o\cdot A}{W}\cdot N_E\cdot N_u \qquad (23)$$

Introducing $w_o A/W$ as from tab.1, deppending on α , it results $\chi = N_u/N_P$.

5. Some tests and applications. Tests intend firstly to point the practical program ability to evaluate the "snap through buckling" situations. Therefore some simple cases, as that in fig.5a wich were able to have an analitical solution, were used. The program gave very accurate agreedment with the theory.

A simple modulus (fig.5b) experiment was performed.

The program was used for the analysis of some barrel vaults structures, as in fig.6, and some other space structures. Various imperfections and loads scenery was tested using the program.

The program was also tested against some experimental results on a barrel vault model.

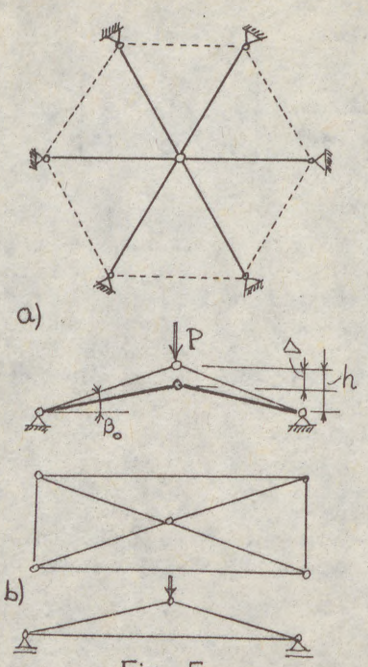

Fig. 5.

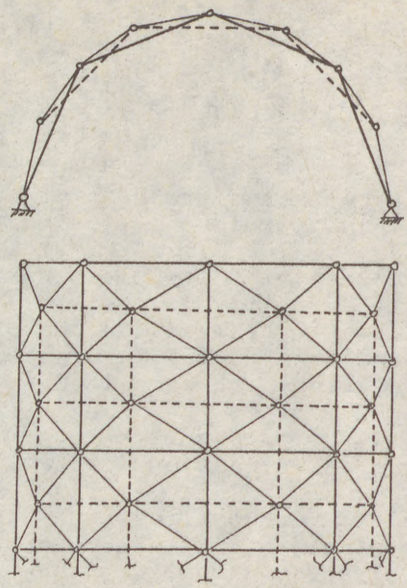

Fig. 6.

It is to be noticed that for some applications, as that in fig.6, the program use is indispensable, the classical analysis results and our results being essentialy different.

More tests, mainly aiming at a better imperfection level adoption, are now in progress.

6. Conclusions. Structural behaviour and ultimate load capacity of a space structure are fundamentally affected by its imperfections.

An accurate analysis can't be done in absence of an adequate computer program. An algorithm for such a program was introduced.

References.

1. Commission des Communautes europeennes. EUROCODE 3: Regles unifiees communes pour le construction en acier. Luxembourg, 1984.

2. ECCS - European Recommendations for Steel Construction. ECCS-EG 77-1E, 1977.

3. NBN B51-002. Carpantes en acier. Calcul par la methode des etats-limites., Bruxelles, 1988.

4. * * * Stahlbau Handbuch. Stahlbau-Verlags-GmbH., Koln, 1982.

DOTZEV, Valentin (1)

PRESERVATION OF LOAD CARRYING CAPACITY AND STABILITY OF SPACE STEEL STRUCTURES WHEN A FAILURE OF A BAR OCCURS

INTERNATIONAL COLLOQUIUM
STABILITY OF STEEL STRUCTURES
BUDAPEST, HUNGARY, 1990
PRELIMINARY REPORT

SUMMARY: Space structures are usually highly statically indeterminate, which causes a high degree of structural safety. They have a built-in reserve of strength, enabling a structure to take local overloading or the consequences of a bar failure. In the paper the results from a study carried out in CESSI are discussed. Its main purpose is to clarify the behaviour of a space bar structure when a member is excluded off the work due to an accident.

One of the most dynamicly developing branches of metal construction industry in Bulgaria recently is the erection of multipurpose, multifunctional public buildings with space steel tube-bar roofings. A system similar to the well known MERO and MArchI systems is applied. The basic unit of the system is a rod pyramid on a rectangular basis, obtained by adjoining uniformly long steel electrowelded tubes to unified structural nodes by means of an axial bolted connection. The type of the connector is shown on fig.1.

---

(1) Research Assosiate in CESSI, Sofia

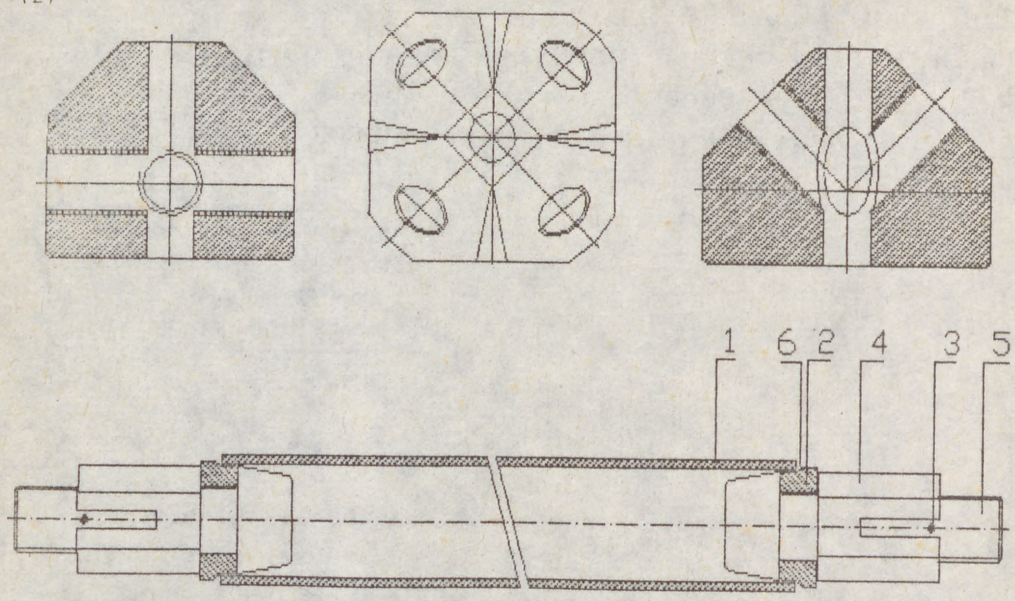

Figure 1

The advantages of the system - light selfweight at small construction hight, possibility for flexible architectural layouts and almost unlimited form generation, easy transportation, assembly and erection, etc. lead to design and building of numerous structures with most variable configurations over large spans (60 m. and more), consisting of a great number of elements (6000 bars and more).

The rapid spread of tubular space steel structures as well as some disadvantages of the tube-bar elements caused by the imperfect production technology set the problem of safety and reliability of this type of structures.

The design reliability of a steel structure is ensured by the accurate solution of two main tasks:

1. correct determination of the quality of the building material, production and erection, which define a multidimensional Space of Quality (SQ). In the process of exploitation it continuously changes; the accumulation of impairs by unfavourable mechanic, chemical and other harmful actions leads to shrinking of SQ, while some phenomena as flattening

(3)
the peaks of stress concentrators cause its expansion.

2. accurate estimate of the type and the magnitude of the various loadings which define the Space of Status (SS). It changes constantly in time, following the changes of the loadings.

Each engineering structure is considered to be safe and serviceable only until the pulsating space of status is enveloped by the space of quality [1].

PREREQUISITES OF THE STUDY

The investigation of this problem for the tubular space structures shows the following.

The buildings covered by steel space structures (SSS) are subjected to different loadings:

- self weight,
- live load (suspended ceilings, lighting, ventilation, etc.),
- snow load,
- temperature influence,
- seismic loading.

The accumulated experience in computer aided analysis of SSS in our institute indicates that the dimensional forces for most of the structural members are obtained on the basis of the self weight, live and snow load combination. For the various in configuration structures the percentage of such members varies between 80% and 95%. The nature of the above mentioned loads is relatively simple, besides their maximal values could be rather accurately foreseen in the design phase. This enables us to state that the limit space of status for the space bar structures can be reliably forecast.

The precise determination of the space of quality turned to be far more difficult, because it depends mainly on the imperfections and production defects of the elements. The problems for the structures produced and erected in Bulgaria arise mainly from the following facts:

(4)

- The welded seam, adjoining the sleeve to the tube (item 6 on fig 1) is performed semiautomatically. As yet the production enterprise does not possess adequate equipment for supersonic control so that reliably to guarantee the quality of the weld seams. This might lead to implanting in the structure members with lower load capacity than the calculated one;

- The actual length of a member depends on the tolerances of accuracy of its compounds (length, diameter and thickness of the tube, diameter of the sleeve cone, length of the nut,etc.). When assemling a structure with numerous members these tolerances might accumulate unfavourably and affect the assembly. In case of an attempt of length adjustment of members in place, which is strongly not recomended, it might lead to inserting significant initial forces which added up to the exploitational ones might cause a failure of a separate member.

In order to study the behaviour of a space structure when a given member is excluded off the overall work of the structure a series of analyses was carried out in CESSI, based on the software developed [2]. Here the results from the consecutive analysis of a tubular space structure with dimensions 24/24/3 (fig.2.) are discussed.

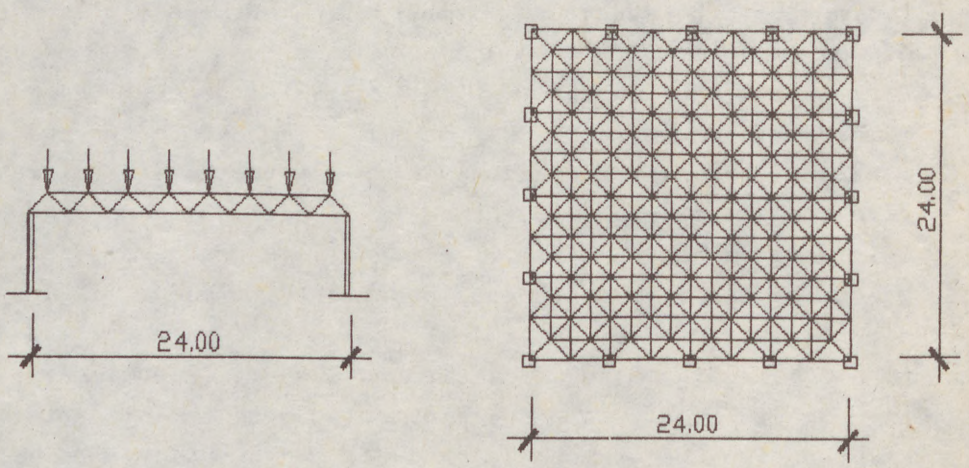

Figure 2

(5) SOLUTION SCHEME

The ivestigation has been carried out in the following sequence:

1. The structure is analysed for a distributed vertical load acting upon the upper grid as concentrated in the nodes forces. The allocation of this load corresponds to the combination of self weight and snow load, which in this case is the dimensional combination for 87% of the members. Its value is chosen so that to cause in the most heavily loaded elements forces near the limit load carrying capacity for the chosen set of members.

2. A series of solutions is performed at the assumption that each time one of every basic type of tube members has failed and this particular member is substituted by a pair of forces acting along the axis of the excluded member and applied at its end nodes. The following cases are considered:

- a tube situated at the middle of the upper grid;
- a tube situated at the middle of the lower grid;
- a tube situated near the support of the lower grid;
- a support diagonal member;
- a tensile diagonal situated near the support;
- a grid member in the vicinity of a rarefied zone.

The results of this series of solutions are used for tracing the way of redistribution of forces in the members near the defected one and for estimating their magnitude.

3. The member forces when a given member has been excluded are obtained according the following formula:

$$N_I^F = N_I^S + N_J^S \qquad (1)$$

where: N_I^F is the force in the I^{-th} member of the structure at failure of the J^{-th} one,

N_S^I is the service force in the I^{-th} member,

N_S^J is the service force in the defected member before the accident,

is the percentage of the J^{-th} member force, which is to be redistributed to a I^{-th} member after the accident.

(6)

RESULTS FROM THE SOLUTION'S SERIES

On the next few figures the redistribution of the forces after a failure of some of the basic types of members is illustrated. The members which get an extra compression force in consequence of the accident are presented with a dense line. The ones getting an additional tension force are shown with a hatched line. The members whose forces after the accident practically coincide with the service ones are presented with a thin line.

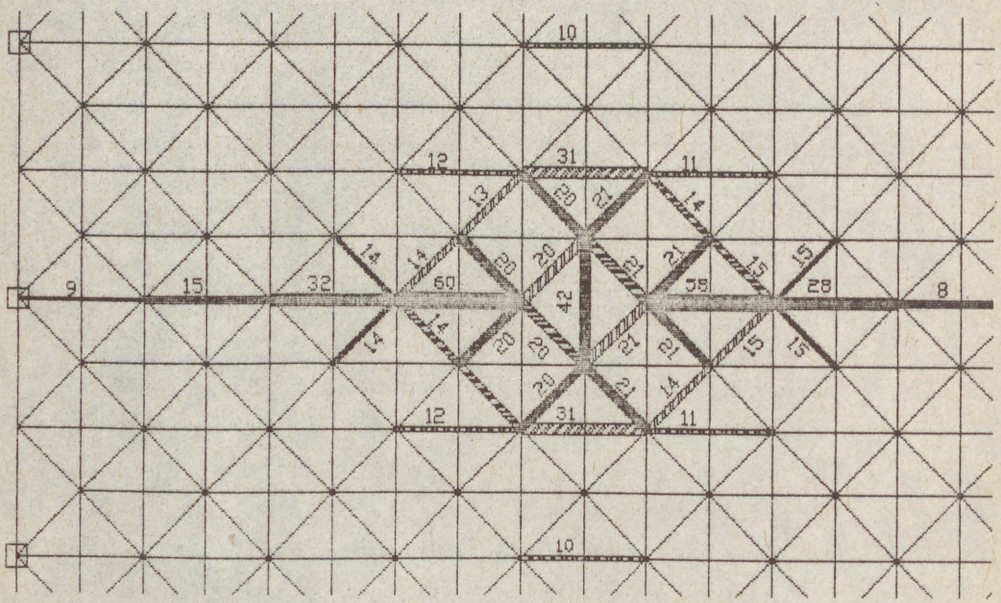

Figure 3 - failure of a tube situated at the middle of the lower "tensile" grid.

In this case the next parallel to the defected member elements get the maximum extra tension force - 31% of the defected member's force. A member from the upper grid situated just over the failed member gets the maximum supplementary compression force - 42% due to the redistribution.

(7)

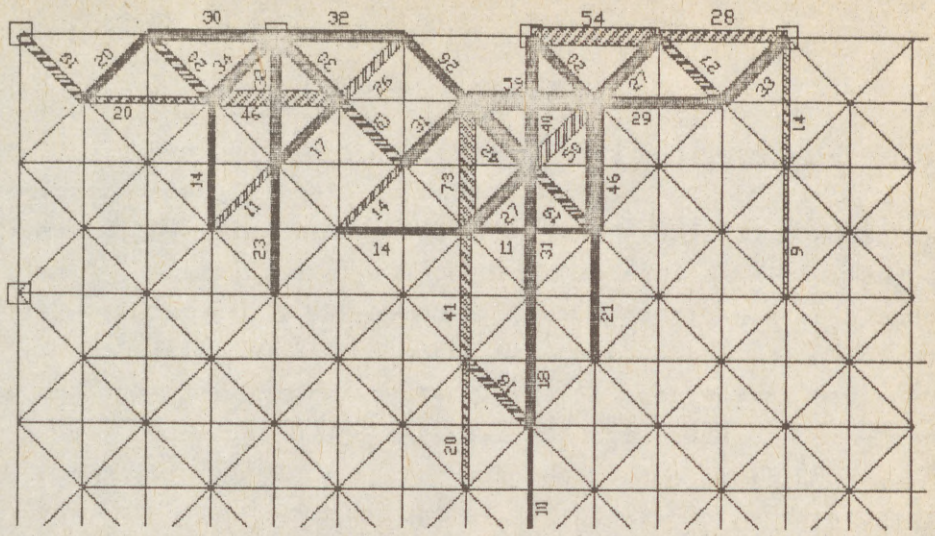

Figure 4 – A support diagonal member excluded.

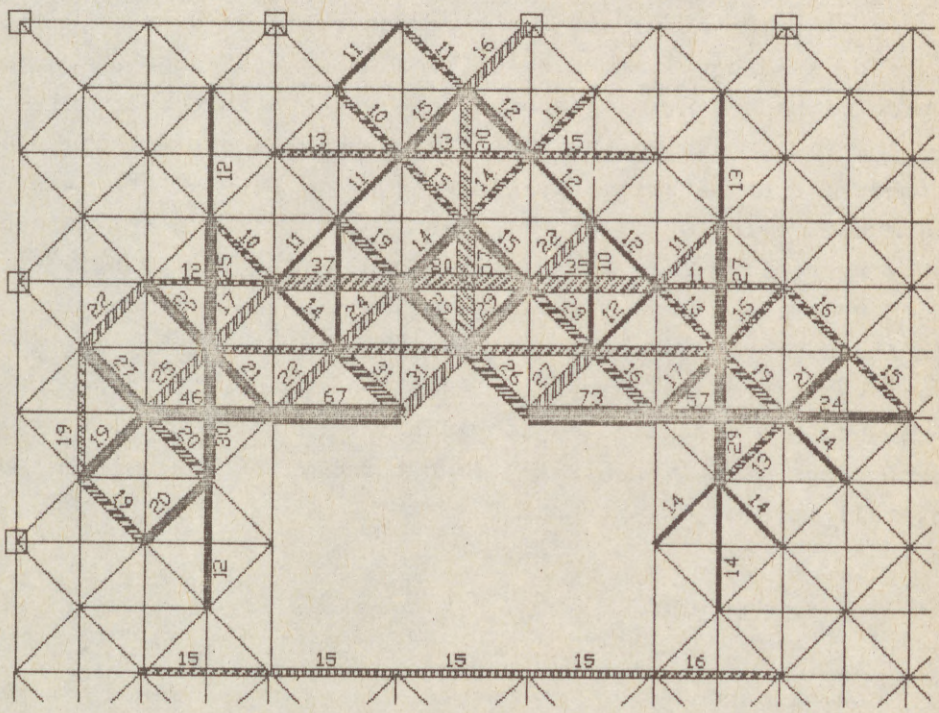

Figure 5 – failure of an element near a rarefied zone.

(8) ANALYSIS OF THE RESULTS

The following conclusions can be drawn on the basis of the analysis of the results obtained from the investigation:

1. Due to the high degree of static indeterminacy of space bar structures the inner forces are very well redistributed when a failure of a bar occurs. The additional forces of practical significance (it's assumed 10% redistribution of the force in the defected member to be considered significant) are received in the zone in the immediate vicinity to the failed bar - two to three modules away in each direction.

2. The additional forces received by the members in the vicinity of the defected bar do not exceed the reserves foreseen in the design codes by means of the overloading factor, work condition and material safety factors. That is why a failure of a bar does not cause the breakdown of the structure as a whole.

3. The above statement is not valid in case of a failure of a member from a rarefied zone or of a support bar, which might cause a collapse of the whole structure.

4. Though in the case of excluding a support diagonal member a considerable overloading of some bars occurs, the defected member's forces are distributed in the nearby zones only partially. This can be explained in the following way. When the load carrying capacity of a compressed member (such as the support diagonal) is exceeded, because of the particularity of the space bar structures the rest of the structure prevents the unrestricted approach of the nodes of the failed bar. Consequently this bar is not fully excluded from the overall work of the structure.

REFERENCE:

1. Кузнецов В.В. и кол. Развитие металлических конструкций. Работы школы Н.С. Стрелецкого, Стройиздат, Москва 1987.

2. Dotzev V., Nesheva I., CAD of space steel structures, 15-th Conference on Steel Space Structures, Prague 1988.

1

GALAMBOS, Theodore V. [1]
XYKIS, Constantine [2]

THE EFFECT OF LATERAL BRACING ON THE STABILITY OF STEEL TRUSSES

INTERNATIONAL COLLOQUIUM
STABILITY OF STEEL STRUCTURES
BUDAPEST, HUNGARY, 1990
PRELIMINARY REPORT

Summary: Results of two analytical studies of three-dimensional rigid space trusses are reported and compared to experimental results. Single trusses as well as two and three braced truss systems were investigated by finite element analysis for the elastic buckling strength of the system. The effects of the following parameters were investigated: Axial and flexural stiffness of the bracing, the brace end-conditions, the number of trusses, and the effect of bracing only the top chord.

1. INTRODUCTION

Light preengineered and prefabricated trusses are very popular in North America for roofs and floors in institutional and industrial buildings. These trusses are known as "steel joists" and they are fabricated by welding. The chords are made from two angles or cold-formed hat shapes, and the webs may be solid round bars, double angles, or single angles welded to one side of the chord, or their crimped ends may be placed between the two chords. The design of these trusses is governed by the Standard Specifications of the Steel Joist Institute (Steel Joist Institute, 1990). They are available in standard sizes from about 200 mm to 1800 mm in depth and they may be up to 45 m long. The selection is made by the engineer by referring to a load table. The manufacturer designs these joists by computer automation according to the rules in Reference 1.

The trusses are strong and stiff in their plane, but they are very flexible out-of-plane. They must therefore be properly braced prior to the application of any construction load. This paper is a report of a continuing study on the lateral stability of such braced truss-systems. Some aspects of the study were reported in the proceedings of the 1986 Stability Colloquium (Galambos,

[1]Professor of Civil Engineering, University of Minnesota
[2]Structural Engineer, Onan Corporation, Minneapolis

1988). Here we will describe further analytical studies and comparisons to a test.

2. ASSUMPTIONS AND ANALYSIS OF THE BRACED TRUSS MODEL

The system of trusses and braces is shown schematically in Fig. 1. The trusses to be braced are designated as "joist" on this figure. They are supported by the heavier trusses called "joist girder." These are braced by the joists, which in turn are braced by the members designated as "bridging" in Fig. 1. We are here concerned with the analysis of the joist-bridging system after the bridging is in place and the construction loads are placed at the points where the bridging lines intersect with the joists.

Bridging may be either "horizontal" or "diagonal" (see Fig. 1). Horizontal bridging is preferred because it is easier to install, but diagonal bridging is required for joists over 12 m in length. The bridging consists of very small angles which are designed for a maximum slenderness ratio of 300 for horizontal and 200 for diagonal bridging. Since these bracing elements can act only in tension, their ends must be anchored to a separate lateral load resisting structural system. The spacing of the bracing is specified according to the elastic Euler buckling formula for the top chord with an effective length of 0.9 times the spacing between the bracing lines such that the elastic critical stress is approximately 30 percent of the yield stress under construction load. The joists will thus buckle in the elastic range.

The assumptions for the analysis of the truss-bracing system are as follows:

1) elastic behavior is specified up to and during buckling;

2) equilibrium is formulated on the buckled shape, using small deflection theory;

3 the forces due to planar behavior at the instant of buckling are those determined from a first-order analysis of a planar truss with articulated joints;

4) for purposes of the buckling analysis all members in the three-dimensional joist-bridging structure are continuously connected;

5) the cross sections retain their original shape;

6) the cross section is idealized as a tee-shape having zero warping rigidity;

7) loads are applied vertically at the points of lateral bracing to the top chord at truss panel points.

The differential equations for the elastic lateral-torsional deformations are (Galambos, 1968; Vlasov, 1961; Timoshkenko, 1961):

$$EI_y\, u^{iv} + P\,(u^{ii} + y_o \phi^{ii}) = 0$$

$$EI_x \, v^{iv} + P \, (v^{ii} - x_o \phi^{ii}) = 0$$

$$EI_w \, \phi^{iv} + (Pr_o^2 - GK_T) \, \phi^{ii} + P \, (y_o u^{ii} - x_o v^{ii}) = 0$$

where EI_x, EI_y, GK_T and EI_w are, respectively, the out-of-plane flexural stiffness, the in-plane flexural stiffness, the St. Venant torsional stiffness and the warping stiffness. The latter stiffness is zero for a tee-shape. The coordinates u, v and ϕ are respectively, the out-of-plane deflection, the in-plane deflection and the torsional rotation of the member. P is the axial force in the member from a first-order pre-buckling truss analysis, and x_o and y_o are the coordinates of the shear center (for a tee-shape $x_o = 0$); r_o is the polar readius of gyration with respect to the sher center.

The differential equations are solved and exact expressions are obtained for the stiffness matrix of each element. These are 12 x 12 matrices. The element stiffness matrices are then all assembled into the global stiffness matrix of the 3-dimensional structure. For any applied vertical force, the axial forces in each element are determined by first-order analysis. These axial forces are then substituted into the global lateral-torsional stiffness matrix and the value of the determinant is calculated. This process is repeated until it is ascertained that for the lowest value of P the determinant becomes equal to zero. The applied load corresponding to this condition is the buckling load of the system. The resulting global stiffness matrix is quite large and it requires a large computer to solve the determinant. Analytically it was complicated to work out the proper transformation matrices (see Ref. 6).

Because of the large computational effort required, only systems with one (Masoumy, 1980) and two and three joist systems (Xykis, 1988) were solved.

3. DESCRIPTION OF THE SOLVED SYSTEMS AND DISCUSSION OF THE RESULTS

The details of the joist are presented in Fig. 2. The joist is loaded on the top chord at the third points of the span at a panel point. These points are laterally braced, as are the points on the bottom chord directly below the load. The truss thus has 49 elements. This particular joist was chosen because it is identical to one physically tested by Leigh (1971).

The first finite element study was performed by Masoumy (1980) on a one joist system as shown in fig. 3. The single joist was braced at the centroid of the top and bottom chord by a horizontal brace of varying length (20, 100 and 200 times the least radius of gyration of the bridging). The ends of the bridging were either fixed (1), pinned (2), or on rollers (3).

The second finite element study was performed by Xykis (1988) on a two-joist (Fig. 4) and a three-joist (Fig. 5) system. The ends of each bridging line were fully anchored. Between the joists either horizontal or diagonal bridging was used.

The results of the study are presented in Tables 1 and 2. These tables give the computed critical load at one load point (P in Fig. 2). In the case

of multiple joists each brace point is loaded. Thus for the 3-joist system there are 6 loads P.

The following observations can be made from these analytical experiments:

1) The support conditions at the ends of the bridging do not affect the buckling capacity appreciably (compare conditions 1, 2 and 3 in Table 1).

2) The flexural stiffness of the bridging members has a significant effect on the buckling load (compare results between cases where only axial stiffness, and axial and flexural stiffness, is considered in Tables 1 and 2).

3) The buckling load is only slightly reduced if only the top chord is braced (Table 1, second row and third row).

4) The analysis slightly underestimated the experimental buckling load (8.45 versus 10.54 kN) which was conducted with a fully rigid brace permitting only vertical movement of the joist at that location.

5) The Euler buckling load for the top chord alone is somewhat above that computed by finite element analysis, but somewhat below the test load.

6) The two finite element analyses give comparably close answers in overlapping cases (Table 1, footnote).

7) There is little difference between the two and the three joist systems if horizontal bridging is used (e.g., compare 11.57 and 12.10, or 17.17 and 17.39 kN in Table 2), but the difference becomes significant if the bridging is diagonal (compare 14.28 and 17.26 kN in Table 2).

8) Diagonal bridging is more effective in increasing the buckling load than horizontal bridging.

These two analytical studies (Refs. 6 and 7) were very elaborate and expensive as regards both theoretical derivation and computer effort. They showed that an actual bridged joist system may have considerable reserves beyond the strength predicted by the simple design theory. However, these conservative rules represent minimal conditions one can confidently count on if the ends of the bridging lines are anchored.

4. CONCLUSION

This paper presented the results of two analytical studies on the elastic buckling strength of single and multiple braced trusses. The effect of the following parameters was examined: axial and flexural stiffness of the bracing, the brace end-conditions, the number of trusses in parallel, and the effect of bracing only the top chord.

5

5. REFERENCES

1. Steel Joist Institute, "Standard Specifications, Load Tables, and Weight Tables for Steel Joist and Joist Girders" 1990.

2. T. V. Galambos, "Bracing of Light Roof Trusses" in "Stability of Steel Structures", Akademia Kiado, Budapest, 1988.

3. T. V. Galambos, "Structural Members and Frames" Prentice-Hall, Englewood Cliffs, New Jersey,1968.

4. V. Z. Vlasov "Thin-Walled Elastic Beams," National Science Foundation Translation, 1961.

5. S. P. Timoshenko and J. M. Gere "Theory of Elastic Stability", McGraw-Hill, New York, 1961.

6. C. Xykis, "Lateral Torsional Stability of Non-Linear Rigid Space Frame Systems" Ph.D. Thesis, University of Minnesota, Minneapolis, MN, 1988.

7. G. Masoumy, "Lateral Torsional Buckling of Steel Joists and Joist Systems", D.Sc. Thesis, Civil Engineering Dept., Washington University, St. Louis, May 1980.

8. J. M. Leigh, "Bridging Spacing for Longspan Steel Joists" Research Report No. 19, Civil Engineering Dept., Washington University, St. Louis, Dec. 1971.

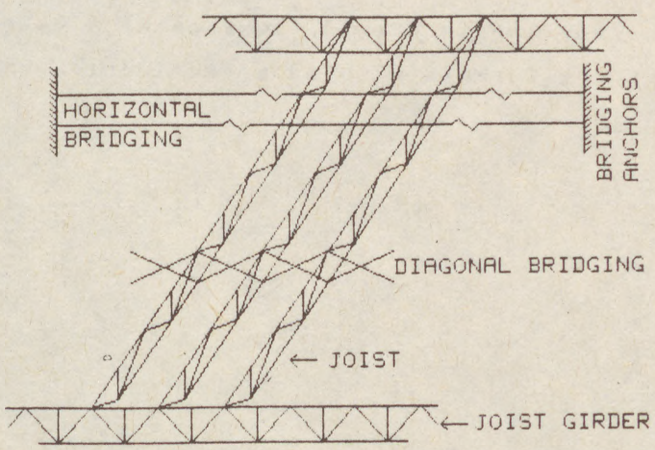

FIG.1 JOIST AND BRIDGING SYSTEM

6

Table 1 Results from Masoumy's (Ref. 7) Analysis of 18.29m long Joist (Fig. 3)

Brace Stiffness Criteria	Brace End Conditions	P_{cr}
Axial Stiffness Only	——	8.45kN #
No Movement of Brace Point	——	8.45kN ### #####
Axilal Stiffness Only Only Top Chord Is Braced	——	8.18kN
Axial and Flexural Stiffness		
L_b/r_b=20	#1, Fig.3	16.45kN ##
	#2	15.84kN
	#3	15.79kN
L_b/r_b=100	#1, Fig.3	12.32kN
	#2	11.61kN
	#3	11.57
L_b/r_b=200	#1, Fig.3	10.72kN
	#2	10.23kN
	#3	10.19

8.63kN from Ref.6

16.19kN from Ref.6

10.54kN from experiments (Ref.8, average of 3 tests)

9.16kN from Euler formula with an effective length of 0.9

7

Table 2 Results of Xykis' (Ref.6) Analysis of 18.29m long Joist (Figs. 4 and 5)

Bridging Type (Figs.4 and 5)	Bridging Size	Brace Stiffness Criteria of Horizontal Bridging	Number of Parallel Joists	P_{or}
Horizontal	2L25X25X3	Axial Stiffness	2	11.57kN
Horizontal	2L25X25X3	Axial Stiffness	3	12.10kN
Horizontal	2L25X25X3	Axial & Flexural	2	17.17kN
Horizontal	2L25X25X3	Axial & Flexural	3	17.39kN
Diagonal	2L25X25X3	Axial Stiffness	2	14.28kN
Diagonal	2L25X25X3	Axial Stiffness	3	17.26kN
Diagonal	2L25X25X3	Axial & Flexural	2	19.08kN
Horizontal	2L32X32X6	Axial & Flexural	2	24.29kN

8

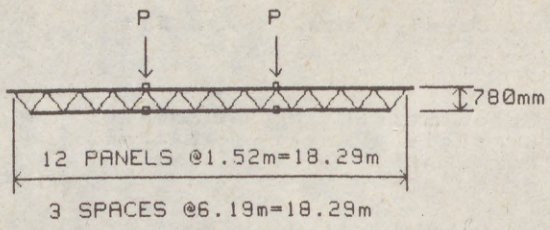

▫ POINTS OF LATERAL BRACING
TOP CHORD: 2L 64X64X6mm
BOTTOM CHORD: 2L 51X51X6mm

FIG. 2 JOIST USED IN TESTS AND IN ANALYSES

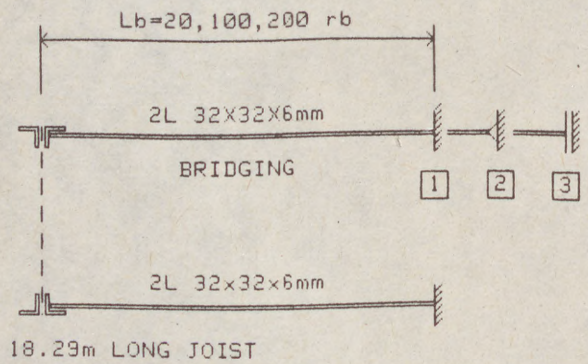

FIG. 3 MASOUMY'S ANALYTICAL MODEL (REF.7)

9

9

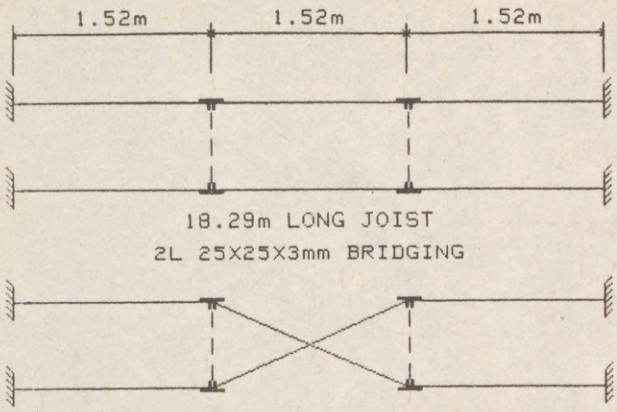

FIG. 4 XYKIS' 2-JOIST MODEL (REF.6)

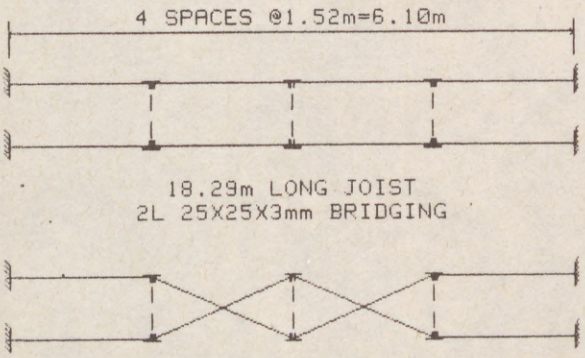

FIG. 5 XYKIS' 3-JOIST MODEL (REF.6)

/1/
KRA
KRA

WAS

Sum
exp
by
fai
in
exp
sit
sta
pri
to
of
gus
tha
mea
the
wer
mec
the
cau

the
pro
par
the

/1/

/2/

/1/
KRATĚNA, Jindřich /1/
KRATĚNOVÁ, Marie /2/

WAS OR WAS NOT THE LOSS OF STABILITY THE REASON OF THE FAILURE OF AN ICE-HOCKEY HALL IN CZECHOSLOVAKIA?

INTERNATIONAL COLLOQUIUM
STABILITY OF STEEL STRUCTURES
BUDAPEST, HUNGARY, 1990
PRELIMINARY REPORT

Summary: In December, 1981, a large sports hall collapsed. The expert opinions elaborated by the forensic experts appointed by the state authorities concluded that the cause of the failure consisted in the buckling of the diagonal bar situated in the main framework of the structure. On the other hand, the expert counsels for the defence specified the crack of welds, situated in one frame gusset, as the cause of the failure and stated that the buckling of the diagonal bar could not be the primary cause. In the end the lawsuit resulted in the endeavour to prove whether the cause of the failure had been the buckling of the diagonal bar or the crack of the welds in the frame gusset. It was necessary to give a more convincing proof than that based on theoretical solution only. Therefore, experimental measurements were carried out on a steel model of the gusset, the scale being 1 : 1. Besides, 1 : 25 silicone rubber models were produced which served for the demonstration of failure mechanism and for the verification of the modified length of the diagonal bar. Experimental measurement demonstrated that the cause of failure consisted in the inferior quality of welds.

The decision of the cause of the failure is usually made by the court which evaluates the data submitted by both the prosecution and the defence. As the state authorities taking part in court proceedings are not experts in technical matters, they appoint authorized experts. If the case is very complex,

---

/1/ Chief Research Fellow, Institute of Theoretical and Applied Mechanics, Czechoslovak Academy of Sciences, Prague
/2/ Assistant Professor, Faculty of Civil Engineering, Czech Technical University, Prague

/2/
two authorized experts and sometimes a specialized institute are appointed.

The authorized expert must approach his task with the highest responsibility, as both the prosecution and the decision are based on his conclusions. Although it is the court that decides, it is necessary to realize that it is the very expert on whose opinion the court bases its decision, which gives the court the guidance as to how to decide. The court actually merely formulates the technical conclusions of the expert in legal terms. If the expert comes to erroneous conclusions and insists on them during court proceedings regardless of the objections of the defence, the endeavours of the latter to disprove or at least to throw some doubt on the accusation is always made considerably difficult. This is due to the fact that the court prefers believing the experts appointed by the state authority then those engaged by the defence.

Several years ago a serious failure of the structure of a big sports hall took place in December, only about two months after it had been put into operation. In the course of the six years following the failure several expert opinions were elaborated both by the experts authorized by the state authority and by those engaged by the defence, all of which were based on only theoretical computations. Their conclusions were diametrally different. In the course of court proceedings which lasted several years the dispute finally culminated in the endeavour to prove whether the failure was due to the buckling of an important structural member /opinion of authorized experts of the prosecution/ or to the failure of the welds in one gusset of the structure /opinion of the defence/.

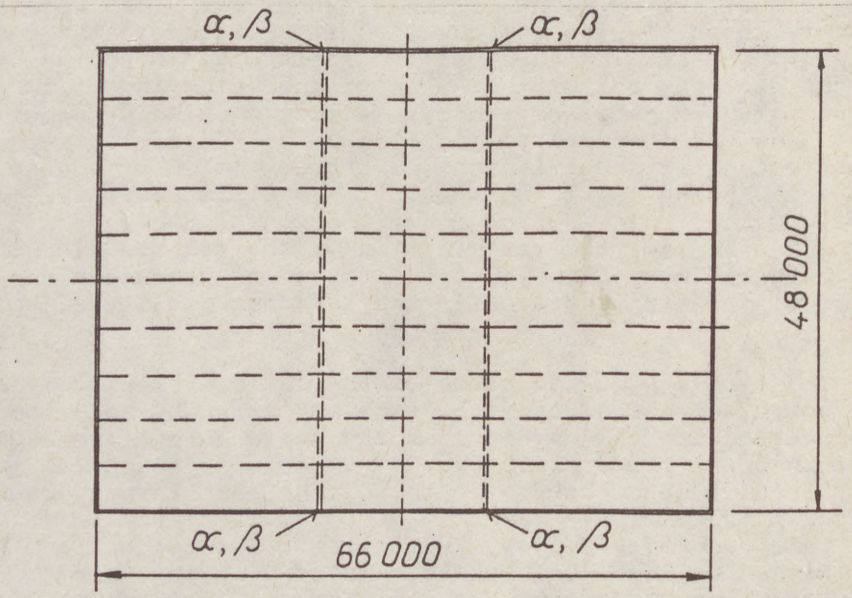

Fig.1. Schematic plan of the hall

/3/

The steel structure under consideration was of an unusual design featuring a special system of main frameworks and characterized by favourable economic parameters. The whole building, sized 48 x 66 m in plan, was divided in longitudinal direction into approximate thirds by two transverse frameworks /Fig.1/ which supported directly the longitudinally continuous latticed purlins supporting the roof of the hall. The unusual structural system of principal transverse frameworks had four hinges in every framework /Fig.2/. This system has been patended in Czechoslovakia and used for the construction of several major structures of various design.

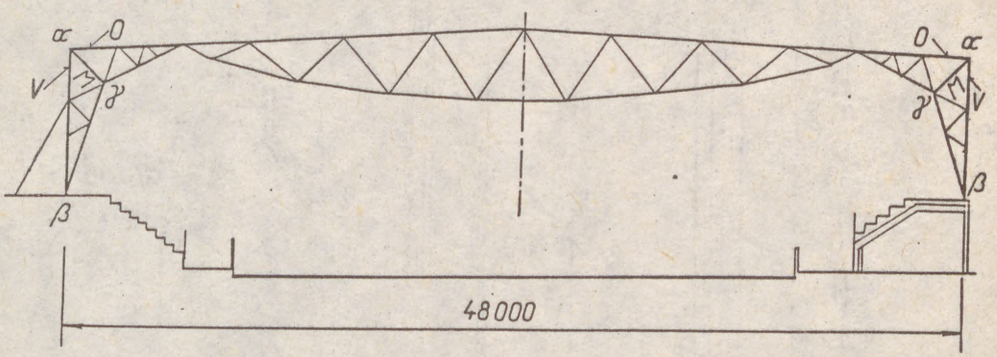

Fig.2. View of one of the two main frameworks

The gusset marked α in Fig.2 was highly exposed to stresses, as it joined three bars, i.e. the vertical bar V consisting of two stiffened UE 18 channels, the upper chord O made of a U 30 channel, and the compressed diagonal M, also made of a U 30 channel. The structural design of the gusset α resulted in a complex arrangement of the contact surfaces of the individual sections mutually jointed by a system of welds which had to guarantee the transmission of all forces in the node /Fig.3/. For the sake of clarity only one half of the symmetrical gusset α is shown in the drawing.

After the failure of the structure defects were ascertained both in the design and in the actual execution of the steel structure. Structural analysis did not contain the dimensioning of the diagonal M. It has been ascertained that the diagonal did not satisfy the requirements of the respective standard. One of the authorized experts stated that the failure had been due to the buckling of that bar. The other expert who had been concerned primarily with the quality of welds stated that the failure was due to the failure of the welds in the gusset β. The revision expertise of an specialized institute excluded the failure of the welds in the gusset β as the cause of the collapse of the structure and supported the opinion of the expert who had maintained that the collapse was due to the

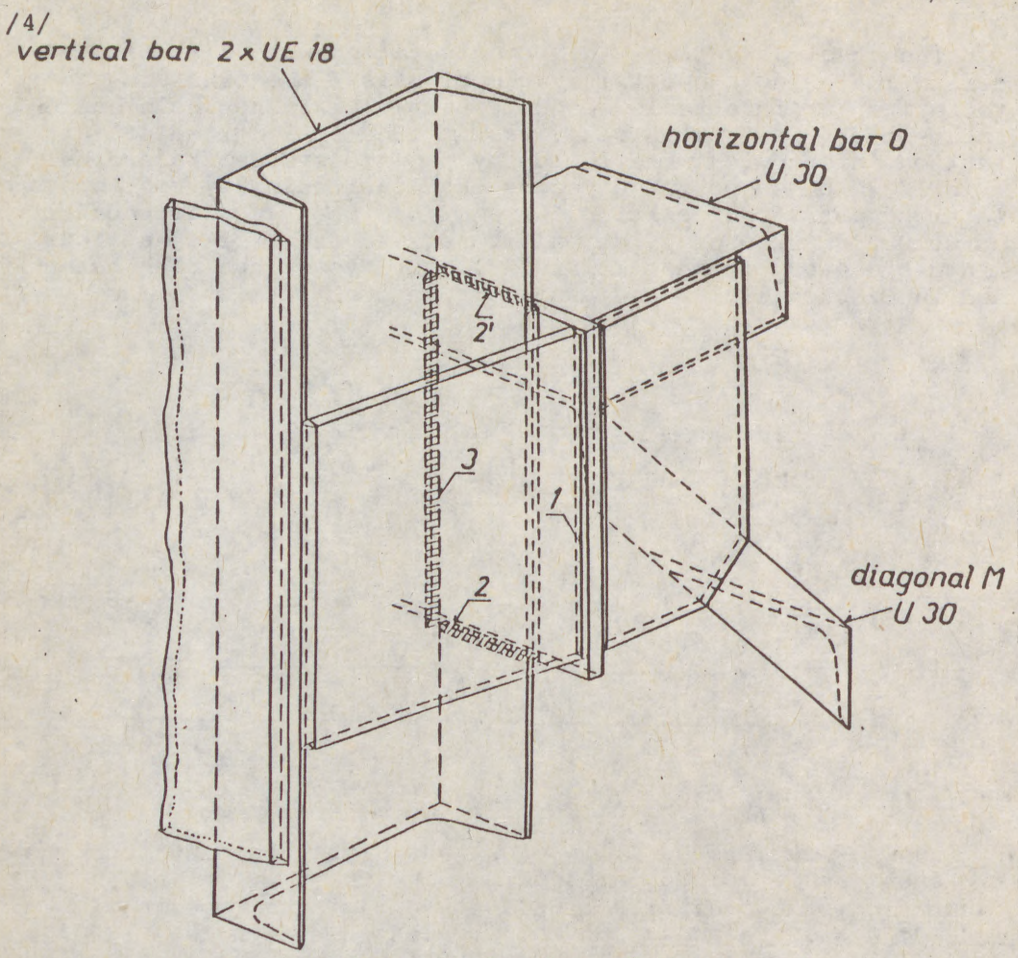

Fig.3. Schematic drawing of the gusset

buckling of the diagonal M . During court proceedings all experts insisted on their conclusions and qualified continuously the objections of the defence as technically unacceptable.It should be stressed that the opinions of both the appointed experts and those submitted by the defence in the first years after the collapse of the structure were based only on theoretical computations.

During on-site investigations, however, one of the appointed experts ascertained also serious defects in the execution of the welds, particularly in the gussets α and β . This expert than indicated the gusset β as the cause of failure, having calculated that at the moment of failure the stress in the welds of the gusset α was merely 122.01 MPa. The expertise of the institute subsequently corrected that value to 150 MPa. On the basis of such computations the institute could state, indeed that the failure of the welds in the gusset α could

/5/
not have been the cause of the collapse of the structure. This statement was seemingly supported also by the shape of the collapsed diagonals M . It should be noted that the structure had 4 gussets α , of which 3 ruptured and one remained intact. It has been proved by testimony of witnesses that the collapse of the structure began in the place of failure of the gusset α. The majority of experts, however, overlooked an important fact. The shape of the diagonals M with ruptured gussets /Fig.4/ differed from the shape of the diagonal with the intact gusset /Fig.5./.

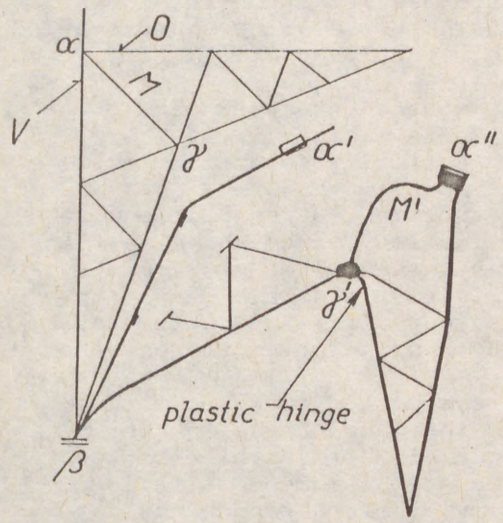

Fig.4. Column parts of the framework after failure with the ruptured gusset α /three of four cases/

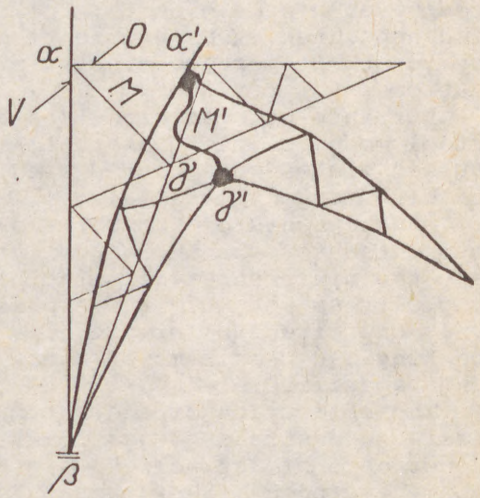

Fig.5. Column parts of the framework after failure with the intact gusset α /one case of four only/

Apart from the defects of the quality of welds /insufficient dimensions, insufficient root penetration, or incomplete root penetration/ it was ascertained that the producer of the steel structure had not followed the instructions of the working drawing. Two important long load-bearing welds in the gusset α /marked "3" in Fig.3/ were omitted and substituted with four short welds, marked "2" and "2´" respectively.

In spite of all ascertained defects of welds all experts appointed by the state authority continued to insist that the failure of the welds in the gusset α could not have caused the collapse. This conclusion, however, was based on unrealistic calculations of stresses in the welds of the gusset α , on the erroneously determined buckling length of the bar M and on the erroneously determined decisive yield point of the material of the diagonal.

The defence objected that the primary buckling of the dia-

/6/
gonal M could not have given rise to the rupture of the welds in the gusset α . Therefore, the collapse could not have been due to the buckling of the diagonal M , but the rupture of the welds in the gusset α . This opinion was supported, on the one hand, by the computation, on the other hand by the very fourth gusset which had remained intact; its diagonal buckled during the collapse of the structure and yet the gusset α did not rupture.

Although the defence submitted sufficient theoretical proofs of the incorrect character of the conclusions presented by appointed experts, the court was still convinced that the appointed experts were right. Therefore, it was necessary to submit more convincing proofs than theoretical computations.

For this purpose experimental measurements were made on a steel model of the gusset α on the scale of 1 : 1. The gusset plates were coated with an optically sensitive layer of birefringent material.

On the basis of PhotoStress measurement a few places were subjected to more thorough investigation. Since the directions and the differences of principal stresses were determined by Photostress method, it was possible to fix strain gauges in only one direction of principal stress after the photoelastic coating had been removed there. Both principal stresses were thus specified.

The aplication of the PhotoStress method combined with resistance strain gauges revealed that the stress in the upper part of the weld No. 1 /Fig.3/ in horizontal direction must have been higher than 355 MPa at the moment of failure. Should the welds be of good quality, their strength would have been 430 - 450 MPa. With regard to the ascertained serious defects of the welds the conclusion was justified that during the collapse of the structure their strength indubitably was exhausted which resulted in their failure. The results of measurements thus refuted the theoretical computations of appointed experts, according to which the stresses were considerably lower.

It is worth mentioning that an other group of experts calculated the weld stresses, by the Finite Element Method, independently of the experiment; their results were in very good agreement with the experimental ones.

Apart from the gusset α also models of the edge latticed column were made of silicone rubber on the scale of 1 : 25 and used for the demonstration of the mechanisms of the collapse of the structure, the verification of the buckling length of the diagonal M and the demonstration of the fact that after the failure of the diagonal the welds in the gusset α could no longer rupture.

Only the experiment /since theoretical computations of the experts of the defence could not persuade the court/ refuted the main argument of the revision experts maintaining that, should the rupture of the welds in the gusset α occured

/7/
first, the shape of the bars *M* and *O* after the collapse of the structure would have to be approximately the same. Since the bar *O* had been almost straight and the diagonal *M* heavily deformed, the experts insisted on their incorrect conclusions. Their great error consisted in their assumption of the instantaneous failure of the whole complex system of welded joints of the gusset *α* . The gusset *α* failed in a short period, but this period was of sufficient duration to enable a certain deformation of the diagonal due to the rotation of the jointed ends of the bars *M* and *O* . The crack initiated in the upper part of the gusset, where the maximum stress values were measured. The gradual opening of the crack necessarily resulted in the deformation of the diagonal /Fig.6/. When

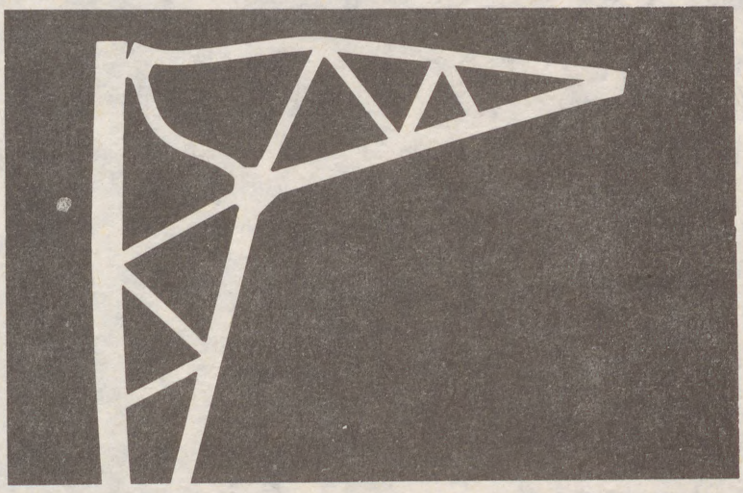

Fig.6. Silicone rubber model - demonstration of the deformation after the iniciation of the crack in the upper part of the gusset *α*

the welds ruptured completely the diagonal *M* had been partly deformed; however, the deformation was not due to its buckling. Subsequently the tensile force of the bar *O* , which equalled exactly the resistance of the diagonal *M* , deformed the diagonal by bending into its final shape /Fig.7/. In the lower chord of the latticed structure a plastic hinge originated close to the gusset *γ* which enabled such deformations of the bars *O* and *M* .

The silicone rubber models also represented objective evidence that after buckling of the diagonal *M* the gusset *α* could not have cracked. Fig.8 shows high level of stresses in the gusset *α* in the case of non buckled diagonal bar *M* . If the diagonal *M* buckles, the stresses in the gusset *α* diminish to lower values which is demonstrated in Fig.9 and therefore the welds in the gusset *α* cannot crack after the buckling of the diagonal bar *M* .

/8/

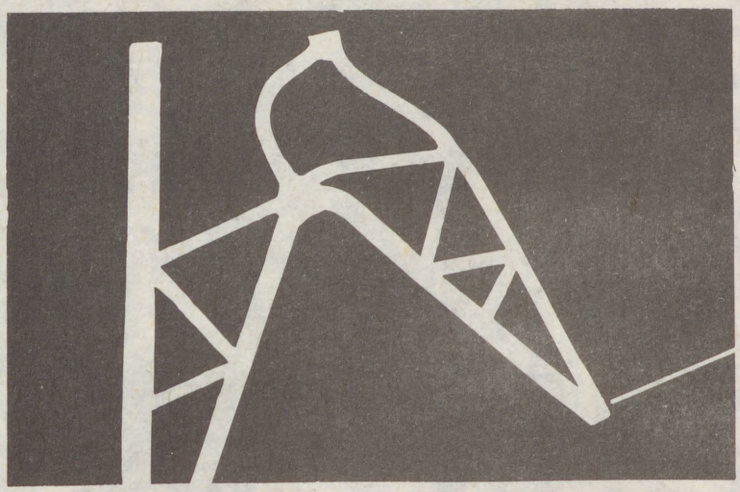

Fig.7. Silicone rubber model - demonstration of the definitive position after the failure

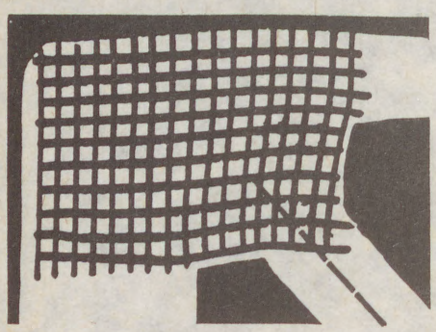

Fig.8. Silicone rubber model - demonstration of the high level of stresses in the gusset α with the non-buckled diagonal bar M

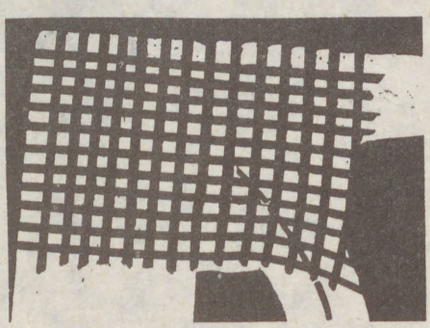

Fig.9. Silicone rubber model - demonstration of low level of stresses in the gusset α after the buckling of the diagonal bar M

(1)
LUKJANOV Konstantin (1)
SILVESTROV Anatoly (2)

DESIGN CONCEPTS TO PROVIDE THE STABILITY OF STEEL TRUSSES DURING ERECTION

INTERNATIONAL COLLOQUIUM
STABILITY OF STEEL STRUCTURES
BUDAPEST, HUNGARY, 1990
PRELIMINARY REPORT

Summary: The theoretical basis of design methods of steel trusses stability out of plane at their erection and further temporary fastening to the supports during their erection is considered. Theoretical ideas about stability of thin-walled open profile bars and centrally compressed bars on the elastic basement stability were used. A design method of trusses general stability at their erection and a magnitude of safety factor of their stability was based on the position of limit state design method accepted in the USSR.

At the erection of separate trusses it's nessesary to provide their stability out of plane both at lifting and at temporary fastening to the supports till installation of roof braces according to design.

The methods of trusses general stability design existing in USSR earlier were based on the design of their compressed top chords stability out of trusses plane, and top chords were considered as bars, subjected to longitudinal bending caused by forces of trusses dead load. In some cases such method led to the overestimation of trusses safety factor of stability.

Theoretical and experimental investigations made by authors [1]; [2] showed that actual out of plane stability margin of truss at its erection in the most cases exceeded their design magnitude obtained with written above design scheme. Further the

---

(1) Cand.Sc. (Eng.), Vice-Director of VNIPIPromstalconstruktsiya, Moscow, USSR.
(2) Dr.Sc.(Eng.), Professor of Steel Structures, Dnepropetrovsk Civil Engineering Institute

(2)
design of flat trusses general stability at the erection was given and the truss was considered as a bar system consisting of chords and elements of lattice .

Considering a design scheme of truss with parallel chords at its erection with attachment to one point in the middle of the span (Fig.1) let's establish the following assumptions:

- weight of truss is uniformly distributed along its length and concentrated along the line of averaged chords and lattice centre of gravity at the distance H_o from upper chord;

- rigidity of truss at its bending out of plane EI_y equals to sum of upper and lower chord's rigidity in the middle of its span;

- torsion rigidity of the truss is negligible;

- centre of gravity and torsion centre of truss coinside.

Considering a truss as a thin-walled open profile bar and using the theory of stability of such bars, created by V.Z.Vlasov one can write down differential equations of steel truss with parallel chords at its erection in following form:

$$EI_y U^{IV} + (M_z \theta)'' = 0 \qquad (1)$$

$$EI_\omega \theta^{IV} + M_z U'' = 0 \qquad (2)$$

where M_z - bending moment in the plane of truss;
E - steel elasticity modulus;
I_ω - torsion inertia moment of truss cross section;
U - displacement of truss centre of gravity axis in the direction of axis "z";
θ - angle of rotation of truss cross section along "x" axis.

Equation (1) describes the equilibrium of truss bending out of its plane and equation (2) describes truss equilibrium at torsion. With the help of simple transformations one can express torsion inertia moment of truss cross section with approximate formula:

$$I_\omega = H^2 \frac{I_\ell \cdot I_u}{I_\ell + I_u}; \qquad (3)$$

where H - height of a truss;
I_ℓ and I_u - cross section inertia moments of lower and upper truss chords accordingly.

Bending moment in plane of truss equals to:

$$M = g \frac{x^2}{2}; \qquad (4)$$

where g - linear weight of truss.

(3)
Twice integrating equation (1) we´ll have

$$EI_y\, U'' + M_z \theta = Ax + B = 0, \qquad (5)$$

Since because of consideration of boundary conditions A=0; B=0. So, joint consideration of equations (2) and (5) leads:

$$EI_\omega\, \theta^{IV} - \frac{M_z^2}{E\, I_y}\, \theta = 0 \qquad (6)$$

Involving non-dimentional coordinate

$$\xi = \frac{x}{L} \quad \text{and marking parameter}$$

$$n = \frac{g L^4}{2 HE \sqrt{I_\ell \cdot I_u}}\ ; \qquad (7)$$

where L - span of truss, we´ll obtain generalized equation of equilibrium:

$$\theta^{IV} - n^2 \xi^4 \theta = 0 \qquad (8)$$

Solution of this equation is fulfilled due to expansion of cross section rotation angle in a power series:

$$0 = a_o \xi^{m_o} + a_1 \xi^{m_1} + \ldots + a_i \xi^{m_i} \qquad (9)$$

Not having presented here mathematical transformations, fulfilled to solve equation (8) taking into account equation (9), we have obtained a magnitude of truss critical linear weight:

$$g_{cr} = \frac{160 HE (I_\ell + I_u)}{L^4} \cdot \beta \qquad (10)$$

where β - ratio of ordinate of truss cross section centre of gravity to a half of truss height.

In those cases when an erection of truss is fulfilled not according to scheme in Fig.1 but with symmetrical attachment to two upper chord points, which are situated at the distance of $l = L$, the solution of differential equations of truss equilibrium at erection leads to magnitude of critical weight:

$$g_{cr} = \frac{160 HE (I_\ell + I_u)}{L^4} \cdot \beta \cdot \gamma \qquad (11)$$

$$\gamma = \frac{6}{20 (1 - \alpha) - 5 (1 - \alpha)^4 - 9} \qquad (12)$$

The authors also considered the questions of truss chords cross sections change along its length [5].

One should also mark that at $\alpha = 0.54$ out of plane stability of trusses with parallel or slightly inclined chords (1: 10) is practically always provided and at $\alpha > 0.54$ the loss of stability may take place because of buckling of compressed upper chord: this case is not considered by us because such attachment

of trusses is not used, as a rule, at the erection. Solution of equation (11) can be used for trusses which are commonly used in industrial buildings in the USSR.

Evaluating out of plane stability of trusses installed and attached to the supports according to the scheme in Fig.2 or additionally fixed to upper chord joints with erection brace, as our experimental investigations showed, the main thin-walled open-profile bars hypothesis about not-deformativity of bar's contour is violated.

It is connected with that at considered ways of truss attachment the loss of its general stability is accompanied by more considerable buckling of compressed upper chord than that lower tensioned chord. However in this case identification of out of plane truss stability with stability of its compressed chord at flexibility of chord out of truss plane more than 250 - 300 leads to underestimation of truss real stability margin.

An existance of bending rigidity of lattice elements and torsional rigidity of lower chord enables, at considerable flexibilities of upper chord pointed above, elastic fixions of this chord and increases its stability at the action of truss dead load.

Considering a design scheme in Fig.2 one should mark that at a number of truss panels more than four, in analogy with the design stability of compressed chords of bridges at an open air and trusses on elastic support of compressed chord in joints at the expense of lattice elements bending and lower chord torsion, may be rather exactly changed by distributed elastic Winkler foundation (model of design) with valiable along the length factor of rigidity of the foundation C.

$$C = \frac{1}{1/c_\ell + \varphi H}, \qquad (13)$$

where c_ℓ - coefficient of foundation rigidity, depending upon bending rigidity of lattice structural elements built in absolutely torsionally rigid lower chord;

φ - an angle of lower chord twist at single displacement of upper chord at its buckling out of truss plane when there are lattice elements having absolutely high bending rigidity.

One can see, that averaged value C_ℓ equals to:

$$C_\ell = \frac{3E}{L} \sum_1^n \frac{I_i}{\ell_i^3} \qquad (14)$$

where I_i and l_i - inertia moment of i - element of lattice out of truss plane and its length accordingly;

n - the number of lattice elements.

Magnitude φ in formula (13) changes along the truss depending upon the form of compressed chord buckling and can be defined with the help of equlibrium differencial equation of lower chord

at its twist:

$$M_t = GI_t \cdot \frac{d\varphi}{dx} ; \qquad (15)$$

where M_t - torsional moment;
GI_t - torsional rigidity of lower chord.

Hence

$$\varphi = \frac{H}{2GI_t}\left(\frac{L^2}{4} - x^2\right) \qquad (16)$$

And so, coefficient of foundation rigidity in solving problem depends on "x" coordinate. Let's determine averaged value of this coefficient:

$$\bar{C} = \frac{2}{L}\int_0^{L/2} c \cdot dx \qquad (17)$$

Integrating expression (17) with account of (13), (14) and (16) we notice that for principal trusses

$$C_\ell \gg \frac{8GI_t}{H^2L^2} \qquad (18)$$

With account of (18) solution of integral equation (17):

$$\bar{C} = 2\,C_{\ell.ch} \ln \frac{C_\ell}{C_{\ell.ch.}} , \qquad (19)$$

where $C_{\ell.ch.} = \frac{2GI_t}{H^2L^2}$

The design scheme of truss at its temporary fastening to the supports is shown in Fig.2. It's considered because of weak elastic support of compressed chord with box elements and bottom chord occured on one half-wave (Fig.2). The truss uniformly loaded due to own weight and compressed forces transferred to the chord by braces, will be proportional to the distances from the middle of the span.

Compressed linear efforts equivalent to them will be distributed according to the curve in Fig.2c.

Critical force for the longitudinal compressed top chord of truss at the averaged elastic foundation according to the solution (4) could be expressed by formula

$$N_{cr} = N_E + N_C \qquad (20)$$

where N_E - Euler critical force;
N_C - critical force for infinitely long centrally compressed rod at the elastic foundation.

For this case

$$N_E = 5{,}12\,\frac{EI_u \cdot 4}{L^2} , \quad N_{cr} = 2\sqrt{\bar{C}\,EI_u} \qquad (21)$$

Hence, the value of truss critical mass at its temporary fastening to the supports is equal to (scheme in Fig.2):

(6)

$$g_{cz} = 164 \frac{E I_u H}{L^4} \left(1 + \frac{L^2}{10} \sqrt{\frac{\bar{c}}{E I_u}} \right). \quad (22)$$

In the cases when value q_{cz}, calculated by formula (23) is less than linear mass of truss multiplied by the coefficient of stability margin k_y (which is considered below) the top chord of truss besides fastening to the supports should be additionally attached during the erection with distance bars or flexible braces. Solution of this task at any number of intermediate upper chord braces is not considered here and given in paper [2] written by the same authors. One should only mark that in case of flexible braces use made of steel rope it's necessary to take into account both elastic ductility of flexible braces, considering their deflection and initial tension as additional forces in truss structural elements, caused by tension of inclined flexible braces [5]. The authors have also considered the change of chords cross sections along the truss lenght at evaluation of critical linear weight of a truss temporary attached to the supports [5]. It should be marked that theoretical methods erection truss stability evaluation have been rather exactly confirmed by the experimental investigations of authors.

So, verification of out of plane stability of steel trusses both at their erection and at temporary attachment to the supports can be fulfilled with formular:

$$g_{cz} \geqslant k_y \cdot g \quad (23)$$

where g_{cz} - critical value of truss linear weight, defined by methods considered above;
g - linear weight of truss, defined with the help of working drafts;
k_y - index of stability margin.

A value of stability margin index should be taken considering the general thesis of accepted in the USSR limit state design of structures. So, using the main unequality describing a first group limit state, which a loss of stability of structure is referred to, one can write down cornformably to considering tasks:

$$g \cdot \gamma_f \cdot k_d = N \leqslant F = g_{cz} \frac{\gamma_c}{\gamma_m \cdot \gamma_n} \quad (24)$$

where N - ultimite generalized force;
F - ultimite load-carrying capacity;
γ_f - reliability index concerning load;
k_d - dynamic coefficient;
γ_c - index concerning structure working conditions;
γ_m - reliability index concering steel;
γ_n - reliability index concering purpose of structure.

So, stability margin (23) must be given from the condition

(7)

$$k_y = \frac{\gamma_f \cdot k_d \cdot \gamma_m \cdot \gamma_n}{\gamma_c} \qquad (25)$$

The authors of the paper , having fulfilled an analysis of design factors in formula (26), based [3] the values of stability margin factor. So for steel trusses made of low carbon steel during their erection lifting k_y = 1.7 and during their temporary attachment k_y = 2.6.

Finally it should be marked that considered methods out of plane stability evaluation of steel trusses equilibrium at their erection are given in the building codes and manuals [5].

REFERENCES

[1] Лукьянов К.И., Сильвестров А.В.,Зайденберг А.И. : Обеспечение устойчивости плоской формы изгиба стальных ферм при подъеме. Промышленное строительство №1,1972,стр 7-9.

[2] Лукьянов К.И., Сильвестров А.В.,Зайденберг А.И. : Обеспечение устойчивости металлических ферм в процессе монтажа . Промышленное строительство №4,1974,стр 14-17.

[3] Лукьянов К.И., Сильвестров А.В. : О структуре и величине коэффициента запаса устойчивости металлических ферм при подъеме. Известия вузов. Строительство и архитектура №1,1975,стр 8-10

[4] Ржаницын А.Р.: Устойчивость равновесия упругих систем. Гостехтеориздат.Москва ,1955.,стр 348-355.

[5] Справочник монтажника.Монтаж стальных и железобетонных конструкций .Москва.Стройиздат,1980,стр 799-814.

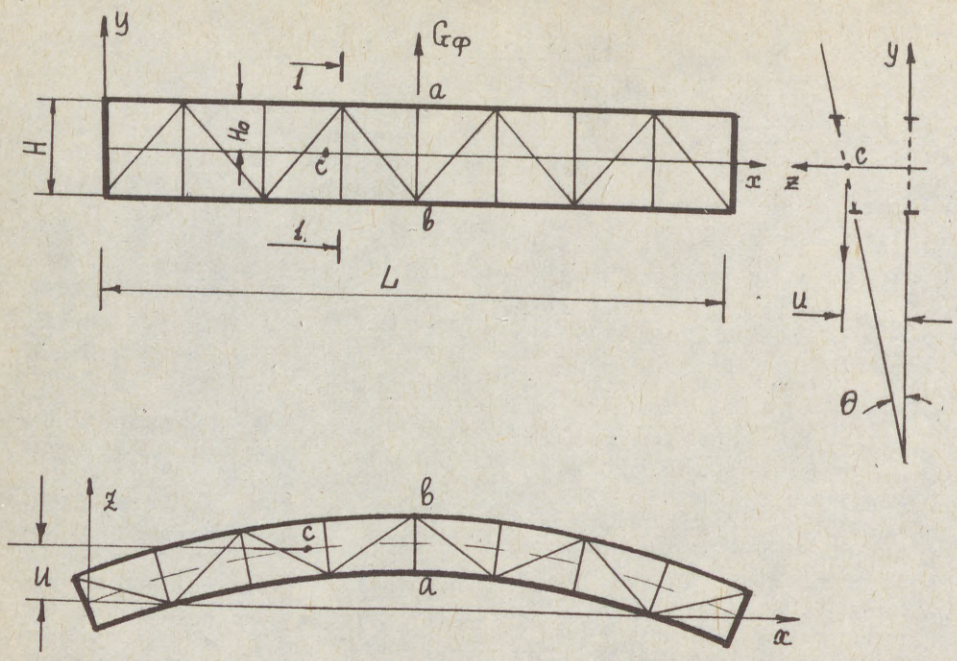

Фиг. 1

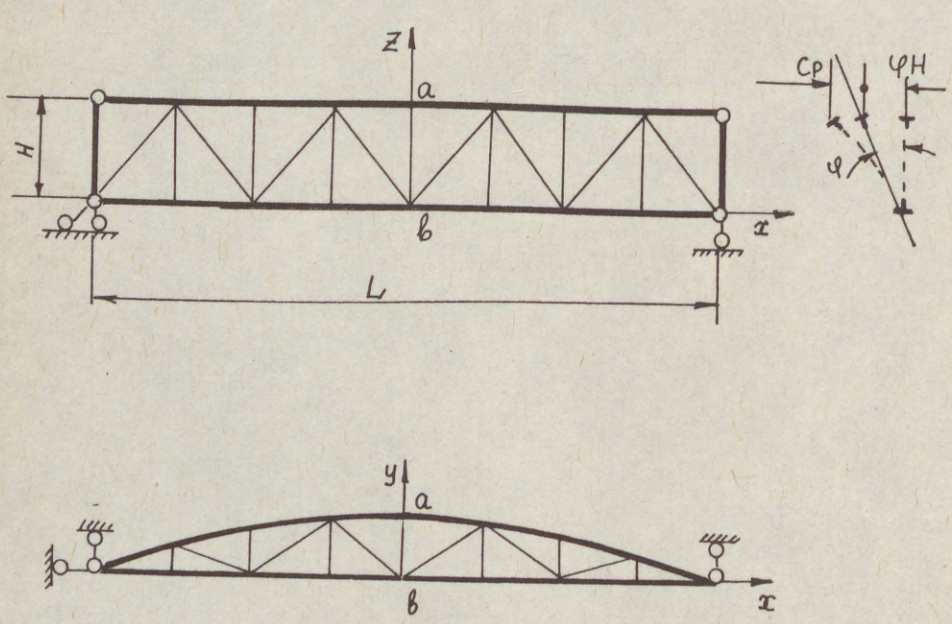

Фиг. 2

(1)
PLÁTTHY, Pál (1)

A SPECIAL PROBLEM OF THE PLASTIC INSTABILITY

INTERNATIONAL COLLOQUIUM
STABILITY OF STEEL STRUCTURES
BUDAPEST, HUNGARY, 1990
PRELIMINARY REPORT

Summary: The paper is based on the instability of through-type bridges of the varying height top-beams, with upper wind braces, which instability is caused by impact loads. It can be proved that vehicles with high loadings are very dangerous in respect with such bridges, since impact force acting on the wind braces would pull the upper chord of the top-beam to the middle of the bridge.

Before World War II. steel truss bridges were constructed with top-beams of the varying height. At such structures - if they were through-type ones - upper wind braces could often be placed in the middle segment of the span. This formation has the risk that vehicles with higher than the allowable loading deteriorate the compression chord of the top-beam in the middle segment of the span that might cause the collapse of the bridge even at low speed of the vehicle (low impact force). Four road bridges were deteriorated in Hungary in the past 20 years due to such cause. The last such catasrophe was caused at the village of Gesztely on the bridge on the river Hernád, in Fall, 1988, by a shovel hauled by a truck, when its jib got caught in the upper wind braces (Figs.1.a. and b.).

Deterioration procedure of the above mentioned bridge is shown in Fig. 2. The first crossing of the upper wind brace, - due to the impact force - pulls the chords of the top-beam, along with the columns, to the middle of the bridge (also see Fig. 1.). Therefore the elements, those of laterally displacing, of the top-beams drop out from load-

---

Professor, Department of Steel Structures,
Technical University Budapest

(2)

Fig. 1.a.

Fig. 1.b.

(3)

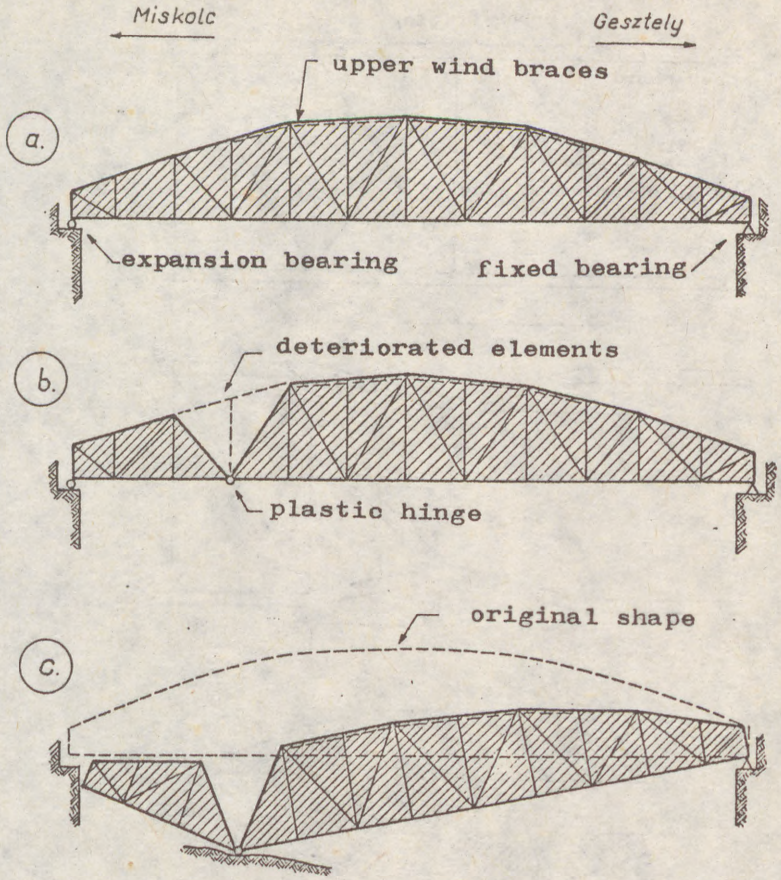

Fig. 2.

bearing; top-beams divide into plates that are connected - at the level of the lower chord - only by a part with relatively little stiffness. The connection, due to the large bending moment, transforms into a plastic hinge, and the top-beams, becomeing mechanism , collapse.

To describe the procedure, denote the geometric data according to Fig. 3., where details "a" and "b" show the top-view of the bridge, and detail "c" shows the side view of the bridge, respectively, before and during deterioration. If neglecting the change in length (elongation, compression) of the elements, the relations between the geometrical data marked can be relatively easily determined, and the motion of the structure during deterioration can be described by mathematical methods.

Besides the geometrical correlation, the displacement, e, of upper chords, loaded by compression force, N, and transversal force, Q, can be determined with good approxi-

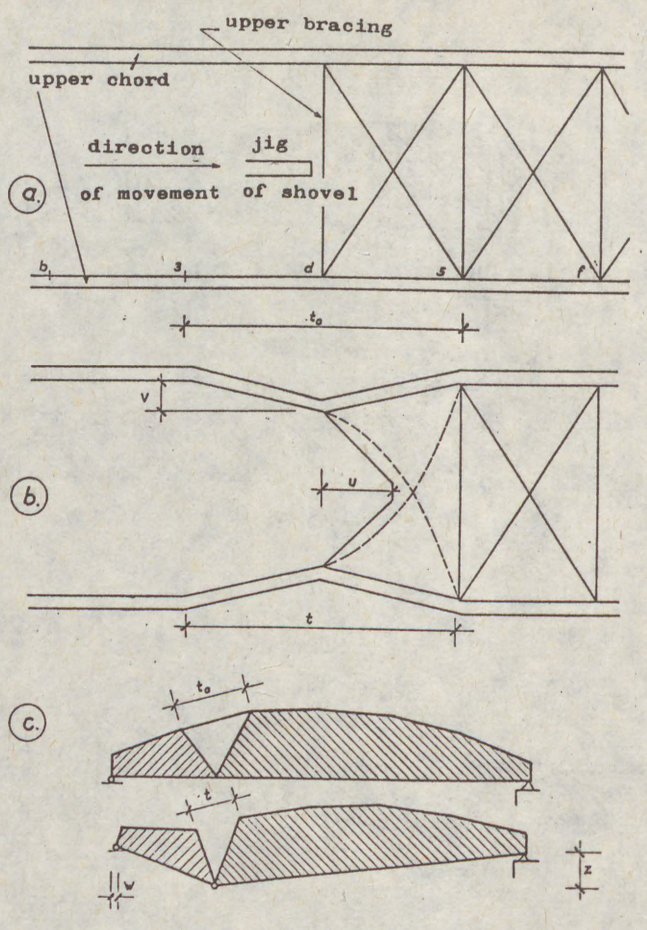

Fig. 3.

mation. The compression force, N, is caused by the dead load and the live load on the bridge, while the transversal load, Q, is caused by the tensile effect of the crossing, deforming due to impact. The value Q has a critical value, Q_c, in a given case, just causing of the chord, and the unstable state of the bridge. At the same time, from the displacement, e, corresponding to Q_c, all other displacements can be determined, therefore all data of Fig. 4. showing the simplified top-view. This way there is the possibility to make an energy-balance, for what let's assume the followings.

The kinetic energy of the vehicle of the mass, m, and the velocity, v, at the moment of the impact:

$$E_k = \frac{mv^2}{2}$$

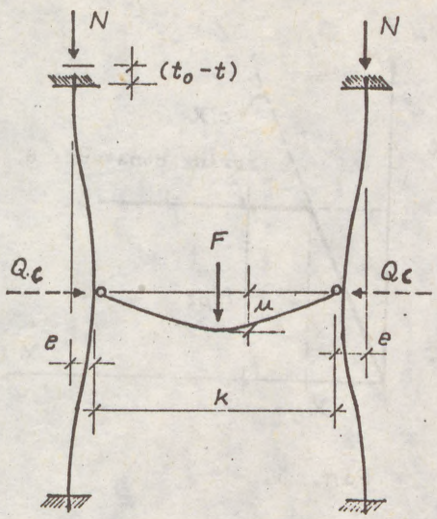

Fig. 4.

If, in this moment, the crossing is loaded by a force of F, then the approximate transversal tensile force acting on the top-beam is:

$$Q \cong \frac{Fk}{4u}$$

Taking this into consideration:

$$F_c \cong \frac{4u}{k} Q_c$$

However in the given case, not the force, F_c, is desired, but the critical velocity, v_c, of the vehicle. This means the minimal velocity at which unstable state just occurs. Since in this case the transformation of the kinetic energy is approximately equal to the work of the external forces, the following equation can be described:

$$\Delta E_k = E_k = L_k = \int N dt + \int F du$$

From this

$$v_c \approx \alpha \frac{2L_k}{m}$$

where α is a magnification factor, necessary, because the mathematical model does not consider the stiffness of the lower chord (work must be performed for the formation of plastic hinges). The problem, up to a certain degree, is analogous with the problem of the model shown in Fig. 5., where the falling down of the pinned column is prohibited

(6)

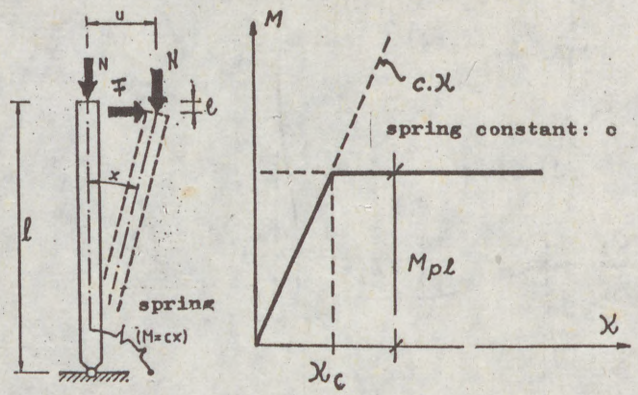

Fig. 5.

by an elastic-plastic spring.

Finally let's mention that, at the Hernád-bridge, collapsed in Fall, 1988, the critical velocity of the impacting vehicle came out to be 12 km/h, that calls for the extremely dangerous character of the structures considered.

— x —

(1)
SAVELYEV V.A. (1)

STABILITY OF RETICULATED METAL SHELLS

INTERNATIONAL COLLOQUIUM
STABILITY OF STEEL STRUCTURES
BUDAPEST, HUNGARY, 1990
PRELIMINARY REPORT

Summary: The paper contains the results of investigation into the effect of relative cell sizes of reticulated shells on the value of the critical load. A practical technique for determination of the bar design length factor in the plane normal to the surface for reticular metal shells with rigid joints, and, besides, formulae for calculation of critical loads for hinged-bar spherical shells have been proposed, the initial deviations of joints and non-uniformity of loading being taken into account.

1. Statement of the problem

In the majority of members of reticulated shells used as frameworks of large-span roofs the main loads give rise to compressive forces, therefore the most important problem of designing reticulated shells is provision of their stability.

The behaviour of a reticulated shell which is a bar system is equivalent to that of a solid shell with reduced thickness and modulus of elasticity. Therefore, the solid analogue method is the basis of the most present-day recommendations on examination of stability of reticulated spherical shells.

The upper critical load for a spherical reticulated shell with triangular cells is calculated by the formula:

$$p = 2\sqrt{6}\,\frac{EAi}{lr^2}\,, \qquad (1)$$

---

(1) Leading Researcher of TSNIIProektstalkonstruktsiya named after Melnikov of Gosstroy of the USSR, Moscow

(2)

where E - modulus of elasticity;
A - cross-sectional area of the bar;
l - average length of the bar (average distance between the joints);
i - radius of gyration of the bar section normally to the surface (along the joint axis);
r - radius of curvature of the spherical surface on which the reticulated shell joints are located.

In the course of numerous experiments carried out on solid spherical shells it was found out that the critical load value is considerably affected by the initial deviations of the surface from its spherical form and by the non-uniformity of the load application. Therefore, a decreasing coefficient is usually introduced the value of which is in the range of c=0.17 to c=0.33. For example, Wright (Wright, 1965 [1]) recommends the value of c=0.327.

However, the practice of designing reticulated metal shells shows that formula (1) gives some overstated values of the critical load in the mentioned range even when decreasing coefficients are taken into account (Schönbach, 1969 [2]).

Apparently, this is accounted for by the fact that it is derived proceeding on the assumption that the behaviour of the structural material is elastic, so it cannot be used directly at checking the total stability of bar shells. The critical load calculated by formula (1) cannot be a criterion of the reticulated dome total stability, as well as the Euler formula cannot be a stability criterion of a low-carbon steel bar the flexibility of which is less than =100. Besides, formula (1) does not take account of the reticulated shell discrete nature, namely, the reticulation thickness, relationship between the cell size and the surface curvature radius.

2. Reticulated shells with rigid joints

To introduce clarity into the solution, a diagram should be considered which includes archs of three directions intersecting in joints at the angle of 60° (Fig. 1). The stability of archs of any two directions is maintained by the third-direction archs that serve as their elastic supports. Archs of the first two directions are interconnected and are distorted simultaneously.

Let a non-dimensional parameter be introduced which will characterize the relative size of the reticulated shell cell:

$$\nu = \frac{l}{\sqrt{ri}} \qquad (2)$$

The critical load for an infinitely long bar on elastic supports is determined by the following expression:

$$N = \xi^2 \frac{EAi^2}{l^2} \qquad (3)$$

(3)

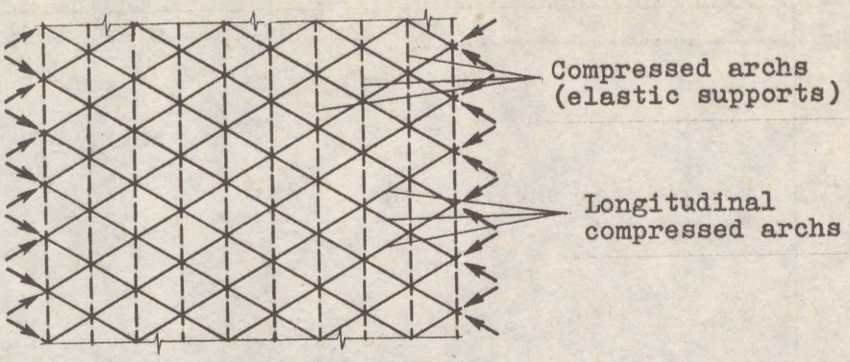

Fig. 1 Design scheme of a reticulated shell in the form of a system of compressed archs on elastic supports

Parameter ξ may be found due to solution of equation (3):

$$\nu^2 = \frac{4\xi^2 \cdot (1 - \cos\xi)}{(1 + \sqrt{\sin\xi / \xi})^2} \quad . \tag{4}$$

Having equated the critical load (3) to the critical load of the bar with the design length $l_o = \mu l$:

$$\xi^2 \frac{EAi^2}{l^2} = \frac{\pi^2 EAi^2}{(\mu l)^2} \quad , \tag{4'}$$

one may obtain

$$\mu = \frac{\pi}{\xi} \quad . \tag{5}$$

The upper critical load corresponding to the critical load N is equal to :

$$p' = N \frac{2\sqrt{3}}{rl} = 2\sqrt{6}\, E \frac{Ai}{lr^2} \cdot \frac{\xi^2}{\nu^2\sqrt{2}} = 2\sqrt{6}\, E \frac{Ai}{lr^2} \cdot k. \tag{6}$$

Expression (6) differs from (1) in the factor

$$k = \frac{\xi^2}{\nu^2\sqrt{2}} \tag{7}$$

which takes account of the dependence of the upper critical load on the relative size parameter of the reticulated shell cell.

In Fig. 2 there is a plot of factor k against parameter . The plot shows that at $\nu < 2$ the value of k is practically equal to 1. The value of factor k falls with the increase of parameter ν . In point $\nu = \sqrt{8\pi^2} \approx 3$ factor $k = \pi/4$. This point corresponds to the rigidity of elastic supports at

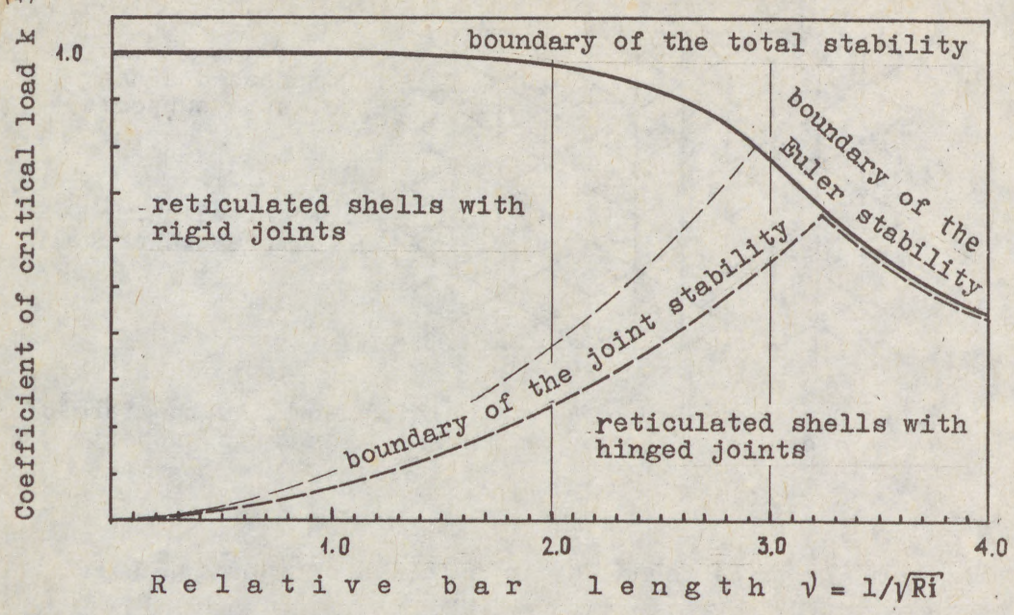

Fig. 2 The plot of critical load versus the bar length

which their behaviour is absolutely rigid. At $\nu > 3$ the bar free length is equal to the distance between joints, and the value of parameter ξ is constant and equal to π. Factor k is inversely proportional to ν^2 :

$$k = \frac{\pi^2}{\sqrt{2}\,\nu^2}. \tag{8}$$

The range of $\nu < 2$ may be conditionally called the range of a thick reticulation in which the critical load does not depend on the bar length. At $2 < \nu < 3$ (the range of the cell medium sizes) the critical load decreases with the increase of ν. At $\nu < 3$ the total buckling becomes impossible. In this range of parameter ν variation which may be conditionally called the range of a thin reticulation, the load-carrying capacity is determined by the stability of individual bars at a free length equal to the distance between joints, independently of the fact if the bars are rigidly connected or hinged in the joints.

If the bars are hinged and $\nu < 3$, the joints buckling occurs. The critical load may be determined by the formula (Timoshenko, 1946 [4]):

$$N = \frac{EAl^2}{8r^2}, \tag{9}$$

(5)
which was derived for an infinitely long equal-span articulated-link chain on discrete elastic supports.

This load corresponds to the distributed load

$$p = \frac{\sqrt{3}\, EAl}{4r^3}. \qquad (10)$$

The decreasing coefficient of the critical load is equal to:

$$k = \frac{1}{8\sqrt{2}}\, \nu^2. \qquad (11)$$

The dependence of k on ν is shown in the plot of Fig. 2 by means of a thin dash-dot line. Below it will be shown that an axially symmetric form of buckling (pressing-through of individual joints) gives a 1.5 times less value of the critical load (thick dash-dot line in the plot).

The practical procedure of checking the load-carrying capacity of a reticulated shell with rigid joints includes the following. According to the plot of Fig. 3, a coefficient of the bar design length is determined at buckling normally to the surface, depending on the value of the cell relative size parameter ν. The bar design flexibility is calculated as

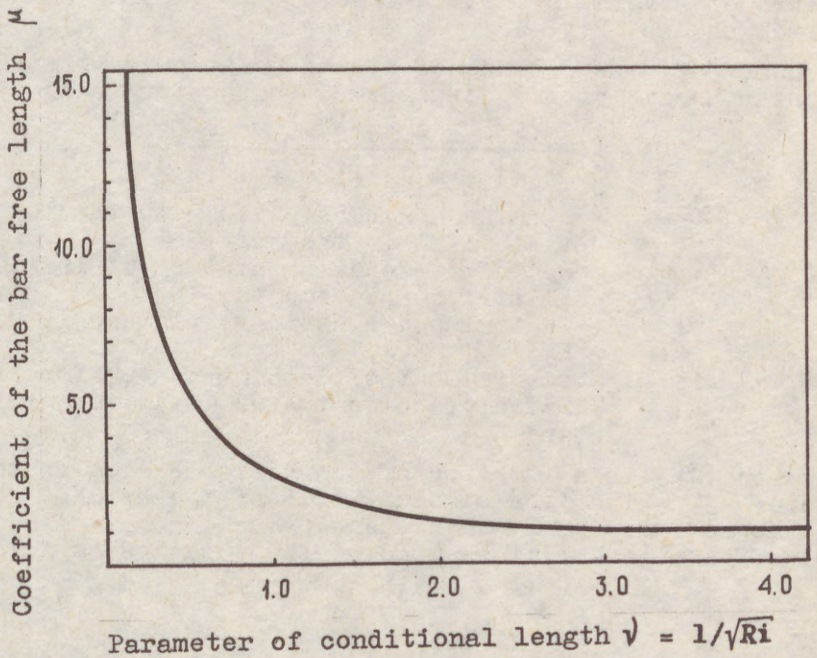

Fig. 3 Plot for determining the free length of a reticulated shell bar normally to the surface

(6)

follows: $\lambda = \mu l/i$, and, according to the corresponding standard relationships, the longitudinal stability coefficients are determined with or without account of bending moments. (Stability check at central or eccentric compression). The design values of longitudinal forces and bending moments may be obtained by means of static design of a reticulated shell according to the linear theory.

3. Hinged-bar shells

Single-reticulation shells with hinged joints are generally used in construction of roofs of small and medium-size spans. In most cases, performance of hinged joints is necessitated by the structural considerations - fabrication of a hinged three-dimensional joint consisting of several bars is not so difficult as that of a rigid one. In some cases, for example, for collapsible reticulated shells, a hinged joint is necessary for provision of structural transformation.

The plot of Fig. 2 shows that, as a whole, hinged bar shells are less stable than shells with rigid joints; their range of variation of geometrical parameter at which the upper critical load is maximal: $3 < \sqrt{} < 3.6$ is comparatively narrow.

In papers (Savelyev, 1966 [5]) and (Savelyev, 1973 [6]) various discrete design schemes are analyzed on the assumption of simultaneous pressing-through towards the centre of curvature of several symmetrical joints of sloping hinged-bar spherical shells (Fig. 4).

For scheme "a", the dependence of the joint concentrated load k on the non-dimensional displacement parameter is as follows:

$$P = 2EA\beta^3 \frac{3(1 - \zeta_o - \zeta)(2 - 2\zeta_o - \zeta)\zeta}{4(1 - m) + 2(2m + 1)(\zeta_o + \zeta)}, \qquad (12)$$

where $\beta = \frac{l}{2r}$ - sloping angle of the bar to the tangential plane in the joint;

$\zeta_o = \varphi_o/\beta$; $\zeta = \varphi/\beta$ - non-dimensional parameters of initial and elastic displacements;

φ_o; φ - initial and elastic sloping angles of bar KM;

$m = Pm/P$ - coefficient of loading non-uniformity or ratio of concentrated loads in joints M and K.

Expression (12) is a function of one variable displacement parameter ζ which is a sloping angle of the bar KM. The general view of diagram $P - \zeta$ is analogous to the solid shell diagram. The upper critical load of the joint is as follows:

$$P = 2EA\beta^3 = \frac{EAl^3}{4r^3} \qquad (13)$$

which conforms to the equivalent distributed load:

$$p = \frac{EAl}{2\sqrt{3}r^3} \qquad (14)$$

(7)

a)

c)

Fig. 4

The

This
obta
Fig.

The
to a
more

sche

sche

Sche
chai
with

The
that
non-

(7)

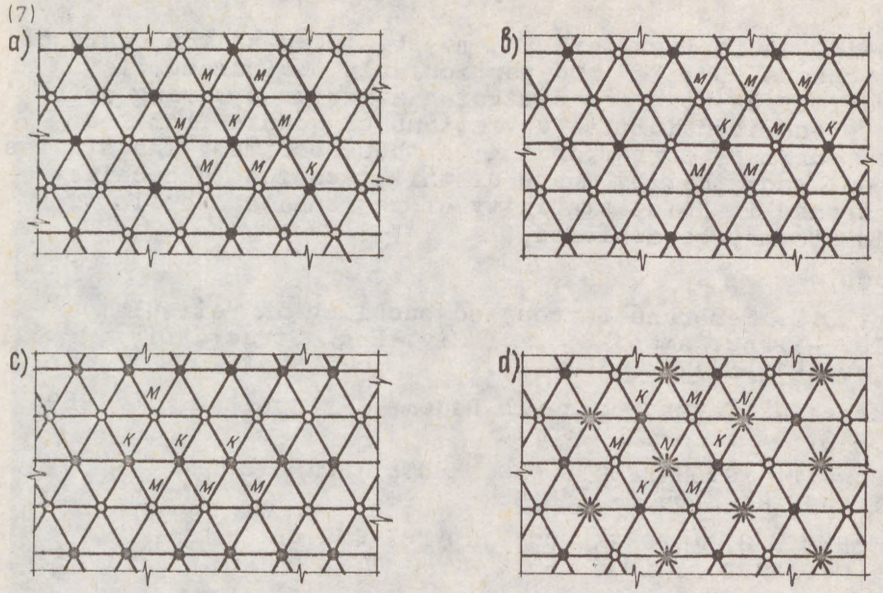

Fig. 4 Design schemes of hinged-bar shells: a, b, c - with one parameter of deflection; d - with two parameters of deflection

The corresponding coefficient k is equal to:

$$k = \frac{\nu^2}{12\sqrt{2}} \tag{15}$$

This value is 1.5 times less than the upper critical load obtained in the past (11). The relationship (15) is shown in Fig. 2 by a thick dash-dot line.

The design scheme of Fig. 4a is not the only one which leads to a single-parametric solution. In Fig. 4b,c there are two more analogous schemes that give the following solutions:

scheme "b" $$P = 3EA\beta^3 \frac{2(2 - 2\zeta_o - \zeta)(1 - \zeta_o - \zeta)}{3(1 - m) + (3m + 1)(\zeta_o + \zeta)}; \tag{16}$$

scheme "c" $$P = 3EA\beta^3 \frac{2(2 - 2\zeta_o - \zeta)}{3(1 - m) + 2(m + 1)(\zeta_o + \zeta)} \tag{17}$$

Scheme "c" is the above mentioned scheme of a hinged-link chain on elastic supports. The upper critical load coincides with expression (10) obtained beforehand.

The comparison of relationships (12), (16) and (17) shows that, in general case, at random initial shape deviations and non-uniformities of joint loads, the scheme of a joint buck-

(8)

ling in Fig. 4a is less safe and may be taken as the basis of design. Schemes "b", "c" and particularly two-parametric scheme "d" may be used for designing structures having artificially prescribed initial deviations of joints from the spherical surface, corresponding to these schemes. The studies carried out show that by means of this technique a considerable increase in joint stability of reticulated shells with hinged joints may be achieved.

References

1. Wright D.T. Membrane forces and buckling in reticulated shells. - Proc. Amer. Soc. of Civ. Eng. Struct. Div., 1965, V. 91, ST1, p. 173-201.

2. Schönbach W. Netzkuppeln als Radome. - Stahlbau, 2, 1969, s. 33-43.

3. Лейтес С.Д. Устойчивость сжатых стальных стержней. -М.: Госстройиздат, 1954.- 186 с.

4. Тимошенко С.П. Устойчивость упругих систем. -М.,Л.: ОГИЗ Гостехиздат, 1946. -532 с.

5. Савельев В.А. Устойчивость сетчатых куполов. - В кн.: Металлические конструкции. Работа школы проф. Н.С.Стрелецкого. М.: Стройиздат, 1966, с.325-339.

6. Савельев В.А., Ломбардо И.В. Приближенный метод расчета односетчатых куполов по деформируемой схеме.- В кн.: Материалы по металлическим конструкциям, М.: Стройиздат, 1973, вып.17, с.120-126.

SESSION 10

TUBULAR STRUCTURES

(1)

LANDOLFO, Raffaele [1]
MAZZOLANI, Federico M.[2]

THE INFLUENCE OF THE VARIATION THROUGH THE THICKNESS OF RESIDUAL STRESSES IN TUBULAR COLUMNS

INTERNATIONAL COLLOQUIUM
STABILITY OF STEEL STRUCTURES
BUDAPEST, HUNGARY, 1990
PRELIMINARY REPORT

SUMMARY: Previous experimental measurements of residual stresses in steel hollow profiles showed a predominant flexural distribution through the wall thickness instead of the classical constant distribution. The novelty of such result induced to carry on a systematic research of the influence of this kind of flexural distribution on the load bearing capacity of tubular columns. The analytical models necessary to the simulation calculations were derived from the experimental evidence of several test results. The simulated curves are here compared with both the ECCS buckling curves and the ones based on the classical residual stress distributions.

1. PREVIOUS DEVELOPMENTS

The systematic research on residual stresses started in USA at the beginning of the sixties. The main purpose was both to define models and to account their influence on the load carrying capacity of steel members [Johnston, 1966].
Furthermore, this problem spread out in Europe in the range of activity of the European Convention for Constructional Steelwork, faced to the preparation of the stability approach which was introduced in the ECCS Recommendations [Ballio and Mazzolani, 1985].
Also Italy, during the seventies, participated to this activity and several measurements of residual stresses were done on IPE and HE profiles [Mazzolani, 1972]. These results were exploited to interpret the buckling behaviour of "industrial columns" [Mazzolani, 1973].
The objects of these studies were mainly the double T shapes and very few contributions were given in the field of hollow sections until the beginning of the eighties.
In 1983 the Cometube in cooperation with the Committee of European Communities and with the financial aid of CECA, sponsored a common research program with the participation of several European laboratories (TNO, Delft; University of Karlsruhe; University of Naples; Polytechnic of Kingston; CETIM of Senlis, France; University of Liege).

---

1 Research fellow, University of Naples, Italy

2 Professor of Structural Engineering, University of Naples, Italy

(2)

The main purpose of this research was to compare the different methods for measuring residual stresses in square hollow sections made of steel with different forming processes. The discussion of the final results led to a complete judgement on the reliability of each method [Grimault and Rondal, 1985].

A very new aspect of the residual stress distribution was emphasized from the test done at the University of Naples [Mazzolani, 1985]. The most significant pattern of residual stresses was a quasi-linear variation along the wall thickness from external compressive to internal tensile values, whereas the classical distribution constant along the cross-section was practically negligible. At a consequence, this produced unexpected influences on the buckling behaviour [Faella et al., 1985].The importance of this discovery suggested to carry out an additional research on the remaining specimens of hollow sections in order to provide analytical models of residual stress distribution and to develop a systematic investigation of their influence of the buckling behaviour of tubular columns [Landolfo et al., 1989]. The conclusive results of this research line are summarized in this paper.

2. TESTING DATA

The experimental results, which the numerical exploitation is based upon, are obtained from two series of test developed at the University of Naples. The first belongs to the common Cometube-CECA program [Mazzolani, 1985], the second was further carried out in autonomous way [Landolfo et al., 1989]. Both series utilized the same type of specimens, which come from tubular steel profiles with square cross-section 200x200x8. They are formed by means of three different manufacturing procedures.

According to the purpose of this investigation, the only cases of welded sections are mentioned here, in particular:

-type A, cold formed welded shape with releasing;

-type B, cold formed welded shape without releasing.

They are made of steel with f_y varying from 420 to 450 Nmm^{-2} .Four specimens of type A plus four specimens of type B were tested in total.

3. THE MEASURING METHOD

The method used for measuring residual stresses in the samples of steel hollow sections belongs to the category of the so-called "sectioning methods", which were first applied in the USA by the Column Research Council (CRC) around 1950 and later introduced into Europe.

They are based on releasing residual stresses by mechanically subdividing the specimen into an appropriate number of parts. The new equilibrium condition corresponds to a shape modification and, as such unloading processes are essentially elastic, it is therefore possible using Hooke's law to measure deformations in order to deduce the stress state which caused them.The longitudinal cuts were made by means of a disk-type milling cutter. The number of strips was 24 in the first series (fig. 1,a) and 40 in the second series (fig. 1,b). In the last case both longitudinal and transversal strains were measured. The strain measurements were made by means of mechanical extensometers.

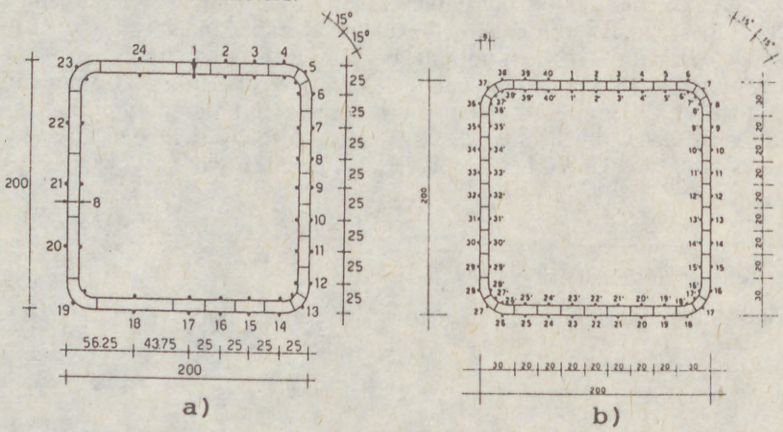

FIG.1

4. RESIDUAL STRESS DISTRIBUTIONS

From the examination of testing results we can point out some general aspects. The internal stress state of the hollow sections of specimens is mainly flexural, with a very large variation of stresses through the thickness of the wall.

The order of magnitude of the highest longitudinal residual stresses at the edges of the thickness is of about 100 Nmm^{-2} for sections of type A and of about 400 Nmm^{-2} for sections of type B. Obviously, these differences strictly depend upon the manufacturing procedures (with or without releasing).

At the contrary, the means values of longitudinal residual stresses are very low in both cases (about 5% of the edge values). The prevalence of the flexural behaviour with respect to the extensional one has been also emphasized during test by the large curvature of the strips after cutting.

The amount of transversal residual stresses has been always lower than longitudinal ones. Their distribution is quite constant through the thickness according to an extensional pattern. The degree of magnitude of transverse values is approximately around 10% of the longitudinal ones. It seems to be, therefore, reasonable to neglect transversal residual stresses in the evaluation of column buckling, by accounting the longitudinal residual stresses only.

5. DISTRIBUTION MODELS

From the above mentioned test results the model of distribution of longitudinal residual stresses is given in fig.2,a. This diagram is referred to the mean line of one side of the square perimeter of the profile and gives both variations along the side and through the thickness. The variation along the side is constant from 100% in the central portion to 35% at the corners. The variation through the thickness is governed by the ratio σ_r/f_y, which values coming from tests are:

0.26 for type A

0.77 for type B

In view of the simulation calculations, together with the proposed model, also the classical model of longitudinal residual stresses is considered, as it is shown in fig.2,b.

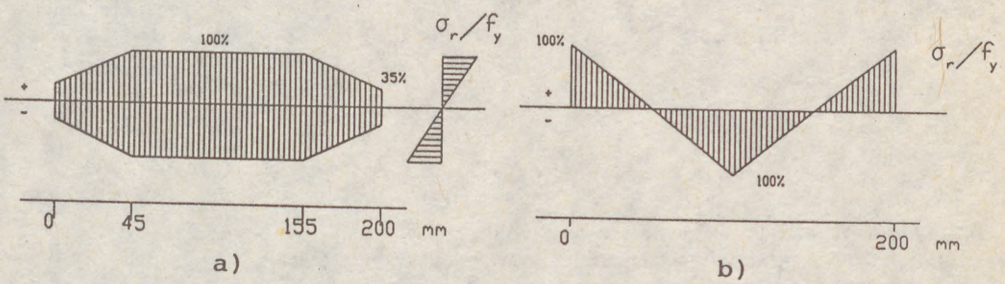

FIG.2

For the parametric analysis the following values of the ratio σ_r/f_y are proposed for both models: 0.00; 0.25; 0.50; 0.75; 1.00.

As it is usually assumed, an initial curvature of the column with a mid-span displacement $v_0 = L/1000$ is considered in all simulation calculations.

6. SIMULATION RESULTS AND CONCLUSIONS

The simulated curves for columns of type A and type B are evaluated by means of the distribution model given in fig.2,a on the bases of testing results. In fig.3, these curves are compared with the European curves a_o ,a ,b and c. For the profiles under examination the reference curves are:

- curve a_o, for heat treated box sections (in this case type A)
- curve a , for welded box sections (in this case type B)

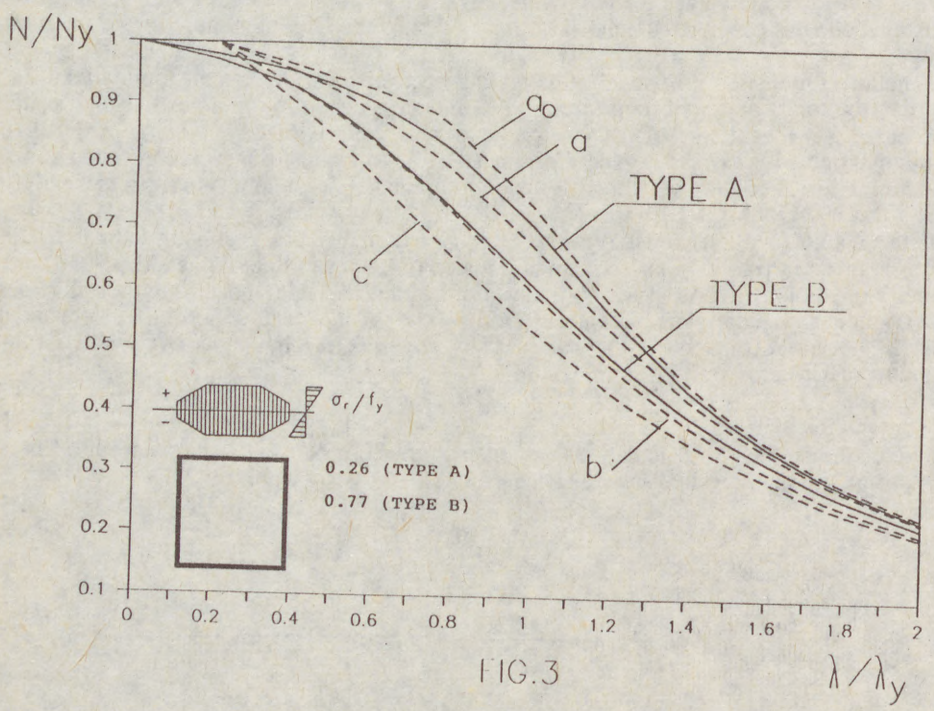

FIG.3

From the comparison in fig.3 we can observe that:

- curve of type A profiles is intermediate between curves a_o and a;
- curve of type B profiles is very close to curve b.

So, both curves based on the experimental data lie always below the corresponding reference curves, which therefore are not conservative. This discrepancy with the codified assessment calls the attention on the necessity of further deep investigations on this subject.

A first attempt in this direction is given here by means of a parametric analysis which consider all possible values of the ratio σ_r/f_y and compare the results of proposed and classical models of residual stresses (fig.2, a and b).

Fig.4 gives the simulated curves based on the model of fig.2,a by varying the ratio σ_r/f_y from 0.00 to 1.00. We can note the coincidence of curve a_o with the case of absence of residual stresses. The most unfavorable case (σ_r/f_y = 1.00) should not be considered completely unexpected for box sections welded in the corners.
The simulated curves based on the classical model of fig.2,b are given in fig.5 for the same values of the ratio σ_r/f_y.

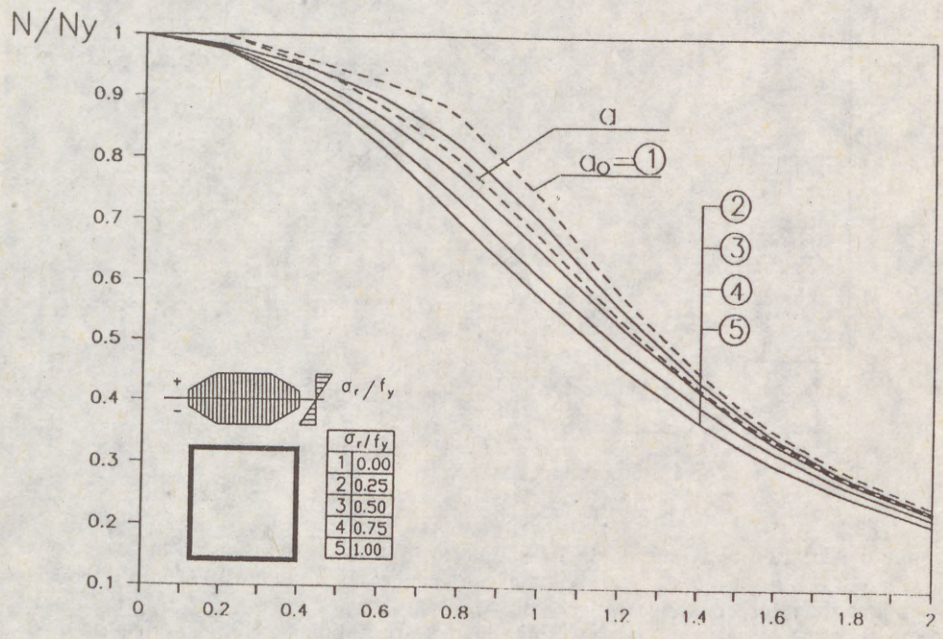

FIG.4

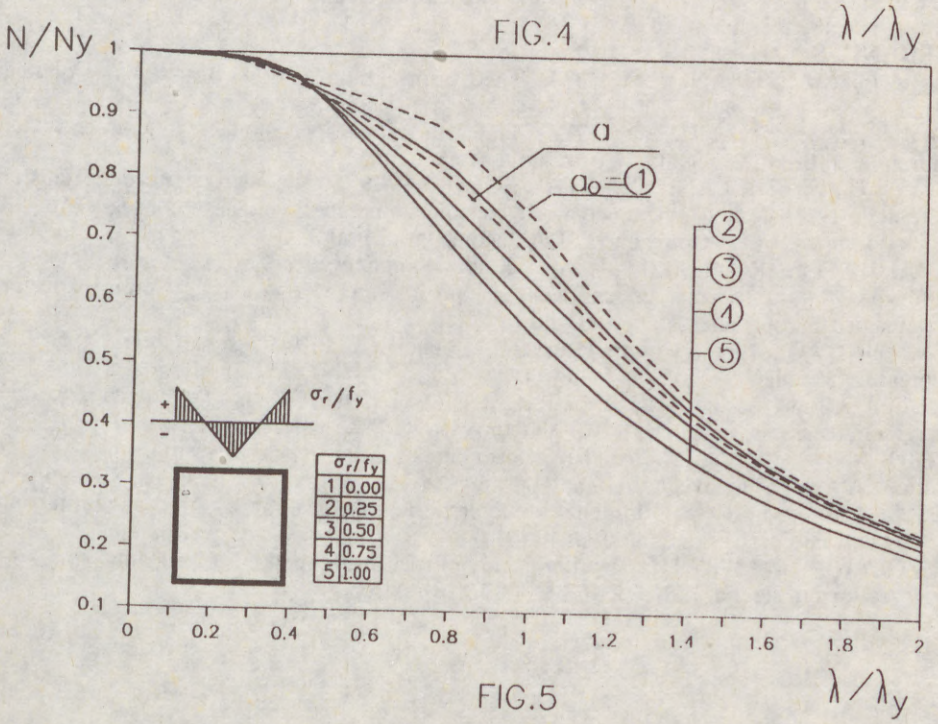

FIG.5

(6)

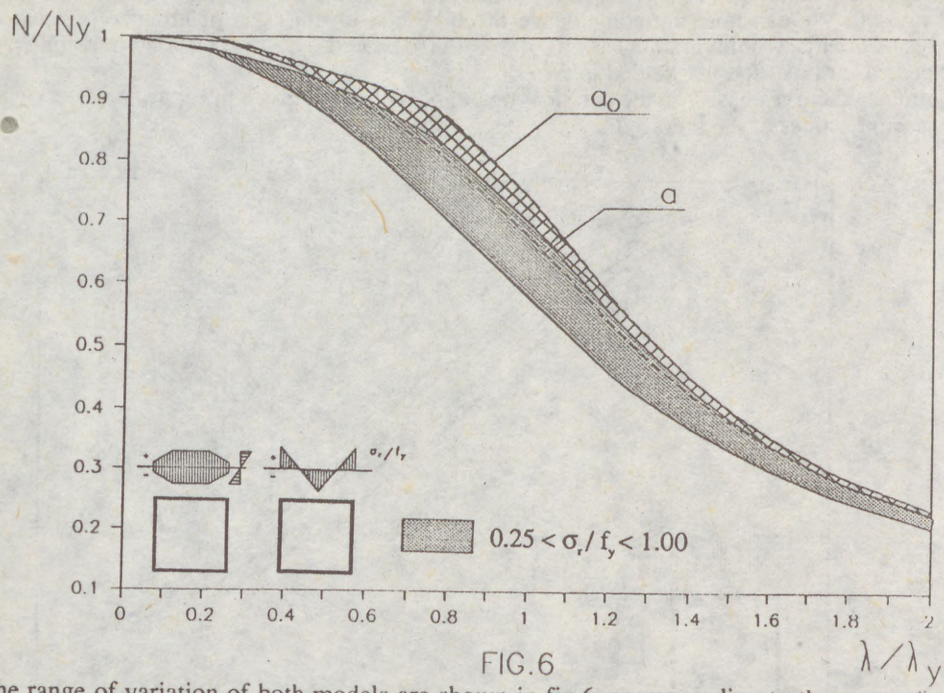

FIG.6

The range of variation of both models are shown in fig.6, corresponding to the cases of σ_r/f_y from 0.25 to 1.00. Both models approximately cover the same range of variation, which lies always below the reference range between curves a_o and a.

It means that the assessment of buckling checks for tubular columns must be revised according to these results.

REFERENCES

BALLIO, G., MAZZOLANI, F.M., 1983, "Theory and Design of Steel Structures", Chapman and Hall

DADDI, I., MAZZOLANI, F.M., 1972, "Determinazione sperimentale delle imperfezioni strutturali nei profilati in acciaio", Costruzioni Metalliche N°5

FAELLA, C., MAZZOLANI, F.M., TALARICO, G., 1985, "La. variazione delle tensioni residue nello spessore dei tubi in acciaio: Determinazione sperimentale e conseguenze sulla capacità portante", Atti X Convegno C.T.A., Montecatini (Italy)

GRIMAULT, J.P., RONDAL, J., 1985, "Etude comparative de differentes méthodes de mesure des contraintes résiduelles dans les profils creux en acier", Commission des Communautes Europeennes, Rapport Final

JOHNSTON, B.G., 1966, "Column Research Council Guide to Design Criteria for Metal Compression Members", 2nd Edn, Wiley

LANDOLFO, R.,MAZZOLANI, F.M., TALARICO, G., 1989, "Misura delle tensioni residue nelle sezioni a cassone in acciaio", Atti XI Convegno C.T.A., Anacapri (Italy)

MAZZOLANI, F.M., 1972, "Analisi sperimentale delle tensioni residue nei profilati metallici", Atti del 1° Convegno AIAS, Palermo

MAZZOLANI, F.M., 1973, "Influenza delle imperfezioni strutturali sulla instabilità delle colonne in acciaio", Costruzioni Metalliche N°6

MAZZOLANI, F.M., 1985, "Comparative study of measuring methods of residual stresses in hollow sections in steel", ECSC 7210-SA-308 Research report

(1)
MENDERA, Zbigniew (1)

BUCKLING STRENGTH OF CIRCULAR THIN-WALLED TUBE COLUMNS

INTERNATIONAL COLLOQUIUM
STABILITY OF STEEL STRUCTURES
BUDAPEST, HUNGARY, 1990
PRELIMINARY REPORT

SUMMARY: Steel bars and tubular shells of circular cross-section under axial or eccentric compression have been considered. Such elements are widely used in various technological fields such as aviation, shipbuilding or civil engineering (space trusses, pipelines, reservoirs, stacks, off-shore structures, etc.). The problem has been considered in the convention of semi-probabilistic limit states method, i.e. method of partial safety factors commonly used in structural standard design. The idea of this method is to compare, in the conditions of safety, design values of load effects with the design values of load capacity of a structure, justified in semi-probabilistic way. Thus safety parameters of certain required probability are found.

The load-carrying capacity of steel bars and tubular shells of circular cross-section under compression has been discussed. The formulas considering separately the effect of column buckling and thin-walled cylindrical shell local buckling have been quoted. A general and local buckling interaction formula of circular tube columns has been derived for the whole elastic-plastic range.

---

(1) Professor of Civil Engineering, Cracow Technical University

(2)

1. COLUMN BUCKLING OF CIRCULAR TUBES

The load capacity of slender compressed steel tubes is determined by their strength, buckling taken into account:

$$\sigma \leq f_d \cdot \varphi , \qquad (1)$$

where: σ - stress from design loads,

$f_d = \frac{f_y}{\gamma_m}$ - design strength of steel,

f_y - yield point of steel (characteristic value),

γ_m - safety factor of material,

φ - column buckling factor.

Column buckling factors have long been well known and tabulated in design standards. However, it is only recently that uniform analytic formulas have been proposed for their description in the whole elastic and elastic-plastic ranges [Maquoi and Rondal 1978, Murzewski 1982, Mendera a)1986], additionally classifying them on the basis of the bar cross-section profile and production technology.

For circular tube columns, considering total geometric and structural imperfections the following formula is recommended [PN-89/B-03200, 1989]:

$$\varphi = (1 + \bar{\lambda}^4)^{-1/2} , \qquad (2)$$

where: $\bar{\lambda} = \frac{\lambda}{\lambda_k}$ - slenderness parameter (relative slenderness),

$\lambda = \frac{l_b}{i}$ - bar slenderness,

$\lambda_k = \pi \sqrt{\frac{E_o}{f_d}}$ - transient slenderness,

$E_o = \frac{E}{\gamma_E}$ - design modulus of elasticity,

γ_E - coefficient of transition from mean value E to design value E_o (after PN-89/B-03200 : $\gamma_E = 1{,}33$).

(3)

2. THE EFFECT OF IMPERFECTIONS ON THE STABILITY OF CYLINDRICAL SHELL IN ELASTIC RANGE

So far local buckling factors of thin-walled cylindrical shells have been described incompletely and theoretical estimations differ significantly from the results of experimental tests.

The critical stress of an ideal cylindrical shell of an average length under axial compression, corresponding with the bifurcation point in the linear-elastic problem, was defined by [Timoshenko, 1910] :

$$f_{cr}^{i} = \frac{E}{\sqrt{3(1 - v^2)}} \frac{t}{r} , \qquad (3)$$

which, when shell contour slenderness is formulated as the shell radius to shell thickness $\lambda_1 = r/t$ and Poisson ratio for steel $v = 0,3$ is adopted, gives the known formula:

$$f_{cr}^{i} = 0,6 \frac{E}{\lambda_1} . \qquad (4)$$

Real shells, however, are far from ideal and one should be prepared not only for their residual stresses but also for initial deformations of the order of the shell thickness, which can generally be called imperfections. Therefore it is advisable to introduce a reduction coefficient in the form of elastic imperfections parameter:

$$k(\lambda_1) = \frac{f_e}{f_{cr}^{i}} = \frac{f_e}{0,6\ E/\lambda_1} . \qquad (5)$$

In paper [Mendera, b)1986], using the experimental data and having verified the hypothesis that the distribution of critical values can be approximated by Weibull´s distribution function, the elastic imperfections parameter on the level of design values was defined:

$$k(\lambda_1) = 3,3\ \lambda_1^{-1/2} \qquad (6)$$

and as a result, critical design strength in the elastic range:

$$f_e = k(\lambda_1)\ f_{cr}^{i} = 3,3\ \lambda_1^{-1/2} .0,6\ E\ \lambda_1^{-1} = 2\ E\ \lambda_1^{-3/2} . \qquad (7)$$

(4)

3. STABILITY OF CYLINDRICAL SHELLS IN ELASTIC-PLASTIC RANGE

To derive a uniform formula for the limit strength of a cylindrical shell under axial compression Rankine-Merchant interaction formula of limit load carrying capacity, generalized by [Murzewski, 1974], was used in paper [Mendera, b)1986] for cases where the mechanisms of elastic and plastic instabilities are random independence:

$$f_u^{-1/u} = f_d^{-1/u} + f_e^{-1/u} \quad , \tag{8}$$

where: $f_u = f_d \cdot \varphi_1$ - limit design strength of shell,

f_d - design strength of steel,

$f_e = 2 E \lambda_1^{-3/2}$ - critical design strength of shell in elastic range,

u - generalized parameter of elastic-plastic imperfections (u=0,25-1), after experimental data,

φ_1 - local buckling factor of shell.

After the substitution of the above notation in expression (8), we can formulate the stability factor φ_1 of cylindrical shell of any kind of steel, valid for the whole range of shell contour slenderness, in the following way:

$$(f_d \varphi_1)^{-1/u} = f_d^{-1/u} + (2 E \lambda_1^{-3/2})^{-1/u} \quad ,$$

hence

$$\varphi_1^{-1/u} = 1 + \left(\frac{2E}{f_d} \lambda_1^{-3/2}\right)^{-1/u} \tag{9}$$

and using the transient slenderness expression:

$$\lambda_{1k} = \left(\frac{2 E}{f_d}\right)^{2/3} \tag{10}$$

we finally obtain:

$$\varphi_1 = (1 + \bar{\lambda}_1^{3/2u})^{-u} \quad , \tag{11}$$

where $\bar{\lambda}_1 = \frac{\lambda_1}{\lambda_{1k}}$ - shell slenderness parameter and $\lambda_1 = \frac{r}{t}$.

(5)

Four classes of technological imperfections of cylindrical shells in the elastic-plastic range can be distinguished. The fabrication technology (structural imperfections) and shell manufacture precision (geometric imperfections) are taken into account, independent of the parameter of elastic imperfections $k(\lambda_1)$ introduced earlier.

Thus the following formulas of limit nondimensional design strength of cylindrical shells , included in the particular classes of imperfections, are obtained:

- <u>shell class a</u> (minor imperfections): $u = 1/4$

$$\varphi_1 = (1 + \bar{\lambda}_1^{\,6})^{-1/4} , \qquad (12a)$$

- <u>shell class b</u> (medium imperfections): $u = 1/2$

$$\varphi_1 = (1 + \bar{\lambda}_1^{\,3})^{-1/2} , \qquad (12b)$$

- <u>shell class c</u> (large imperfections): $u = 3/4$

$$\varphi_1 = (1 + \bar{\lambda}_1^{\,2})^{-3/4} , \qquad (12c)$$

- <u>shell class d</u> (very large imperfections): $u = 1$

$$\varphi_1 = (1 + \bar{\lambda}_1^{\,3/2})^{-1} . \qquad (12d)$$

In this way four boundary curves are obtained after formulas (12a) to (12d), defined by factors of stability φ_1.

For a cylindrical shell under eccentric compression or bending a correction is introduced in formula (12):

$$\varphi_{1e} = \varphi_1 \left(1{,}1 - 0{,}1 \frac{\sigma'}{\sigma}\right) \leq 1 , \qquad (13)$$

where σ' denotes extreme stress in section whose absolute value is smaller (or equal) to σ ; tensile σ' is marked with "-".

Thus for pure bending the formula is:

$$\varphi_{1b} = 1{,}2\ \varphi_1 \leq 1 . \qquad (14)$$

(6) (7)

4. GENERAL AND LOCAL INSTABILITY INTERACTION IN LONG AND THIN-WALLED CYLINDRICAL SHELLS UNDER COMPRESSION

In order to derive an interaction factor φ_i of general instability (buckling of bar) and local instabiliy (bulging of shell) we shall use the postulate that the condition of column buckling is considered till value $f_d \cdot \varphi_1$, which amounts to the condition of local instability being considered till value $f_d \cdot \varphi$. Then the condition of interaction stability of shell bar under longitudinal compression can be written as follows:

$$\sigma = \frac{F}{A} \leq f_d \cdot \varphi_i \tag{15}$$

where
$$\varphi_i = \varphi \cdot \varphi_1' \equiv \varphi_1 \cdot \varphi', \tag{16}$$

φ and φ_1 after formulas (2) and (12b), respectively,

while
$$\varphi' = (1 + \bar{\lambda}^4 \cdot \varphi_1^2)^{-1/2}, \tag{17}$$

$$\varphi_1' = (1 + \bar{\lambda}_1^3 \cdot \varphi^2)^{-1/2}, \tag{18}$$

which after substitution into formula (16) gives:

$$\boxed{\varphi_i = (1 + \bar{\lambda}^4 + \bar{\lambda}_1^3)^{-1/2}}. \tag{19}$$

The interaction effect of general and local instabilities has been illustrated, after formula (19), in Fig.1.

The buckling strength condition of circular thin-walled tube columns under compression and bending can be written:

$$\frac{F}{A} \varphi_i^{-1} + \frac{M}{W} (1{,}2 \cdot \varphi_1)^{-1} \leq f_d, \tag{20}$$

but this is a conservative approach.

(7)

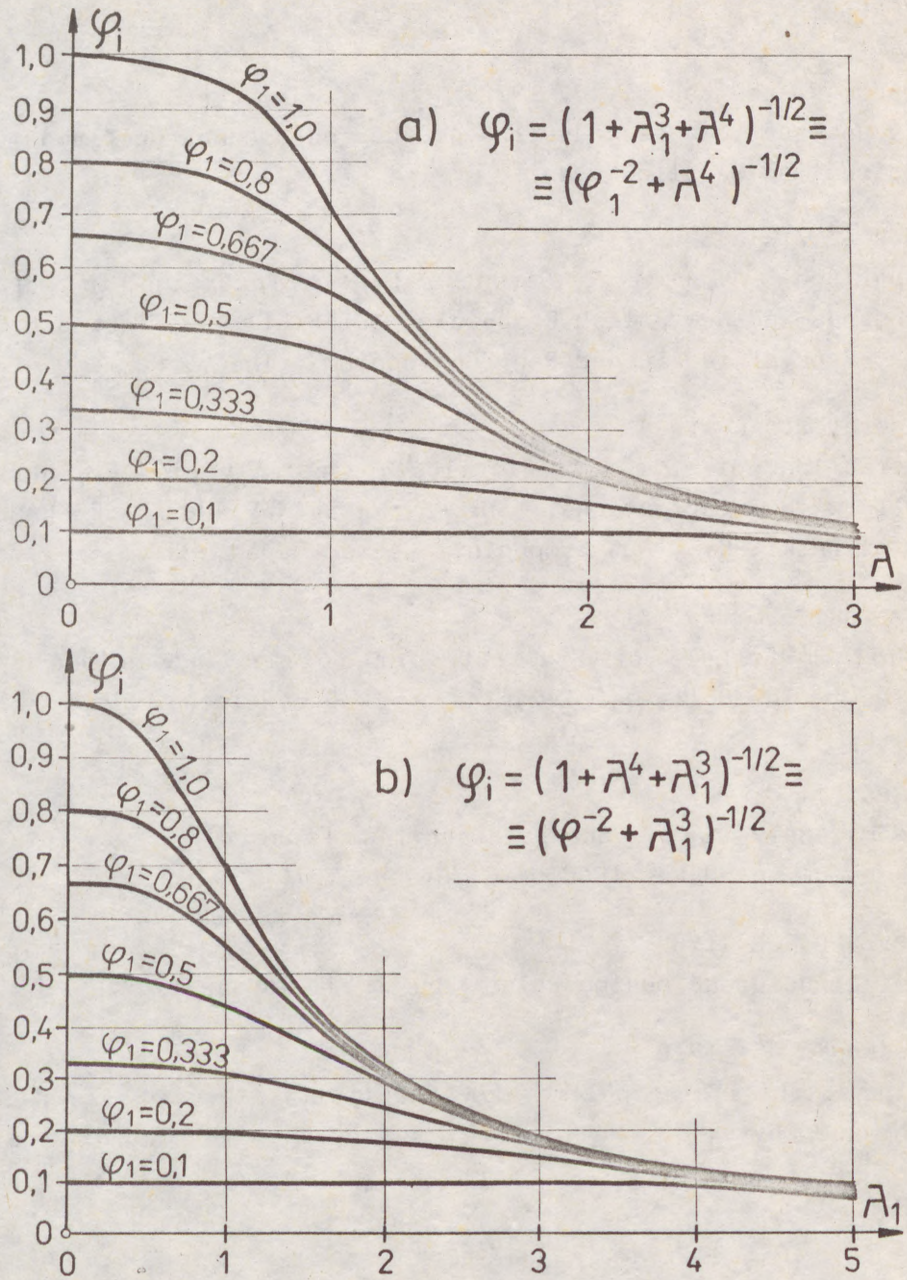

Fig.1 Interaction of general and local instabilities

(8)

REFERENCES

Maquoi, R. and Rondal, J. 1978
Mise an équation des nouvelles courbes européennes de flambement, Construction Métalique, No 1.

Mendera, Z. a)1986
Comparison of Buckling Strength Curves According to Foreign Standards and New Polish Proposals, "STABILITY OF STEEL STRUCTURES", Proc.of the Second Reg. Colloquium, Tihany, Hungary, Vol.I

Mendera, Z. b)1986
Interaction of Elastic Plastic Instability in Cylindrical Shells with Imperfections, "SHELLS, MEMBRANES AND SPACE FRAMES", Editor Heiki, K., IASS Symposium, Osaka, Japan, Vol.1, pp.17-24.

Murzewski, J. 1982
A Uniform Formula of Stability for Columns, Beams and Steel Plates, (In Polish), Inżynieria i Budownictwo, No 5/1982, Warsaw.

Murzewski, J. 1974
Random Analysis of Shells Carrying Capacity, Proc. of the Symphosium on SHELL STRUCTURES, Cracow 1974.

PN-89/B-03200, 1989
Steel Structures, Design Rules (Draft 5), Warsaw 1989.

Timoshenko, S. 1910
Einige Stabilitätsprobleme der Elastizitätstheorie, Z. angew. Math. und Phys., 58, No 4.

(1)
NIEMI, Erkki (1)
RINNEVALLI, Jussi (2)

BUCKLING TESTS ON COLD-FORMED SQUARE HOLLOW SECTIONS OF STEEL Fe 510

INTERNATIONAL COLLOQUIUM
STABILITY OF STEEL STRUCTURES
BUDAPEST, HUNGARY, 1990
PRELIMINARY REPORT

Summary: Buckling tests were conducted on cold formed square hollow sections made of steel Fe 510. The range of slenderness L/i was from 20 to 140 in steps of 10. The whole series contained 39 tests. The test pieces were aligned in the loading frame such that the initial eccentricity always equalled exactly L/1000, simulating the assumed initial curvature of real columns. This method resulted in a narrow scatter band which agreed rather well with the ECCS curve c. Using a reduced tangent modulus in calculation of the relative slenderness, which accounts for the effect of residual stresses, the results are shown to fit well with the different ECCS curves.

INTRODUCTION

Structural hollow sections are ideal for compressed members in steel structures owing to their large radii of gyration, i, and their large torsional stiffnesses.

Square and rectangular hollow sections are manufactured by two basic methods: (i) hot rolling and (ii) cold forming. The products made by these methods differ in some respects. One difference of concern is the residual stress state.

The residual stresses are rather low in hot rolled sections and their effect on buckling strength is small (Stamenkovic 1983). Therefore the use of the European buckling curve, a, is fully justified in the case of hot rolled sections (ECCS 1976, 1978).

However, in the cold-forming process residual stresses are produced, which are rather high. Depending on the forming process, i.e. whether a circular

(1) Professor of Steel Structures, Lappeenranta Univ. of Technology
(2) Research Assistant, Lappeenranta Univ. of Technology

(2)
tube is formed first, or the rectangular section is formed directly, the residual stress pattern is different. In the former case there are high bending stresses in the flat walls, whilst the membrane stresses are negligible (Huhdankoski 1982). At the inside surface of the section the magnitude of the compressive residual stress may be close to the yield strength of the material.

The effect of residual stresses on the buckling strength of conventional hot rolled wide flange beam sections and similar sections is understood well (Schulz 1968). Based on this knowledge and extensive test series, the European buckling curves have been developed. They make a distinction between different cross section types and fabrication methods depending on the effect of the residual stresses. However, due to their specific residual stress pattern, the cold formed rectangular sections show a different buckling behaviour, which does not fit well with the ECCS buckling curves (Niemi 1985).

In addition to the residual stresses, cold-formed sections differ from hot rolled profiles due the strain-hardening, which strengthens the material during the forming process. The actual yield strength of the finished product is much higher than that of the virgin steel strip. Therefore there has been some uncertainty about how the design strength should be specified by the design rules. The European draft proposal (Eurocode 3, 1988) proposes two alternative ways for calculating the buckling strength of cold-formed hollow sections:

(i) curve b may be used in connection with the yield strength of virgin steel material;
(ii) curve c shall be used in connection with the design strength based on tests on the cold finished section.

The above proposal is a compromise which allows the use of standard curves, but which does not give very good consistency with the real buckling behaviour of the cold-formed hollow sections. Some earlier studies of the effect of residual stresses on the buckling behaviour of rectangular hollow sections cold finished from a circular cold formed section (Huhdankoski 1982, Rokkanen 1983), have led to an alternative proposal, which uses a reduced tangent modulus in calculating the relative slenderness (Niemi 1985).

This paper presents the results of a new test series conducted at Lappeenranta University of Technology. The project is not yet completed, a refined analysis of the results is currently being yndertaken.

MATERIALS AND METHODS

Material and testing programme

Square hollow sections of cross section 100·100·5 mm made of steel Fe 510 D were tested. All tested material was from one batch, manufactured by first forming and welding a round tube, which then was finished to the final square shape. Thirteen different lengths were chosen corresponding to

(3)
slenderness values L/i equal to 20, 30 ... 140.

Material properties

The yield strength, f_y, was determined using tensile coupon tests. The results are given in Table 1 as the average values of two tests. For the virgin material, R_{eH}, and for the flat side and corner area of the cold-finished section, $R_{p0.5}$, were determined. In addition to these, a weighted average yield strength over the whole cross section was calculated. Due to the initial crookedness of the tensile coupons the definition $R_{p0.5}$ was found to describe test piece yielding better than the usual $R_{p0.2}$.

Table 1. Mechanical properties measured from the virgin material and the cold finished product

Sample	Yield strength N/mm²	U.T.S N/mm²	Elongation A5 %
Virgin material	356	485	35
Flat side	423	480	
Corner	535	546	
Weighted average	444	492	

Specimen dimensions

All dimensions and cross sectional areas are given in Table 2. The length of a specimen was measured with an accuracy of 0.5 mm, and the cross sectional height and width with a resolution of 0.01 mm. The specimens were weighed in order to calculate the average cross sectional area using a density value of 7850 kg/m³. The given values of inner radius are average values determined with an accuracy of 0.1 mm.

Testing arrangements

The pinned joint end conditions were achieved by following the instructions given in Refs. (Huber 1958, Tebedge 1976). The principle is shown in Fig. 1. The rolling cylinder parts and the flat counterparts were made of hardened steel. The centre line of the cylinder was placed just at the end of the specimen such that the length of the specimen corresponds to the distance between the fictitious pin joints.

The compressive load was generated by using a hydraulic jack with a capacity of 1 MN. The loading rate was about 6.9 MPa/min according to guidance given in Ref. (Tebedge 1976). The force was measured by an in-house built force transducer which was calibrated by an authorized testing laboratory of the Technical Research Centre of Finland. The largest measuring error was found to be 0.58%.

(4)

The lateral displacement of the specimen mid-point was measured by three potentiometers coupled such that the average end displacement was subtracted from the mid-point displacement. The load-displacement curves were produced by an x-y plotter. A fourth potentiometer was arranged to record the load-shortening curve on the same paper.

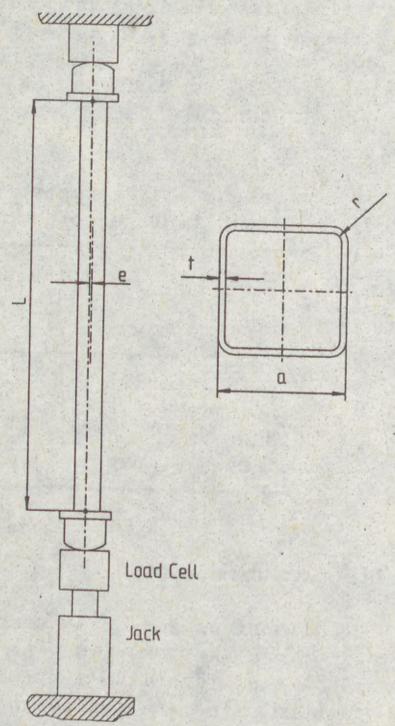

FIGURE 1. Principle of the testing conditions

Out-of-straightness and eccentricity measurements

The deviation of the specimen centre line from the straight line through the end cylinder mid-points was measured with a resolution of about 0.2 mm, using a thin piano wire and a measuring tool with a millimeter scale. The measurements were made under a pre-load of 5% of the predicted ultimate load according to (Tebedge 1976). The errors caused by the torsional and distortional deviations were automatically corrected. The specimen end eccentricities were adjusted such that a mid-point eccentricity of L/1000 was achieved.

Location of the weld

In some specimens the weld was located in the plane of buckling. The direction of buckling is indicated in Table 2 as follows:

A: weld on the convex side
C: weld on the concave side

A weld not located in the buckling plane is indicated by B or D.

RESULTS AND DISCUSSION

The test results are given in Table 2. The relative slenderness values $\bar{\lambda}$ have been calculated using an elastic modulus of 210000 MPa and a yield strength value of 423 N/mm², measured from the flat face of the square section. The extra strain hardening in the coners has not been taken into account.

Figure 2 shows how the results fit the ECCS curve c, which is recommended for use by Eurocode 3. There are 8 data points slightly under the curve. The largest deviation on the unsafe side is 2.4%. However, it should be noted that in this test series the initial eccentricity was always equal to L/1000, which represents a small fraction of the initial crookedness of real columns. Therefore, quite a high fraction of these results could be allowed to lie under the design curve. The determination of this is left to the code writing bodies.

Figure 3 shows how the results fit the ECCS curve b, when the yield strength of the virgin material is used. This alternative method recommended by Eurocode 3 largely underestimates the load bearing capacity in the regime of small slenderness.

Figure 4 shows how the results fit the ECCS curve a, using the virgin steel yield strength again, but replacing the elastic modulus by a lower tangent modulus $E_t = 0.8 \cdot E$. The value of E_t was chosen such that only 4 data points fall slightly under the a-curve. This value of tangent modulus, $E_t = 0.8 \cdot E$ yields safe predictions in combination with the highest ECCS curve, a.

Figure 5 shows the fit with curve c, when the yield strength is taken as the weighted average over the whole cross section. The fit is now very good, although the fraction under design curve is rather large. The use of a slightly reduced tangent modulus of 200500 N/mm² would give almost an ideal fit.

The rather good fit of the results with the ECCS curves in Figures 4 and 5 has a physical explanation. On the inside surface of this type of hollow section there are rather high compressive residual bending stresses, which cause premature local yielding at low load levels. This is revealed in the low apparent value of elastic modulus, which could be determined from stub column tests. In this paper this reduced modulus has been called the tangent modulus.

(6)

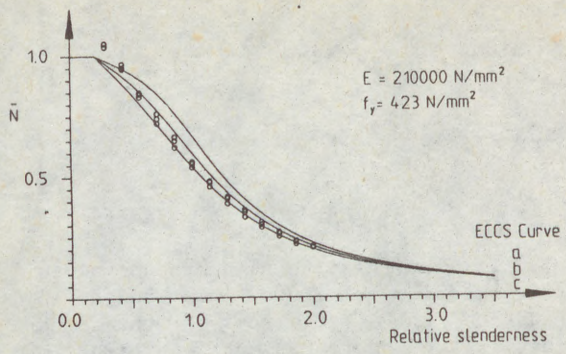

FIGURE 2. Test results compared with ECCS curves. Flat side yield strength.

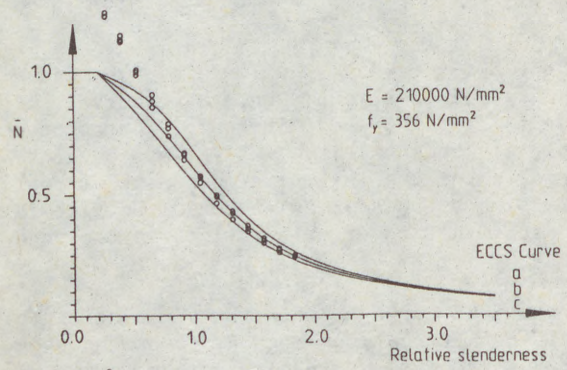

FIGURE 3. Test results compared with ECCS curves. Virgin material yield strength.

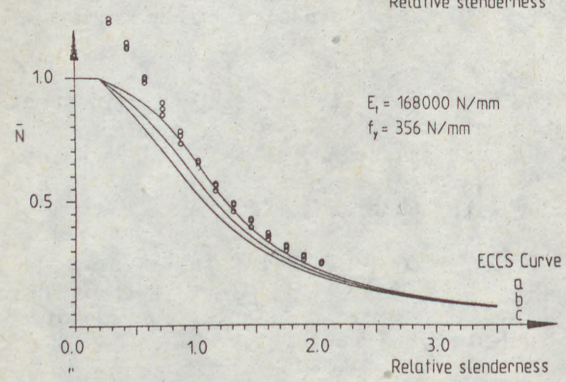

FIGURE 4. Test results compared with ECCS curves. Virgin steel yield strength and reduced tangent modulus.

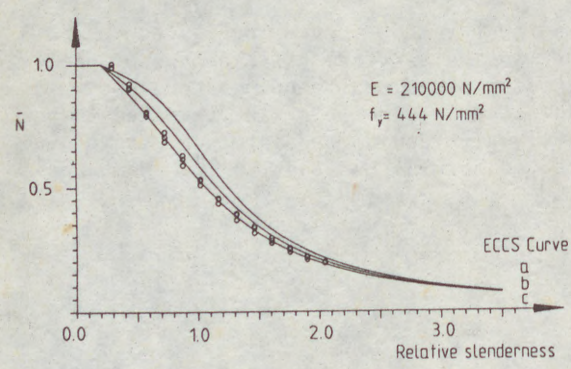

FIGURE 5. Test results compared with ECCS curves. Weighted average yield strength.

(7)

Table 2 Test piece dimensions and test results

Test no.	a mm	t mm	r mm	L mm	A mm^2	i mm	P_u kN	f_y N/mm^2	$\frac{f_c}{f_y}$	$\bar{\lambda}$	Weld pos.
1	100.12	4.93	8.1	766	1804.4	38.31	791	423	1.036	0.286	A
2	100.11	4.87	8.3	766	1812.7	38.31	796	423	1.038	0.286	B
3	100.08	4.96	8.3	765	1806.8	38.26	803	423	1.051	0.286	C
4	100.11	4.96	8.1	1149	1802.4	38.29	725	423	0.951	0.429	C
5	100.12	4.90	8.2	1149	1790.5	38.31	715	423	0.944	0.428	D
6	100.12	4.95	8.1	1149	1802.4	38.30	736	423	0.965	0.428	A
7	100.13	4.96	8.3	1531	1809.7	38.28	648	423	0.847	0.571	A
8	100.11	4.94	8.3	1528	1800.8	38.28	640	423	0.840	0.570	D
9	100.11	4.89	8.3	1529	1799.6	38.30	631	423	0.829	0.570	C
10	100.12	4.97	8.4	1916	1811.8	38.27	567	423	0.740	0.715	C
11	100.13	4.96	8.3	1915	1806.1	38.28	581	423	0.760	0.715	A
12	100.10	4.95	8.2	1916	1798.9	38.28	547	423	0.719	0.715	B
13	100.11	4.93	8.2	2301	1802.0	38.30	505	423	0.663	0.858	C
14	100.11	4.91	8.1	2300	1791.7	38.31	491	423	0.648	0.858	C
15	100.11	4.96	8.2	2302	1810.0	38.28	475	423	0.620	0.859	B
16	100.12	4.95	8.0	2679	1807.3	38.31	411	423	0.538	0.999	D
17	100.14	4.98	8.1	2679	1811.7	38.29	430	423	0.561	1.000	C
18	100.11	4.91	8.1	2679	1795.4	38.31	421	423	0.554	0.999	C
19	100.11	4.96	8.4	3059	1807.3	38.27	364	423	0.476	1.142	C
20	100.11	4.96	8.0	3059	1803.5	38.30	367	423	0.481	1.141	C
21	100.10	4.92	8.0	3059	1794.8	38.31	348	423	0.458	1.141	D
22	100.14	4.96	8.3	3449	1808.0	38.29	313	423	0.409	1.287	C
23	100.14	4.96	8.4	3450	1807.7	38.28	317	423	0.415	1.287	A
24	100.14	4.91	8.3	3449	1791.3	38.31	293	423	0.387	1.286	B
25	100.12	4.95	8.3	3832	1788.5	38.29	250	423	0.330	1.430	D
26	100.11	4.94	8.3	3829	1794.9	38.28	273	423	0.360	1.429	A
27	100.13	4.93	8.4	3832	1798.5	38.29	268	423	0.352	1.430	C
28	100.15	4.94	8.1	4209	1804.1	38.32	220	423	0.288	1.569	B
29	100.15	4.97	8.4	4209	1811.4	38.28	229	423	0.299	1.571	C
30	100.14	4.92	8.1	4208	1795.2	38.32	235	423	0.309	1.569	A
31	100.13	4.94	8.2	4597	1795.7	38.30	190	423	0.250	1.715	B
32	100.08	4.92	8.3	4597	1786.0	38.28	197	423	0.261	1.716	C
33	100.12	4.97	8.2	4597	1800.0	38.28	204	423	0.268	1.715	A
34	100.13	4.93	8.3	4976	1790.8	38.30	165	423	0.218	1.856	B
35	100.14	4.96	8.4	4975	1803.9	38.28	177	423	0.232	1.857	A
36	100.13	4.92	8.2	4977	1788.0	38.31	172	423	0.227	1.856	C
37	100.13	4.93	8.2	5355	1781.8	38.30	153	423	0.203	1.997	B
38	100.06	4.96	8.3	5358	1797.4	38.26	157	423	0.206	2.001	A
39	100.11	4.96	8.3	5360	1795.6	38.28	159	423	0.209	2.000	C

CONCLUSIONS

From this buckling test series with cold formed square hollow sections of steel Fe 510 using an initial eccentricity of length/1000, the following conclusions may be drawn:

(8)

1. The two alternative methods for determining design strength given by the Eurocode 3 proposal are conservative in the low slenderness regime, but less conservative in the high slenderness regime.
2. It is possible to take account of (i) the strain hardening and (ii) the effect of residual stresses by defining the yield strength and a tangent modulus in such a way that the results fit well with any of the design curves a to c.
3. The initial eccentricity of L/1000 led to a narrow scatter band. However, it remains to be decided how large a fraction of these results are allowed to fall below the design curve.

ACKNOWLEDGEMENT is given to Company Rautaruukki Oy for financial support and the supplied materials.

REFERENCES

ECCS, 1976, Manual on Stability of Steel Structures. ECCS, June 1976.

ECCS, 1978, European Recommendations for Steel Constructions. European Construction for Constructional Steelwork (ECCS), March 1978.

EUROCODE No.3, 1988, Design of Steel Structures. Part 1 - General Rules and Rules for Building. Preliminary Version (July 1988).

HUBER A.W., 1958, Fixtures for Testing Pin-End Columns. ASTM Bulletin n:o 234, p. 41-45.

HUHDANKOSKI E., 1982, Buckling of Cold-Formed Rectangular Hollow Sections. Lappeenranta University of Technology, Department of Mechanical Engineering. Lappeenranta 1982, 91 p. (In Finnish)

NIEMI E., 1985, Buckling of Cold-Formed Rectangular Hollow Sections. United Nations, Economic Commission for Europe, Steel Committee: Seminar on Steel Tubes and their Raw-Material Quality Requirements. Helsinki 13-17 May 1985.

ROKKANEN A., 1983, Effect of Precompression on the Buckling Strength of Cold-Formed Rectangular Hollow Sections. Lappeenranta Univ. of Technology, Department of Mechanical Engineering. Lappeenranta 1983, 123 p. (In Finnish)

SCHULZ G., 1968, Die Traglastberechnung von planmässig mittig belasteten Druckstäben aus Baustahl unter Berücksichtigung von geometrischen und strukturellen Imperfektionen. Universität von Graz.

STAMENCOVIC A. & GARDNER M.J., 1983, Effect of Residual Stresses on the Column Behaviour of Hot-Finished Steel Structural Hollow Sections. Proc. Instn. Civ. Engrs, Part 2, 1983, 75, Dec., pp. 599-616.

TEBEDGE N. & TALL L., 1976, Procedure for Testing Centrally Loaded Columns. Tech. Mem. No. 4, Lehigh Univ. Fritz Eng. Lab. Rep. No. 351.6. In: B.G. Johnston, Guide to Stability Design Criteria for Metal Structures, p. 554-588.

(1)
SHERMAN, Donald R. [1]

IMPACT OF CODE DIFFERENCES FOR TUBULAR MEMBERS

INTERNATIONAL COLLOQUIUM
STABILITY OF STEEL STRUCTURES
BUDAPEST, HUNGARY, 1990
PRELIMINARY REPORT

Summary: This paper discusses the impact on the design strength of tubular members caused by differences in specifications from various regions of the world. The specifications that are considered are the latest limit states design codes from five regions. Both circular and rectangular hollow sections manufactured by either hot-formed or cold-formed methods are considered.

The first comparison deals with the column buckling strength. Codes differ not only in the design equations but also in whether a distinction is made between hot- and cold-formed tubes. The design strengths resulting from these differences can be over 20%. The comparisons continue with the consideration of local buckling in thin-walled members in both axial compression and in bending. Not only do the equations for the local buckling strength differ, but the codes vary on whether an interaction with overall column buckling is considered. The conclusion of the paper is that the same tube, particularly thin circular sections, used in various parts of the world may have a significantly different design strength. Some possible reasons for these differences are stated.

Introduction: The purpose of this paper is to discuss the impact that the differences in design codes from various regions of the world have on the deign of tubular members. Both circular hollow sections (CHS) and square hollow section (SHS) are considered, with the latter designation including rectangular sections. This paper supplements the information in Chapter 9 - Tubular Structures of the 2nd edition of "Stability of Metal Structures:

[1] Professor of Civil Engineering
University of Wisconsin-Milwaukee, USA

(2)

A World View" [SSRC 1989.] Since the "World View" contains the actual code equations and criteria, they will not be repeated here.

As the "World View" indicates, there are numerous codes that have specific criteria for tubular members. These codes are in both allowable stress design and limits states design formats. Table 1 lists the the codes used in this paper as being representative of five regions of the world. Two codes are included for North America because they are significantly different and widely used in the United and Canada respectively.

Table 1 - Regional Design Codes

Region	Designation in this paper	Reference
Australia	AUS	AS-DR87164
East Europe	E. EUR	STAS 10108/0 1978
Japan	JAP	AJI 89
North America	US	AISC-LRFD-1986
	CAN	CSA S16.1-M89
West Europe	EC3	EC3 84

All of the codes that have been selected for the comparisons are in the limit states design format. They are the latest structural codes in the various regions and should represent the most current viewpoints regarding the design of tubular members. Other codes primarily intended for pressure applications of cylinders or storage tanks contain criteria for axial and bending loads, but these are not generally used for structural members. Bridge specifications have criteria for box sections that are intended for box plate girders and are not used for manufactured tubular members.

Tubes are produced in accordance with product specifications in various countries. These specifications generally contain chemistry requirements, dimensional tolerances and mechanical properties for both hot-formed and cold-formed tubes. In some cases cold-formed tube may be hot-finished for final sizing or heat treated to reduce the level of the residual stresses. The specified yield strengths generally range from 250 to 350 MPa with hot-formed tubes having lower strengths. In some regions of the world, only one type of tube may be produced.

Column Buckling Under Axial Compression: Of the six codes under consideration AUS, CAN and EC3 use multiple column curves that differ for hot- and cold-formed tubes. The other codes use a single column curve that applies to any type of tube. In Fig. 1 the limit state design strength for hot-formed tubes, ϕN, normalized by the yield load, N_y, is plotted against the nondimensional column slenderness parameter

(3)

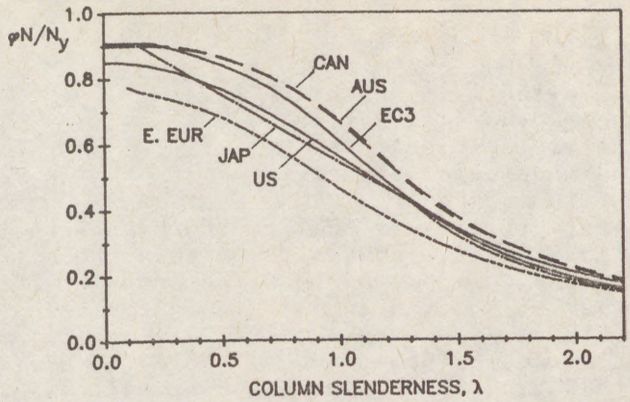

FIG. 1 – COLUMN CURVES FOR HOT–FORMED TUBES

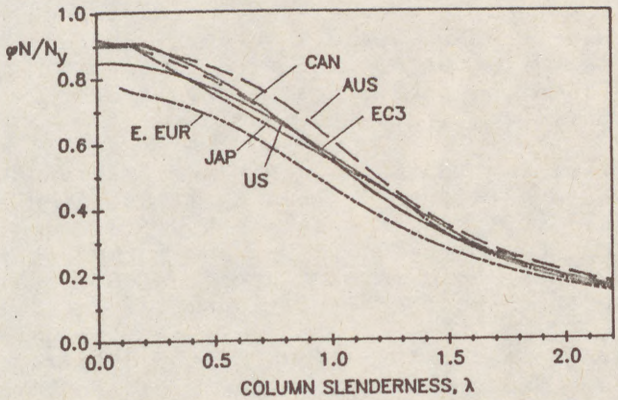

FIG. 2 – COLUMN CURVES FOR COLD–FORMED TUBES

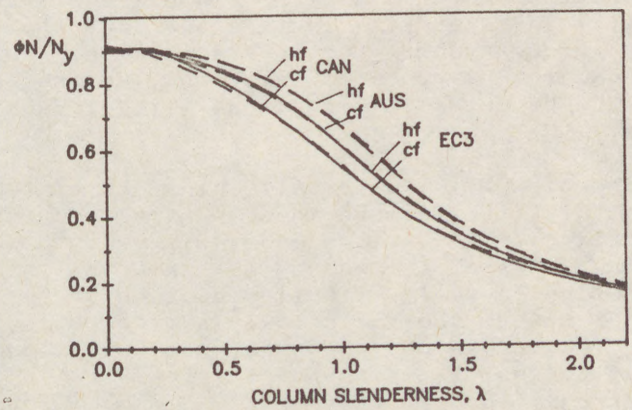

FIG. 3 – HOT & COLD–FORMED COLUMN CURVES

$$\lambda = \frac{KL}{\pi r}\sqrt{\frac{\sigma_y}{E}}$$

where KL = the effective length
r = the radius of gyration
σ_y = the yield strength
E = the modulus of elasticity.

CAN and AUS are very similar and are the highest curves while JAP and US are also similar. EC3 falls between these two sets and E.EUR is lower than all of them. Differences of over 20% occur at a slenderness of about 0.9, which is a typical value for many columns in building structures. Fig. 2 is a similar plot of column curves for cold-formed tubes. Here the differences are much less with CAN, EC3, JAP and US being quite similar. However, it should be noted that there are different ways in which the yield strength is defined. In some cases it is determined from tension coupons taken from the wall of the finished tubular product while in others, the coupon is from the virgin plate material before the tube is formed. In still other cases, yield is a measured or calculated average value for the full cross section.

The differences in the way that AUS, CAN and EC3 distinguish between hot- and cold-formed tubes is illustrated in the column curves of Fig. 3. In CAN the strength difference is greater than in AUS and EC3. Also the curve for hot-formed tubes in EC3 is very similar to the cold-formed curve in AUS. The CAN column curves follow the SSRC recommendations [Galambos, 1988.]

There are some valid reasons for the differences in the column curves. Codes which use higher load factors for determining the design load can justify the use of higher column curves. Codes that adopt a single column are placing an emphasis on simplicity in design or reflecting the fact that only one manufacturing process dominates in that region. For example, hot-formed SHS are not produced in the US, so the relatively low position of the US curve in Fig. 1 has little practical significants.

Local Buckling of CHS: If the wall thickness of a CHS is sufficiently thin, the failure mode in axial compression will be by local buckling. The various codes differ in how they treat local buckling. All of the codes contain a wall slenderness limit that defines a fully effective section where local buckling will not occur before the yield load is reached and does not have to be considered in design. However, the wall slenderness parameter may be just the diameter/thickness ratio (D/t) or it may include the yield strength, $\sigma_y D/t$. In addition, there are differences in the limiting value of the parameter. For thin sections, the equations to determine the local buckling strength also differ and some codes do not even permit the use of thin

(5)

sections. A final difference in the codes is whether an interaction between local and overall column is considered. Table 2 is a comparison of these factors in the various codes.

Table 2 - Provisions for CHS Local Buckling in Compression

	Wall Slenderness Parameter	D/t Limit	Provisions for Thinner	Local-Column Interaction
AUS	$\sigma_y D/t$	$22750/\sigma_y$	YES	YES
E.EUR	$\sigma_y D/t$	$27600/\sigma_y$	YES	NO
JAP	D/t	90	YES	NO
US	$\sigma_y D/t$	$22600/\sigma_y$	YES	YES
CAN	$\sigma_y D/t$	$23000/\sigma_y$	NO	---
EC3	$\sigma_y D/t$	$21150/\sigma_y$	NO	---

σ_y is the yield strength in MPa.

The impact of the code differences reflects the local buckling equation, the column buckling equation and the interaction criteria. With all these variables, it is difficult to make a general comparison. Therefore, Table 3 has been generated to show the the normalized design strength, $\phi N/N_y$, for two column slenderness factors that are at the extremes of the range of practical columns and three D/t ratios. A cold-formed CHS has been used since this is the most likely produce for a thin tube and the yield strength is 350MPa.

Table 3 - Normalized Design Strengths for Thin CHS
($\phi N/N_y$ for Cold-Formed CHS with σ_y = 350MPa)

	λ = 0.6			λ = 1.5		
D/t =	60	100	200	60	100	200
AUS	.80*	.54	.28	.34*	.31	.22
E.EUR	.64*	.64*	.40	.27*	.27*	.27*
JAP	.71*	.71*	.59	.32*	.32*	.32*
US	.73*	.63	.59	.33*	.32	.32
CAN	.75*	not allowed		.32	not allowed	
EC3	.76*	not allowed		.31	not allowed	

* controlled by column buckling only

The D/t ratio of 60 excludes local buckling in all of the codes and the value is included in the Table to reflect the influence of the column equation. The Table shows that the local buckling interaction has a greater influence for shorter columns and that there are considerable regional differences.

In the older allowable stress codes, it was common for the allowable bending stress in thick CHS to be the same as for other shapes and in thin CHS to be the same as for axial compression, with the same limiting D/t. This usually resulted in a discontinuity in design strength at the D/t limit. With the advent of limit states codes, compacts sections were allowed to reach the plastic moment, which is relative high for CHS due to their large shape factor. Therefore, some research has been

(6)

conducted to study the inelastic local buckling of CHS in bending. This research is reflected in some of the codes which present specific criteria for bending of CHS.

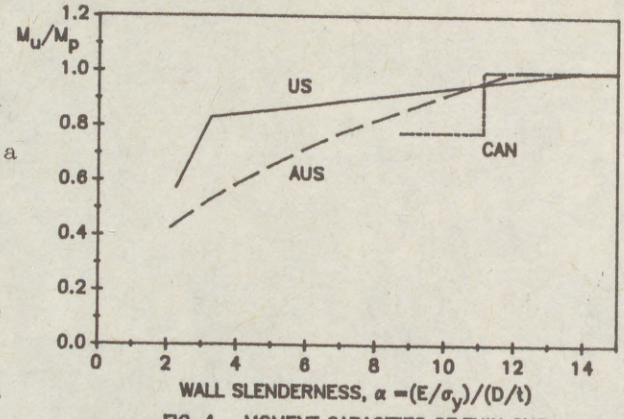

FIG. 4 — MOMENT CAPACITIES OF THIN CHS

The "World View" draft is not entirely clear on the bending criteria for CHS in some regions. However, it appears that AUS and US have specific provisions for bending while the others still use the axial compression criteria when the tube are thin, although CAN imposes a new D/t limit for the plastic moment. The criteria for AUS, US and CAN are compared in Fig.4 where the ultimate moment, M_u (without the resistance factor ø), normalized by the plastic moment, M_p, is plotted against the wall slenderness parameter $\alpha_c = (E/\sigma_y)/(D/t)$. The differences in the limits and strength for thin CHS are significant.

Local Buckling of Thin SHS: All of the codes specify a limiting width thickness ratio, b/t, that defines a thin walled SHS. In some cases this differs for hot- and cold-formed sections. Most codes consider an interaction between local and column buckling. Usually the interaction is a modification of the column slenderness and a reduction in the column strength equation based on an effective area (Q factor) calculated from and effective width of the thin elements. However, the equations for the effective widths differ in the various regions. Table 4 summarizes the different approaches that are used.

Table 4 - Provisions for Thin SHS in Axial Compression

	b/t Limit	b_e Calculated?	Form of Interaction
AUS	cf $632/\sqrt{\sigma_y}$ hf $712/\sqrt{\sigma_y}$	YES	Q for λ and column Eq.
E.EUR	*	NO	Limit raised for axial load reduced below column Eq.
JAP	cf 36 hf $733/\sqrt{\sigma_y}$	NO	Lower of col Eq. & N_{cr} Eq.
US	$625/\sqrt{\sigma_y}$	YES	Q for λ and column Eq.
CAN	$577/\sqrt{\sigma_y}$	YES	Q for λ and column Eq.
EC3	$690/\sqrt{\sigma_y}$	YES	Q for λ and column Eq.

*function of aspect ratio, σ_y and column slenderness

(7)
Although CAN and EC3 do not have different limits for hot- and cold-formed sections, they do use multiple column curves that causes a difference in the normalized strength.

With the large differences in the codes it is impossible to make a general comparison of the strengths. Therefore, the comparisons for thin SHS are made for one size, 406 x 406 x7.9mm, with σ_y of 350MPa. This square section has one of the largest b/t, 47.2, that are normally produced. It should illustrate the largest impact on the comparison. In some codes, the exact determination of the axial load capacity of a thin SHS is an iterative process since the equations for effective width includes a stress level, which is a function of the effective properties of the member. However, it is conservative to use the stress level based on the column slenderness of a fully effective section. This has been done in Table 5 for two column slenderness ratios. The capacity base on the full section is included to show the extent on the reduction for the thin section.

Table 5 - Normalized Design Strengths for Thin SHS
($\phi N/N_y$ for 406 x 406 x 7.9mm SHS with σ_y = 350MPa)

	λ = 0.6		λ = 1.5	
	Full	Reduced	Full	Reduced
AUS	.84	.60	.37	.32
E.EUR	.64	.64	.27	.27
JAP	.71	.58	.32	.32
US	.73	.66	.33	.33
CAN	.75	.61	.32	.32
EC3	.76	.62	.31	.29

Only E.EUR has no reduction for this section, but this code also has the lowest strength form the column curve. AUS and EC3 are the only codes that have a strength reduction for the long column, but these are relatively small. The final strengths are reasonably close considering all the differences in the codes.

There is insufficient information in the draft of "World View" to compare the bending capacities of thin SHS. AUS, US and EC3 use the same b/t limits to define when the yield moment can be achieved as were used for axial compression. JAP and CAN have higher limits for bending. AUS, US and CAN define a lower limit for a compact section where M_p can be achieved. AUS, US, CAN and EC3 use the same effective width expressions that were used for axial compression and the moment capacity of a thin section is based on an effective section modulus. Since these changes are relatively minor, it is to be expected that the comparisons between the regions will be similar to thin SHS in axial compression.

(8)

Conclusions: The equations and approaches used in the design of tubular members differ significantly in various regions of the world. The differences in the column strength can vary by more than 20%, although this difference is less for cold-formed tubes. There may be some justification for the differences in column strengths since the codes use different load factors and in some regions, the cold-formed tube is the dominant type used. The greatest difference is design strengths are for thin CHS tubes. The codes give much closer results for thin SHS even though the provisions on the codes are in different forms.

It is difficult to state why the difference exist. However, it should be noted that in most codes, the primary emphasis is for other types of shapes and tube design provisions are relatively new and may not have received as close a scrutiny. A desire by code writers for simplicity vs. refinement can also create differences. The use of single vs. multiple column curves or complex interaction expressions illustrate this. There may also be differences in regional data bases and philosophies of using lower bound or mean approximations of the data. All of these factors combine to create the code differences.

It is not the purpose of this paper to judge which codes are superior or more correct. However, code writers in the various regions can see how the results obtained by their code fit with others. If they appear out of line, it may be desirable to re-examine the basis for the provisions and justify their use.

References:

AS-DR87164, Draft Australian Standard for Steel Structures, 1987.

STAS 10108/0, Civil, Industrial and Agricultural Buildings-Design of Steel Structural Members, Romainian State Standard, 1978.

AJI 89, Standard for Limit State Design of Steel Structures (Draft), Architectural Institute of Japan, 1989.

AISC-LRFD-1986, Load and Resistance Factor Design, Specification for Structural Steel Buildings, American Institute of Steel Construction, 1986.

CSA S16.1-M89, Steel Structures for Buildings, (Limit States Design) CAN3-S16.1-M89, Canadian Standards Association, 1989.

EC3 84, Eurocode n.3 Common Unified Rules for Steel Structures, EUR 8849 EN-1984.

Galambos, T.V. (editor), GUIDE TO STABILITY DESIGN CRITERIA FOR METAL STRUCTURES, 4th Edition, Structural Stability Research Council, John Wiley & Sons, New York, 1987.

SSRC, STABILITY OF METAL STRUCTURES - A WORLD VIEW (Draft), 2nd Edition, Structural Stability Research Council, 1989.

(1)

WATANABE, Eiichi *1
SUGIURA, Kunitomo *2
KANOU, Masato *3
TAKAO, Michiaki *4
EMI, Susumu *5

HYSTERETIC BEHAVIOR OF THIN TUBULAR BEAM-COLUMNS WITH ROUND CORNERS

INTERNATIONAL COLLOQUIUM
STABILITY OF STEEL STRUCTURES
BUDAPEST, HUNGARY, 1990
PRELIMINARY REPORT

Summary: The hysteretic behavior of steel thin tubular beam-columns under cyclic bending and axial compressive force is investigated experimentally, where the overall load-deformation characteristics considering the local instability of thin plate/shell elements are discussed. Special attention is paid to the effect of the presence of axial compressive force and the use of round corners on the ductility after its ultimate state in view of the aseismic design consideration. From this study, it is found that the axial compressive force may reduce the strength and ductility considerably, and also that round corners may be desirable compared with sharp edges for the ductility improvement without significant loss of strength, and for their beautiful looking.

I. INTRODUCTION

As concerned with the computation of the ultimate strength of steel beam-columns under combined loadings such as axial compressive force, shear force and bending, it has been becoming relatively easy to obtain thanks to the new developments in computations such as Finite Element Method(FEM). However, it is still considered to be a difficult task to analyze the load-deformation relationship including the local failure characteristics such as buckling of thin plate/shell elements of tubular beam-columns. In recent days, the necessity to assess the actual reliability of structures against expected severe loadings such as strong ground motions and wave motions has emerged and an investigation on the basic characteristics of the cyclic behavior in addition to the strength under monotonically

*1 Professor of Civil Engineering, Kyoto University
*2 Research Associate of Civil Engineering, Kyoto University
*3 Research Engineer, JIP Engineering
*4 Graduate Student of Civil Engineering, Kyoto University
*5 Manager, Hanshin Expressway Administration and Technology Center

(2)

applied loads has been carried out.

It has been well known that a properly designed steel structural member would suffer a certain degree of damage, but would not collapse instantaneously due to the ductility of material itself, namely, large inelastic deformation capability of steel. From the intensive experimental investigations on the cyclic load-deformation behavior of thin tubular beam-columns, remarkable results have been obtained in the recent(Fukumoto et al., 1985a/b, PWRI, 1984, Watanabe et al., 1988, Kanou, 1989 and Shimizu, 1989). When cyclic loads are applied, the plate/shell elements such as flanges and webs, are subjected to the alternating cyclic stress/strain. Consequently ,the effect of local deformation due to instability of plate/shell elements on the overall load-deformation relationship of the entire member has been discussed. Fukumoto et al.(1985a,b) have shown the cyclic buckling of plate elements and box members by a series of experiments. They indicated a fact that the strength and stiffness of members become smaller as the number of cycles increases after its ultimate strength is reached. This is so called a brittle type of failure the steel structure might suffer in the severe loading environment in case of insufficient ductility. Authors(Watanabe et al., 1988) also have conducted a series of experiments on the cyclic behavior of thin-walled steel members, namely stiffened box member, under alternating bending and a constant axial compressive force.

In the present study, the emphasis is placed on the effectiveness of the round corners for ductility considering the effect of presence of axial compressive force, in order to evaluate the cyclic performance of tubular beam-columns, and also to provide the basic cyclic characteristics for the design criteria.

II. DESCRIPTION OF EXPERIMENTS

According to the 1973/1980 JSHB code, the axial compressive stress, σ_c, and the compressive bending stress, σ_{bc}, must satisfy the following inequality:

$$\frac{\sigma_c}{\sigma_{ca}} + \frac{\sigma_{bc}}{\sigma_{ba}} \leq 1 \qquad (1)$$

where σ_{ca} and σ_{ba} refer to the allowable axial compressive stress and bending compressive stress, respectively. Nakai et al.(1982a,b) have surveyed the proportion of σ_c and σ_{bc} for 88 steel rigid fame bridge piers(such as shown in Fig. 1 schematically) in Osaka area, which have been already constructed based on 1973 JSHB Code.

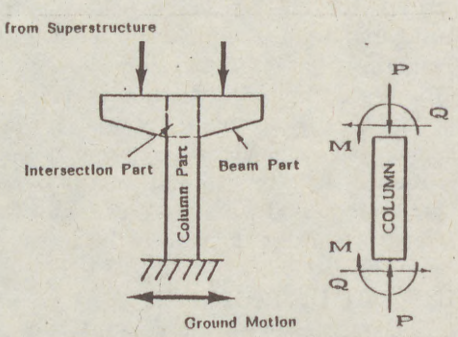

Fig. 1 T-shaped Steel Bridge Pier

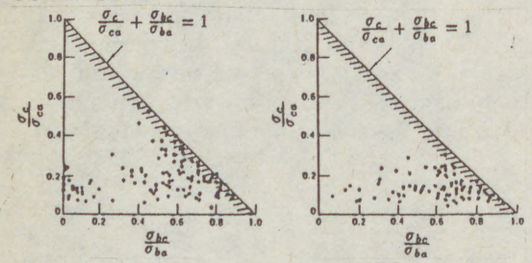

(a) in-plane (b) out-of-plane

Fig. 2 Proportion of Axial/Bending Stresses

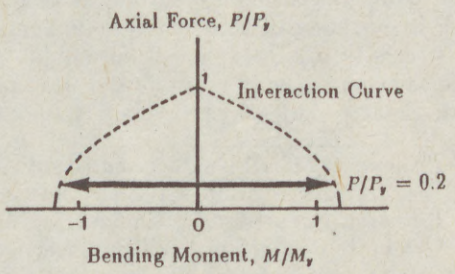

Fig. 3 Loading Sequence in This Test

(3)

Fig. 2 illustrates their results showing the correlations of axial stresses due to axial compressive force (mainly due to the weight of superstructure) and bending moment(due to lateral force such as seismic and wind forces). It is observed that the values of σ_c/σ_{ca} scatter about 0.2 and that the values of σ_{bc}/σ_{ba} scatter uniformly between 0 and 1.0. Taking these observations into consideration, the test specimens are designed, and subjected to the cyclic bending with the constant axial thrust of $P/P_y = 0.2$ as shown in Fig. 3, where P_y is the yielding axial force. In addition, the cyclic bending without axial compression is also applied to single out the effect of presence of axial compressive force on the cyclic bending characteristics of strength and ductility.

The test specimens are classified into two types A(tubular with sharp corners) and B(tubular with round corners). In addition, among type B, three types(B1, B2 and B3) are classified again with respect to the difference of welding positions. The shapes and nominal dimensions of test specimens are shown in Fig. 4(generalized width-to-thickness ratio of plate/shell element: $R_f = \frac{B}{t_f}\sqrt{\frac{12(1-\nu^2)}{K_E\pi^2}\frac{\sigma_y}{E}}$ =1.01 for A-type and 0.63 for B-type; $R_w = \frac{D}{t_w}\sqrt{\frac{12(1-\nu^2)}{K_E\pi^2}\frac{\sigma_y}{E}}$ =1.17 for A-type and 0.79 for B-type; and $R_c = \sqrt{\sqrt{3(1-\nu^2)}\frac{\sigma_y}{E}}\frac{R}{t_c}$ =0.14 for B-type). These specimens were assembled from thin structural steel plates by welding and cold-forming, whose material properties were tested by No. 5 JIS standard test specimen(Young's Modulus:$E = 2.20 \times 10^6$ kgf/cm^2; Yielding Stress:$\sigma_y = 2521$ kgf/cm^2; Poisson's Ratio:$\nu = 0.292$; Ultimate Stress: $\sigma_u = 3781$ kgf/cm^2; and the strength increase by cold-forming was observed to be about 10%).

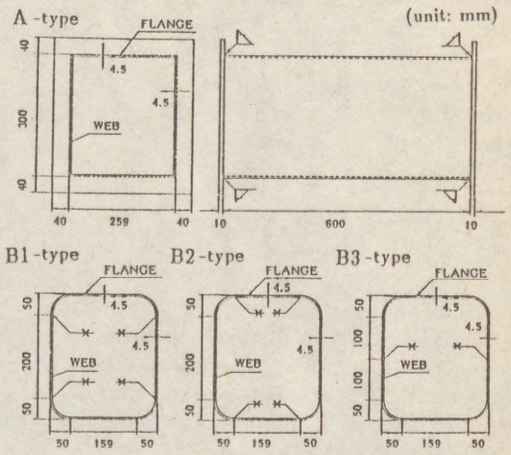

Fig. 4 Dimensions of Test Specimens

The residual stresses were measured for all types of specimens, using sectioning method to relieve longitudinal stresses by cutting the specimen into narrow strips across the cross section for half of section. Several results of measurement(A and B1 types) are illustrated in Fig. 5. It is obvious that the maximum magnitude of the tensile residual stress almost reaches the yielding stress at the welding lines, and also the maximum magnitude of the compressive residual stress is generally distributed almost uniformly at about $0.2 \sim 0.3\ \sigma_y$ between welding lines. The effect of cold-forming to make round corners on residual stress distribution is insignificant.

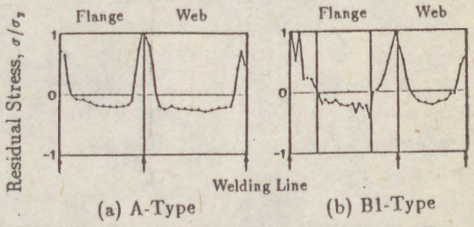

Fig. 5 Residual Stress Distribution

The testing set-up is shown in Fig. 6. The closed-loop servo-controlled hydraulic actuators are used to apply the constant axial force and cyclic bending on the specimen. The specimen connected with nondestructive beam-columns at both ends by high tension bolts, is set as a simple beam on the testing bed(roller supports) and subjected to cyclic lateral loads at two points vertically, so that the test specimen is considered to have an uniform alternating bending moment. The axial compressive force is applied as its reaction force

(4)

from tensioning the PC bar installed inside the specimen. Here, the application of the axial compressive force is manually controlled and set to be a constant value(either $0.0P_y$ or $0.2P_y$) from the beginning to the end of test, and that of the alternating bending is controlled by microcomputer to trace the specific average curvature-time history, namely ramp-wave with a constant amplitude. The details of this automated structural testing system at Kyoto University, can be referred to references(Niwa et al., 1983 and Kanou, 1989).

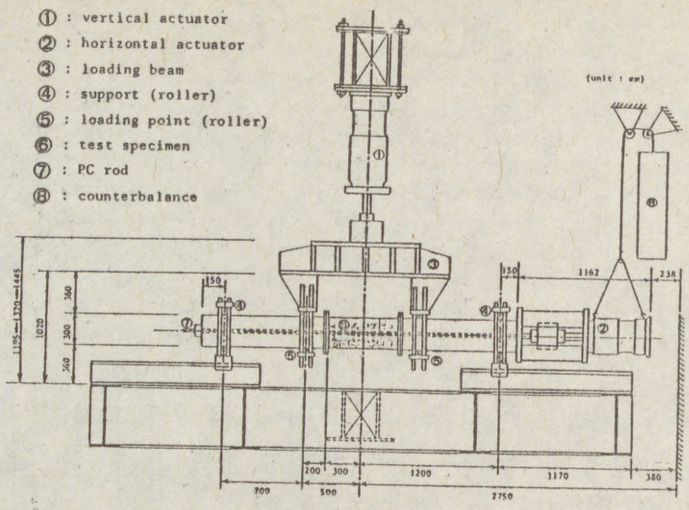

Fig. 6 Testing Set-up

III. PRELIMINARY INVESTIGATION OF ROUND CORNER EFFECT

The general-purpose finite element program, MSC/NASTRAN, is used to investigate the basic characteristics, such as strength and ductility, of the tubular beam-column segment with sharp edges and round corners subjected to monotonically increased biaxial loads, namely bending and axial compressive force.

Considering the symmetry of geometry of test specimen, loading, etc., the quarter section of test specimen is analyzed as shown in Fig. 7. In order to give uniform bending to the test section, the rigid body is connected at both ends of test section and its vertical displacement at point, "I", is controlled. The isoparametric shell element is used and the descretization of analyzed section of tubular with sharp corners and round corners is shown in Fig. 8.

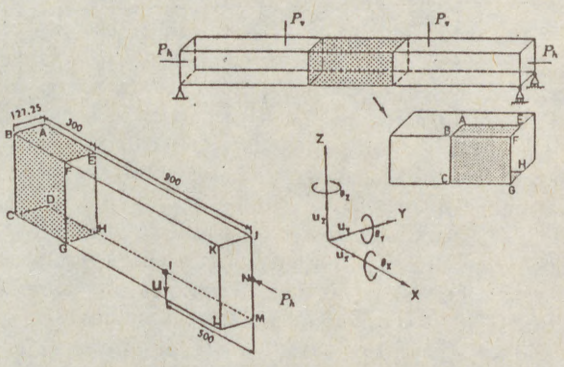

Fig. 7 Finite Element Modeling of Test Specimens

The material property is assumed to be elastic-perfectly plastic(σ_y = 2400 kgf/cm^2; $E = 2.1 \times 10^6$ kgf/cm^2; $\nu = 0.3$; and Von Mises criterion as yielding condition for biaxial stress state is employed).The computation was made for cases of a) bending only, b)~d) bending under constant axial compressive force(P/P_y=0.2, 0.33 and 0.5), and e) axial compressive force only.

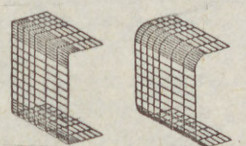

Fig. 8 Mesh of Analyzed Model

Fig. 9 shows the relationships of bending moment vs. curvature and the axial compressive force vs. axial short-

ening for both types of cross sections under given biaxial loading histories, a) to e). Here, bending moment, curvature, axial force and axial shortening are normalized by their yielding values, M_y, ϕ_y, P_y and ϵ_y respectively. It is obviously understood that the deformation capability after the ultimate state has been reached is improved by placing the round corners. In cases of a), b), c) and d), the bending deformation at peak bending moment for round corner is larger than that for sharp edge, and strength deterioration after the peak for round corner is less significant than that for sharp edge. The difference of deformation capability between two cross sections seems to be larger under the larger axial compressive force. In case of e), the sharp peak is not observed for round corner; on the other hand, the sudden drop of bending moment is obtained for sharp edge. The interesting point here is that the shortening of beam-column segment occurs under the monotonically increased bending deformation and its magnitude for round corners is relatively smaller than that of sharp edges. These observations are mainly due to the smaller width-to-thichness ratio of flat portion of flange/web elements in case of round corners.

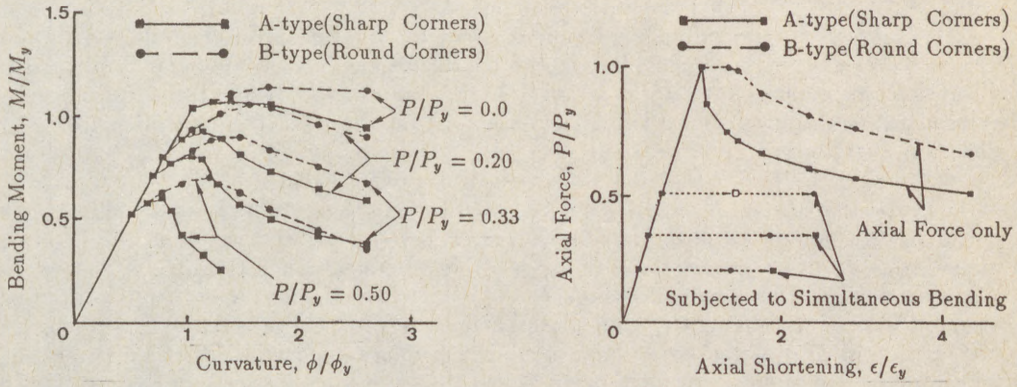

(a) Bending Moment-Curvature (b) Axial Force-Shortening

Fig. 9 Load-Deformation Curve of Tubular Beam-Columns

The interaction curves for both cross sections are shown in Fig. 10. It shows that the advantage of placing round corners for thin tubular beam-columns in terms of strength, may be significant in the case of bending. Although the absolute load-carrying capacity may decrease(considering smaller 2nd moment of inertia), the tubular with round corners may lead to the economical use of material strength(yielding strength) and the more ductility after its ultimate state is expected. Therefore, this type of cross section may be prefered for structures which are required to have large ductility, such as aseismic structures.

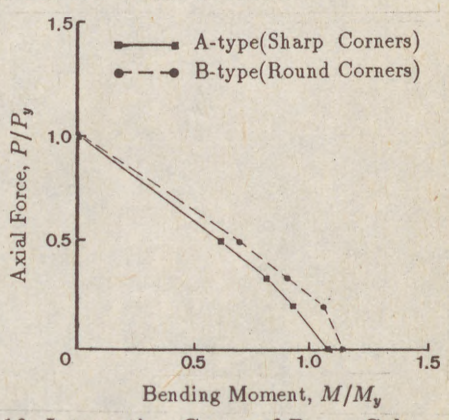

Fig. 10 Interaction Curve of Beam-Columns

IV. TEST RESULT AND DISCUSSION

Fig. 11 is showing the bending moment(M)-curvature(ϕ) relationships for the tubular section with sharp corners(A-1) and that with round corners(B1-1) under monotonically increased bending with constant axial compressive force($0.2P_y$), where the bending mo-

ment and curvature are normalized by their yielding values, M_y and Φ_y, respectively. It can be understood from this comparison that the ductility after the ultimate strength has been reached is improved by placing round corners, where the definition of ductility used here is how much deformation can be undertaken without losing large amount of strength. Although the absolute load-carrying capacity may slightly decrease by placing round corners(2nd order moment of inertia is smaller), this ductility improvement is attractive on the aseismic design viewpoint of the structures.

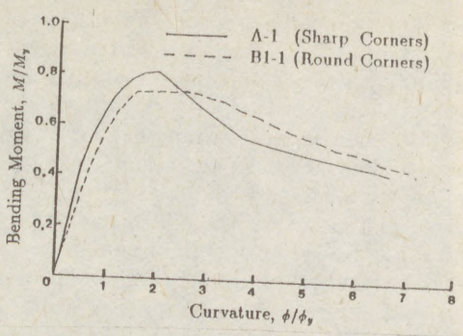

Fig. 11 Monotonic Bending Moment-Curvature Curve

Fig. 12 shows the cyclic bending moment-curvature relationship for A1 type(A-2) and B1 type(B1-2) of test specimens, where the curvature cycle with constant amplitude is applied until an approximate stabilization of loop is attained and then the amplitude was increased for next curvature cycles. It is observed that the peak bending moment under a constant curvature amplitude cycle could be stabilized quite rapidly and maintained during several cycles before the ultimate strength has been reached(5th cycle of ϕ/ϕ_y=1.42 for A-2 and 11th cycle of ϕ/ϕ_y=2.47 for B1-2) even though there exists a local yielding with stress redistribution of the initial residual stress cycle by cycle; whereas, the peak bending moment steadily decreases as the number of cycles increases once the ultimate strength has been reached. This result may suggest the development of new design phylosophy of aseimic structures assembled by thin plate/shell elements: The ultimate strength under static/monotonically increased loads is not always guaranteed and either post-buckling strength or deformability beyond this ultimate state is important to assess the safety of structures under severe loadings.

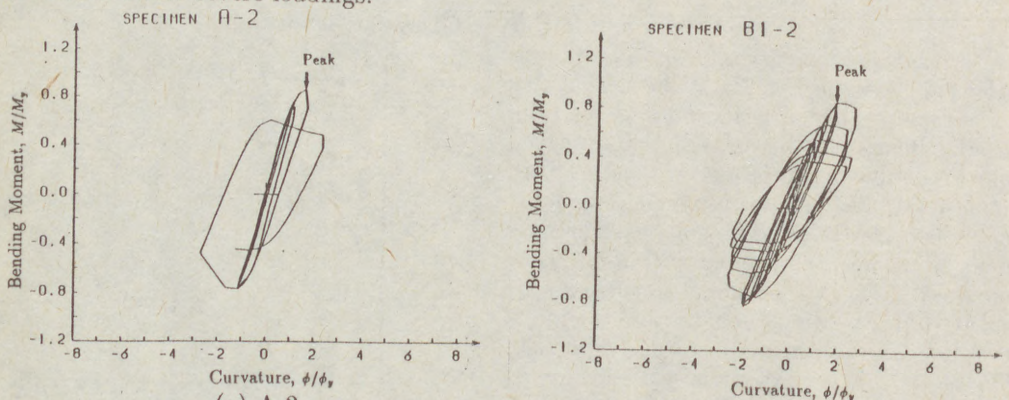

(a) A-2 (b) B1-2

Fig. 12 Cyclic Bending Moment-Curvature Curve

Fig. 13 shows the mode/magnitude change of out-of-plane deformation of plate/shell elements(Flange 1:lower; Web 1 and Flange 2:upper) during cyclic loading tests(A-2 and B1-2). The magnitude of out-of-plane deformation is normalized by its maximum value at each measurement. It is observed that the magnitude of out-of-plane deformation before the ultimate state is reached is as small as its initial value, but it began to concentrate within small area and increased rapidly after the ultimate strength was obtained.

Here, the deterioration of strength under cyclic loadings may be called as "generalized low-cycle fatigue" of thin steel tubular

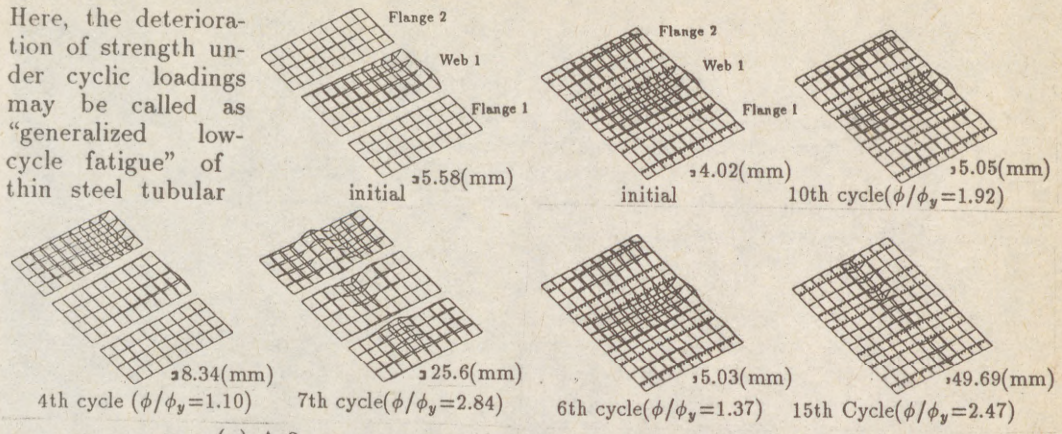

(a) A-2 (b) B1-2

Fig. 13 Mode/Magnitude of Out-of-Plane Deformation

structural members including local instability. This phenomena is a result of local buckling of plate elements subjected to in-plane compressive stress so that the presence of axial compressive force is considered to affect the strength and post-buckling strength of structures.

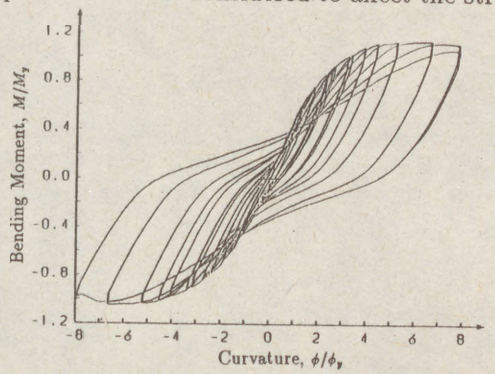

(a) P/P_y=0.0

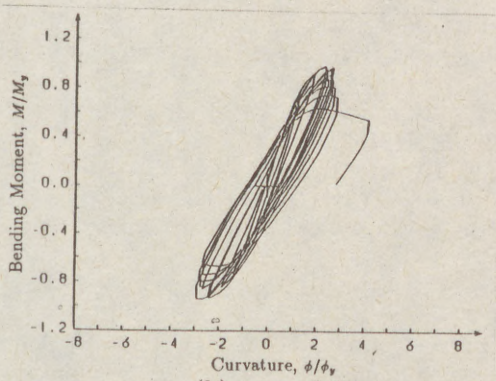

(b) P/P_y=0.2

Fig. 14 Bending Moment-Curvature Curve (B2-type)

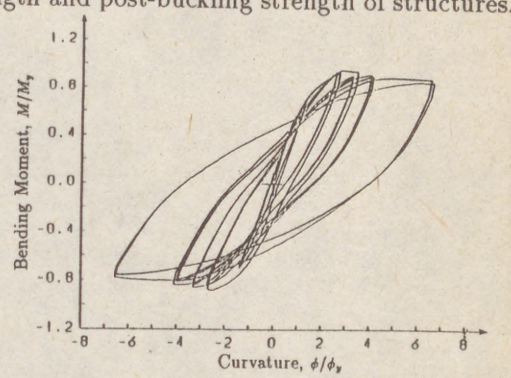

(a) P/P_y=0.0

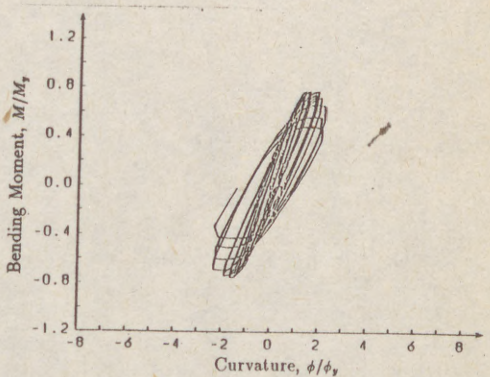

(b) P/P_y=0.2

Fig. 15 Bending Moment-Curvature Curve (B3-type)

(8)

This can be explained by Figs. 14 and 15 showing the cyclic curves of B2/B3 test specimens with/without axial compressive force. When the axial compressive force is not acting, the peak bending moment could be maintained even under relatively large curvature(the stiffness may decrease). On the contrary, the peak bending moment would decrease cycle by cycle in case of the presence of axial compressive force. Although Fukumoto et al.(1985b) have shown a case of cyclic deterioration of peak bending moment inspite of no axial compressive force, this is why they used relatively large plate width-to-thickness ratio compared with the present test specimens.

V. CONCLUSIONS

The basic characteristics of the inelastic behavior of steel tubular beam-columns under alternating bending and constant axial compressive force has been investigated analytically and experimentally in order to provide the basis as the ultimate/limit state design criteria.

Special attention has been placed on the effectiveness of the use of round corners to improve ductility which is one of important design considerations for aseismic structures. The tubular with round corners can improve the ductility without a significant loss of strength. The deterioration of strength and ductility under the presence of axial compressive force was profound and it can be considered as low-cycle fatigue of structures considering the local instability.

REFERENCES

Fukumoto, Y. and Kusama, H., 1985a, "Local Instability Tests of Plate Elements under Cyclic Uniaxial Loading," Journal of Structural Engineering, ASCE, Vol.111, No.5, pp.1051–1067.

Fukumoto, Y. and Kusama, H., 1985b, "Cyclic Bending Tests of Thin-walled Box Beams," Proc. of JSCE, Structural Engng./Earthquake Engng., Vol.2, No.1, pp.141–151.

Japan Road Association, 1973, 1980, "Specifications for Highway Bridges(JSHB)," Tokyo, Japan(in Japanese).

Kanou, M., 1989, "The Study on Strength and Ductility of Steel Piers subjected to Cyclic Bending," M.S. Thesis, Kyoto University, Kyoto, Japan(in Japanese).

MSC/NASTRAN, "User's Manualls and Application Manuals"

Nakai, H., Kawai, A., Yoshikawa, O., Kitada, T. and Miki, T., 1982a, "A Survey on Steel Rigid Frame Bridge Piers:part 1," The Bridge and Foundation Engineering, Vol.16, No.6, pp.35–40(in Japanese).

Nakai, H., Kawai, A., Yoshikawa, O., Kitada, T. and Miki, T., 1982b, "A Survey on Steel Rigid Frame Bridge Piers:part 2," The Bridge and Foundation Engineering, Vol.16, No.7, pp.43–49(in Japanese).

Niwa, Y., Watanabe, E. and Isami, H., 1983, "Automated Structural Testing using Microcomputer system," Proc. of JSCE, No.332, pp.145–158.

Public Works Research Institute(Ministry of Construction), 1984, "Perfectly Alternating Loading Tests on Steel Pier Models,", P.W.R.I. Report No.2147(in Japanese).

Schaeffer, H.G., 1972, "MSC/NASTRAN Primer: Static and NOrmal Modes Analysis," Schaeffer Analysis, Inc., New York, U.S.A.

Shimizu, H., 1989, "Hybrid Experiments of Steel Box-type Bridge Piers," M.S. Thesis, Kyoto University, Kyoto, Japan(in Japanese).

Watanabe, E., Emi, S., Isami, H. and Yamanouchi, T., 1988, "An Experimental Study on Strength of Thin-walled Steel Box Beam-columns under Repetitive Bending," Proc. of JSCE, Structural Engng./Earthquake Engng., Vol.5, No.1, pp.21–29.

SESSION 11

SHELLS

(1)
ANDRIANOV, Igor (1)
VERBONOL, Vladimir (2)

STRINGER SHELL STABILITY INVESTIGATION WITH UNDERCRITICAL STATE IN NONAXISYMMETRIC BENDING MOMENTS CONSIDERATION

INTERNATIONAL COLLOQUIUM
STABILITY OF STEEL STRUCTURES
BUDAPEST, HUNGARY, 1990
PRELIMINARY REPORT

Summary: Experimental study of the behaviour stringer shell, under longitudinal stress (Costirko V., Crasovsky V., 1988) shows that their undercritical deformation is essentially momentous both in longitudinal and critical directions, thus differing form the isotropic case. In many cases the main cause of the considerable differences in experimental value of critical load and teoretical calculation based on hypothesis on axisymmetric of undercritical condition is neglection of specific features of undercritical deformation. We shoud stress that experiments under study were held on samples with littl initial geometrical imperfection, besides the choise of sample typesize was made in such a way that the effects of coupled buckling were excluded. In the present paper the study of stringer shell stability taking into account bending moments

(1) Candidate of physics and mathematics, Institute of Civil Enginering, Dnepropetrovsk
(2) Candidate of Technical Sciens, Institute of Chemistry and Technology, Dnepropetrovsk.

(2)

of nonlinear and nonaxisymmetric undercritical condition was made with the help of asymptotic approuch. Thus it differs form the kmown numerical solutions. Boundaries of application of the simplified design model have been determined.

Undercritical state is described by Sanders equations, stringers are considered as Kirchof's bars with tension-compression (EF_1) and flexural (EJ_1) rigidities and eccentricity e_1 relatively the median surface of the casing.

If a shell is effectively stable during axial compression it is characterized by the following estimates

$$\varepsilon=\frac{1}{k}\sim a^{1/2},\quad \varepsilon_1=\sqrt{\frac{D_{11}}{B_{22}R^2}}\sim a^{1/2},\quad \varepsilon_2=\frac{D_{22}}{D_{11}}\sim a^{3/4},\quad \varepsilon_3=\frac{D_{33}}{D_{11}}\sim a^{3/4},$$
$$\varepsilon_4=\frac{B_{22}}{B_{11}}\lesssim 1,\quad \varepsilon_5=\frac{B_{33}}{B_{11}}\lesssim 1,\quad \varepsilon_6=\frac{e_1}{R}\sim a^{1/2}. \qquad (1)$$

Here k - is the number of the stringers, D_{11}, D_{22}, D_{33}, B_{11}, B_{22}, B_{33} - rigidities of stiffened shell, $a=h/(\sqrt{12}R)$.

Undercritical deformation problem is asympthotically splitted to the average problem (which describes the axisymmetric component of the stress-strain conditions) and the local problem - on the stiffeners' spacing.

The average problem solution consists of the solution without moments and of the non-linear fringe effect

$$w_0=\exp(-b_2\xi)(C_1\sin b_1\xi+C_2\cos b_1\xi)+\exp[b_2(\xi-l)]\times$$
$$\times[C_3\sin b_1(\xi-l)+C_4\cos b_1(\xi-l)+TR\nu_{21}/B_2.$$

Where $b_i=0.5\left[RD_1^{-1}(2D_1^{1/2}B_2^{1/2}+(-1)^i T'R)\right]^{1/2};\ i=1,2;$

$$T'=T-\frac{2K_{11}\nu_{21}}{R},\quad B_2=B_{22}(1-\nu\nu_{21}),\quad \nu_{21}=\frac{\nu B}{B_{11}},$$
$$D_1=D_1-\frac{K_{11}^2}{B_{11}},\quad K_{11}=k\frac{EF_1e_1}{2\pi R},$$

T - axial compression, C_1 - C_4 - const.

(3)

The local fringe problem solution also consists of two components. The first component describes the bending of the panel between the ribs.

$$
\begin{aligned}
w_1 &= \frac{1}{\pi a^2 k^3}\left(\gamma\frac{\partial^3 u_0}{\partial\xi^3} - \alpha\frac{\partial^4 w_0}{\partial\xi^4}\right) F_4(\eta),\\
u_1 &= \frac{2}{\pi k(1-\nu)}\left(\beta\frac{\partial^2 u_0}{\partial\xi^2} - \gamma\frac{\partial^3 w_0}{\partial\xi^3}\right) F_2(\eta) -\\
&- \frac{2\nu}{\pi(1-\nu)k^5 a^2}\left(\gamma\frac{\partial^4 u_0}{\partial\xi^4} - \alpha\frac{\partial^5 w_0}{\partial\xi^5}\right) F_6(\eta),\\
v_1 &= -\frac{1+\nu}{\pi k^2(1-\nu)}\left(\beta\frac{\partial^3 u_0}{\partial\xi^3} - \gamma\frac{\partial^4 w_0}{\partial\xi^4}\right) F_3(\eta) +\\
&+ \frac{1}{\pi k^4 a^2}\left(\gamma\frac{\partial^3 u_0}{\partial\xi^3} - \alpha\frac{\partial^4 w_0}{\partial\xi^4}\right) F_5(\eta) +\\
&+ \frac{\nu(1+\nu)}{\pi k^6 a^2(1-\nu)}\left(\gamma\frac{\partial^5 u_0}{\partial\xi^5} - \alpha\frac{\partial^6 w_0}{\partial\xi^6}\right) F_7(\eta).
\end{aligned}
\qquad (2)
$$

Here

$$
\alpha = \frac{EJ_1}{BR^3}, \quad \beta = \frac{EF_1}{BR}, \quad \gamma = \frac{EF_1 e_1}{BR^2};
$$

$$
F_{2n}(\eta) = \frac{(-1)^{n-1}(2\pi)^{2n}}{2(2n)!} B_{2n}(\varphi_1), \quad F_{2n-1}(\eta) = -\frac{dF_{2n}(\eta)}{d\varphi_1},
$$

$$
\varphi_1 = \frac{k\eta}{2\pi}, \quad F_i(\varphi_1) = F_i(\varphi_1 + m), \quad i = 1,2,\ldots,7;
$$

$$
m = 1,2,\ldots,k; \quad B_{2n}(\varphi_1) = \sum_{j=1}^{\infty}\frac{1}{j^{2n}}\cos j^{2n}\varphi_1 .
$$

The second component - the stress conditions locatized beside the fringe - is described by the linear equations of the bending and of the plane stressed condition of the semi-strips fixed on the ribs. The evident form of the component is found with the help of Cantorovitch method.

The asympthotic splitting made it possible to have the simplified stability equations (lines above symbols signify variations).

(4)

$$\frac{K_{11}}{R}\left[\frac{\partial^3 \bar{u}_0}{\partial \xi^3}+\frac{1}{R}\frac{\partial \bar{w}_0}{\partial \xi}\frac{\partial^3 w_0}{\partial \xi^3}\right]-\frac{D_{11}}{R^2}\frac{\partial^4 \bar{w}_0}{\partial \xi^4}-\frac{D_{22}}{R^2}\frac{\partial^4 \bar{w}_0}{\partial \eta^4}+$$

$$R\bar{N}_{22}+\frac{\partial^2 \bar{w}_0}{\partial \xi^2}N_{11}+\frac{\partial^2 w_0}{\partial \xi^2}\bar{N}_{11}+\frac{\partial^2 \bar{w}_0}{\partial \eta^2}N_{22}+\frac{\partial \bar{w}_0}{\partial \eta}\frac{\partial N_{22}}{\partial \eta}=0,$$

here

$$\bar{N}_{11}=\frac{B_{11}}{R}\left(\frac{\partial \bar{u}_0}{\partial \xi}+\frac{1}{R}\frac{\partial w_0}{\partial \xi}\frac{\partial w_0}{\partial \xi}\right)-\frac{K_{11}}{R^2}\frac{\partial^2 \bar{w}_0}{\partial \xi^2},$$

(3)

$$\bar{N}_{22}=\iint\frac{\partial^2 \bar{N}_{22}}{\partial \xi^2}\,d\eta\,d\eta,$$

$$\frac{\partial \bar{u}_0}{\partial \xi}=-\iint\frac{\partial^2 \bar{w}_0}{\partial \xi^2}\,d\eta\,d\eta-\frac{1}{R}\int\frac{\partial^2 w_0}{\partial \xi^2}\frac{\partial \bar{w}_0}{\partial \eta}\,d\eta+$$

$$+\iint\frac{\partial^3 w_1}{\partial \eta\,\partial \xi^2}\frac{\partial \bar{w}_0}{\partial \eta}\,d\eta\,d\eta.$$

Fringe conditions for equation (1) are:

C1 - C4 : $\bar{w}=0,\quad \bar{\theta}_1=0;$

S3, S4 : $\bar{w}=0,\quad \bar{M}_{11}=0.$

The desired values $\bar{w}$ and T are expressed as expansions:

$$\bar{w}=\bar{w}_0+\varepsilon^{1/2}\bar{w}_1+\varepsilon\,\bar{w}_2+\dots$$

$$T=T_0+\varepsilon^{1/2}T_1+\varepsilon\,T_2+\dots$$

Then the disturbance method combined with the Galerkin method is used.

The design diagram in which the undercritical deformation is considered with regard to stiffeners' discreteness and the buckling is considered within the limits of constructional orthotropic theory with the help of equations (1). The members which contain the inaxisymmetrical components of undercritical stress-strain condition are small, if

$$k^4 \gg a^2 \qquad (4)$$

(5)

The next design models are marked out:

Design models		Undercritical deformation characteristic	Design diagram	
			Undercritical deformation	buckling
I		no moments	constructional orthotropy	constructional orthotropy
II		axisymmetrical bending	- " -	- " -
III	a	inaxisymmetrical bending	stiffeners' discreteness consideration	- " -
	b			stiffeners discreteness consideration

If one takes into account the discontinuity which is conditioned by the stiffeners' discreteness the analysis demonstrates the stringer bending: in the direction of the shell surface external normal vector if the stiffeners are external or in the direction of the internal normal vector if the stiffeners are internal (Fig.1).

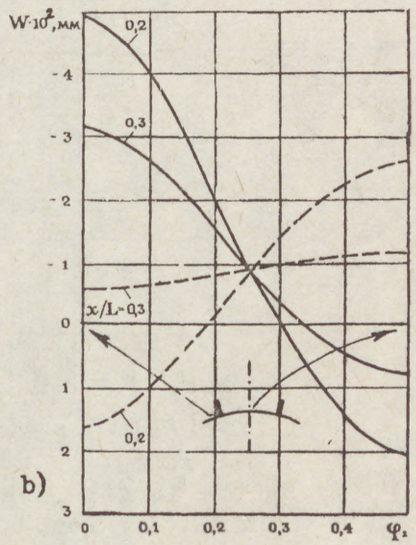

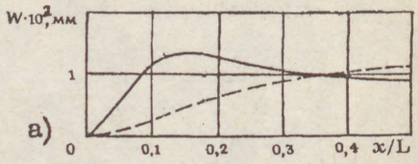

Fig.1.

Undercritical sags for axisymmetric (a) and in axisymmetric (b) undercritical deformation (design model II, III).

(6)

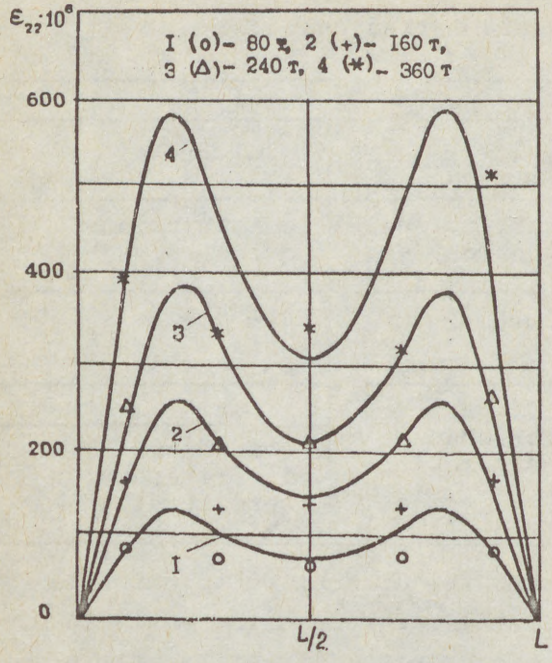

Fig.2. Appliability of desifn model III is also illustrated by its comparison with the experiment data. (Dowling P.J. and others, 1982).

The effect of undercritical bending is greater when the flexural rigidity of stiffeners and the eccentricity of compressive load are higher or the relative length of the shell is smaller. Then the assumption of undercritical state axial symmetry is quantitatively and qualitatively inadequate.

The most pronounced effect of inaxisymmetric bending moments will be when the specimens with external stiffeners have hinge supports and only the casing is externally loaded (Fig.3).

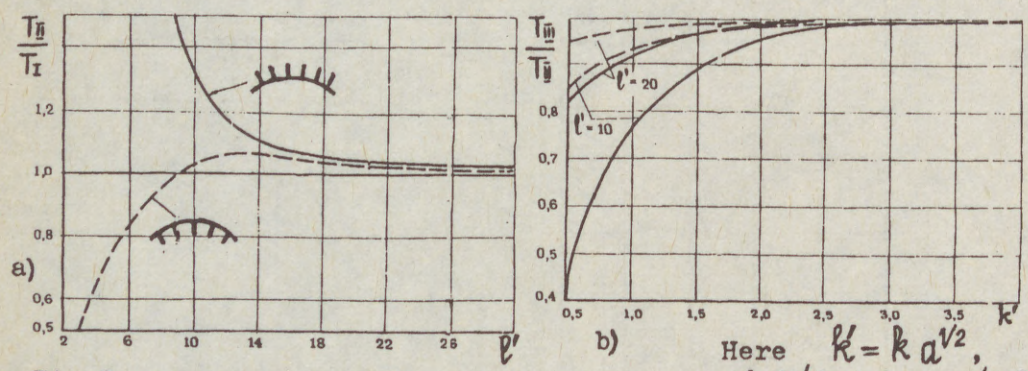

Fig.3.
Critical load values relationships for different undercritical deformation models and for middle stiffened specimens ($\varepsilon_2^{-1}=500$, $\varepsilon_4^{-1}=1.8$)

Here $k'=k\,a^{1/2}$, $l'=l/l_f$, ($l_f=a^{1/2}\varepsilon_2^{-1/4}$ - estimation of the length of fringe effect zone)

(7)

The stability of inaxisymmetric undercritical bending which is conditioned by the stiffeners discreteness is effected slightly if

$$k > (1.5 \div 2)\, a^{-1/2} \qquad (5)$$

and the effect of longitudinal bending is small when

$$l > (15 \div 18)\, a^{1/2}\, \varepsilon_2^{-1/4} \qquad (6)$$

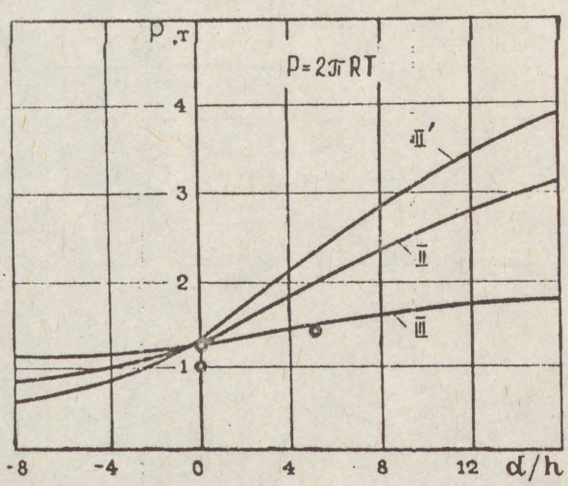

Fig.4. The relationship of critical load and load eccentricity ($\varepsilon_2^{-1} = 1236$, $\varepsilon_4^{-1} = 2{,}3$)

- when only longitudinal undercritical bending is taben into account
  - II' - finite differences analysis method
  - II - the proposed analysis method (design model II);
- when longitudinal and circular undercritical bendings are taben into account
  - III - the proposed analysis method (design model IIIb)
  - o - experiment data.

When $k=36$, $l=L/R=1.12$ ($k'=0.68$, $l'=6.8$) and the loading is inaxisymmetric (Fig.4) the error caused by disregard of the bending in the circular direction will be around 300% for sags if the load eccentricity $d=5h$, some 28% for critical load and the error increases with the eccentricity (Fig.4).

(8)

It was shown that critical loads would be effected more seriously by the stiffeners' discreteness in undercritical state than by variant components if

$$\ell \gg a^{1/2} \qquad (7)$$

The analysis makes it possible to formulate the stringer shell main parameters' estimates which define the applicability limits of design models:

Design models	I	I	III	
			a	b
Construction parameters estimates (relationship number)	(1) (5) (6)	(1) (5)	(1) (7)	(1)

Костырко В.В., Красовский В.Л., 1988. Исследование влияния эксцентриситета приложения осевой сжимающей нагрузки на устойчивость стрингерных оболочек. Гидроаэромеханика и теория упругости. С. 75-81.

Dowling P.J., Harding T.E., Agelidis N., Fany W. 1982, Buckling of ortogonally stiffened cylindrical shells used in offshore engineering. Buckling of shell: Proc. of a state - of - the - Art Collogium, P. 239.

(1)
EGGWERTZ , Sigge (1)
SAMUELSON, Lars Å (2)

DESIGN OF SHELL STRUCTURES WITH OPENINGS SUBJECTED TO BUCKLING

INTERNATIONAL COLLOQUIUM
STABILITY OF STEEL STRUCTURES
BUDAPEST, HUNGARY, 1990
PRELIMINARY REPORT

Summary:

Shell structures are often designed to carry compressive loads which may cause buckling. Openings and cutouts in the shell are known to reduce the carrying capacity, sometimes to a substantial degree. Although extensive research has been devoted to the problem, very few attempts have been made to incorporate the results into existing design codes. One reason for this may be the fact that even the design of simple shell elements under uniform loading conditions is complex and the emphasis has been to develop design methods for these standard cases. The present paper discusses a number of problems associated with cutouts in shells subjected to buckling. Simple design rules are proposed based on theoretical (finite element analysis or equivalent) and experimental results.

1. Introduction

The various problems associated with shell stability analysis have attracted enormous attention during the last decades. Since the shell theory leads to very complex equations general closed form solutions exist only for very restricted problems. In the design codes, most of the available data are, therefore, based on test results. This policy is reasonable in cases of shells of uniform thickness and subjected to uniform load distributions, but may not be applicable to structures where, for instance, external disturbances dominate the picture. Such disturbances may be caused by holes and cutouts in the shell.

---

(1) Professor, Bloms Ingeniörsbyrå, Sundbyberg, Sweden
(2) Professor, The Swedish Plant Inspectorate, Stockholm

(2)
Several investigators have studied the behavior of shells with cutouts, primarily through extensive testing. A comprehensive summary of the literature was given by Knödel and Schulz,1985, and the reader is referred to their paper for a reasonably complete list of available results. The report also discusses possible methods for design of shells with respect to the influence of the hole. For the sake of brevity, only a few of the more important investigations will be summarized in the present report.

In the case of **circular** openings in elastic cylindrical shells, the tests show that the reduction in the load carrying capacity is a deterministic function of the hole diameter. The effect of plastic strains in the vicinity of the hole has not yet been satisfactorily investigated. Tests on shells with reinforced openings indicate that the reinforcement may restore the carrying capacity of the shell to a level equal to that of the shell without a hole provided the hole diameter does not exceed about 20 percent of the cylinder diameter.

Rectangular openings provide a more complex problem and, the design of the shell against instability should be based on slightly different criteria. If the behavior of the shell is well understood, the design of an adequate stiffening arrangement should, however, be straight-forward.

The present paper discusses some of the results presented in the literature in view of a proposed design procedure. Finite element analyses are carried out in order to verify the assumed stress distribution at the edge of the hole and to demonstrate the load carrying capacity reduction caused by the hole.

2. Summary of available results

The work by Knödel-Schulz, 1985, gives test results for cylinders under axial compression and bending, see Fig.1. The figure includes both circular and rectangular openings, which appears to be one of the reasons for the fairly high scatter in the test results. Limiting test results to circular openings, results according to Miller, 1982, Starnes, 1970, Tennyson,1968, and Toda, 1980, are shown in Fig 2, where the scatter is considerably less pronounced.

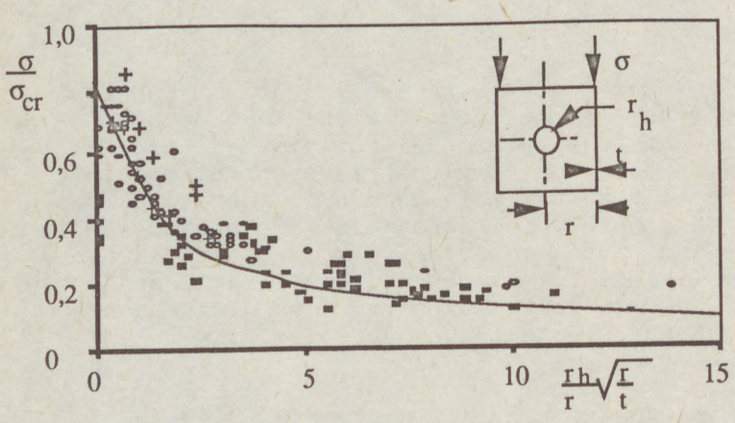

Fig. 1 Experimental buckling loads of cylinders with a hole and subjected to axial compression, according to Knödel-Schulz, 1985

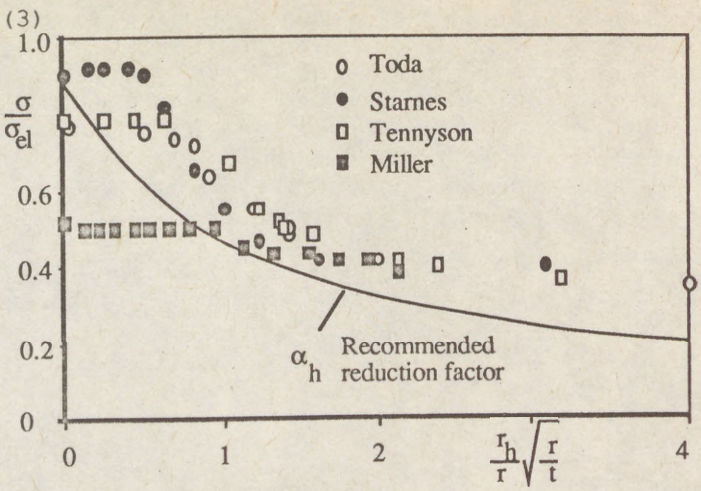

Fig. 2. Thinwalled cylinders with different hole sizes. Experimental buckling load divided by the classical buckling load.

Miller, 1982, also carried out tests on cylinders under internal or external pressure in combination with axial compression. In most of his tests he studied the influence of stiffening of the hole edge.

Rectangular cutouts are favored in some applications, such as chimneys and skirts carrying pressure vessels or process towers. Extensive testing of thinwalled cylinders in bending has been reported by Öry et al, 1984, who also studied the efficiency of various stiffening arrangements.

So far very little information is available on buckling in the elastic-plastic range and further tests using for instance mild steel specimens should be welcomed.

3. Numerical analysis

Since the effect of a cutout on the carrying capacity of a shell should be of a deterministic nature, finite element analysis of the buckling behavior appears to form a realistic approach. Moreover, the theory may easily be extended to include plasticity effects and thus give a better grasp of the entire process.

A cylindrical shell according to Fig.3 was subjected to axial compression. According to the classical theory, the buckling stress of the cylinder is:

$$\sigma_{el} = 0.6\ E\ \frac{t}{r} = 240\ \text{MPa} \qquad (1)$$

The carrying capacity of the shell would be according to the ECCS recommendations, 1987:

$$\sigma_u = 0.75 \cdot \alpha \cdot \sigma_{el} = 61\ \text{MPa}$$

where

$$\alpha = \frac{0.83}{\sqrt{1 + 0.01\ \frac{r}{t}}} = 0.339 \qquad (2)$$

Thus, buckling would not be affected by plasticity for the com-

(4)
plete shell provided the yield stress exceeds 200 MPa. A numerical analysis of the shell without hole was carried out by use of BOSOR4 in order to determine the natural buckling mode of the shell. The results are shown in Fig 4. Based on the results a portion of the cylinder was cut out for analysis by means of ANSYS. The mode, included in Fig 4, gave a buckling stress of σ_{el} = 243 MPa in good agreement with the classical and BOSOR4 values although the model apparently should be improved.

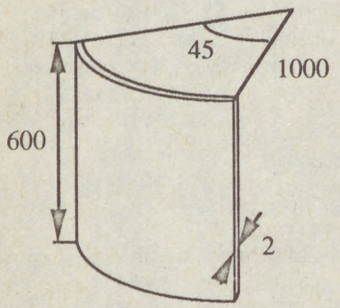

Fig. 3. Thin walled sample cylinder. Horisontal edges simply supported

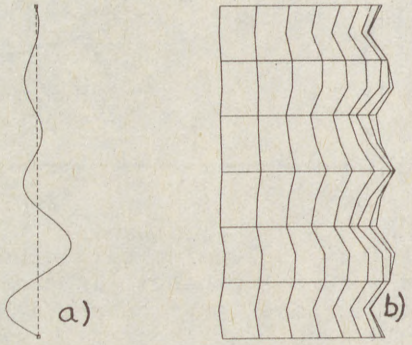

Fig. 4. Buckling modes of the sample cylinder according to **a)** BOSOR 4 and **b)** ANSYS

In the next step, a hole was modeled according to Fig.5. Both circular holes and rectangular cutouts were studied. A linear analysis was carried out in order to determine the stress distribution in the prebuckling state. Typical results are shown in Fig.6 and 7 for two different hole configurations. It may be noted that the stress level at the edge of the circular hole is usually of the order of 3, and the stress level in the rest of the shell is nearly uniform. In Fig. 6, K_T = 4 is observed. This is due to the fact that the load is applied as a uniform stress and not as a uniform displacement. The rectangular hole, however, creates a stress concentration in the shell itself which may cause local shell buckling. The effect is even more pronounced if the edge is reinforced.

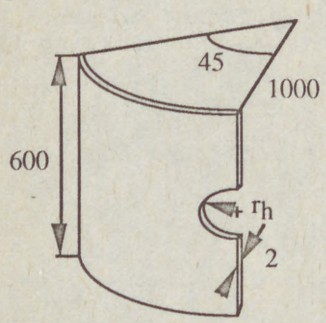

Fig. 5. Hole geometry

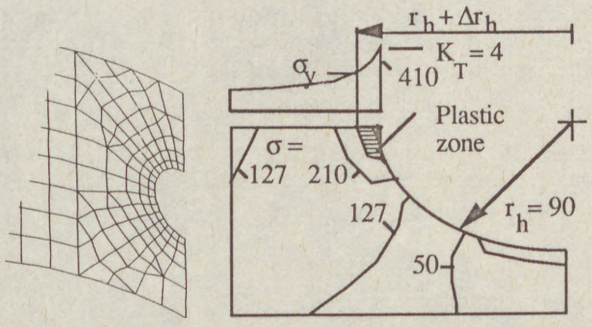

Fig 6. Model of cylinder with a hole and the resulting stress distribution around the large hole

(5)
Buckling analysis was carried out for the model given in Fig.6. Preliminary results show, however, that the critical stress is higher than the value indicated by the test results shown in Fig.1. For r_h=22.5, σ_{cr}=0.89 whereas $\alpha_h\sigma_{el}$=0.60 and for r_h=90 σ_{cr}=(0.42) and $\alpha_n\sigma_{el}$=0.32. This is a consequence of the fact that the buckling analysis is based on the linear prebuckling state. Since the local deflections in the vicinity of the hole will increase as the collapse load is approached, a reasonably accurate estimate of the buckling behavior can only be achieved through a nonlinear collapse analysis. Such analyses are being carried out at the present time (Sept 1989) and the results will be presented at the Tihany Conference.

Large openings are mostly stiffened and the different codes provide rules for the design of the stiffening system. The model shown in Fig.6 was reanalyzed with stiffening around the cutout edge as prescribed by the Swedish Pressure Vessel Code, 1987. The resulting stress distribution is shown in Fig.7a. It is evident that the stress concentration around the circular hole is practically eliminated by the reinforcement, while the stresses in the shell adjacent to the corner of the square cutout, Fig.7b, are of the order of twice the average membrane stress.

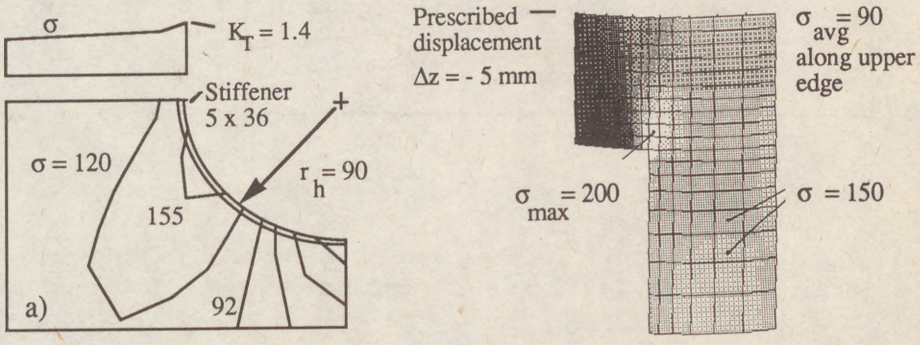

Fig. 7. Stress distributions around circular **a)** and rectangular **b)** reinforced cutouts in a cylinder under axial compression

4. Proposed simplified design procedure

Assume that the reduction of the carrying capacity of a shell under axial compression with a **circular** opening of radius r_h is independent of the imperfection distribution of the shell. Then it may be assumed that:

$$\alpha_h = f(r_h, r, l, t) \qquad (3)$$

A reasonable, lower bound curve is introduced in Fig.1. Not all test results fall above the curve, but most of the tests that do not, have a different geometry (rectangular) or other factors (plasticity) have influenced the results. The same curve is shown in Fig.2. The curve may be represented by the expression:

(6)

$$\alpha_h = \frac{0.83}{\sqrt{1 + 2.12(r_h/\sqrt{rt})^{1.4}}} \qquad (4)$$

Introduction of stiffening was shown to restore the carrying capacity of the shell considerably. Inspection of the data available indicates that a fully reinforced hole of diameter r_{hs} causes the same reduction as an unreinforced hole of radius $r_h = 0.4\ r_{hs}$. The reduction factor may be written as:

$$\alpha_{hs} = \frac{0.83}{\sqrt{1 + 0.588(r_h/\sqrt{rt})^{1.4}}} \qquad (5)$$

α_h and α_{hs} are shown in Fig.8 where some reduction factors α of the complete cylinder are indicated.

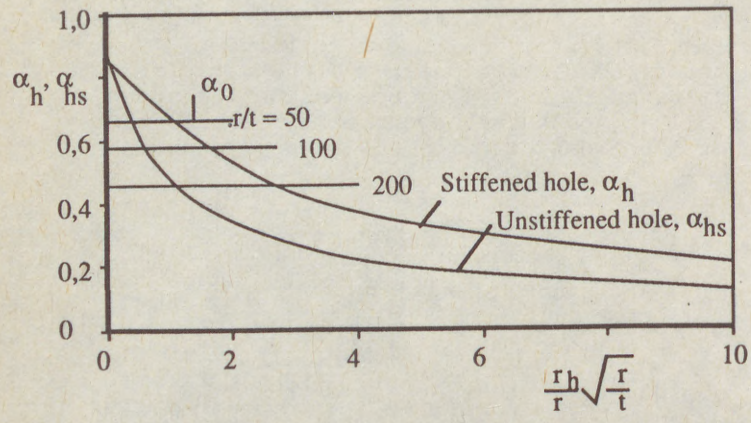

Fig. 8 Recommended design curves for cylinders with circular holes and subjected to axial compression

α_h and α_{hs} are applicable in the case of elastic buckling only. The reduction due to plasticity may be added in the following manner:

Assume that the design analysis provides a lower bound of the elastic (average) buckling stress of

$$\sigma_{elr} = \alpha_h\ \sigma_{el} \qquad (6)$$

An unreinforced circular hole causes a stress concentration factor of 3.0. This means that if $\sigma_{elr} \geq \sigma_y/3$, local plastic deformations will occur lowering the carrying capacity of the shell, see Fig.7. The reduction in the carrying capacity corresponds to that of a circular hole with an effective radius r_{eff} of

$$r_{eff} = r_h + \Delta r_y \qquad (7)$$

where Δr_y is the length of the plastic zone. r_{eff} is used to calculate a new value of the reduction factor η_{heff}. This factor is then used in Eq (4) without further iterations, and the carrying capacity is given by either of the two values.

(7)

$$\sigma_u = 0.75\alpha_h\sigma_{el} \qquad \text{if } \alpha_h\sigma_{el} \leq f_y/2 \quad \text{or} \tag{8}$$

$$\sigma_u = f_y\left[1 - 0.4123\left(\frac{f_y}{\alpha_h\sigma_{el}}\right)^{0,6}\right] \qquad \text{if } \alpha_h\sigma_{el} \geq f_y/2 \tag{9}$$

Rectangular cutouts may be analyzed as follows: Since the horizontal edge is unloaded, the triangular section of the shell above the cutout is practically stress free. The load applied to the shell above the triangle then has to be shifted to the edges of the hole where a concentration of the loading is obtained., see Fig.9. The edge, unstiffened or stiffened must be able to carry the total force acting at the edge.

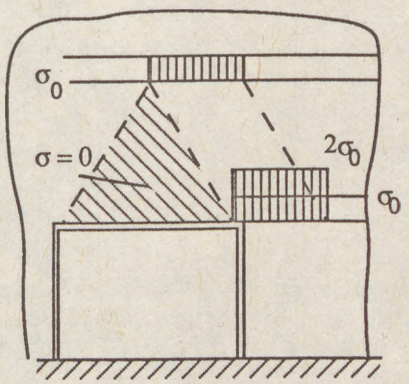

Fig. 9. Simplified model of stress distribution in the shell caused by a rectangular cutout

First, calculate the local stress in the shell at the corner from the assumption that the stress 'not carried by the hole' is shifted and added to the average stress at the corner. The local load is then equal to two times the average load and this value should be used to evaluate the buckling capacity of the shell.

Secondly, the vertical reinforcement must be designed for an axial force equal to: (b = the width of the cutout)

$$F = 2(b/2)t\sigma_0 \tag{10}$$

It should be noted that a reinforcing beam at the upper edge of the hole has to be extremely stiff in order to have any significant influence on the stress redistribution in the shell. See Knödel-Schulz, 1985, Öry et al, 1984, and Samuelson, 1985. While it is easy to design the vertical beam for the applied forces, the local stresses in the shell are often limiting factors with respect to the stability. Introduction of stiffening rings and stringers may be required, see discussion by Öry et al, 1984.

(8)

5. Discussion

A simple design procedure for cylindrical shells with circular and rectangular cutouts and subjected to axial compression is proposed based on classical theory and experimental and numerical (Finite Element) results. The method is as easy to use as the code formulas available for complete shells and should be a valuable tool for the practicing engineer. Further tests are required for final verification of the buckling behavior in the plastic range and slight changes may be required in the proposed formulas. Extension of the method to other types of shells and loading conditions should be easy to carry out.

REFERENCES

Almroth, B. O. and Holmes, A. M. C., 1972: Buckling of shells with cutouts, Experiments and analysis. Int. J. Solids & Structures, Vol. 8.

Knödel, P. und Schulz, U., 1985: Das Beulverhalten von biegebeanspruchten Zylinderschalen mit grossen Mantelöffnungen. Berichte Versuchsanstalt für Stahl, Holz und Steine, Karlsruhe, 4. Folge, Heft 12.

Miller, C. D., 1982: Experimental study of the buckling of cylindrical shells with reinforced openings. Chicago Bridge & Iron Company, CBT-5388, presented at ASME/ANS Nuclear Engineering Conference, Portland, Oregon.

Öry, H., Reimerdes, H.G. und Tritsch, W., 1984: Beitrag zur Bemessung der Schalen von Metallsilos. Der Stahlbau, Jahrgang 53, Heft 8.

Samuelson, L. Å., October 1985: Buckling of cylindrical shells under axial compression and subjected to localized loads. Paper presented at Euromech Colloquium 200, Mátrafüred, Hungary

Starnes, J. H., 1970: The effect of a circular hole on the buckling of cylindrical shells. Ph. D. Thesis, California Institute of Technology, Pasadena, CA

Tennyson, R. C., November 1968: The effects of unreinforced circular cutouts on the buckling of circular cylindrical shells under axial compression. J. Engineering for Industry, ASME, p. 541-546.

Toda, S., 1980: Experimental investigation on the effects of elliptic cutouts on the buckling of cylindrical shells loaded by axial compression. Trans. Japan Society Aero Space Sciences, Vol. 23. No. 59, p. 57-63.

Tryckkärlsnormer 1987 (Swedish Pressure Vessel Code 1987), Stockholm

(1)

EL-MABRUK, Mohamed (1)

EL-AZHARI, Sanusi (1)

EL-WAKIL , Emad (2)

STABILITY OF THIN CYLINDRICAL SHELLS A SIMPLIFIED METHOD

INTERNATIONAL COLLOQUIUM
STABILITY OF STEEL STRUCTURES
BUDAPEST, HUNGARY, 1990
PRELIMINARY REPORT

Abstract: The buckling behaviour of a simply supported perfect thin cylindrical shell under pure bending was studied by an approximate method. The formulation of the approximate method was done by treating the strip of the shell at the maximum compression stress as a beam on elastic foundation subjected to axial compression and the foundation stiffness depends on the material of the shell, its radius and thickness.
An approximate expression for the critical moment is derived and the found results were compared very well to those found by classical analysis.

Introduction: Cylindrical shells have an important applications in many types of structures like air craft, space vehicles, large tanks, power-generating equipment, etc.
Cylindrical structures might be required to carry static and/or transient loads such as compression, bending and/or torsion, either as a pure load or as a combined load.
Whenever any of these kinds of loads is applied to a thin shell structure, it is necessary to investigate the failure of thin shell structures.
Previously, there were several investigation in this field, most of them solved this problem by driving an expressions based on an approximation of the potential energy, most of the studies involved pure axial compression but in a few cases bending loads were applied.
EL-MABRUK[1] in (1983), investigated the buckling and post buckling and effect of initial imperfection of a thin cylindrical shell under pure bending by driving an expression of a differential equations based on approximate form of the potential energy for thin shells.
EL-AZHARI et al [2] applied the approximate method to the vibration of a axisymmetric circular cylindrical shell to find the natural frequencies and their mode shapes. They considered the cylindrical shells as a beam on elastic foundation and their results were very close to those found by using the closed form solution [3] .

(1) Asst. Professor of Civil Engineering, El-FATEH UNIVERSITY.
(2) Graduate student of Civil Engineering, EL FATEH UNIVERSITY.

The main purpose of the present study is to find an approximate solution to this problem, which gives approximate expression to the bucking moment without using digital computers, because the calculations of the buckling stress by using an approximation of the potential energy form as given in [1] , take a long time by using digital computers with the use of various trignometric series.

The comparison of the results between the approximate method and the method of approximation of potential energy form due to pure bending, and due to axial compression is studies for different R/t ratios.

Approximate Method Analysis:
Notation of the problem

Solution of the buckling of the cylindrical shell subjected to pure bending by using an approximate method which considers the strip at the maximum compression stress in the case of a pure bending as a beam on elastic media (foundation) subjected to axial compression load, which can be explained as follows:

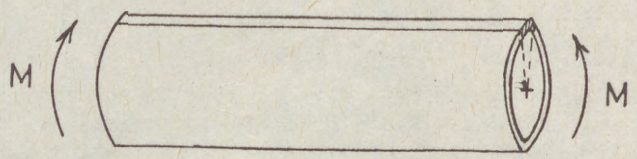

Fig. 1(a) : Thin Cylinder under consideration.

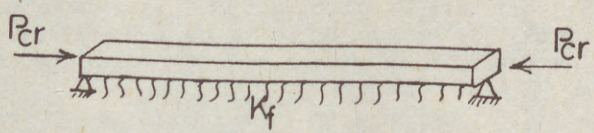

Fig. 1(b) : Strip on elastic foundation.

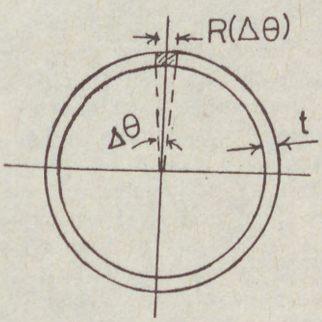

Fig. 1(c) : Cross-section of the cylinder.

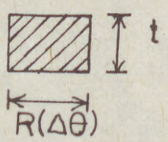

Fig. 1(d) : Cross-section of the strip.

Critical load and Stress Analysis:

The well known beam on elastic foundation equation can be written as :

$$EI \frac{d^4y}{dx^4} + P \frac{d^2y}{dx^2} + K_f y = 0 \qquad (1)$$

Where E,I,P & K_f defined in last page. Taking account the simply supported boundary condition (y=0 and y"=0 at X=L), the solution to this equation can be assumed as $y = an \sin \frac{n\pi X}{L}$ (2)

by substituting the equation (2) into equation (1), leads to

$$\frac{n^4 \pi^4 EI}{L^4} - P \frac{n^2 \pi^2}{L^2} + K_f = 0 \qquad (3)$$

Let $P_E = \frac{\pi^2 EI}{L^2}$

and substitute this value in equation (3), leads to

$$Pcr = n^2 \left(1 + K_f \frac{L^4}{n^4 \pi^4 EI}\right) P_E \qquad (4)$$

Minimize Eq.(4) with respect to n to get the lowest Pcr, leads to

$$n^2 = \frac{L^2}{\pi^2} \sqrt{\frac{K_f}{EI}} \qquad (5)$$

by substitution of the value of n into Eq.(4), the critical load takes this form

$$Pcr = 2\sqrt{K_f EI} \qquad (6)$$

Where

$$K_f = \frac{Et}{R} R(\Delta\theta), \text{ and } I = \frac{R(\Delta\theta)}{12} t^3$$

by substituting the value of K_f and I, in Eq.(6),leads to

$$Pcr = 0.5774 \frac{Et^2}{R} R(\Delta\theta) \qquad (7)$$

by taking the cross-sectional area of strip or $R(\Delta\theta)t$ and

$$\sigma_{cr} = \frac{Pcr}{Area}$$

$$\sigma_{cr} = \frac{0.5774(Et^2/R)\ R(\Delta\theta)}{R(\Delta\theta)\ t}$$

$$\therefore \sigma_{cr} = 0.5774 \frac{Et}{R} \qquad (8)$$

Approximate Critical Moment Expression:

The Critical moment expression can be found as follows :

$$\sigma_{cr} = \frac{I_{cr}}{Area}$$

$$P_{cr} = \sigma_{cr} \times Area = \frac{M_{cr}\, y}{I_{sh.}} \times Area$$

$$= \frac{M_{cr}\, R}{\pi R^3 t} R(\Delta\theta)t$$

$$\therefore \quad P_{cr} = \frac{M_{cr}}{\pi R^2} R(\Delta\theta) \qquad (9)$$

by equating eq.(7) to eq. (9), one can get

$$\frac{M_{cr}}{\pi R^2} R(\Delta\theta) = 0.5774 \frac{Et^2}{R} R(\Delta\theta)$$

$$M_{cr} = 0.5774 \frac{Et^2}{R} \times \pi R^2$$

$$\therefore M_{cr} = (1.81379)ERt^2 \qquad (10)$$

Classical Analysis:

The classical analysis given in [1] for a simply supported thin cylindrical shell subjected to pure bending is based on minimization of an approximate expression for the potential energy for thin cylindrical shell which gives a system of three linear partial differential equations (P.D.E) in the three displacement components with variable coefficients.
The solution of this system is given by the following two forms.

$$\left.\begin{aligned} U^* &= \cos \frac{m\pi x}{L} \sum_{n=o}^{\infty} A_n \cos n\theta \\ V^* &= \sin \frac{m\pi x}{L} \sum_{n=1}^{\infty} B_n \sin n\theta \\ W^* &= \sin \frac{m\pi x}{L} \sum_{n=o}^{\infty} C_n \cos n\theta \end{aligned}\right\} \qquad (11)$$

For Symmetric buckling mode, as shown in figure (2), and

$$\left.\begin{aligned} U^* &= \cos \frac{m\pi x}{L} \sum_{n=1}^{\infty} A_n \sin n\theta \\ V^* &= \sin \frac{m x}{L} \sum_{n=o}^{\infty} B_n \cos n\theta \\ W^* &= \sin \frac{m\pi x}{L} \sum_{n=1}^{\infty} C_n \sin n\theta \end{aligned}\right\} \qquad (12)$$

For antisymmetric buckling mode as shown in figure (3), by substituting into the system of linear partial differential equation by the two forms of solutions leads into a system of Linear ordinary differential equations in form of eign value problem which can be written in the following form $AX=K_b BX$, where K_b is the eign value of the problem (critical stress ratio $= \sigma_b / \bar{\sigma}_c$) and X is the eign vector and the size of the system of equations equals n ($1 \longrightarrow \infty$).
By solving the eign value problem by an iterative method to get the lowest value of Kb for different wave lengths, where for each value of ($m\pi R/L$) the iteration performed in two directions, one in Kb and the other in size of the system (n) in order to get the lowest value of Kb for a fixed value of R/t ratio. This value are tabulated in table (i).
The Critical moment resulted from this analysis can be written in the following forms

$$M_{cr} = \frac{\sigma_b \times I_{sh}}{R}$$

$$M_{cr} = (\bar{\sigma}_c \times Kb) \frac{I_{sh.}}{R}$$

$$M_{cr} = 1.90138\, K_b\, ER t^2 \qquad (\text{for } \nu = 0.3) \qquad (13)$$

Where

$$\bar{\sigma}_c = \frac{E}{[3(1-\nu^2)]^{\frac{1}{2}}} t/R \qquad (14)$$

"theoretical critical stress in case of axil compression"

$$\bar{\sigma}_c = 0.6052 \frac{Et}{R} \qquad (\text{for } \nu = 0.3)$$

and

$$\bar{\sigma}_b = 0.6052\, Kb \frac{Et}{R} \qquad (\text{for } \nu = 0.3) \qquad (15)$$

Discussion of the Results:

The critical stress formulated by the approximate method, by treating the strip of the shell at the maximum compressive stress as a beam on elastic foundation is given by Eq.(8). The computed values of minimum buckling stress ratio (Kb) for various cases of R/t=100,200,300,400, 500,1000 and 2000 are calculated by an iterative method using the derived equations in ref.[1] for symmetric and antisymmetric buckling modes, these values are tabulated in table (i).

The two expressions for the critical moments by the approximate analysis and by the classical analysis are given by Eq.(10) and Eq.(13) respectively. The critical stresses by the approximate analysis, by the classical analysis under axial compression, and by the classical analysis under pure bending are given by Eq.(8) , Eq.(14),and Eq.(15) respectively.

The computed values of critical stresses due to various cases for R/t = 100,200,300,400,500,1000 and 2000 are tabulated in table (ii).

The variation of critical stresses by the approximate analysis and the critical stresses due to the pure bending given in [1] for symmetric buckling mode is plotted in figure (4), and the variation of the critical stresses by the approximate analysis and the critical stresses due to axial compression (σ_c) as a function of R/t is plotted in figure (5), and the variation of critical stresses due to pure bending and the critical stresses due to axial compression as a function of R/t is plotted in figure (6).
The variation of Kb with $(m\pi R)/L$ for the case of R/t = 100 for symmetric and antisymmetric buckling is plotted in figure (7), and the variation of minimum buckling stress-ratio (Kb) with R/t for symmetric and antisymmetric buckling is plotted in figure (8).
By comparing the values of the critical stresses of the different methods, one can get that discrepancies in the results calculated by the classical method is higher than the critical stresses calculated by the approximate method in the case of R/t = 100, by not more than 8 percent, and in the case of R/t = 1000, not more than 6 percent.
The critical stresses for axially compressed cylinder are higher than the critical stresses calculated by the approximate method by less than 5 percent.
By comparing the critical stresses due to axial compression to those due to pure bending, one can get that the critical stresses due to pure bending are higher than the critical stresses due to axial compressin in the case of R/t = 100 by less than 4 percent and in the case of R/t = 1000 by less than 2 percent.
In order to use the classical analysis method to find the lowest buckling stress-ratio tabulated in table (i) with accuracy upto three decimal places, one has to use the eign value of a system of size (19) for R/t = 100, and of size (29) for R/t = 1000, which takes a long computer time, in the other hand the critical stress by the approximate analysis is given by the simple form given in eq.(8).

Conclusion: By comparing the values of the critical moments found by the approximate analysis to those found by the classical analysis one can recommend to use the very simple approximate analysis derived in this study wirh a very reasonable accuracy especially for very thin shells with no need use computer for solving a very lengthy problem as in case of the classical analysis.

References:

(1) EL-MABRUK, M.A., (1988), "Initial post buckling behaviour of thin. cylindrical shells under pure bending, and effect of initial antisymmetric imperfections on the buckling moment", Ph.D dissertation, University of Southern California, U.S.A.

(2) EL-AZHARI,S.A., and HUTCHINSON,J.R.,"Axisymmetric vibration of circular cylindrical shell", J. of thin shells ,in press.

(3) HUTCHINSON, J.R., EL-AZHARI, S.A., (1986),"Vibration of Cylindrical. Shell", J. of applied mechanics.

TABLE (i)

Minimum Buckling Stress - Ratio (K_b)

($\nu = 0.3$)

R/t	100		200		300		400		500		1000		2000	
	$\frac{m\pi R}{L}$	K_b	$\frac{m\pi R}{L}$	K_b	$\frac{m\pi R}{L}$	K_b	$\frac{m\pi R}{L}$	K_b	$\frac{m\pi R}{L}$	K_b	$\frac{m\pi R}{L}$	K_b	$\frac{m\pi R}{L}$	K_b
Antisymmetric Buckling	16.0	1.031	21.9	1.025	27.0	1.021	30.9	1.019	35.0	1.017	55.3	1.011	80.0	1.009
Symmetric Buckling	12.1	1.070	23.0	1.014	29.0	1.008	34.1	1.007	38.1	1.007	55.1	1.007	79.0	1.005

TABLE (ii)

Variation of Critical Stress with R/t

R/t	100	200	300	400	500	1000	2000
$\frac{\sigma_b}{E} \times 10^{-3}$ Due to pure bending (Symmetric Buckling)	6.476	3.067	2.035	1.525	1.218	0.609	0.304
$\frac{\sigma_b}{E} \times 10^{-3}$ Due to Pure Bending (Antisymmetric Buckling)	6.237	3.103	2.060	1.543	1.231	0.612	0.305
$\frac{\sigma_{cr}}{E} \times 10^{-3}$ Due to axial compression	6.052	3.026	2.017	1.513	1.211	0.605	0.303
$\frac{\sigma_{cr}}{E} \times 10^{-3}$ (By approximate method)	5.774	2.882	1.925	1.443	1.155	0.577	00.288

Notation

L, R, t	Length, radius and thickness of the cylinder
E	Modulus of elasticity
ν	Poisson's ratio
K_f	Constant modulus of foundation
R, θ	Polar coordinates
M	Bending moment
K_b	Buckling stress ratio for bending ($\sigma_b / \bar{\sigma}_o$)
σ_b	Maximum stress due to bending moment.
$\bar{\sigma}_o$	Theoretical compression buckling stress $= \frac{E}{[3(1-\nu^2)]^{\frac{1}{2}}} \, t/R$
P	Axial load
P_E	Euler load
$I_{sh.}$	Shell moment of inertia (cylinder)
I	Strip moment of inertia (rectangle)
$\frac{m\pi}{L}$	Wave length.

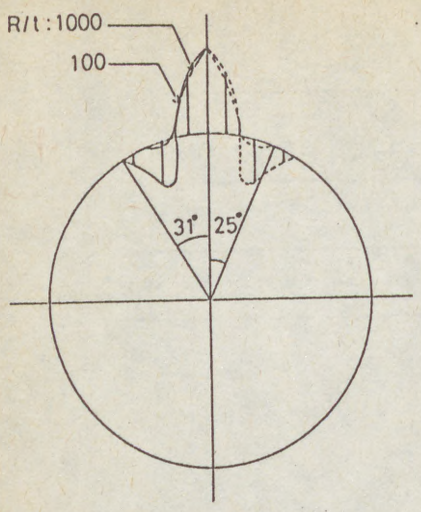

Fig.(2): Symmetric Buckling Shapes.

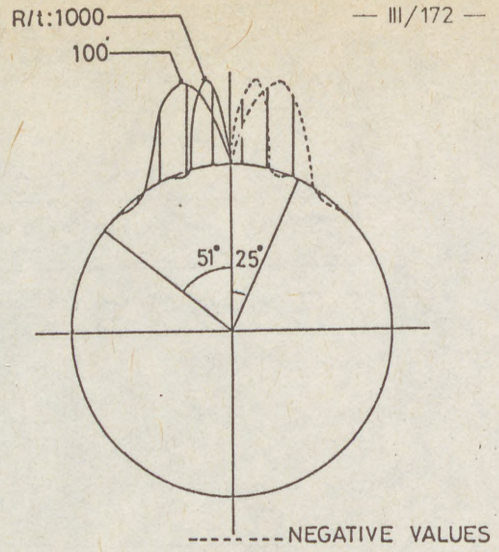

Fig.(3): Antisymmetric Buckling Shapes.

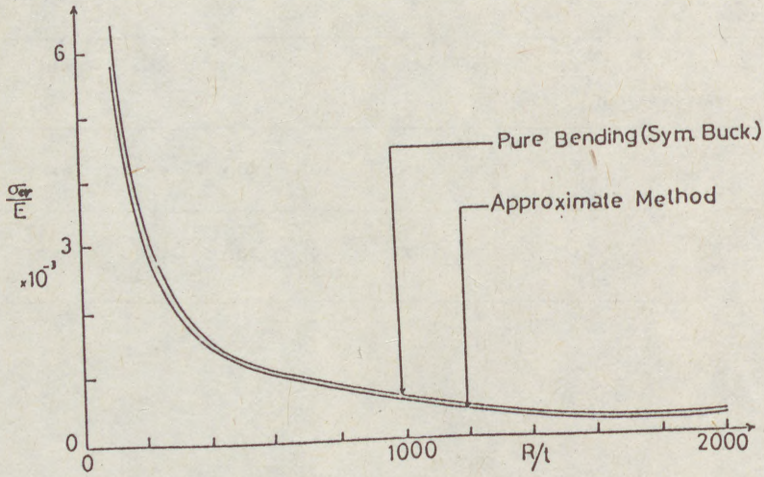

Fig.(4): Variation of Critical Stresses as a function of R/t.

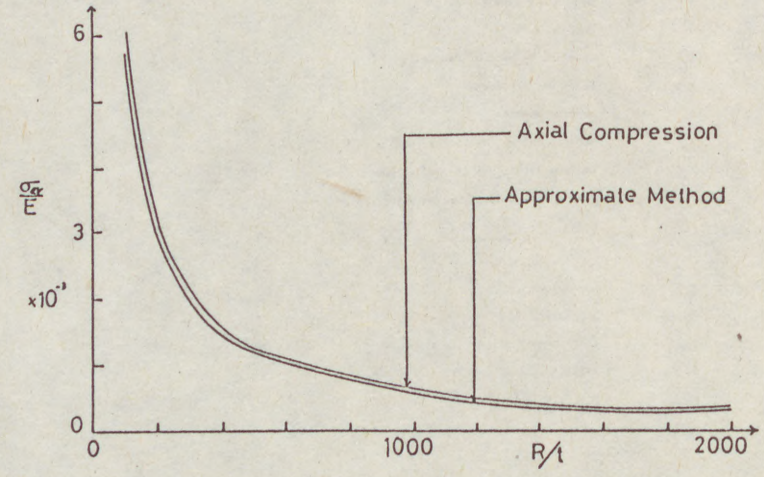

Fig.(5): Variation of Critical Stresses as a function of R/t.

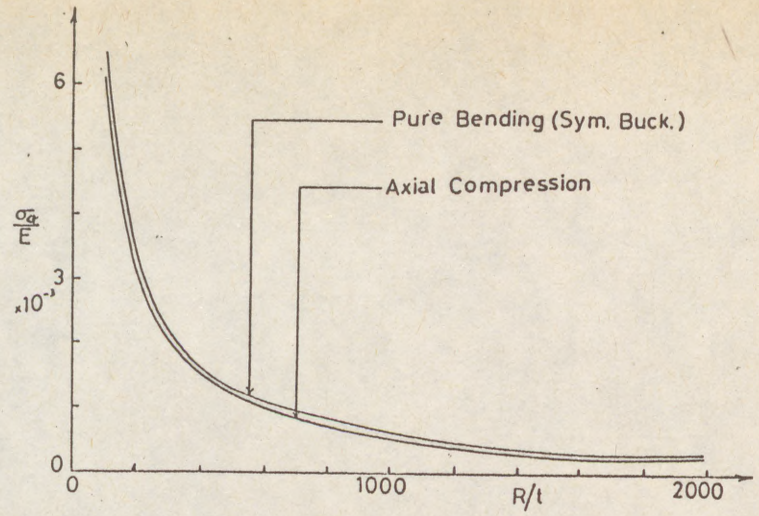

Fig.(6): Variation of Critical Stresses as a Function of R/t.

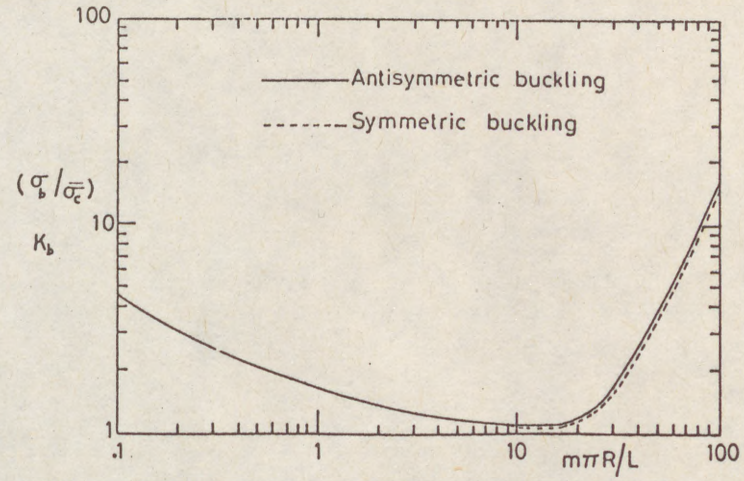

Fig.(7): Variation of Buckling Stress Ratio as a Function of $\frac{m\pi R}{L}$ (R/t=100)

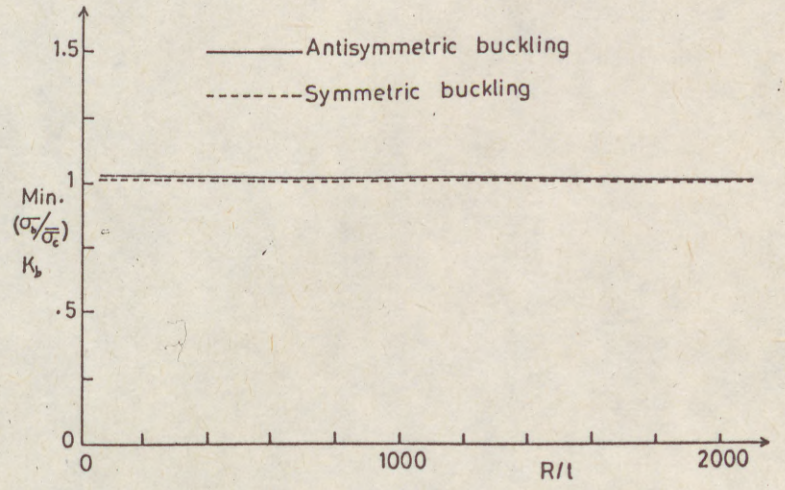

Fig.(8): Variation of Min. Buckling Stress Ratio as a Function of(R/t).

László P

Summary:
shells i
also int
the buck
shown t
deformat
analogou

Sta
(aeolotr
and many
shells a
referenc
author h
shallow
[1972] f

The
shells
generali
shallow
account.

(1)

László P. Kollár (1)

BUCKLING OF GENERALLY ANISOTROPIC SHALLOW SHELLS WITH TRANSVERSE SHEAR DEFORMATION

INTERNATIONAL COLLOQUIUM
STABILITY OF STEEL STRUCTURES
BUDAPEST, HUNGARY, 1990
PRELIMINARY REPORT

Summary: The paper develops the differential equation system of buckling of shells in the case of general anisotropy, taking transverse shear deformation also into account. A closed form solution is derived for the determination of the buckling load which can be applied for a wide range of cases. It is also shown that, in the case of isotropy, the effect of transverse shear deformation can be taken into consideration with a simple formula which is analogous to Föppl's theorem.

1. Introduction

Stability analysis of isctropic, orthotropic, and generally anisotropic (aeolotropic) doubly-curved shells has been investigated by several authors, and many papers can be found in the literature on the buckling of anisotropic shells and plates which take shear deformation also into account (see our references and those of [Kollár, 1990b] and [Kollár and Dulácska, 1984]). The author has dealt in a previous paper [Kollár, 1990a] with the buckling of shallow shells and generalized the results of Dulácska [1969] and Gergely [1972] for aeolotropic shells.

The aim of this paper is to show how can be extended these results for shells with shear deformation. Our work can be considered as the generalization of [Dulácska, 1969], in which he has dealt with the buckling of shallow sandwich shells with thin faces, taking a special orthotropy into account.

(1) Research fellow, Research Group for Applied Mechanics of the Hungarian Academy of Sciences, Technical University of Budapest

(2)

2. Assumptions and notations

Let the equation of the middle surface of the shell be

$$z = z(x, y) \quad ,$$

where x and y are the cartesian co-ordinates of the ground plane.

The internal forces acting on a shell element are shown in Fig. 1.

The external loads acting on a shell element are the distributed forces p_1, p_2, p_3 and the distributed moments M_1, M_2 (Fig. 1). It should be noted that the components of the load do not follow the co-ordinate axes x, y and z, but are tangents to the middle surface in planes parallel to the co-ordinate planes xz, yz (p_1, p_2, M_1, M_2) and normal to the surface (p_3).

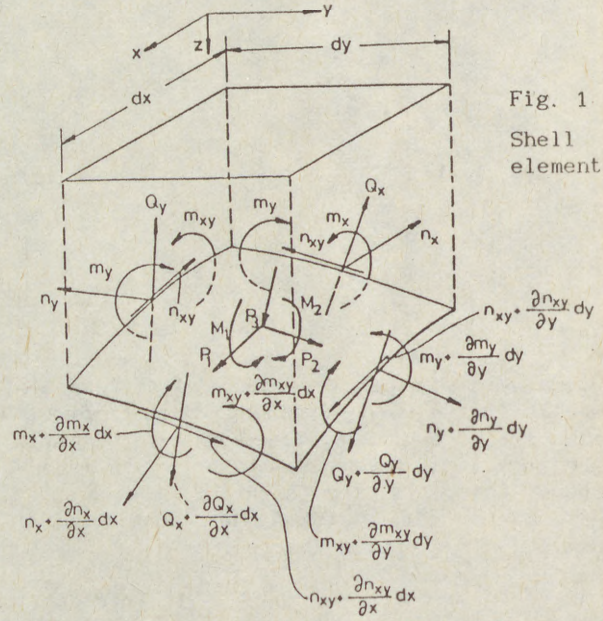

Fig. 1
Shell element

We assume that the material of the shell is homogeneous and linearly elastic. The middle surface of the shell is shallow, so that, we can use the assumptions of the shallow shell theory [Flügge, 1973].

The displacements of an arbitrary point of the middle surface are described by the components u, v and w, which have the same directions as the load components p_1, p_2 and p_3. The rotations of the cross sections are denoted by ϕ_x and ϕ_y respectively.

3. Equations of shallow shells

The **equilibrium equations** for the element shown in Fig.1 (using the assumptions of shallow shells) are as follows [Flügge, 1973] :

$$\frac{\partial n_x}{\partial x} + \frac{\partial n_{xy}}{\partial y} + p_1 = 0 \quad , \qquad \frac{\partial n_y}{\partial y} + \frac{\partial n_{xy}}{\partial x} + p_2 = 0 \quad ,$$

$$n_x \frac{\partial^2 z}{\partial x^2} + n_y \frac{\partial^2 z}{\partial y^2} + 2n_{xy} \frac{\partial^2 z}{\partial x \partial y} + \frac{\partial Q_x}{\partial x} + \frac{\partial Q_y}{\partial y} + p_3 = 0 \quad ,$$

$$\frac{\partial m_x}{\partial x} + \frac{\partial m_{xy}}{\partial y} - Q_x - M_1 = 0 \quad , \qquad \frac{\partial m_y}{\partial y} + \frac{\partial m_{xy}}{\partial x} - Q_y - M_2 = 0 \quad .$$

(3)

These can be written in the following matrix form :

$$\mathbf{p} = \Theta\,\mathbf{n} \quad , \tag{3.1}$$

where **p** and **n** are the vectors of loads and internal forces as follows

$$\mathbf{p} = \begin{bmatrix} p_1 \\ p_2 \\ p_3 \\ M_1 \\ M_2 \end{bmatrix} \quad , \qquad \mathbf{n} = \begin{bmatrix} n_x \\ n_y \\ n_x \\ m_x \\ m_y \\ m_{xy} \\ Q_x \\ Q_y \end{bmatrix} .$$

and Θ is the following operator matrix :

$$\Theta = \begin{bmatrix} -\frac{\partial}{\partial x} & 0 & -\frac{\partial}{\partial y} & 0 & 0 & 0 & 0 & 0 \\ 0 & -\frac{\partial}{\partial y} & -\frac{\partial}{\partial x} & 0 & 0 & 0 & 0 & 0 \\ -\frac{\partial^2 z}{\partial x^2} & -\frac{\partial^2 z}{\partial y^2} & -\frac{2\partial^2 z}{\partial x \partial y} & 0 & 0 & 0 & -\frac{\partial}{\partial x} & -\frac{\partial}{\partial y} \\ 0 & 0 & 0 & \frac{\partial}{\partial x} & 0 & \frac{\partial}{\partial y} & -1 & 0 \\ 0 & 0 & 0 & 0 & \frac{\partial}{\partial y} & \frac{\partial}{\partial x} & 0 & -1 \end{bmatrix}$$

We denote the strains of the middle surface by $\varepsilon_x, \varepsilon_y$ and γ_{xy}, its changes in curvatures by κ_x, κ_y and κ_{xy}, the transverse shearing strains by γ_x and γ_y.

The deformation components of the shell can be calculated from u, v, w, ϕ_x and ϕ_y. These are the **compatibility equations** :

$$\mathbf{e} = \Theta^{*}\,\mathbf{u} \, , \tag{3.2}$$

where

(4)

$$\Theta^* = \begin{bmatrix} \frac{\partial}{\partial x} & 0 & -\frac{\partial^2 z}{\partial x^2} & 0 & 0 \\ 0 & \frac{\partial}{\partial y} & -\frac{\partial^2 z}{\partial y^2} & 0 & 0 \\ \frac{\partial}{\partial y} & \frac{\partial}{\partial x} & -\frac{2\partial^2 z}{\partial x \partial y} & 0 & 0 \\ 0 & 0 & 0 & -\frac{\partial}{\partial x} & 0 \\ 0 & 0 & 0 & 0 & -\frac{\partial}{\partial y} \\ 0 & 0 & 0 & -\frac{\partial}{\partial y} & -\frac{\partial}{\partial x} \\ 0 & 0 & \frac{\partial}{\partial x} & -1 & 0 \\ 0 & 0 & \frac{\partial}{\partial y} & 0 & -1 \end{bmatrix}, \quad \mathbf{e} = \begin{bmatrix} \varepsilon_x \\ \varepsilon_y \\ \gamma_{xy} \\ \kappa_x \\ \kappa_y \\ \kappa_{xy} \\ \gamma_x \\ \gamma_y \end{bmatrix}, \quad \mathbf{u} = \begin{bmatrix} u \\ v \\ w \\ \phi_x \\ \phi_y \end{bmatrix},$$

and Θ^* is the adjoint of Θ.

Since the material of the shell is linearly elastic, the relation between the internal forces and deformations is defined by the following **constitutive equation** :

$$\mathbf{n} = \mathbf{M}\,\mathbf{e} \quad , \tag{3.3}$$

where **M** is the stiffness matrix. **M** is symmetrical and has constant elements:

$$\mathbf{M} = \begin{bmatrix} T_{11} & T_{12} & T_{13} & C_{14} & C_{15} & C_{16} & 0 & 0 \\ T_{12} & T_{22} & T_{23} & C_{24} & C_{25} & C_{26} & 0 & 0 \\ T_{13} & T_{23} & T_{33} & C_{34} & C_{35} & C_{36} & 0 & 0 \\ C_{14} & C_{24} & C_{34} & B_{11} & B_{12} & B_{13} & 0 & 0 \\ C_{15} & C_{25} & C_{35} & B_{12} & B_{22} & B_{23} & 0 & 0 \\ C_{16} & C_{26} & C_{36} & B_{13} & B_{23} & B_{33} & 0 & 0 \\ 0 & 0 & 0 & 0 & 0 & 0 & S_{11} & S_{12} \\ 0 & 0 & 0 & 0 & 0 & 0 & S_{12} & S_{22} \end{bmatrix} . \tag{3.4}$$

The vectors of internal forces (**n**), deformations (**e**) and displacements (**u**) contain 21 unknown functions, the equations of equilibrium (3.1), deformations (3.2) and Hooke's law (3.3) yield 21 equations. Eliminating the internal forces and deformations, we obtain the following equation for the displacements :

$$\mathbf{p} = \Theta\,\mathbf{M}\,\Theta^*\,\mathbf{u} \quad . \tag{3.5}$$

(5)

4. Governing equations of buckling

For the investigation of stability the change in geometry has to be taken into account. The vector of internal forces before buckling is denoted by $\mathbf{n}_D$, and the middle surface of the shell is given by the function z_D which contains the deformations due to $\mathbf{n}_D$ as well. The displacements, deformations and internal forces during buckling are denoted by $\mathbf{u}_B$, $\mathbf{e}_B$ and $\mathbf{n}_B$ respectively.

The shell is shallow, so that the function of the middle surface of the shell can be written in the following way :

$$z = z_D + w_B ,$$

where w_B is the third element of $\mathbf{u}_B$.

Let us introduce the following notations :

$$\Theta_2(z)=\begin{bmatrix} 0 & 0 & 0 & 0 & 0 & 0 & 0 & 0 \\ 0 & 0 & 0 & 0 & 0 & 0 & 0 & 0 \\ -\frac{\partial^2 z}{\partial x^2} & -\frac{\partial^2 z}{\partial y^2} & -\frac{2\partial^2 z}{\partial x \partial y} & 0 & 0 & 0 & 0 & 0 \\ 0 & 0 & 0 & 0 & 0 & 0 & 0 & 0 \\ 0 & 0 & 0 & 0 & 0 & 0 & 0 & 0 \end{bmatrix},$$

$\Theta_2^*(z)$, which is identical with the transpose of $\Theta_2(z)$, further the operators

$$\Theta_1 = \Theta - \Theta_2(z) , \qquad \Theta_1^* = \Theta^* - \Theta_2^*(z) .$$

Θ_1 and Θ_1^* do not depend on z.

Introducing these into (3.5), and neglecting those terms which contain second and third power terms of the displacements, we obtain a homogeneous linear differential equation system, on the basis of which the buckling load can be calculated :

$$\left[[\Theta_1 + \Theta_2(z_D)] \, \mathbf{M} \, [\Theta_1^* + \Theta_2^*(z_D)] + \Theta_3 \right] \mathbf{u}_B = 0 . \qquad (4.1)$$

where

$$\Theta_3=\begin{bmatrix} 0 & 0 & 0 & 0 & 0 \\ 0 & 0 & 0 & 0 & 0 \\ 0 & 0 & \left[-n_{xD}\frac{\partial^2}{\partial x^2} - n_{yD}\frac{\partial^2}{\partial y^2} - n_{xyD}\frac{2\partial^2}{\partial x \partial y}\right] & 0 & 0 \\ 0 & 0 & 0 & 0 & 0 \\ 0 & 0 & 0 & 0 & 0 \end{bmatrix},$$

and n_{xD}, n_{yD} and n_{xyD} are the elements of $\mathbf{n}_D$.

(6)

5. Determination of the buckling load

As a rule, we can solve Eq.(4.1) only numerically, as is usual in the literature. Now we present a simple analytical solution for a special case. Let the function of the middle surface be of the second order as follows :

$$z_D = -\frac{1}{2R_x}x^2 - \frac{1}{2R_y}y^2 \quad ,$$

and let the membrane forces be constant, provided that $n_{xyD}=0$, further that the stiffness matrix has the following special form :

$$\mathbf{M}_o = \begin{bmatrix} xx & xx & & & \\ xx & xx & & & \\ & & x & x & \\ xx & xx & & & \\ xx & xx & & & \\ & & x & x & \\ & & & & x \\ & & & & x \end{bmatrix} .$$

We assume the displacement functions in the following form :

$$u_B = u\cos\frac{\pi}{l_x}x \sin\frac{\pi}{l_y}y \quad , \quad v_B = v\sin\frac{\pi}{l_x}x\cos\frac{\pi}{l_y}y \quad , \quad w_B = w\sin\frac{\pi}{l_x}x\sin\frac{\pi}{l_y}y$$

$$\phi_{Bx} = \phi_x\cos\frac{\pi}{l_x}x\sin\frac{\pi}{l_y}y \quad , \qquad \phi_{By} = \phi_y\sin\frac{\pi}{l_x}x\cos\frac{\pi}{l_y}y \quad ,$$

where l_x and l_y are the half wavelengths of buckling in the directions x and y respectively.

These functions can be used for the investigation of the local buckling of shallow shells [Kollár and Dulácska, 1984], nevertheless, they satisfy the boundary conditions in several cases as well.

Let us introduce these functions into (4.1). These satisfy the differential equation system only if the coefficients of each trigonometrical function vanish. Hence, we obtain from (4.1) five linear equations, which can be written in the following matrix equation :

$$\left[\mathbf{A}\,\mathbf{M}_o\,\mathbf{A}^T - \lambda\,\mathbf{B}\right]\mathbf{U} = 0 \quad . \qquad (5.1)$$

where $\mathbf{A}^T$ is transpose of $\mathbf{A}$:

$$\mathbf{A}^T = \begin{bmatrix} -\alpha & 0 & 1/R_x & 0 & 0 \\ 0 & -\beta & 1/R_y & 0 & 0 \\ \beta & \alpha & 0 & 0 & 0 \\ 0 & 0 & 0 & \alpha & 0 \\ 0 & 0 & 0 & 0 & \beta \\ 0 & 0 & 0 & -\beta & -\alpha \\ 0 & 0 & \alpha & -1 & 0 \\ 0 & 0 & \beta & 0 & -1 \end{bmatrix}, \quad \mathbf{B} = \begin{bmatrix} 0 & 0 & 0 & 0 & 0 \\ 0 & 0 & 0 & 0 & 0 \\ 0 & 0 & 1 & 0 & 0 \\ 0 & 0 & 0 & 0 & 0 \\ 0 & 0 & 0 & 0 & 0 \end{bmatrix}, \quad \mathbf{U} = \begin{bmatrix} u \\ v \\ w \\ \phi_x \\ \phi_y \end{bmatrix}$$

(7)

and

$$\lambda = -n_{xD}\alpha^2 - n_{yD}\beta^2 , \qquad \alpha = \frac{\pi}{l_x} , \qquad \beta = \frac{\pi}{l_y} .$$

We can obtain the buckling (bifurcation) load from the condition of singularity of the coefficient matrix in Eq. (5.1) :

$$\det\left[\mathbf{A}\,\mathbf{M}_o\,\mathbf{A}^T - \lambda\,\mathbf{B}\right] = 0 . \qquad (5.2)$$

The buckling load calculated from (5.2) depends on the parameters α, β and we have to minimize it with respect to these two parameters.

These results are the generalisation of those of Dulácska [1969, Eq.(9.1)], where he neglected the stiffnesses outside the main diagonal of stiffness matrix (3.4).

This formula can be applied e.g. for (simply supported) *plates* provided that $1/R_x = 1/R_y = 0$. In this case the displacement functions satisfy also the boundary conditions if $l_x = a/n$ and $l_y = b/m$, where a and b are the side lengths of the plate and n, m are integer numbers.

In the case of **isotropic material** our formulas become more simple. In this case :

$$T_{11} = T_{22} = T = \frac{t\,E}{(1-\nu^2)} , \qquad T_{12} = \nu T , \qquad T_{33} = T(1-\nu)/2 ,$$

$$B_{11} = B_{22} = B = \frac{t^3 E}{12(1-\nu^2)} , \qquad B_{12} = \nu B , \qquad B_{33} = B\,(1-\nu)/2 ,$$

$$S_{11} = S_{22} = S , \qquad C_{ij} = 0,$$

where E ad ν are Young's modulus and Poisson's ratio of the shell, respectively, and t is the thickness of the shell. Introducing these into (5.2) we obtain, after rearranging ,

$$\lambda = n_T + \left[\frac{1}{n_B} + \frac{1}{n_S}\right]^{-1} \qquad (5.3)$$

where

$$n_T = T(1-\nu^2)\,\frac{\left[\frac{\alpha^2}{R_y} + \frac{\beta^2}{R_x}\right]^2}{\left[\alpha^2+\beta^2\right]^2} , \qquad n_B = B\left[\alpha^2+\beta^2\right]^2 , \qquad n_S = S\left[\alpha^2+\beta^2\right] .$$

Applying these formulas for an axially compressed sandwich cylinder we obtain the results of Hegedűs [1979]. Formula (5.3) shows the effect of the shearing deformation on the buckling load. The form of the last term of this simple formula is identical with the "Dunkerley-type" expression of Föppl, which can be used for the calculation of the lowest critical load of elastic structures having different stiffnesses.

7. CONCLUSIONS, FURTHER APPLICATIONS

We have derived the governing equation of buckling of generally anisotropic shallow shells with shear deformation and we obtained an expression for the determination of the bifurcation load assuming a sinusoidal buckling shape which satisfies the differential equation system of buckling and in many cases also the boundary conditions.

These results can be generalized for sandwich shells with thick faces and a closed form solutions can be found in the case of an arbitrary second order middle surface assuming a doubly sinusoidal buckling mode in a skew co-ordinate system [Kollár, 1990b].

References

Allen, H. G. (1969) : Analysis and Design of Structural Sandwich Panels. Pergamon Press. Oxford etc.

Banavalkar, P. V. and Gergely, P. (1972) : Analysis of Thin-Steel Hyperbolic Paraboloid Shells. Proc. ASCE **98.** Structural Division, 2605-2621.

Dulácska, E. (1969) : Vibration and stability of anisotropic shallow shells. Acta Techn. Hung. **65.**, 225-260.

Fischer, M. (1974) : Das Beulproblem der flachen, orthotropen, hyperbolischen Paraboloidschale. Der Stahlbau. **43.** 52-61.

Flügge, W. (1973) : Stresses in Shells . 2nd edition. Springer, Berlin etc.

Gergely, P. (1972) : Buckling of Orthotropic Paraboloid Shells. Proc. ASCE **98.** Structural Division, 395-398.

Hegedűs, I. (1979) : Buckling of axially compressed cylindrical sandwich shells. Acta Techn. Hung. **89.**, 377-387.

Jones, R. M. and Morgan, H. S. (1975) :Buckling and Vibration of Cross-Ply Laminated Circular Cylindrical Shells. AIAA Journal, **13.** 664-671.

Jones, R. M. (1975) : Mechanics of Composite Materials. McGrow-Hill, New York etc.

Kollár, L. and Dulácska, E. (1984) : Buckling of Shells for Engineers. J. Whiley & Sons, Chichester etc. and Akadémiai Kiadó, Budapest,

Kollár, L. P. (1990a) : Buckling of Generally Anisotropic (Aeolotropic) Shallow Shells. Acta Techn. Hung.(At press.)

Kollár, L. P. (1990b) : Buckling of Generally Anisotropic Shallow Sandwich Shells. Submitted to the J. of Reinforced Plastics and Composites.

Pomázi, L. (1986) :Remarks to the stability of asymmetrically built and loaded sandwich plates. Proc. of the Euromech Colloquium No 200, Mátrafüred, Hungary, 5-7. Oct. 1985. Post-buckling of elastic structures. Edited by J. Szabó, assistant editors :Zs. Gáspár and T. Tarnai. Akadémiai Kiadó, Budapest, 253-275.

Reissner, E. (1955) : On some Aspects of the Theory of Thin Elastic Shells. Journal Boston Soc. of Civ. Eng. **42.** 100-133.

Stein, M. (1986) : Nonlinear theory for Plates and Shells Including the Effect of Transverse Shear. AIAA Journal, **24.** 1537-1544.

Vinson, J. R. and Sierakowski, R. L. (1986) : The behaviour of structures composed of composite materials. Martinus Nijhoff Publishers, Dordrecht etc.

(1)
MANDARA, Alberto (1)
MAZZOLANI, Federico (2)

TESTING RESULTS AND DESIGN PROCEDURES FOR AXIALLY LOADED ALUMINUM ALLOY CYLINDERS.

INTERNATIONAL COLLOQUIUM
STABILITY OF STEEL STRUCTURES
BUDAPEST, HUNGARY, 1990
PRELIMINARY REPORT

Summary: After recalling the basical theoretical principles on the buckling strenght of aluminum alloy cylinders under axial compression, a comparison between theoretical and experimental data is made, in order to find out the approach that better fits the experimental evidence. At the same time a new expression of the knockdown factor α, accounting for imperfections, is proposed. Finally, a practical method for design and check of aluminum cylinders is presented here.

THEORETICAL FOREWORDS: An axially loaded perfect cylinder, having mean radius R and wall thickness t, simply supported at the edges, and under the hypothesis of pure membrane stress before buckling, fails in elastic-plastic range under the following stress:

$$\sigma_{cr} = \eta \, \sigma_{cr,e} \qquad (1)$$

where:

$$\sigma_{cr,e} = \frac{E}{\sqrt{3(1-\nu^2)}} \frac{t}{R} \qquad (2)$$

is the elastic bifurcation stress (TIMOSHENKO and GERE, 1961), η is a non dimensional function which takes into account the plasticity effects. If we assume the material

---

(1) Research Fellow, Università di Napoli, Italy.
(2) Professor of Structural Engineering, Università di Napoli, Italy.

(2)

as incompressible ($\nu = 0.5$), then η has the generical form:

$$\eta = f(E, E_t, E_s) \tag{3}$$

where E_t and E_s are the tangent and the secant modulus of the σ-ε law of material, respectively.

According to some existing theoretical approaches, different expressions of η are possible.:

1) Theory of plastic deformations (GERARD, 1957):

$$\eta = \frac{\sqrt{E_t \, E_s}}{E} \tag{4}$$

2) Flow theory (incremental type) (VOL'MIR, 1965):

$$\eta = \sqrt{\frac{E_t}{E}} \tag{5}$$

3) Theory of secant modulus (VOL'MIR, 1965):

$$\eta = \frac{E_s}{E} \tag{6}$$

4) Theory of WEINGARTEN, MORGAN & SEIDE (1960):

$$\eta = \frac{E_s}{E}\sqrt{\frac{E_t}{E}} \tag{7}$$

5) Theory of GERARD & STOWELL (RADHAKRISHNAN, 1956):

$$\eta = \sqrt{\frac{E_t}{E_s}} \tag{8}$$

For aluminum alloys, E_t and E_s values may be easily exstimated by the use of the Ramberg-Osgood's law, whose general form is (MAZZOLANI, 1985):

$$\varepsilon = \frac{\sigma}{E} + \varepsilon_{o,res} \left(\frac{\sigma}{f_o}\right)^n \tag{9}$$

where $\varepsilon_{o,res}$ is the residual strain corresponding to the reference stress f_o and n is an exponent depending on the kind of alloy.

The evaluation of n is made by imposing that equation (9) passes through two values of σ. If f_1 and f_2 are such values, we have:

$$n = \frac{\ln \left(\varepsilon_1 - f_1/E\right)/\left(\varepsilon_2 - f_2/E\right)}{\ln \left(f_1/f_2\right)} \tag{10}$$

where ε_1 and ε_2 are the strain values corresponding to f_1 and f_2, respectively.

Usually for the evaluation of n we assume $f_1 = f_{0.1}$ and $f_2 = f_{0.2}$ so we have:

$$n = \frac{\ln 2}{\ln\left(f_{0.2}/f_{0.1}\right)} \tag{11}$$

that fits fairly well the shape of σ-ε law of material for

(3)

small plastic deformations ($\varepsilon < 1\text{-}2\%$). If the material is strongly strained in plastic range ($\varepsilon > 2\%$), then the value of n can be more approximatively evaluated by assuming $f_1 = f_t$ and $f_2 = f_{0.2}$, being f_t the tensile rupture strength. In this case we have:

$$n' = \frac{\ln (\varepsilon_t - f_t/E)/0.002}{(f_t/f_{0.2})} \qquad (12)$$

Since in both cases $f_{0.2}$ value is used, equation (9) may be more conveniently expressed in the form:

$$\varepsilon = \frac{\sigma}{E} + 0.002 \left(\frac{\sigma}{f_{0.2}}\right)^n \qquad (13)$$

This form makes easier the expressions of E_t and E_s, which result:

$$E_t = \frac{d\sigma}{d\varepsilon} = \frac{E}{1+0.002\ n \frac{E}{f_{0.2}} \left(\frac{\sigma}{f_{0.2}}\right)^{n-1}} \qquad (14)$$

$$E_s = \frac{\sigma}{\varepsilon} = \frac{E}{1+0.002 \frac{E}{f_{0.2}} \left(\frac{\sigma}{f_{0.2}}\right)^{n-1}} \qquad (15)$$

where the exponent n can be expressed by (11) or (12) according to the range of σ-ε curve that one would better interpretate.

INFLUENCE OF IMPERFECTIONS: The values deducted from (1) according to one of the above mentioned theoretical approaches, cannot be directly used in practice, due to the great imperfection sensitivity of axially compressed cylinders. The theoretical buckling load must be corrected by means of a knock-down factor α which accounts for imperfections. So, the expression of the failure load for an imperfect cylinder becomes:

$$\sigma_{cr} = \alpha\ \eta\ \sigma_{cr,e} \qquad (16)$$

It has been experimentally observed that the coefficient α decreases as the R/t ratio increases and assumes values close to unity for very thick cylinders ($R/t < 20$), whose buckling occurs in fully plastic range.

Several expressions of α , deducted by various Authors on the basis of experimental tests, are listed below:

1) $$\alpha = \frac{1}{(1+0.02\ \sqrt{2\ R/t})^2} \qquad (17)$$

(4)

$$\alpha = \frac{0.83}{\sqrt{1+0.01\ R/t}} \qquad (18)$$

2)

$$\alpha = \frac{0.70}{\sqrt{0.1+0.01\ R/t}}$$

$$\alpha = 1.52-0.473\ \log_{10}(R/t), \quad \text{for } R/t < 600$$

3)

$$\alpha = 0.207, \quad \text{for } R/t > 600 \qquad (19)$$

4)

$$\alpha = 18.41/\sqrt[3]{(R/t)^2} \qquad (20)$$

The comparison between equations (17)-(20) is shown in fig. 1. Equation (17) in the only one especially conceived for aluminum alloy cylinders (CLARK and ROLF, 1964), while equations (18) and (19) are the expressions proposed by ECCS (1988) and ASME (MILLER, 1981) Recommendations for steel shells, respectively. Equation (20) is an alternative to (18) proposed by (SALMERI, 1987) in continuous form.

EXPERIMENTAL RESULTS: The experimental program, performed by (MAZZOLANI and MANDARA, 1988) at the Engineering Faculty of Naples, aimed to investigate the buckling phenomenon for axially compressed aluminum alloy cylinders in plastic range. For this reason 8 series of cylinders (91 specimens alltogether having R/t ratio below 40) have been tested. The mechanical and geometrical features of specimens are summarized in table 1. Their imperfection degree were within the tollerances of the ordinary industrial manufacturing of extruded cylinders.

The length of cylinders has proved to have no influence on the buckling phenomenon. In fact, most of samples buckled with two anular folds placed close to the ends of the cylinder (fig. 2).

For each series the experimental results have been statistically exploited by determining the mean value of failure stress σ_{med}, the standard deviation s and the characteristic value of failure stress, defined by equation:

$$\sigma_k = \sigma_{med} - ks \qquad (21)$$

where the constant k depends on the number of tests performed for each series.

COMPARISON BETWEEN EXPERIMENTAL RESULTS AND THEORETICAL PREVISIONS: For each series of specimens the theoretical buckling load has been determined by the use or equation (1) with η supplied by (4)...(8). The quantities E_t/E (14) and E_s/E (15) have been evaluated through the Ramberg-Osgood

law both with exponent n (11) and n' (12). Such values of buckling loads have been compared with the characteristic test data σ_k (21), as shown in table 2.

The percentage scatters between experimental and theoretical results are given in table 3, where the reduced values of buckling load (16) are also shown. The reduction factor α has been computed according to (17), (18) and (19). Equation (20) has not been considered because it supplies results above the unity for the investigated R/t range of values.

It may be noted that the not reduced theoretical results (α = 1) fairly well agree with experimental data only in the case of very thick shells (series 1, 2, 3, 4 and 6); as an exception, equation (8) leads to results in great disagreement with the experimental values. The discrepance increases for thinner cylinders (series 5, 7 and 8), which are more sensitive to initial imperfections.

For this reasons, the theoretical approach which better fits the experimental evidence can be individuated only referring to series 1, 2, 3, 4 and 6, for which one may assume α = 1.

The exam of the theoretical results shows that equation (4) (theory of plastic deformations) better fits the experimental results with scatters on the safe side.

By assuming equation (4) to be valid, and limiting the analysis to series 1, 2, 3, 4 and 6, it is noted that the exponent n, given by (11) results more appropriate as compared with the exponent n' (12) deduced on the basis of $f_{0.2}$ and f_t. This appears fairly plausible since, for the above mentioned series, buckling occurs at compressive stress values not far from $f_{0.2}$, and therefore with small plastic deformations.

On the basis of theoretical results given by equation (4) for series 5, 7 and 8 (cases of imperfection sensitive shells), it has been proved that the expression of α which best fits the experimental data is that proposed by ECCS (1988) for steel shells (18). As an alternative to (18), we may assume the expression:

$$\alpha = \frac{1}{\sqrt{1.20+0.02\ R/t}} \qquad (22)$$

which satisfactorily approximates the values and covers continuously the full geometric range of cylinders. Equation (22) is plotted in fig. 2 together (17)-(20).

CHECK AND DESIGN METHOD: The above results can be conveniently used for the formulation of a design method for axially compressed aluminum alloy cylinders. The method is a slight variant of that proposed in (MANDARA and MAZZOLANI, 1989);

(6)

it links both geometrical and mechanical features (R, R/t, $f_{0.2}$) together with the factored value of external axial load N.

The compressive stress acting along the longitudinal fibers of the cylinder may be expressed by:

$$\sigma = \frac{N}{2 \pi Rt} \tag{23}$$

By imposing that such stress equals the buckling stress,we have:

$$\frac{N}{2 \pi Rt} = \alpha \eta \sigma_{cr,e} \tag{24}$$

where α, η and $\sigma_{cr,e}$ are given by (22), (4) and (2) respectively.

By multiplying both members for $2 \pi t/RE$ equation (24) may be written in the nondimensional form:

$$\frac{N}{R^2 E} = 2 \pi \alpha \eta \frac{\sigma_{cr,e}}{E} \frac{t}{R} \tag{25}$$

By means of suitable manipulation, η may be expressed in function of the nondimensional parameter N/R^2E. In fact, on the basis of (14) and (15), we have:

$$E_t = \frac{E}{1+0.002\, n \frac{E}{f_{0.2}} \left(\frac{N}{2\pi R^2 E f_{0.2}} \cdot \frac{R}{t}\right)^{n-1}} \tag{26}$$

$$E_s = \frac{E}{1+0.002 \frac{E}{f_{0.2}} \left(\frac{N}{2\pi R^2 E f_{0.2}} \cdot \frac{R}{t}\right)^{n-1}} \tag{27}$$

Since α and $\sigma_{cr,e}$ depend on the R/t ratio only, equation (25) may be plotted in the $N/R^2 E$, R/t plane for different values of $f_{0.2}$, as shown in fig. 3. The exponent n has been evaluated according to the formula (MAZZOLANI, 1985):

$$n = f_{0.2}/10 \quad (f_{0.2} \text{ on } N/mm^2) \tag{28}$$

The curves of fig. 3 divide the plane into a safe area (below) and a unsafe area (above). For given values of N, R and $f_{0.2}$, we calcolate the $N/R^2 E$ ratio and, through the appropriate curve, we obtain the design value of the R/t ratio.

For checking stability, it is enough that the point ($N/R^2 E$, R/t), falls below the curve corresponding to the given $f_{0.2}$ value.

(7)

REFERENCES

CLARK, J.W., ROLF, R.L., 1964, "Design of aluminum tubular members", Journal of Structural Division, ASCE.

EUROPEAN CONVENTION FOR CONSTRUCTIONAL STEELWORK (ECCS), 1988, "Buckling of Shells".

GERARD, G., 1957, "Plastic Stability Theory of Thin Shells", Journal of Aeronautical Sciences.

MANDARA, A., MAZZOLANI, F.M., 1989, "On the Stability of Aluminum Alloy Cylindrical Shells under Axial Compression", Costruzioni Metalliche.

MAZZOLANI, F.M., 1985, "Aluminum Alloy Structures", Pitman.

MAZZOLANI, F.M., MANDARA, A., 1988, "Esame comparativo delle teorie elasto-plastiche per cilindri assialcompressi in lega di alluminio sulla base dell'evidenza sperimentale", from the honorary volume to G. Ceradini.

MILLER, C.D., 1981, "Buckling Design Methods for Steel Structures, a State of the Art", Integrity of Off-shore Structures, Proc. Second Symposium, Glasgow.

RADHAKRISHNAN, S., 1956, "Plastic Buckling of Circular Cylinders", Journal of Aeronautical Sciences.

SALMERI, A., SALMERI, M., 1987, "Calcolo diretto dello spessore dei cilindri sottili con modifica del coefficiente di riduzione α ", Giornate Italiane della Costruzione in Acciaio, Trieste.

TIMOSHENKO, S., GERE, J.M., 1961, "Theory of Elastic Stability", 2nd ed. Mc Graw Hill, New York.

VOL'MIR, A.S., 1965, "Stability of Elastic Systems", Foreign Technology Division, Wright-Patterson Air Force Base, Ohio.

WEINGARTEN, A., MORGAN, E.J., SEIDE, P., 1960, "Final Report of Design Criteria for Elastic Stability of Thin Shell Structures", Space Technology Laboratories.

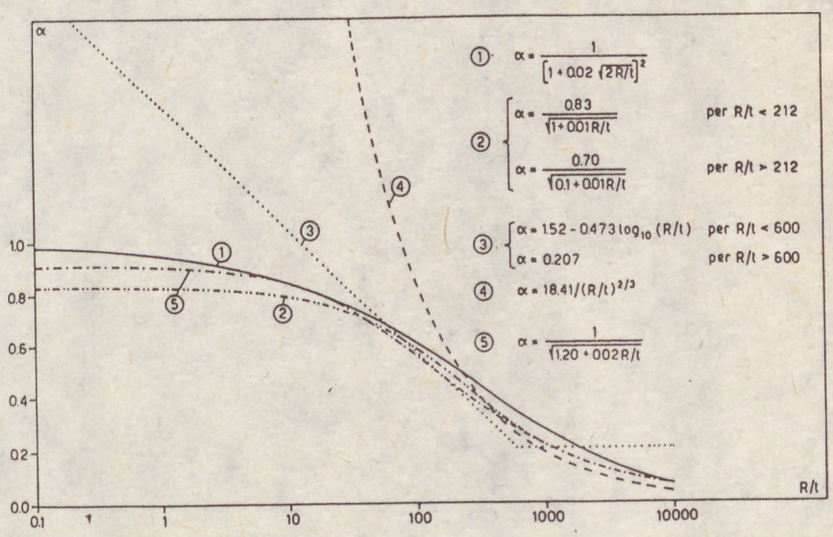

Fig. 1

(8)

SERIES	DENOMINATION	DIMENSIONS		$f_{0.1}$	$f_{0.2}$	f_t	ϵ_t	n	n'
		Rxt (mm)	R/t	(N/mm^2)	(N/mm^2)	(N/mm^2)	(%)		
1	6082	25x2	12.5	253	256	273	12.45	59	66
2	1050 A	27x2	13.5	78	80.5	84.5	14.65	27	88
3	5086	27x1.5	18	218.5	224.5	280.5	12.40	26	18
4	1050 A	30x2.5	12	82.5	85.5	90	15.30	19	84
5	6060	50x2	25	213	218.5	244	14.80	27	39
6	1050 A	60x6	10	33	35	65	42.00	12	9
7	6060	40x1	40	-	188	215	14.2	20(*)	32
8	6060	50x1.25	40	-	188	215	14.2	20(*)	32

(*) Estimated value in absence of $f_{0.1}$

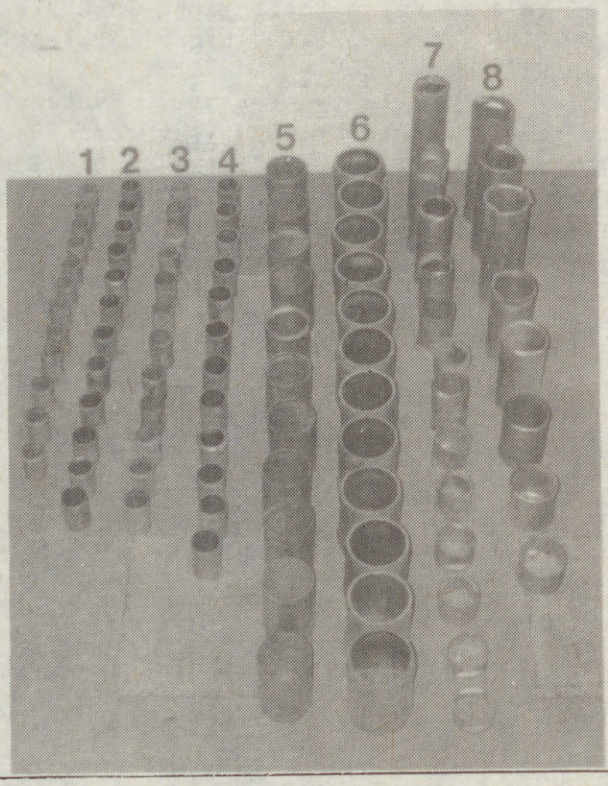

Tab. 1

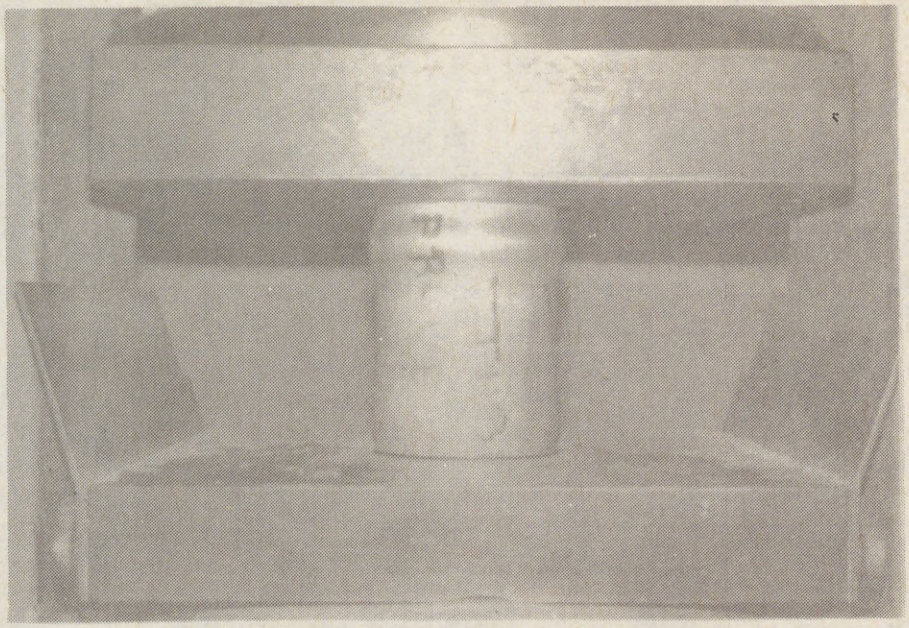

Fig. 2

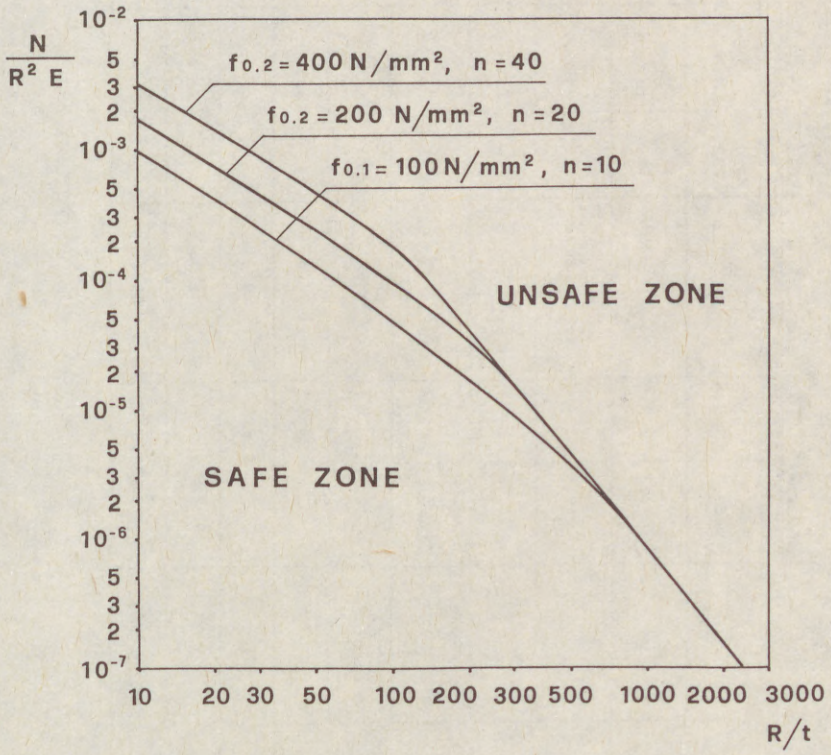
N / R² E
10⁻²
5
3
2
10⁻³
5
3
2
10⁻⁴
5
3
2
10⁻⁵
5
3
2
10⁻⁶
5
3
2
10⁻⁷
f0.2 = 400 N/mm², n = 40
f0.2 = 200 N/mm², n = 20
f0.1 = 100 N/mm², n = 10
UNSAFE ZONE
SAFE ZONE
10 20 30 50 100 200 300 500 1000 2000 3000
R/t

Fig. 3

	SERIES 1 R/t = 12.5 $f_{0.2}$=256 N/mm^2		SERIES 2 R/t = 13.5 $f_{0.2}$=80.5 N/mm^2		S SERIES 3 R/t = 18 $f_{0.2}$=224.5 N/mm^2		SERIES 4 R/t = 12 $f_{0.2}$=85.5 N/mm^2		SERIES 5 R/t = 25 $f_{0.2}$=218.5 N/mm^2		SERIES 6 R/t = 10 $f_{0.2}$=35 N/mm^2		SERIES 7 and 8 R/t = 40 $f_{0.2}$=188 N/mm^2	
	n = 59	n'= 66	n = 22	n'= 88	n = 26	n'=18	n = 19	n'= 84	n = 27	n'= 39	n = 12	n'= 9	n = 20	n'= 32
$\eta = \sqrt{\frac{E_t E_s}{E}}$	259.7	259.0	86.2	81.2	232.7	239.2	93.5	86.4	222.5	219.9	41.9	45.2	188.9	186.7
$\eta = \sqrt{\frac{E_t}{E}}$	263.3	262.1	94.5	82.6	240.9	253.0	104.4	88.1	228.3	223.3	54.3	63.8	194.6	189.5
$\eta = \frac{E_s}{E}$	269.8	268.3	92.6	83.4	249.2	260.9	101.2	88.8	238.3	232.0	46.5	51.1	205.8	199.0
$\eta = \frac{E_s}{E}\sqrt{\frac{E_t}{E}}$	257.9	257.5	83.1	80.6	228.7	232.9	89.4	85.8	219.4	218.0	37.8	39.3	185.7	185.0
$\eta = \sqrt{\frac{E_t}{E_s}}$	441.2	417.2	669.1	334.5	461.6	554.8	810.0	385.2	326.1	271.4	1223.0	1412.2	238.5	201.3
n specimens	12		12		12		11		11		12		21	
σ_{med} (N/mm^2)	286.2		96.8		243.5		94.7		216.3		56.4		169.3	
s	4.23		2.54		2.71		3.97		3.45		0.31		15.18	
k	2.74		2.74		2.74		2.82		2.82		2.74		2.38	
σ_k (N/mm^2)	274.6		89.8		236.1		83.5		206.6		55.6		133.2	

Tab. 2

Tab. 2

		$\alpha = 1$					$\alpha = \frac{1}{\left[1+0.02\sqrt{2R/t}\right]^2}$					$\alpha = \frac{0.83}{\sqrt{1+0.01\ R/t}}$					$\alpha = 1.52-0.473\ \log_{10}(R/t)$				
		1	2	3	4	5	1	2	3	4	5	1	2	3	4	5	1	2	3	4	5
SERIES 1	n = 59	-5.43	-4.12	-1.75	-6.08	60.67	-21.84	-20.76	-18.80	-22.38	32.79	-25.99	-24.97	-23.11	-26.51	25.73	-5.32	-4.00	-1.63	-5.97	60.86
R/t = 12.5	n'= 66	-5.68	-4.55	-2.28	-6.23	51.93	-22.05	-21.12	-19.25	-22.50	25.56	-26.19	-25.31	-23.54	-26.61	18.89	-5.57	-4.44	-21.80	-6.12	52.11
SERIES 2	n = 22	-4.01	5.23	3.12	-7.46	645.10	-21.23	-13.65	-15.38	-24.06	511.40	-25.22	-18.01	-19.66	-27.91	480.50	-5.41	3.69	1.61	-8.82	634.20
R/t = 13.5	n'= 88	-9.58	-8.02	-7.13	-10.24	272.50	-25.80	-24.52	-23.97	-26.35	205.70	-29.55	-28.34	-27.64	-30.07	190.20	-10.90	-9.37	-8.49	-11.56	267.00
SERIES 3	n = 26	-1.44	2.03	5.55	-3.13	95.51	-21.43	-18.66	-15.86	-22.78	55.86	-24.69	-22.04	-19.35	-25.99	49.38	-8.71	-5.49	-2.24	-10.28	81.09
R/t = 18	n'= 18	1.31	7.16	10.50	-1.36	135.00	-19.23	-14.57	-11.92	-21.36	87.33	-22.59	-18.12	-15.57	-24.63	52.37	-6.16	-0.74	2.36	-8.63	117.70
SERIES 4	n = 19	11.98	26.03	21.20	7.07	870.10	-7.12	3.71	0.53	-11.19	704.70	-12.18	-1.94	-4.95	-16.03	660.80	13.05	26.22	22.35	8.09	879.30
R/t = 12	n'= 84	3.47	5.51	6.35	2.75	361.30	-14.17	-12.48	-11.79	-14.77	282.70	-18.85	-17.25	-16.59	-19.41	261.80	4.46	6.52	7.36	3.74	365.70
SERIES 5	n = 27	7.70	10.50	15.34	6.20	57.80	-17.34	-15.18	-11.47	-18.49	21.15	-20.05	-17.97	-14.37	-21.16	17.18	-7.51	-5.10	-0.95	-8.80	35.55
R/t = 25	n'= 39	6.44	8.08	12.29	5.52	31.36	-18.30	-17.04	-13.81	-19.01	0.38	-20.98	-19.76	-16.64	-21.67	-2.48	-8.59	-7.18	-3.56	-9.38	12.81
SERIES 6	n = 12	24.64	-2.34	-16.37	-32.01	21.00	-36.51	-17.72	-29.54	-42.72	17.53	-40.36	-22.71	-33.81	-46.20	16.41	-21.10	2.25	-12.44	-22.82	22.03
R/t = 10	n'= 9	18.71	14.75	-8.09	-29.32	24.40	-31.51	-3.32	-22.56	-40.43	20.40	-35.67	-9.19	-27.27	-44.06	19.10	-14.88	20.14	-3.77	-25.99	25.59
SERIES 7 and 8	n = 20	41.82	46.10	54.50	39.41	70.05	2.04	5.12	11.17	0.31	28.84	0.52	2.48	8.38	-2.20	25.60	8.10	11.36	17.77	6.27	36.48
R/t = 40	n'= 32	40.17	42.27	49.40	38.89	51.13	0.85	2.37	7.50	-0.06	8.74	-1.68	-0.20	4.80	-2.57	6.01	6.84	8.44	13.88	5.86	15.19

1. THEORY OF PLASTIC DEFORMATIONS
2. FLOW THEORY (INCREMENTAL TYPE)
3. THEORY OF SECANT MODULUS
4. THEORY OF WEINGARTEN, MORGAN & SEIDE
5. THEORY OF GERARD & STOWELL

Tab. 3

(1)
TARN

CELL

Summa
spher
honey
show
-dimp
analo

1. IN

In st
are t
tail
(Gion

A thi
press
mond
-gona
of th
ed by

Anothe
spheri
vestig
inform
advanc
tern
mostly
phases

(1) Hu

(1)
TARNAI, Tibor (1)

CELLULAR BUCKLING SHAPE OF COMPLETE SPHERICAL SHELLS

INTERNATIONAL COLLOQUIUM
STABILITY OF STEEL STRUCTURES
BUDAPEST, HUNGARY, 1990
PRELIMINARY REPORT

Summary: Analogy between the post-buckling equilibrium form of complete spherical shells with the mandrel inside and the form of living spherical honeycomb structures is investigated. The primary aim of this paper is to show briefly the typical topological-geometrical properties of the multi--dimple buckling pattern of a complete spherical shell on the basis of this analogy.

1. INTRODUCTION

In stability research on thin elastic shells, circular cylindrical shells are the most intensively studied structures and almost every important detail of their buckling has been cleared up (Kollár and Dulácska, 1984), (Gioncu and Ivan, 1978).

A thin-walled circular cylindrical shell subjected to uniform axial compression, in the advanced phases of the buckling process, buckles in a diamond pattern close to the Yoshimura pattern that is composed of equal n--gonal antiprisms consisting of equal isosceles triangles. The main feature of this buckling pattern is a high order of symmetry that has been confirmed by several experiments (Yamaki, 1984).

Another common shell form is the sphere. Buckling of thin-walled complete spherical shells subjected to uniform external pressure has also been investigated (Kollár and Dulácska, 1984), (Gioncu and Ivan, 1978) but scanty information is available on the buckling pattern especially on that at an advanced stage of the buckling process. Data available on the buckling pattern of complete spherical shells are quite meagre since researchers have mostly dealt with local phenomena and with the buckling shape in the early phases of the buckling process with the formation of a single dimple. The

(1) Hungarian Institute for Building Science, Budapest

(2)

(a)

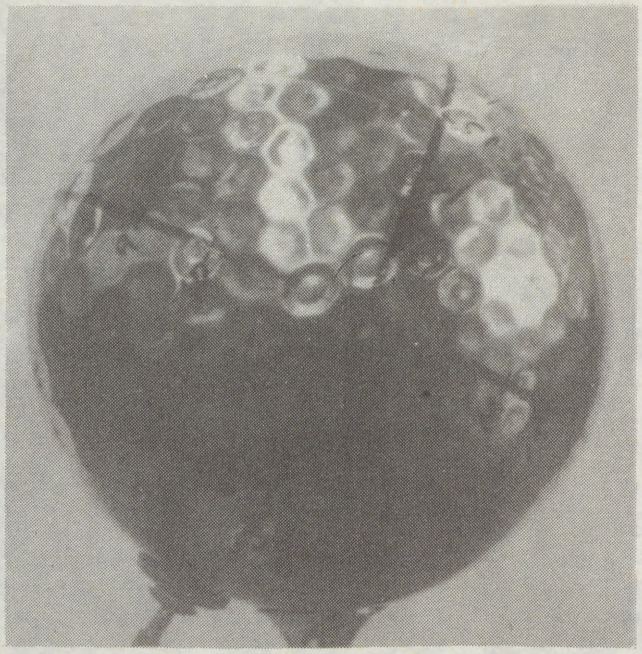

(b)

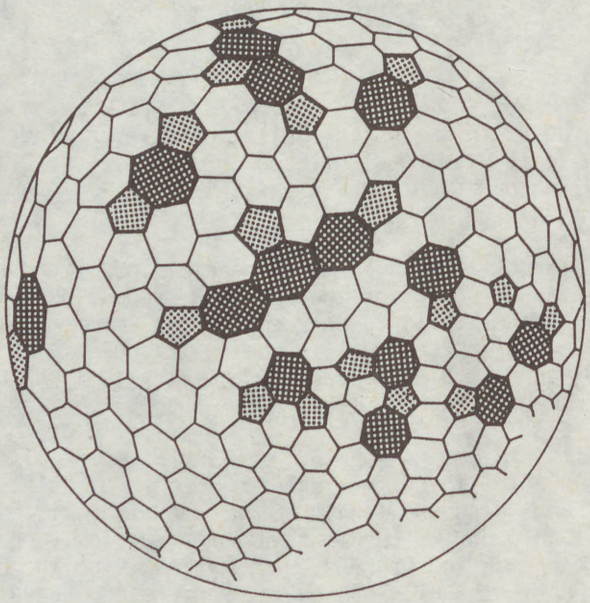

Fig.1. Buckling pattern of a complete spherical shell. (a) Air-system test with wax mandrel inside the specimen (courtesy of Professor N.J. Hoff). (b) Pentagons and heptagons in the buckling pattern.

(3)

(a)

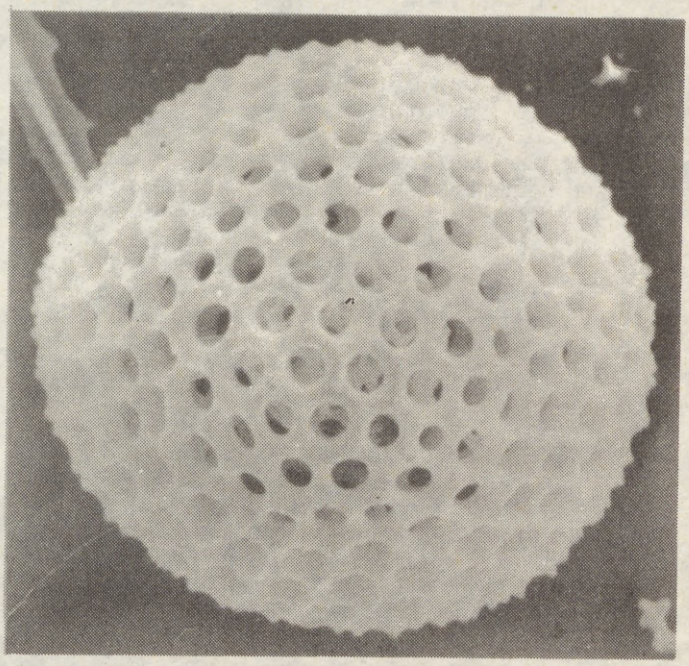

(b)

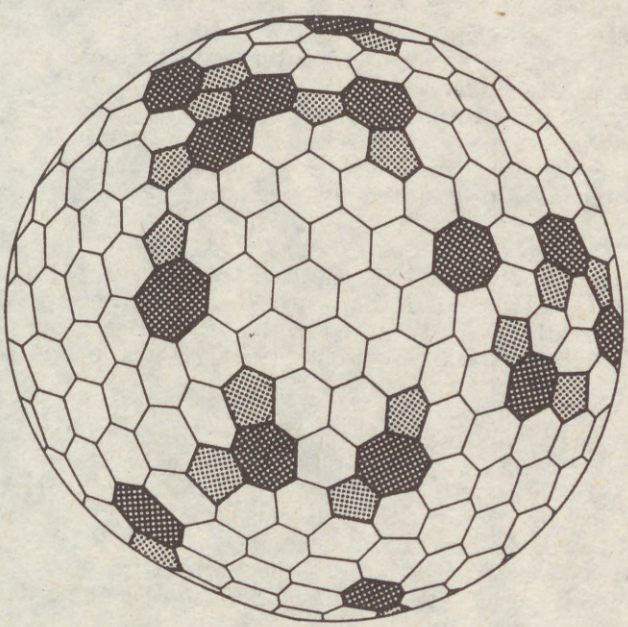

Fig.2. (a) Scanning electron micrograph of a spherical radiolarian (courtesy of Dr. S.A. Kling) and (b) pentagons and heptagons in its network.

(4)

buckling pattern of the sphere, where the buckled state occurs with the formation of a large number of dimples, is not known. It is not known either whether this buckling pattern has certain kind of symmetry.

An interesting idea on the development of the buckling pattern, which is tacitly supposed to be a rounded "polyhedron" with icosahedral symmetry, can be found in (Gioncu and Ivan, 1978). To our knowledge, the only series of experiments, which was executed also in the advanced phases of the buckling process and could produce a large number of dimples forming a honeycomb on the complete spherical surface, was performed at Stanford University by Carlson, Sendelbeck and Hoff (1967).

The aim of this paper is to try to show in brief an outline of the formation of the buckling pattern of complete spherical shells by means of the Stanford experiments (Carlson et al., 1967) and of analogies with spherical honeycomb structures in nature. A more detailed discussion can be found in (Tarnai, 1989).

2. BUCKLING OF COMPLETE SPHERICAL SHELLS

During the buckling process of complete thin-walled spherical shells subjected to uniform external pressure, in general, only one dimple appears which gradually deepens and so leads to collapse of the sphere. However, Hutchinson (1967) and Koiter (1969) have shown that in the initial stage of post-buckling a cellular deflection pattern consisting of hexagons can develop on a part of the shell surface; but the problem is that this deflection pattern cannot be extended to the entire shell surface because, as a consequence of the Euler polyhedron theorem, it is impossible to enclose a simply connected domain of the three-dimensional space by a polyhedron bounded merely by hexagons (D'Arcy Thompson, 1963). A trivalent polyhedron (i.e. a polyhedron in which three edges meet at each vertex) mainly composed of hexagons always need polygons bounded by less than six sides. The Euler Theorem also involves that in a trivalent polyhedron bounded by pentagons and hexagons the number of pentagons is always 12.

Knowing these facts and the idea of Gioncu and Ivan (1978) and certain geometrical arguments (Tarnai, 1989) one can imagine the full buckling pattern of the complete spherical shell as a honeycomb composed of pentagons and hexagons corresponding to a covering system of not necessarily equal circles on the sphere in icosahedral symmetry. Reality, however, shows a different picture.

The quasi-hexagonal cellular buckling pattern, also at the advanced stage of the buckling process, can be realised physically if the inward deflections of the shell are restricted by a mandrel with a small clearance. This principle was applied in the Stanford experiments (Carlson et al., 1967). In the test the mandrel-restricted specimens were gradually evacuated and under external air pressure the shells buckled with a simultaneous formation of a large number of dimples. The resulting buckling pattern of one of the specimens is shown in Fig. 1(a).

Apart from a region along the contour of the sphere we have identified the

buckling pattern of the specimen in Fig. 1(a) and drawn it in Fig. 1(b). Examination of Fig. 1(b) reveals that the buckling pattern contains not only pentagons and hexagons, as expected, but heptagons also, and the buckling pattern has no symmetry at all. It is of interest to observe that many of the dimples in Fig. 1(a) contain circular swelling in the middle as small "anti-dimples".

It is not clear from this experiment whether the honeycomb shape of the buckling pattern with its irregularities is accidental or it represents certain rules generally valid for spherical honeycombs in nature. Since this example of buckling pattern is the only one available to us, to detect the tendencies we have considered analogies with other spherical honeycomb structures in nature.

3. ANALOGIES IN NATURE

Figure 2(a) shows the quasi-hexagonal pattern of the skeleton of a spherical radiolarian. Comparing the line drawing of the buckling pattern of the spherical metal shell (Fig. 1(b)) and the line drawing of the structural network of the radiolarian (Fig. 2(b)) it can be ascertained that:

(1) The honeycombs are asymmetric.
(2) The honeycombs are trivalent "polyhedra" bounded by pentagons, hexagons and heptagons.
(3) It is typical that a pentagon has a heptagon neighbour joined to it by a whole side. (Only one exception is seen in Fig. 1(b) where there is an individual pentagon, i.e. completely surrounded by hexagons.)
(4) It is typical that a heptagon has a pentagon neighbour joined to it by a whole side. (Only one exception is seen in Fig. 2(b) where there is an individual heptagon, i.e. completely surrounded by hexagons.)

One can find three kinds of typical morphological modules in these honeycombs: hexagons, pentagon-heptagon juxtapositions and pentagon-heptagon--pentagon juxtapositions. Occurrence of individual pentagons and heptagons is not frequent, so they may be considered as exceptions.

There is an additional surprising similarity between Fig. 1(a) and Fig.2(a), namely the circular openings in the radiolarian shell seem to have the same morphological properties as the circular "anti-dimples" on the buckled metal shell.

Several other examples of spherical honeycombs and quasi-hexagonal patterns can be found in nature, e.g. certain pollen grains (Bolick, 1981), coated vesicles (Heuser and Evans, 1980), showing morphological properties similar to those in Fig. 1(a).

4. CONCLUSIONS

The morphological resemblance between the buckling pattern of the spherical metal shell in Fig. 1(a) and the shape of the radiolarian shell in Fig.2(a) (and other spherical honeycombs in nature) is striking. Although resemblance is nothing more than simple analogy, it helps to understand and to predict the buckling pattern of complete spherical shells with the mandrel inside.

(6)

The shape of the buckled sphere in Fig. 1(a) has probably been influenced by random imperfections. We beleive that the shape itself is not accidental but some of its details show certain tendencies and in this sense the buckling pattern is typical, and the considered analogy confirms this observation. The main features are enumerated in Section 3.

From all of these it follows that, in a rigorous post-buckling analysis, calculations should be extended to the entire shell surface because of lack of symmetry, that is, calculations cannot be simplified due to symmetry; and the cellular buckling pattern, under which the potential energy is a minimum (stationary), should contain not only pentagons and hexagons but heptagons also, and the distribution of the pentagons and heptagons in the honeycomb should meet the observed tendencies.

Acknowledgement: The research reported here was supported by OTKA Grant No. 744 awarded by the Hungarian Scientific Research Foundation.

REFERENCES

Bolick, M.R. (1980). Mechanics as an aid to interpreting pollen structure and function. Rev. Palaeobot. Palynol. 35, 61-69.

Carlson, R.L., Sendelbeck, R.L. and Hoff, N.J. (1967). Experimental studies of the buckling of complete spherical shells. Exp. Mech. 7(7), 281-288.

D'Arcy Thompson, W. (1963). On Growth and Form, 2nd edn. Reprinted, Cambridge Univ. Press, Cambridge.

Gioncu, V. and Ivan, M. (1978). Buckling of Shell Structures (in Romanian). Editura Academiei, Bucharest.

Heuser, J. and Evans, L. (1980). Three-dimensional visualization of coated vesicle formation in fibroblasts. J. Cell Biol. 84, 560-583.

Hutchinson, J.W. (1967). Imperfection sensitivity of externally pressurized spherical shells. J. Appl. Mech. 34, 49-55.

Koiter, W.T. (1969). The nonlinear buckling problem of a complete spherical shell under uniform external pressure, I-IV. Proc. Kon. Nederl. Akad. Wet. B72, 40-123.

Kollár, L. and Dulácska, E. (1984). Buckling of Shells for Engineers. Akadémiai Kiadó, Budapest/Wiley, Chichester.

Tarnai, T. (1989). Buckling patterns of shells and spherical honeycomb structures. Computers Math. Applic. 17, 639-652.

Yamaki, N. (1984). Elastic Stability of Circular Cylindrical Shells. North-Holland, Amsterdam.

THIELE, Rolf (1)
LEISSNER, Ulrich (2)

STABILIZING EFFECT OF THE INTERNAL PRESSURE IN STEEL SILOS

INTERNATIONAL COLLOQUIUM
STABILITY OF STEEL STRUCTURES
BUDAPEST, HUNGARY, 1990
PRELIMINARY REPORT

Summary: The internal pressure of silos is contributing to the stabilization of the axially loaded imperfect cylinder shell so that the reduction factor of the ideal buckling stress value can be valued higher: $\alpha + \Delta\alpha$. The value $\Delta\alpha$ is quantitatively analyzed by means of several procedures. In practically relevant ranges the plate thickness stepping has a low influence on $\Delta\alpha$ and, thus, on the critical buckling load.

The buckling strength of circular cylindrical shells under axial pressure is of special importance for the thin cylindrical shells of steel silos concerning the safety and economy. The imperfection sensitivity is the reason why the classical critical stress

$$\sigma_{Ki} = 0.605 \cdot E \cdot t/R \qquad (1)$$

will never be achieved in practice. For practical dimensioning there are used experimentally or quasi-theoretically determined reduction factors α , which are fixed in their value by the geometry

(1) Professor of Mechanics, Technische Hochschule Leipzig
(2) Assistant of Mechanics, Technische Hochschule Leipzig

(2)

$$\sigma_{Kr} = \alpha \cdot \sigma_{Ki} \qquad (2)$$

and by constructive measures such as longitudinal and annular bracings. The buckling load increasing effect of the internal pressure for the axially loaded isotropic circular cylinder was the subject of studies made as early as thirty decades ago. A decisive influence quantity is the reliable value of the horizontal pressure of the bulk material in the silo. On it the reduction of the cylinder's imperfection sensitivity is dependent decisively. In a test by simulating the internal pressure with gases it was possible to achieve buckling stresses in the order of the classical values according to equation (1). The computational aquisition of the increase is made by the coefficient $\Delta\alpha$ which is added to the factor according to equation (2) additively

$$\sigma_{Kr} = (\alpha + \Delta\alpha) \cdot \sigma_{Ki} \qquad (3)$$

Depending on the internal pressure parameter

$$\bar{p} = \frac{p}{E} \cdot \left(\frac{R}{t}\right)^2 \qquad (4)$$

there are zwo possibilities when determining $\Delta\alpha$:

- dimensioning solutions which are, in addition to $\bar{p}$, dependent on the ratio R/t within the procedure
- dimensioning solutions in which $\Delta\alpha$ is taken from a combined curve dependent on $\bar{p}$ only.

The first principle is shown quantitatively in Fig. 1 and is based on suggestions of well-known authors and on standards for a practice-relevant ratio R/t = 800. The function characteristic for the second procedure is, with curve 5, given in Fig. 1 as well and is based on a 90 per cent probability. The considerable deviations of the $\Delta\alpha$ values according to the procedures of Fig. 1 will become distinct with their dimonsioning influence of the percentage increase of the buckling loads are contrasted with α of Fig. 2 under consideration of the inter-

(3)

nal pressure relating to the appropriate reduction factor - see equation (3) - which is different from procedure to procedure. High percentage increases will result in procedures which use relatively low values for the reduction factor .

The limitin curve according to ECCS is largely confirmed by test results and by latest theoretical researches for the safety level provided. ECCS gives equation (5) for :

$$\Delta\alpha = (1 - \alpha) \cdot \frac{\bar{p}}{\bar{p} + 0.007} \quad \text{with} \qquad (5)$$

$$\alpha = \frac{0.7}{0.1 + \frac{R}{100 \cdot t}} \quad \text{and deviating from equation} \qquad (4)$$

$$\bar{p} = \frac{p}{E} \cdot \sqrt{\left(\frac{R}{t}\right)^3}$$

The nomograms show distinctly that the supporting effect of the internal pressure reduces heavily with decreasing R/t ratios. A consideration in the plastic strain rangs is not to be recommended for the time being. As far as the suggestions (Fig.1) are related to tests, these are experiments with gas pressure equivalents. Test results for internal pressure load from actual bulk materials are existing to a small degree only.
An analysis of the linterature has produced with equation (3) the result shown in Fig. 3. Moreover, the curve according to ECCS for R/t = 500 is shown for comparsion because $400 < R/t < 500$ was valid for the test cylinders. This curve limits well (Fig. 3) the known test results.
$\Delta\alpha$ is reduced by wall thickness steppings which are indispensable in an economical construction. According to /1/ und /2/ the combination of axial load and internal pressure is possible for the stepped cylinder. For the connected eccentricities e of adjacent sections a reduction of the value $\Delta\alpha$ is to be made. $\Delta\alpha$ is to be reduced with the factor m according to equation (6) for $e \leq 1.1\ t_i$.

(4)

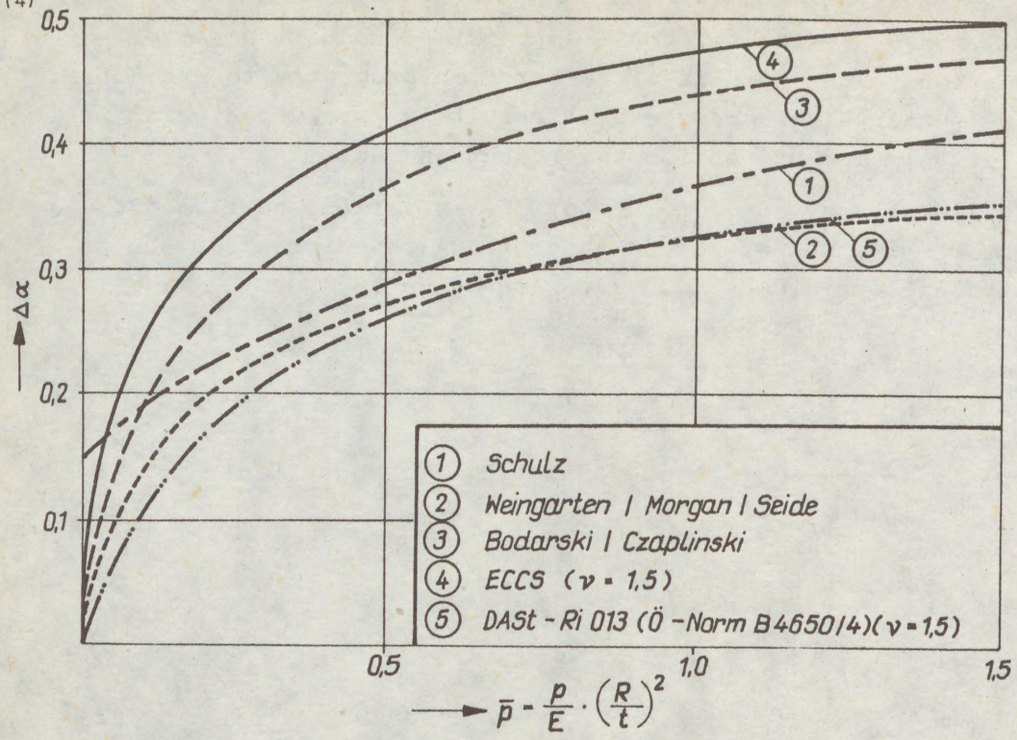

Fig. 1 Buckling load increasing coefficient $\Delta\alpha$ for $\frac{R}{t} = 800$

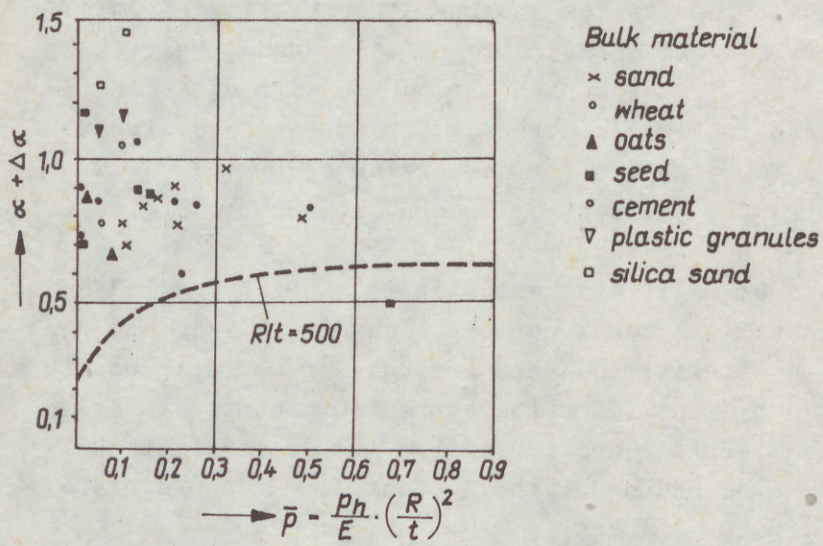

Fig.3 Comparison between buckling loads of axially loaded cylinders with internal pressure by bulk material calculated according to ECCS for R/t = 500, γ = 1,5

(5)

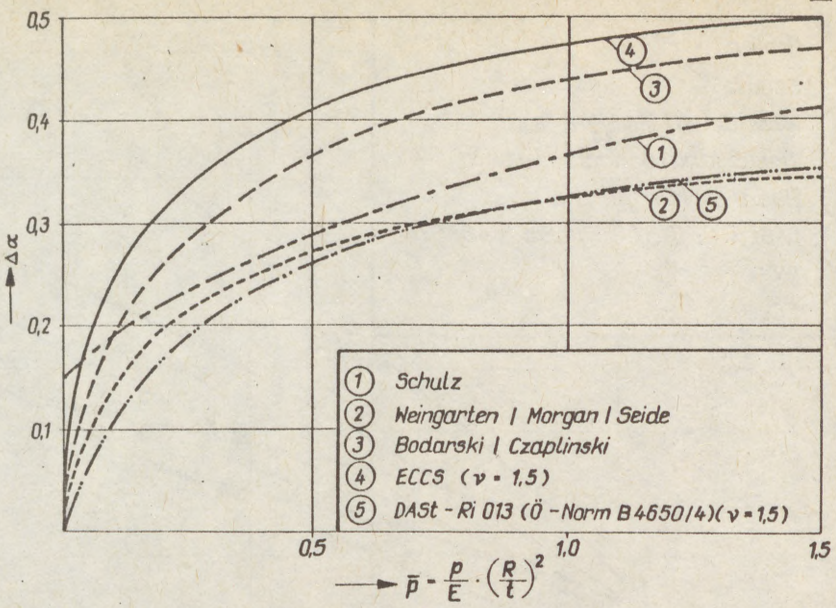

Fig. 1 Buckling load increasing coefficient $\Delta\alpha$ *for* $\frac{R}{t} = 800$

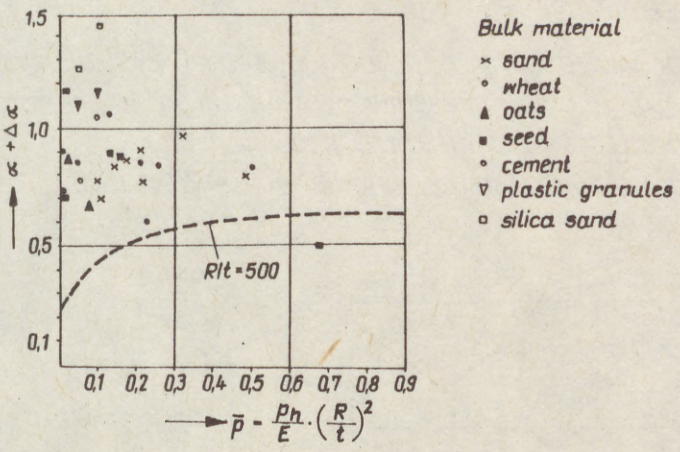

Fig. 3 Comparison between buckling loads of axially loaded cylinders with internal pressure by bulk material calculated according to ECCS for $R/t = 500$, $\gamma = 1,5$

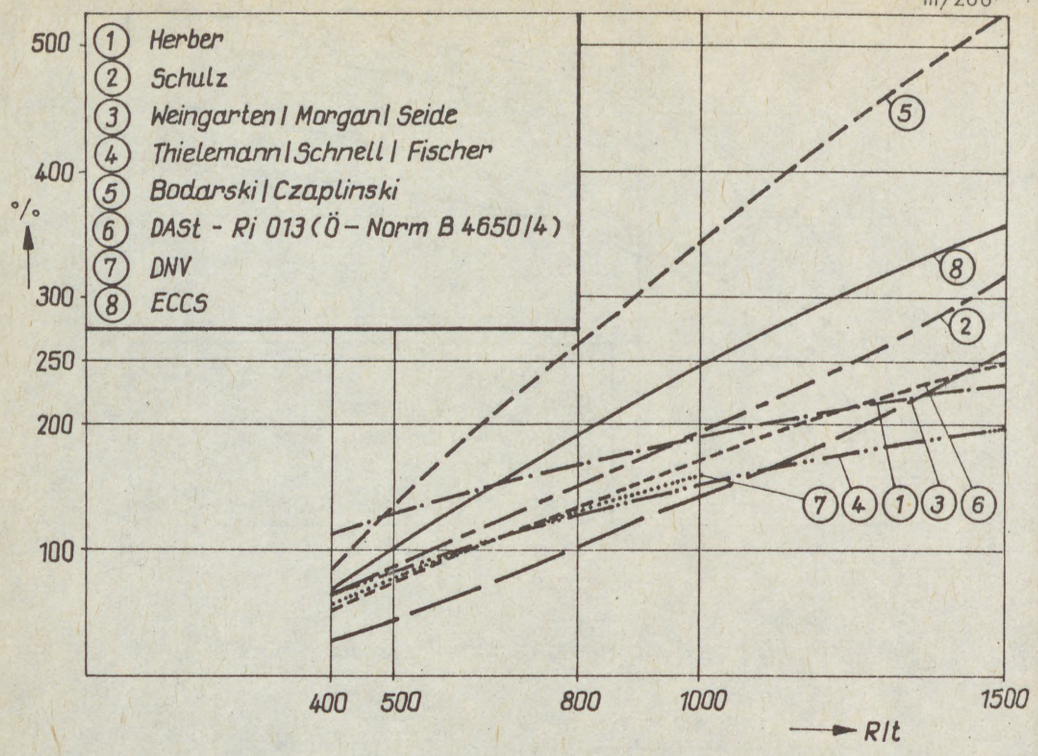

Fig. 2 Percentage increases of buckling loads by the stabilizing effect of the internal pressure relative to the appropriate reduction factors α of different procedures.
$p_h = p = \text{const} = 0{,}1\ N/mm^2$ (in the range of $400 \leq R/t \leq 1500$)

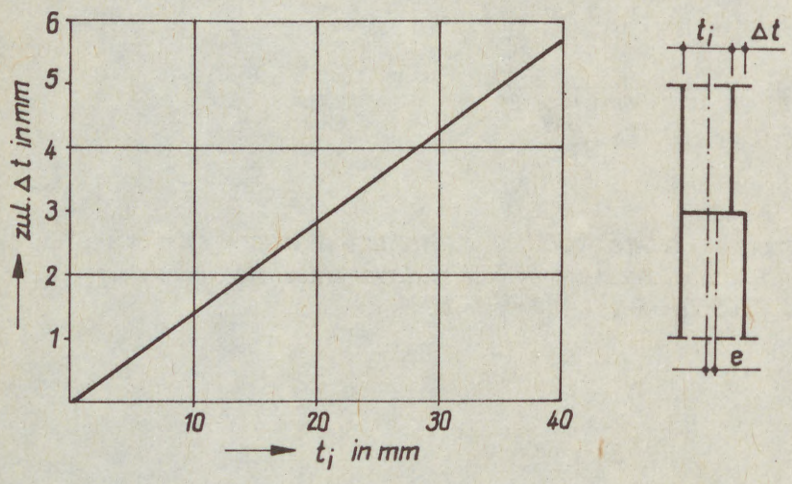

Fig. 4 Permissible misalignment between adjacent sections of axial and internal pressures for $\Delta\alpha_{misalignment} = 0{,}9 \cdot \Delta\alpha$

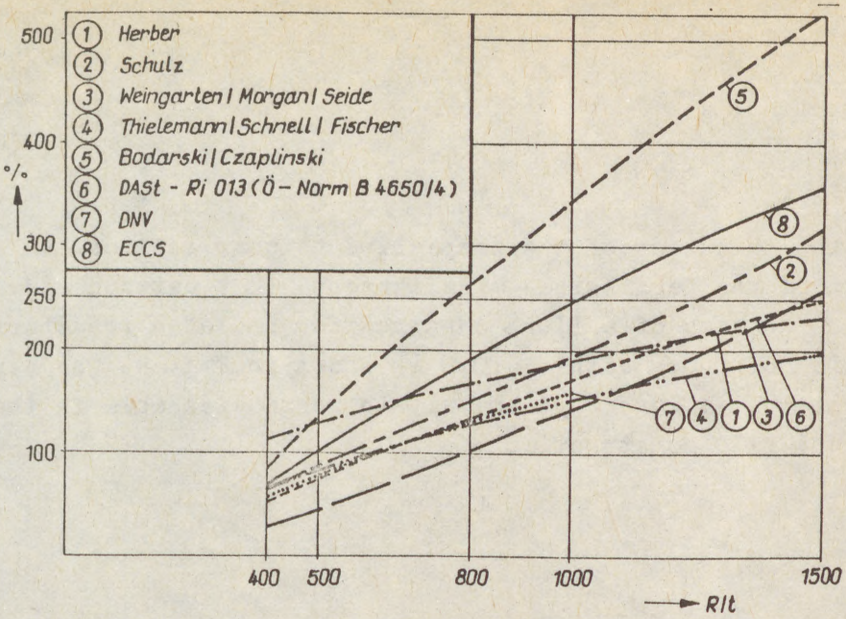

Fig. 2 Percentage increases of buckling loads by the stabilizing effect of the internal pressure relative to the appropriate reduction factors α of different procedures.
$p_h = p = \text{const} = 0{,}1\,N/mm^2$ (in the range of $400 \leq R/t \leq 1500$)

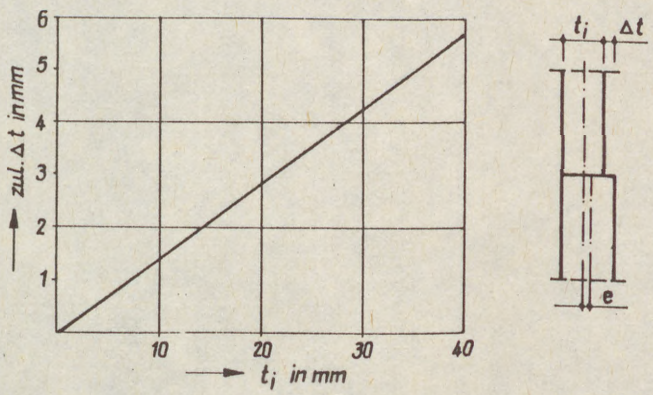

Fig. 4 Permissible misalignment between adjacent sections of axial and internal pressures for $\Delta\alpha_{misalignment} = 0{,}9 \cdot \Delta\alpha$

$$m = 1 - \frac{1.5\, e}{t_i + e} \qquad (6)$$

t_i is the thickness of the respective thinner section. An evaluation of the permissible misalignment Δt between adjacent sections in case of a flush construction and of a predetermined reduction of $\Delta\alpha$ with m = 0.9 is shown in Fig. 4. The permissible values for Δt are within ranges feasible in the practical silo construction.

Bibliography

/1/ DAST-Richtlinie 013, Deutscher Ausschuß für Stahlbau, Beulsicherheitsnachweise für Schalen, 1980

/2/ Ö-Norm B 4650 / 5, Beulung von Kreiszylinderschalen mit abgestufter Wanddicke, 1980

(1)

TURČIĆ, FRANJO[1]

RESISTANCE OF AXIALLY COMPRESSED CYLINDRICAL SHELLS DETERMINED FOR THE MEASURED GEOMETRICAL IMPERFECTIONS

INTERNATIONAL COLLOQUIUM
STABILITY OF STEEL STRUCTURES
BUDAPEST, HUNGARY, 1990
PRELIMINARY REPORT

Summary: The resistance probability characteristics of an axially compressed circular cylindrical geometrically imperfect steel shell (R/t=500, R=3500 mm, t=constant = 7 mm, without any stiffeners) are determined, using probabilistic approach. For this purpose, probability characteristics of the following resistance variables are investigated: geometrical imperfection, wall thickness, and yielding point of material, which were treated as random values. Probable combinations of these three variables are determined by the Monte Carlo method. Real geometrical imperfection is approximated using axysimmetric model, with imperfection amplitudes treated as random values. For each combination of variables corresponding shell resistance is determined, using computer program Bosor 5 for numerically simulated experiments. The total of 50 numerically simulated experiments are made. Very good conformity with known results of laboratory experiments was reached.

1. Introduction

In the scope of the extensive sound research, and in order to find a model for investigation of the reliability index of constructed steel silos ("calibration") it was necessary to determine resistance probability characteristics (mean value, coefficient of variation and probability distribution) (Turčić, 1987,/7/, Milčić, 1981,/6/).
Resistance is a random value depending on several variables, which are also random values. In this paper only three of them are treated as random values: geometrical imperfection amplitudes, wall thickness and material yielding point, while others are treated as determined values.
In the usual design process, the resistance of a real shell is determined on the basis of numerous statistically evaluated experimental results, while geometrical imperfections are limited in the construction process.

---

[1] Associate professor of Steel Structures, University of Zagreb, Faculty of Civil Engineering.

Prescribed geometrical tolerances are sometimes not respected during the process of construction, and then appears a problem of safety level estimation for the known geometrical imperfections.
Some authors have investigated, by using the deterministic approach, possibilities of analytical prediction of resistance, based on the geometrical imperfections measured either on laboratory models or on finished structures (e.g. Arbotz, Babcock, 1978, /1/; Häfner, 1982, /4/).
Probability characteristics of resistance variables are determined in this paper on the basis of a limited number of data collected in Yugoslavia. That is why the assumptions must be further scientifically verified and the results can only serve for further research and information purposes.

2. Probability characteristics of the basic resistance variables

2.1. Wall thickness (t) – The coefficient of variation $v = 0.0232$ and an average relation between the arithmetic mean and nominal value $\bar{t}/t_n = 1.028$ were determined by analysing 1106 data for three different plate thicknesses. If we apply this to $t_n = 7$ mm the following values are obtained: mean value $\bar{t} = 7.19$ mm and standard deviation $\sigma = 0.167$ mm. The normal probability distribution was adopted.

2.2. Yielding point (σ_y) – The total of 2846 data related to the steel quality St 37 (DIN) from three different national sources was analysed. The following results were obtained: $\bar{\sigma}_y = 284$ through 315 N/mm²; $v = 0.081$ through 0.147; $\bar{\sigma}_y/\sigma_y(\text{nom.}) = 1.18$ through 1.31; Hypotheses related to the lognormal and normal probability distribution are acceptable. Following characteristics were adopted for further analysis: $\bar{\sigma}_y = 1.10 \cdot \sigma_y(\text{nom}) = 1.10 \cdot 240 = 264$ N/mm²; $v = 0.11$; (Galamboš, Ravindra, 1978, /3/) as well as the normal probability distribution.

2.3. Initial geometrical imperfections ($w = f(x,\Phi)$) – The total of 3700 individual data obtained by measuring deviation from the ideal cylindrical form collected at five structures located in different zones was analysed(15 individual cylindrical shells for different purposes, of different dimensions, construction details and materials – Turčić 1987, /7/).
The amplitudes of deviation were measured at approx. 8 to 32 measuring points (depending on cylinder's diameter) along the cylinder's circumference at each parallel circular cross section located at each level of circular weld.
An average absolute value of the imperfection amplitude ($/\bar{w}_o/$) and its coefficient of variation were determined for each of these cross sections. The same procedure was carried out for the groups of parallel circular sections and also for groups of shells having equal t and R values (practically equal average absolute amplitude value will be obtained either from positive or from negative imperfections if the circumference remains constant).
It has been noticed that the coefficient of variation varies from 0.62 to 0.93 regardless of the type of material used and also regardless of t, R, R/t $/\bar{w}_o/$ and $/\bar{w}_o//t$ values. It has equally been observed that both normal and lognormal distributions are acceptable for an average absolute amplitude value. Lognormal distribution was used in this paper with the coefficient of variation $v = 0.79$.
The following mean value of the average absolute value of deviation amplitude for the critical parallel circular cross section was adopted: $/\bar{w}_o/ = 0.86t = 6.05$ mm (due to the lack of statistical data for $R/t = 500$).

(3)

3. Approximation of the form of geometrical imperfection

It can be seen from the measuring results that the deviation amplitudes change sign several times both in the direction of circumference and meridian (negative sign towards the center and positive sign out of the cylinder).
The author starts from the assumption that the deviation of both signs is unfavourable for the stability loss.
From the description of the initial occurrence, development and appearance of the buckle figure at the critical cross section (several references, e.g. Wolmir, 1962, /8/), it is visible that the greatest part of the circumference has a deformation of the negative sign ("vales") and only a smaller part has a deformation of the positive sign ("hills"). Number of vales is equal to the number of hills. It seems that after a certain degree of deformation, the hills begin to act as stiffeners - bearing capacity of this cross section increases. If the load is further increased the deformations also increases and similar stability loss occurs in the weakest neighboring cross section.
On this basis, the author thought it possible to approximate well enough the real unsymmetrical form of the initial geometrical imperfection ($w = f(x,\Phi)$) with the axisymmetrical model ($w = f(x)$) of the constant negative amplitude along the entire circumference of the critical cross section (an efficient computer program called Bosor 5, Bushnell, 1976,/2/ is only able to deal with axisymmetrical geometrical imperfection). The amplitude value is equal to the average absolute value of the determined number of measured amplitudes. The number of measurements must be sufficient at points that are uniformly distributed along the circumference.
Shape and dimensional relations of initial geometrical imperfection in the meridional direction, near the critical cross section, are adopted as presented in the doctor's thesis Häfner, 1982, /4/, with the maximal amplitude of negative sign in the critical cross section (not dependant to circular welds) (cf. Fig. 1).

4. Random values combinations of resistance variables

Each individual numerically simulated experiment is made with a single combination of resistance variables random values. Their occurrence probability is the consequence of their probability distributions. Such combinations are obtained by the Monte Carlo method. In this procedure, an arbitrary number of random numbers is determined by means of appropriate random number generators.

a) Random numbers generator for variables with normal probability distribution:

$$x_i = \sigma u_i + \mu \qquad (4.1)$$

$u_i \sim N(0,1)$; $x_i \sim N(\mu,\sigma^2)$;

- wall thickness (t): $t_i = 0.167\ u_i + 7.19$ (4.2)

- yielding point (σ_y): $\sigma_{y,i} = 29.04\ u_i + 264$ (4.3)

(4)

b) Random numbers generator for variable with lognormal probability distribution:

$$y_i = e^{x_i} = e^{\sigma u_i + \mu} \quad \text{.....(4.4)}$$

$u_i \sim N(0,1)$; $x_i \sim N(\mu,\sigma^2)$; $y_i \sim LN(\mu_{LN}, \sigma^2_{LN})$;

$$\mu = \ln \frac{\mu^2_{LN}}{\sqrt{\sigma^2_{LN} + \mu^2_{LN}}}; \quad \sigma^2 = \ln\left(1 + \frac{\sigma^2_{LN}}{\mu^2_{LN}}\right); \quad \text{.....(4.5)}$$

- maximal imperfection amplitude (w_o^a):
$\mu_{LN} \cong |\overline{w}_o| = 6.05$ mm; $\sigma_{LN} \cong 4.78$ mm;
from 4.5: $\mu = 1.56$; $\sigma = 0.69$;

$$w^a_{o,i} = e^{0.69u_i + 1.56} \quad \text{.....(4.6)}$$

(u_i = random numbers of the standard normal probability distribution taken from the book by Lipson, Sheth, 1973,/5/,Table A-48).
Values obtained from the expression 4.2, 4.3 and 4.6 are presented in columns 2, 3, 4, 7, 8 and 9 of the Table 1.

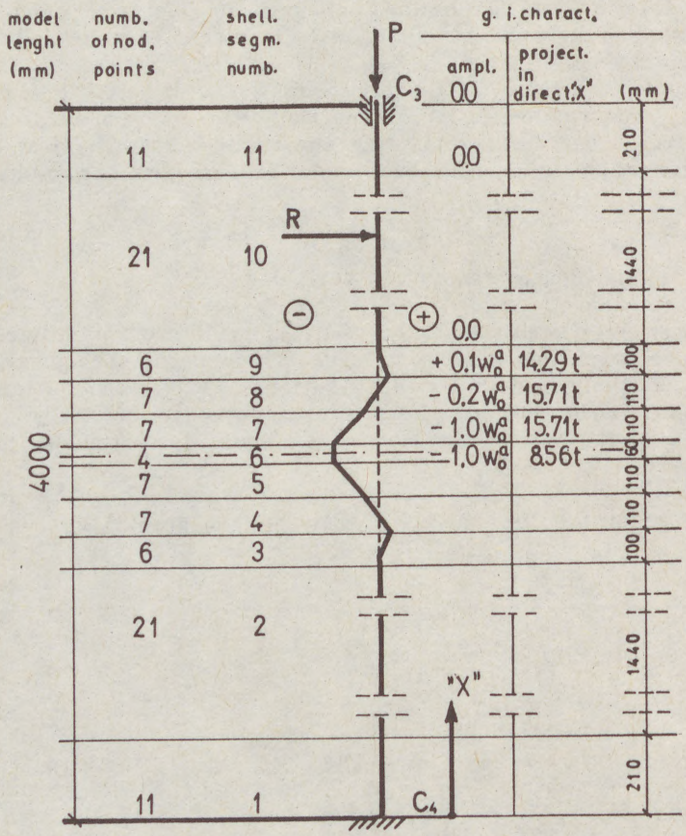

Fig. 1 - *Calculation model (R/t = 500, t = const. = 7 mm)*

(5)

5. Resistance results and calculation model

As stated earlier in this paper, the resistance of the analysed structure model is determined by numerical simulation of experiments for 50 different combinations of resistance variables random values. Numerical simulation is performed by using the computer program Bosor 5 (Bushnell, 1976,/2/). Results are presented in columns 5 and 10 of the Table 1. Calculation model is presented in Fig. 1 and is complemented with the following data:

- constraint conditions: C_3: $w = w' = N_x = v = 0$; C_4: $w = w' = u = v = 0$;
- material: St 37 ... DIN, bilinear stress/strain relation
- total model length: 4000 mm (sufficient for approximation of the shell of middle length)
- number of full waves of the buckle figure along circumference: $n = 12$ (taken in this paper as a constant).

Table 1 – Results of resistance and its variables random values

Anal. n°.	t mm	σ_y N/mm²	w_o^a mm	Pcr N/mm'	Anal. n°.	t mm	σ_y N/mm²	w_o^a mm	Pcr N/mm'
1	2	3	4	5	6	7	8	9	10
1	7.58	279	9.53	625	26	7.04	229	6.28	575
2	7.64	283	7.06	725	27	7.22	205	7.56	575
3	7.28	259	4.80	725	28	7.10	282	4.72	725
4	7.10	281	4.37	775	29	7.24	263	7.27	625
5	7.18	259	4.68	675	30	7.18	261	2.80	925
6	7.18	276	5.33	725	31	7.10	275	5.04	725
7	7.32	242	5.55	675	32	7.08	254	1.25	1225
8	7.16	287	3.79	825	33	7.02	255	7.97	575
9	7.00	270	2.70	925	34	7.14	247	1.27	1225
10	7.32	192	1.16	1075	35	7.08	237	12.94	525
11	7.08	288	6.06	625	36	7.06	263	3.22	875
12	6.98	267	10.61	625	37	7.08	225	4.00	725
13	7.16	299	7.22	625	38	7.44	287	13.50	675
14	7.08	285	10.08	625	39	7.08	282	10.83	675
15	7.50	229	9.13	825	40	7.34	263	1.34	1225
16	7.42	301	3.78	925	41	7.10	200	9.02	525
17	7.32	248	2.44	1025	42	7.08	255	4.47	725
18	7.28	309	3.05	965	43	7.34	281	2.02	1125
19	7.14	288	6.61	625	44	7.18	263	9.42	625
20	7.12	240	6.30	625	45	7.32	256	3.26	925
21	7.02	259	2.24	975	46	6.84	298	6.21	575
22	6.90	260	11.10	575	47	7.22	229	4.84	725
23	7.46	264	4.05	875	48	6.96	259	5.23	675
24	7.32	273	11.71	675	49	7.24	238	10.00	625
25	7.06	282	2.48	975	50	7.26	216	15.24	475

(6)

The resistance results obtained are also shown in Fig. 2 in comparison with the results of laboratory experiments taken from the literature.

Full line represents the range of dispersion of the author's results for R/t = 500 (φ = 0.27 through 0.69). Circle denotes arithmetic mean value $\overline{P}_{cr}$ = 761 N/mm' (coefficient of variation v = 0.2564).

Good correspondence of these results can be noted. It seems that the mean value of the author's results is lower, and the dispersion range is somewhat wider. One of the reasons for this could be that the mean value and coefficient of variation of the maximum amplitude of geometrical imperfection adopted in the analysis are less favorable than those on the models tested in laboratory.

Furthermore, the tests have shown that the hypothesis of lognormal probability distribution is acceptable for the shell resistance.

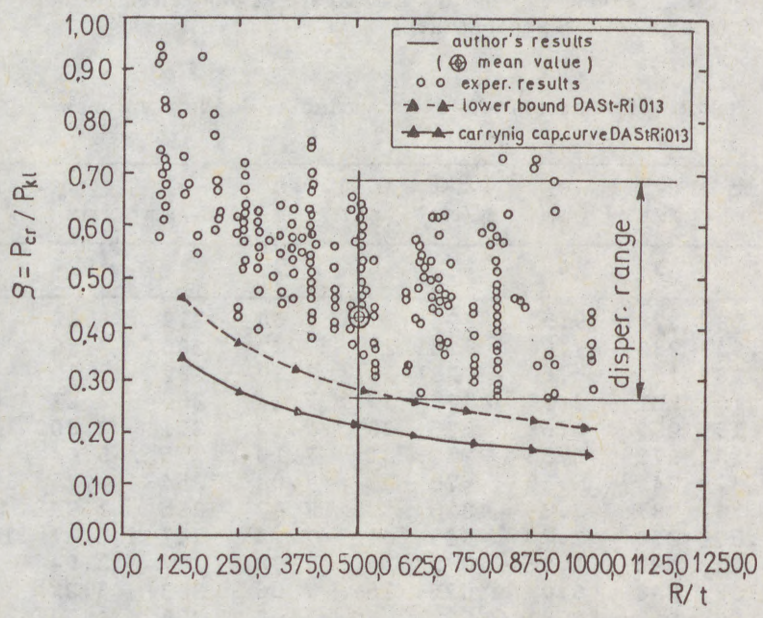

Fig. 2 – Comparison between experimental results and those obtained by the author for R/t = 500 (exper. results from Häfner /4/ – originally from Esslinger/Geier).

6. Conclusions

6.1. – Numerically simulated experiments based on adopted assumptions on the probability characteristics of the resistance variables (t, σ_y, w_o), on the "equivalent" axisymmetrical geometrical imperfection, as well as the application of the Monte Carlo, method resulted in the resistance values for R/t = 500 that comply very well with the published results of the laboratory experiments.

6.2. – The correspondence of results is surprisingly good and, for that reason, it would be interesting to verify the adopted assumptions. In the opinion of

(7)

the author, the easiest way would be to predict, by using the proposed procedure of numerical simulation, the resistance of models tested in laboratory for which the measured geometrical imperfections data are available.

6.3. - Investigations have shown that the influence of σ_y and t variations to the resistance could be neglected with the increase of the geometrical imperfection amplitudes.

6.4. - If it will be confirmed that the applied model of the axisymmetric approximation of geometrical imperfection is good enough, that would enable, among other things, analytical prediction of resistance for some shell structures for the measured geometrical imperfections.

References

/1/ Arbocz, J., CD. Babcock, J.R.: Utilization of Stags to determine Knockdown Factors from measured Initial Imperfections, Delft University of Technology, Department of Aerospace Engineering, Report LR-275, 1978.

/2/ Bushnell, D.: BOSOR-5 - Program for buckling of elastic-plastic shells of revolution including large deflections and creep, Computers & Structures, Vol. 6, pp. 221-239, 1976.

/3/ Galamboš, T.V., Ravindra, M.K.: Properties of Steel for Use in LRFD, Journal of the Structural Division, ASCE, Vol. 104, No. ST9, Proc. Paper 14009, Sept. 1978, pp. 1459-1468.

/4/ Häfner, L.: Einfluss einer Rundschweissnaht auf der Stabilität und Traglast des axialbelasteten Kreisylinders, Dissertation, Institut für Baustatik der Universität Stuttgart 1982.

/5/ Lipson, C., Sheth, N.J.: Statistical Design and Analysis of Engineering Experiments, International Student Edition, Mc Graw - Hill, Inc. 1973.

/6/ Milčić, V.: Ujednačavanje stupnja sigurnosti čeličnih konstrukcija primjenom probabilističkih metoda, Disertacija, Fakultet građevinskih znanosti u Zagrebu, 1981.

/7/ Turčić, F.: Utvrđivanje pouzdanosti plašteva čeličnih cilindričnih spremnika pod vanjskim pritiskom, Disertacija, Fakultet građevinskih znanosti Sveučilišta u Zagrebu, 1987.

/8/ Volmir, A.S.: Biegsame Platten und Schalen, VEB-Verlag, Berlin, 1962.

SESSION 12

COLD FORMED MEMBERS & INTERACTIVE BUCKLING

(1)
AOKI, Tetsuhiko(1)
MIGITA, Yasuhiro(2)
FUKUMOTO, Yuhshi(3)

LOCAL BUCKLING STRENGTH OF CLOSED POLYGON FOLDED SECTION COLUMNS

INTERNATIONAL COLLOQUIUM
STABILITY OF STEEL STRUCTURES
BUDAPEST, HUNGARY, 1990
PRELIMINARY REPORT

SUMMARY: The local buckling behavior of regular polygonal steel short length columns fabricated by welding two half sections made of folded steel plates is described. The polygonal sections are composed of five different section profiles with four to eight sides and each profile has the component plates with one to four varied width to thickness ratios. A total fifteen specimens is used in the compression test sustaining uniform compression stress in the fixed end condition. Accurate measurements of welding and cold-forming residual stresses and geometric imperfections were taken prior to testing and are presented in this paper. The test strengths are compared with the current plate buckling code in Japan and with the ECCS recommendations for the unstiffened circular cylinders. The empirical design formula based on the test data is also presented to predict the local buckling strength of the polygon section columns.

1. INTRODUCTION

The cross section profiles of boxes or pipes have been commonly used in compression members such as piers of highway bridges, columns of rigid frames, and mono-pole tower structures like floodlight towers and transmission towers. In recent years, the possibility of the use of polygonal thin walled steel members has been considered for those structures from a point of view of aesthetics in urban areas and from the demand of such freedom of designs for the shape of steel structures as concrete structures have. There has been, however, few studies on the buckling strength of the polygon section steel members so far, on which the design formulas would have been established.

In this research field, Wittrick and Curzon(1968) had developed a theoretical method on local buckling of long polygonal tubes in combined compression and torsion. Bulson(1969) performed the compression tests and analysis in elastic range for the polygon section members consisting of very thin plates with four to forty sides. The strengths of the polygon

(1) Prof. of Dept. of Civil Eng., Aich Institute of Tech., Toyota, Japan
(2) Associate Prof. of Dept. of Civil Eng., Tokai Univ., Fukuoka, Japan
(3) Prof. of Dept. of Civil Eng., Oosaka Univ., Suita, Oosaka, Japan

(2)

members were estimated replacing them with the pipe sections having the same section areas. Avent and Robinson(1976) conducted the elastic stability analysis for the regular polygon folded plate columns. Kurt and Johnson(1978) also studied analytically the elastic stability of imperfect closed polygon columns concerning in the local buckling domain. These studies are performed related to the elastic buckling analysis.

A more recent study presented by Koseko, Aoki and Fukumoto(1983) describes the experiments and finite strip analysis of the local buckling strength of the short length thin walled steel members with regular and irregular octagonal cross sections in the inelastic domain.

In this paper, the load carrying capacities due to local buckling of the component plates of regular polygonal section members are investigated experimentally. The number of sides of the polygons is changed from four to eight and the width to thickness ratios of the component plates of each specimen is varied from one to four.

The residual stresses caused by welding and folding process and the geometric imperfections are measured prior to the compression test.

2. TEST

2.1 TEST SPECIMENS

Test specimens were fabricated by welding two half section pieces made of folded plates of which nominal thickness is 4.5 mm and the steel grade of nominal tensile strength is 400 N/mm^2. The cross sectional profiles of the specimen consist of rectangular, pentagonal, hexagonal, heptagonal and octagonal regular shapes as shown in Fig.1(a), in which the welded locations in the cross section are indicated by the solid triangular marks. The cross sectional dimensions and properties are listed in Table 1.

Each specimen is named with the short form of the polygon name followed by the plate width in centimeters, as given in Table 1. The total fifteen specimens were prepared for the compression test. For the compression test specimens 1500 mm was cut from the 2300 mm length fabricated members and

Table 1 Nominal Cross Sectional Properties and Maximum Stresses due to Test

Number of Sides	Name of Specimen	Width of a plate b (cm)	Thick-ness t(mm)	Width-Thickness Ratio b/t	Width-Thickness Parameter R	Sectioal Area A (cm^2)	σ_{max} (N/mm^2)	σ_{max}/σ_Y
4	REC-20	20	4.5	44.4	0.86	36.0	261	0.90
	REC-25	25	4.5	55.6	1.07	45.0	201	0.70
	REC-30	30	4.5	66.7	1.29	54.0	210	0.72
5	PEN-24	24	4.5	53.3	1.03	54.0	213	0.74
	PEN-24b	24	4.5	53.3	1.03	54.0	207	0.71
6	HEX-20	20	4.5	44.4	0.86	54.0	251	0.87
	HEX-25	25	4.5	55.6	1.07	67.5	206	0.71
	HEX-30	30	4.5	66.7	1.29	81.0	177	0.61
7	HEP-17	17	4.5	38.1	0.74	54.0	271	0.94
8	OCT-15	15	4.5	33.3	0.64	54.0	278	0.96
	OCT-15b						274	0.95
	OCT-15w						275	0.95
	OCT-20	20	4.5	44.4	0.86	72.0	244	0.84
	OCT-25	25	4.5	55.6	1.07	90.0	206	0.71
	OCT-30	30	4.5	66.7	1.29	108.0	173	0.60

Tensile Yield Strength σ_Y=289 N/mm^2, OCT-15w: All corners are welded

(3)

the rest was used for the measurement of residual stresses or tensile coupon test specimens, as shown Fig. 1 (b),(c).

The compression test specimens have diaphragms near both ends. The strains of local buckling of the component plates and longitudinal displacement were measured in the 1200 mm length between both diaphragms, which corresponds to four times of the largest plate width (b=300 mm) of the test specimens. One octagonal specimen was fabricated by welding eight flat plates at all their junctions to compare with the folded and welded specimens.

From the tensile coupon tests the average yield strength σ_y = 289 N/mm², Young's modulus E = 215000 N/mm² were obtained.

2.2 RESIDUAL STRESSES

The twelve strain gauges were attached on each couple of outside and inside surface of plate elements, around the peripheral of the specimens at the mid length. The method of sectioning was employed to release the residual stresses.

An example of measured residual stress distribution for OCT-15 is shown in Fig. 2. For all measured specimens, the residual stresses of outside and inside surface are almost the same value except in the corner parts, where the cold form effect by folding plate caused the significant difference in the measured values of the both sides. The distributions of the membrane residual stresses after averaging the outside and inside values, taking the half section between two welding lines from the section, are shown in Fig. 3.

The residual stress distributions are categorized into three patterns by the shapes of their compression distributions and the number of corners between the welding locations rather than by the distance between the weldings, as shown in Fig. 3(a), (b) and (c). Fig. 3(a) shows the results of the rectangular sections having two corners between the welding points and They are seemed to be approximately trapezoidal shapes for compression

(a) Cross Sections

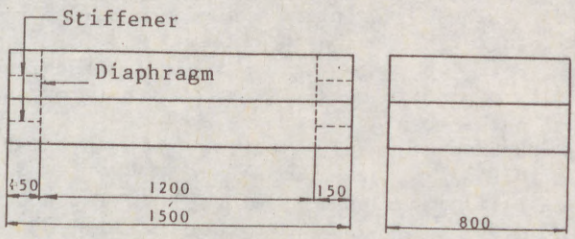

(b) Compression Test Specimen

(c) For Measurement of Residual Stress

Fig. 1 Cross Sectional Profiles and Length of Test Specimens

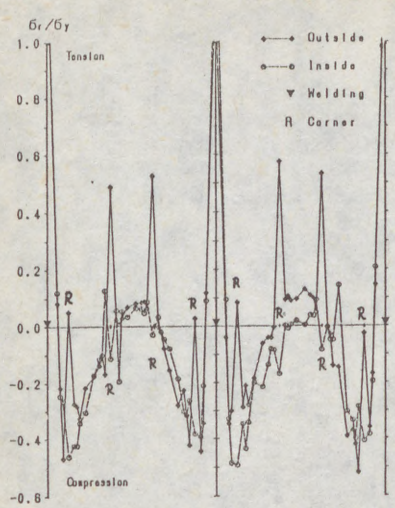

Fig. 2 Residual Stress Distribution in OCT-15

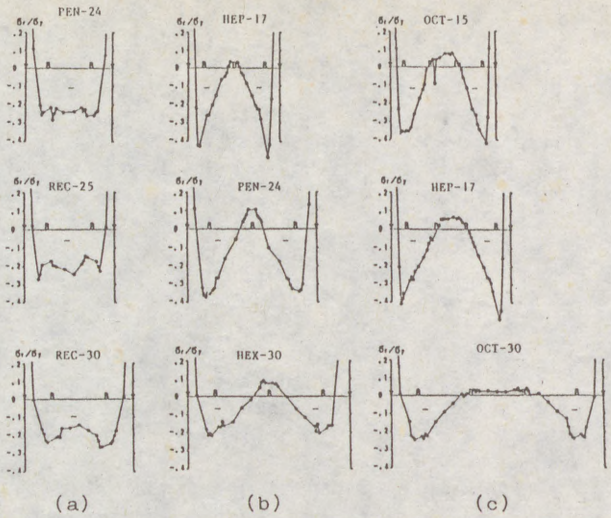

Fig.3 Compressive Residual Stress Distributions

residual stress distributions. The distributions in Fig. 3(b) contain two triangles near the tensile residual stresses at the welding sites, and a small triangle tensile stress at the center, where three corners exist. The distributions of Fig.3(c), being almost the same as those of in Fig.3(b), have four corners and a little trapezoidal tensile residual stresses at the center by the observation. The changes of distribution along with the distance between the weldings are observed in each classification.

The maximum compressive residual stresses were varied 0.25 σy - 0.3 σy for the rectangular sections and 0.22 σy - 0.5 σy for other sections.

2.3 GEOMETRIC IMPERFECTIONS

The geometric imperfections of the component plates forming the thin walled polygonal test specimens were measured by dial gauges to an accuracy of 0.01 mm per reading. Thirteen dial gauges were fixed on a firm steel bar and the straightness was measured prior to the measurement of the geometric imperfections of the plates.

All component plates of the test specimens were divided into grids consisting of six to eight equally spaced lines on the flat part of the plates in the direction of the plate width and thirteen equally spaced measuring points were taken along each line.

The test data for all specimens were analyzed by the least square method using Fourier series expansion consisting of seven terms and the components of the half wave-lengths were obtained.

Examples of measurement results for the specimen OCT-20 are shown in Fig. 4(a) and (b). It was observed in almost all of the specimens that the shape of the geometrical imperfections of the non-welded plates had the one half wave-length mode predominantly, whereas the random ripple modes appeared on the welded plates. The maximum values of imperfections were also found in the welded plates in all specimens except PEN-24 and OCT-15. The value of the maximum imperfection of all specimens was 0.014b(4.24 mm) in the specimen OCT-30, where the plate width b= 300 mm. The mean value of all measured was 1.21 mm which corresponded to 1/1000 of the plate length.

(5)

Fig. 5 shows the geometric imperfections on the cross section at mid length of the specimens, in which the deformations are scaled up to the cross sectional dimensions for the illustration.

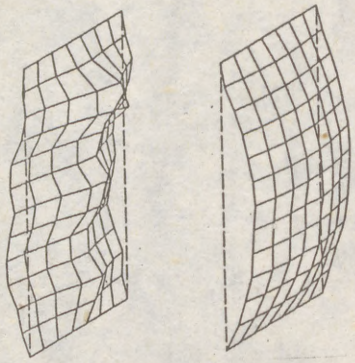

(a) Welded Panel (b) Non-welded Panel

Fig. 4 Examples of Geometric Imperfections (OCT-20)

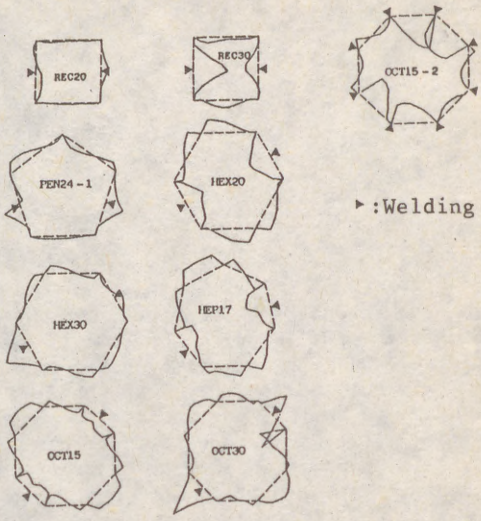

Fig. 5 Geometric Imperfections on the Cross Sections at Mid-length of the Specimens

2.4 COMPRESSION TEST

(1) TEST METHOD

The compression tests were conducted in the fixed end condition setting the specimens between two rigid end plates with a couple of rotational beveled bearing circular plates to adjust the uniform compression stress conditions during loading. The thirteen strain gauges were attached longitudinally on the center line of the component plate which is located the adjacent of the welding plate, where the maximum compressive residual stress were supposed to be contained. The axial displacements were measured with the 1/100 mm accuracy dial gauges attached at the four corners of each test specimen. A test set-up is shown in Fig. 6.

(2) TEST RESULTS

The longitudinal average stress strain curves obtained from the dial gauges as a whole column for octagonal specimens with different width to thickness ratios are shown in Fig. 7. Each curve coincides well with others just before the maximum strength and after that the sudden unloading of the bearing load were observed.

Fig. 8(a) shows the change of strain distributions along the center line of the component plates of the specimen OCT-20. The uniform increasing of the strains along the longitudinal lines are observed until the maximum stress σmax, in spite of the geometry imperfections of the plates. The local buckling mode is also observed clearly from the strain distributions after buckling. Fig. 8(b) shows the stress and strain graph at the several points on the center line shown in Fig.8(a). It can be found from Fig.8(b) that diverging of the strains start from around 0.8 σmax. Examples of local buckling failure after testing are shown in Fig.9.

(3) MAXIMUM STRENGTH

All test specimens caused local buckling in the component plates. The maximum strength points due to the compression test are given in Table 1 and in Fig.10, in which the current plate buckling formula of Japan Highway

(6)

Association's Specification and the ECCS Recommendations curve which gives the lower bound to the unstiffened circular cylinders are also given. An empirical formula [Eq.(1)] based on the present test data is also shown.

$$\sigma max/\sigma Y = 1.35 - 0.55\,R \quad (R>0.636) \qquad (1)$$

$$R = \sqrt{\sigma Y / \sigma cr} \qquad (2)$$

$$\sigma cr = k\frac{E\pi^2}{12(1-\nu^2)}\left(\frac{t}{b}\right)^2 \quad (k=4) \qquad (3)$$

Observing both the test results and Eq.(1) in Fig.10, it can be said that the maximum strength has a close relationship with the width-thickness ratios of the component plates of the polygonal section members. Since the profiles with the smaller width-thickness ratio may have the larger local buckling strength, polygonal section having more sides among the thin walled members with the same cross section area, may become advantageous with regard to the local buckling strength and therefore the ultimate strength before to occur the shell type buckling mode for large number of sides. Considering practical problems such as fabrications, the octagonal section profile may be desirable among polygonal members.

4. CONCLUDING REMARKS

In this paper, an experimental study of load carrying capacity of the stub columns having thin walled regular polygon section was presented. Test specimens were fabricated by folding plates, forming two half of the cross sections and welding them into one section.

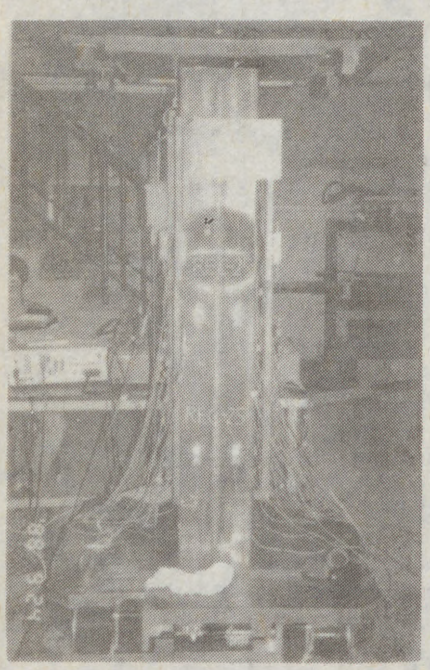

Fig. 6 Test Set-up

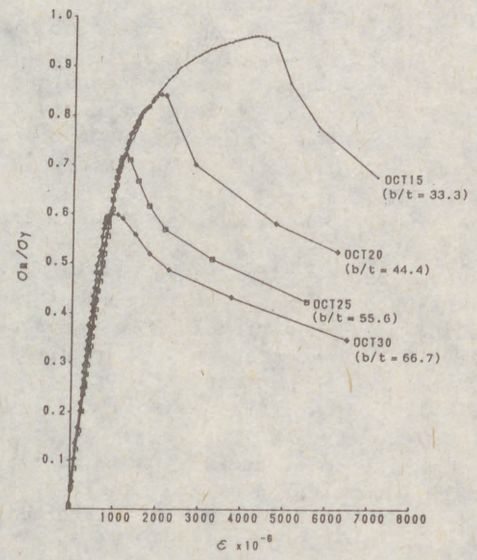

Fig.7 Average Stress-Strain Curves due to Dial Gauges

(7)

(7)

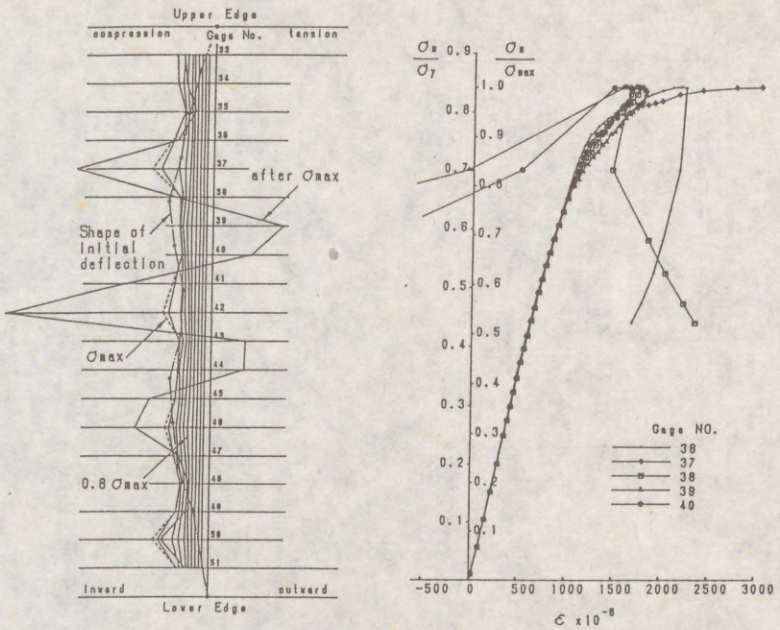

(a)The Change of Strain Distributions along The Center Line

(b)Stress-Strain Relations of the Points on the Center Line

Fig. 8 Examples of the Change of Strains on the Specimen OCT-20

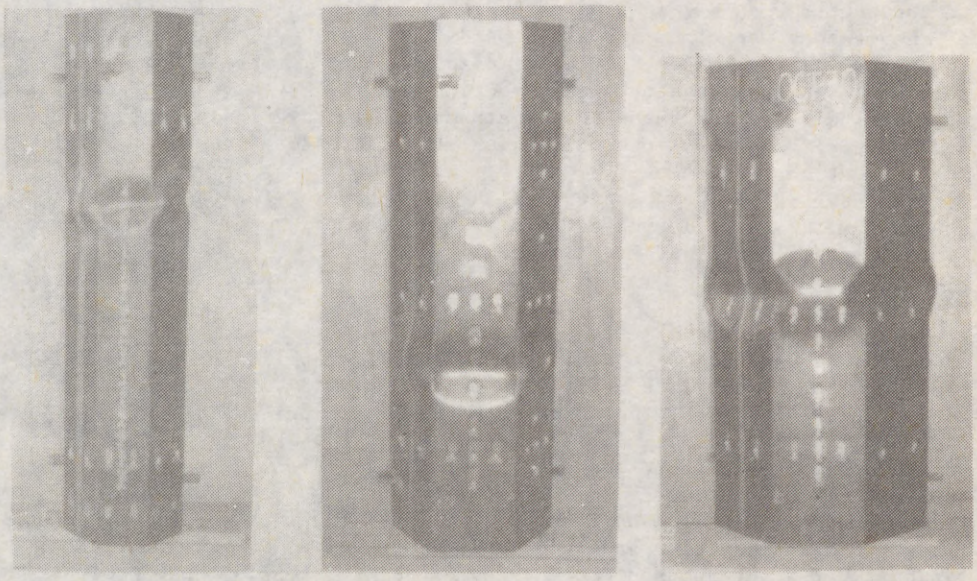

(a) OCT-15

(b) HEX-25

(c) OCT-30

Fig. 9 Local Buckling Failure after Testing

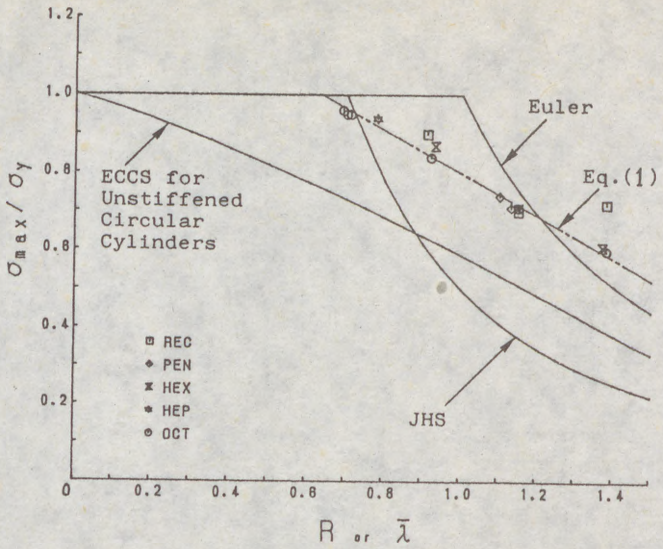

Fig. 10 Experimental Maximum Strengths

The ultimate strength of the uniformly compressed polygon stub columns under the fixed end condition showed stronger interaction with the width-thickness ratios of the component plates than with the cross sectional profiles. The polygonal thin walled short length members, therefore, seems to be better than box section members in respect to the ultimate strength of the members when they are affected directly by the local buckling of the component plates under the condition of uniform compression. Among the polygonal sections, the octagonal section profile may have much possibility in practical use for the structures because of convenience of fabrications and comparatively easy connection with other structural members as well as the aesthetics considerations.

The authors have been conducting the test program for the medium length columns with the polygon sections from a view point of the interaction effect between local and overall buckling.

REFERENCES

1) Avent,R.R. and Robinson,J.H., 1976: Elastic stability of polygon folded plate columns, Proc. ASCE, Vol.102, No.ST5, pp.1015-1029

2) Bulson,P.S., 1969: The strength of thin-wall tubes formed from flat element, Int.J.Mech.Sci., Vol.11, pp.613-620

3) European Recommendations for Steel Construction, 1983: Buckling of Shells, ECCS-CECM-EKS,p.7

4) Koseko,N., Aoki,T. and Fukumoto,Y., 1983: The local buckling strength of the octagonal section steel columns, JSCE, Vol.2, No.330, pp.27-36

5) Kurt,C.E. and Johnson,R.C., 1978: Cross sectional imperfections and columns stability, Proc. ASCE, Vol.104, No.ST12, pp.1869-1883

6)Japan Highway Association, 1980: Spec. for Highway Bridges (Steel Bridge)

7)Wittric,W.H., 1968: A unified approach to the initial buckling of stiffened panels in compression, The Aeronautical Quarterly, Vol.19, pp.265-283

(1)

BEG, Darko[1]

SIMPLIFIED ANALYSIS OF LOCAL AND GLOBAL INSTABILITY INTERACTION OF THIN-WALLED STRUCTURES

INTERNATIONAL COLLOQUIUM
STABILITY OF STEEL STRUCTURES
BUDAPEST, HUNGARY, 1990
PRELIMINARY REPORT

Summary: The simplified method for the analysis of the interaction of local and global instability of thin-walled structures based on the effective-width metod is presented. Several examples, where the results of the presented method are compared with the experimental and numerical ones, are given.

1 INTRODUCTION

In structures with slender cross-sections the interaction of local and global instability might have an essential influence on the load-carrying capacity. The more exact numerical methods, as for example the finite element method (shell elements) and the finite strip method, are not the most convenient for the interaction analysis in everyday practice, because they consume a lot of time for data preparation as well as a lot of computer time. Our major task was to develop a simplified numerical method that would enable quick and simple analysis of the interaction of local and global instability.

2 DESCRIPTION OF THE METHOD

The interaction of local and global instability is a very complicated physical phenomenom being dependent on a great number of parameters. It is most expressive in the area , where the load-carrying capacity of a slender cross-section is approximately equal to the global elastic critical load-carrying capacity. It is mostly influenced by geometrical imperfections that can be either local (imperfection of cross-section shape) or global (geometrical imperfections of longitudinal axes) and by postcritical load-carrying capacity of slender cross sections. The important influences are also due to the residual stresses and the inelastic behaviour of material. We have tried to involve all these essential characteristics of the behaviour of thin-walled structures into our method.

[1] ASSISTANT, UNIVERSITY OF LJUBLJANA, DEPARTMENT OF CIVIL ENGINEERING

(2)
The computer program THIN (Beg, 1984), intended for the nonlinear analysis of space frames with open nondeformable thin-walled cross-section, represents the basis of the method. The geometrical nonlinearity is incorporated by the 2nd order theory and the material nonlinearity by the hyperelastic material that might be used, in the phase of increasing loading, for the simulation of i. e. elasto-plastic material. The shape functions for the lateral displacements and for the torsional rotation are the polynoms of the 6th degree while the element axial force (mixed variationed principle) has been chosen for the independent variable instead of axial displacement. For the calculation of the tangential matrix of a single finite element, Gauss's numerical integration with five integration points was used.

The simplified constitutive equations, which are based on the known effective-width method and which enable the analysis of slender (noncompact) cross-sections, was incorporated into the program THIN. The load-carrying capacity of the cross-section with the local buckling of single parts of the cross-section is not exhausted, because slender metal sheets have quite a post-critical load-carrying capacity. After the local buckling a redistribution of stresses over the cross-section appears and the simplest way to consider this is with effective width method, which supposes that the buckling part is not capable of carrying anymore (Fig. 1). The remaining (effective) part of the cross-section is treated in the same way as compact cross-sections. The ultimate load of the cross-section is achieved when the stress σ_m becomes equal to the yield stress σ_v (it is valid for an ideal elasto-plastic material).

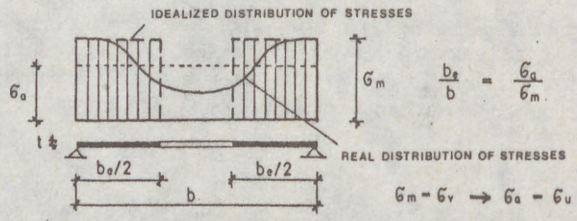

FIGURE 1

In literature, there exist different expressions for the calculation of effective width b_e. The first one was published already in 1932 by von Karman. Most offen appears the expression, proposed by G. Winter on the basis of experimental researches.Von Karman's effective width represents the upper limit of Winter's effective-width. The values of both expressions come very close in great slenderness.

$$\frac{b_e}{b} = \frac{1}{\bar{\lambda}_p} \leq 1.0 \quad \text{....von Karman} \qquad (1)$$

$$\frac{b_e}{b} = \frac{1}{\bar{\lambda}_p}\left(1.0 - \frac{0.22}{\bar{\lambda}_p}\right) \leq 1.0 \quad \text{....G. Winter} \qquad (2)$$

$$\bar{\lambda}_p = \sqrt{\frac{\sigma_m}{\sigma_{cr}}}\,, \quad \sigma_{cr} = K_\sigma \frac{\pi^2 E t^2}{12(1-\nu^2) b^2}$$

Von Karman's formula is suitable for the treatment of cross sections with ideally flat components without residual stresses, while Winter's expression gives in the

(3)
area of mid slenderness ($\bar{\lambda}_p$ - 1.0) rather lower results because it takes into account the influences of geometric imperfections and residual stresses. Both above described expressions for the effective width (Eq. 1 and 2)are incorporated in the program. They are regarding the ECCS Recommendations No. 49, 1987, used also for plates, supported only along one longitudinal edge (i.e. flange of I - profile) and for any linear distribution of stresses along the width.

Let us see, in short, the process of calculating the stress resultants and their derivates (stiffness coeficients) in single integration points. The cross-section can consists of any set of rectangles - subsections that compose the open thin-walled cross-section (in absence of torsion it might as well be closed). To each of these rectangles a linear course of residual stresses along longer sides and its own diagram stress - deformation for normal stress can be prescribed. The diagram is sectional linear and of any shape. The resultants of normal stresses and their derivates are calculated with the help of exact analytical integration over the whole cross-section. The torsional moment of Saint-Venant torsion and appertinent torsional stiffness, which are linked to the shear stress, are calculated according to the method, described in reference (Beg, 1984). The single parts of the cross-section, for which the effective width is determined independently (i.e. flange or web of I - profile), can be composed of one or more subsections.

In the program THIN, the limit state of the slender cross-section and thus of the whole structures is determined by the plastification of the most loaded fibre in the compression part of the slender cross-section. The elasto -plastic reloading of the compression stresses is , however, not possible in the post critical zone. The tension parts of the slender cross-sections and the more compacts parts of them can be plastified.

The described simplified method for the study of the interaction of local and global instability is less exact than i.e. the finite element metnod (shell elements), but it has certain advantages. It enables a simple analysis of bigger structures, it gives the results that are mainly on the safe side (Hancock, 1980, De Wolf, 1974) and it involves all the essential influences, being of interest in the study of interaction. The influence of postcritical load-carrying capacity is incorporated in the effective width method which, in its expressions, takes into account the influence of local geometric imperfections and residual stresses. The influence of the latter ones on the resultants of stresses and stiffness are considered also explicitly by defining arrangement of residual stresses over the cross-section. The global geometric imperfections can be comprised in without difficulties when defining the global geometry of the structure and the nonlinear behaviour of material can be determined as well.

There remains some open questions to be shortly commented upon.

The question of the influence of local geometric imperfections is a very important one. In cross-sections with small local geometric imperfections Winter's effective width (Fig. 2) gives results that are excessively conservative. The next problem which can not be solved in the frame of the treated method is the problem of distortion of the cross-sections. Figure 2a shows the local buckling of the cross-section involved in the effective-width method while the distortion of the cross-section, shown in Fig. 2b, can not be incorporated. The appearance of distortion can be extenuated or even complitely prevented (see Chapter 3) with conveniently arranged stiffeners. The influence of shear stresses on the postbuckling capacity of

(4)
thin plates is also not taken into account.

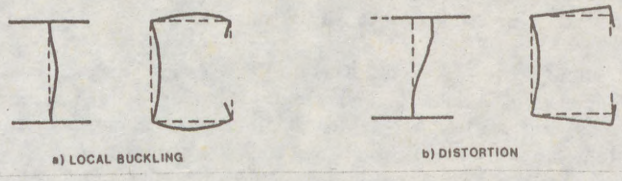

FIGURE 2

3 NUMERICAL EXAMPLES

In literature there is rather a small number of experimental and numerical examples in the field of the interaction of local and global instability. Some of the most cited results have been compared with the results of the computer program THIN.
Fig. 3 presents the analysis of centrically compressed aluminium column of I-profile with slender flanges. The results of the computer program THIN have been compared with the experimental results of Biljaard and Fisher (1953) and numerical results of Davids and Hancock (1987), who used the modified finite strip method. Because the column had very small local and global geometric imperfections, only one finite element and Von Karman's effective width were used. The examples with slender flanges are very sensitive in the weak axis, for i.e., the bending stifness is the function of the third power of the efective witdth of flange. So we get the results, which fits well with the experiments taking into account the real buckling coefficient $K\sigma$=0.739 of flanges, which was defined experimentally. The usual minimum factor $K\sigma$=0.425 would give lower valuos. However, it is evident that in smaller slenderness our results are well on the safe side. It should be taken into account that in our calculation and in the analysis of Davids and Hancock an ideal elastic material was used, while in the highest two experimental results the influence of nonlinear behaviour of material was surely present.

In the next example (Figure 4), the lateral buckling of an aluminium beam with prevented warping of the cross section on the both sides has been treated.The results of THIN are in a very good agreement with the experimental results of Cherry, 1960. All comments regarding the geometric imperfections, the choice of the expressions for the calculation of effective-width and the coefficient $K\sigma$ is equal to the previous example. Because there were not any data about real diagram stess-deformation, the ideal elasto-plastic diagram was used as a rough approximation. Therefore, our results are much lower than the experimental ones in the area where the plastification begins.

In plate girders with compact flanges and slender webs the interaction is somehow less expressive than in latter examples. Inspite of the fact that this type of structures is quite often used in literature, there is not many data about the treatment of plate girders as regards to the interaction of local and lateral buckling.

In our study the simply supported plate girder has been treated at different lengths. The influence of local and global geometric imperfections on the ultimate load has been established. The elastic behaviour of girders was supposed. The lengths were chosen in accordance and thus the influences of elasto-plastic

(5)

behaviour of material and residual stresses would not be dominant even if they are taken into account. The numerical analysis were made by the help of the program FINAS that enabled the nonlinear analysis of structures with the finite element method (Trueb, 1983). The isoparametric doubly curved 8-noded finite elements were used. Every flange was transversally divided into two elements and web into five finite elements. In the longitudinal direction every girder was divided into 36 strips of elements. The geometry and the load are shown in Fig. 5. The global geometric imperfections were supposed in the form of lateral sinusoid imperfection of a compressed flange (one halfwave) with the amplitude e_0 in the middle of the span. The tension flange remained straight. The local geometric imperfections are meant for the web. Along the height of the web one sinusoid halfwave was chosen and along the girder a greater number of halfwaves (amplitude w_0). Any combination of both kinds of imperfections might appear (see Fig. 5). Rather high amplitudes were chosen, so they could not be avoided in manufacturing of plate girders with very slender web (in our case h/d = 250).

The ultimate load was calculated for every length also according to three technical standards (SIA 161 1979, ECCS Recomendations No 31 (1978/1985) and JUS U.E7.101 (1986)). Finally, a comparison with results, gained by the above described method, was made. We used eight finite elements and the same shape of global geometric imperfections than when calculating with computer program FINAS. The effective width of the web was achieved by Winter's formula considering the real value of the coefficient $K\sigma$ ($K\sigma$ = 36.6). Besides the elastic also the elasto-plastic material was taken into account (σ_V = 235.0 N/mm^2). The value of the ultimate bending moment for all examples is shown in Fig. 5.

Because of the limited number of lines in this paper, a detailed comment is not possible. However, we established that:

- while increasing the global imperfection, the load-carrying capacity decreases;
- there does not exist such linear relationship in local geometric imperfection, but the differences in the ultimate load are not so big even the differences in amplitudes are;
- the results according to different standards are in good agreement and are on the safe side (with the exception of exaggerated global amplitude e_0 = 1/300);
- the results according to the presented method are in good agreement with the results of the programe FINAS (see Fig. 6 and 7), where for examples l = 3.26 m and l = 3.60 m the diagrams load-displacement were shown.

(6)

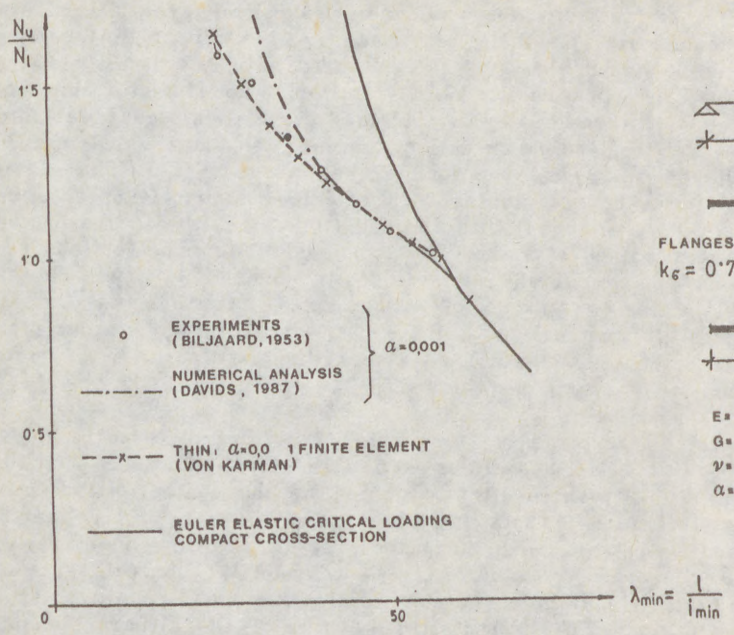

FIGURE 3

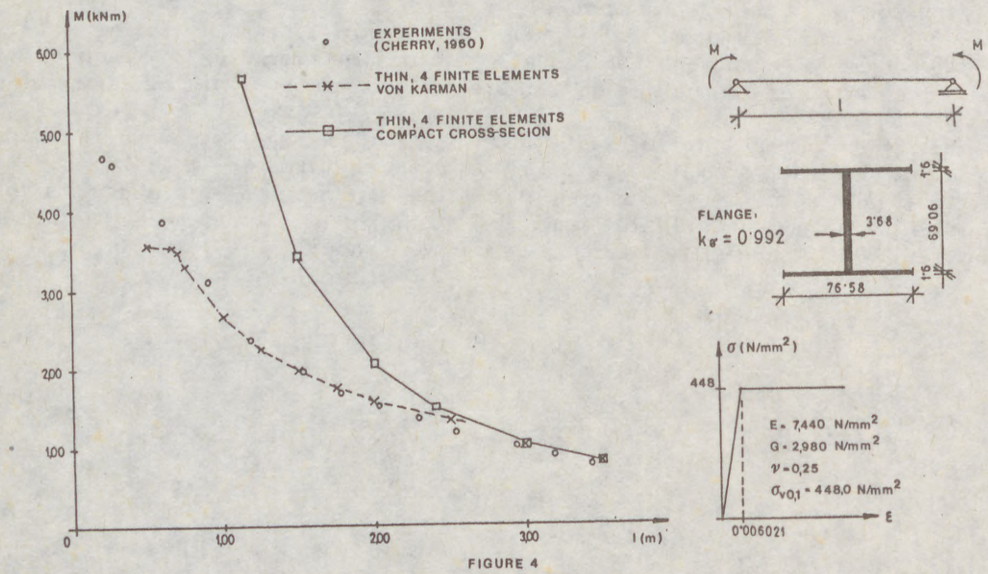

FIGURE 4

(7)

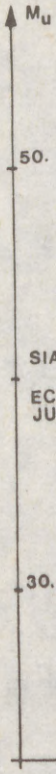

(7)

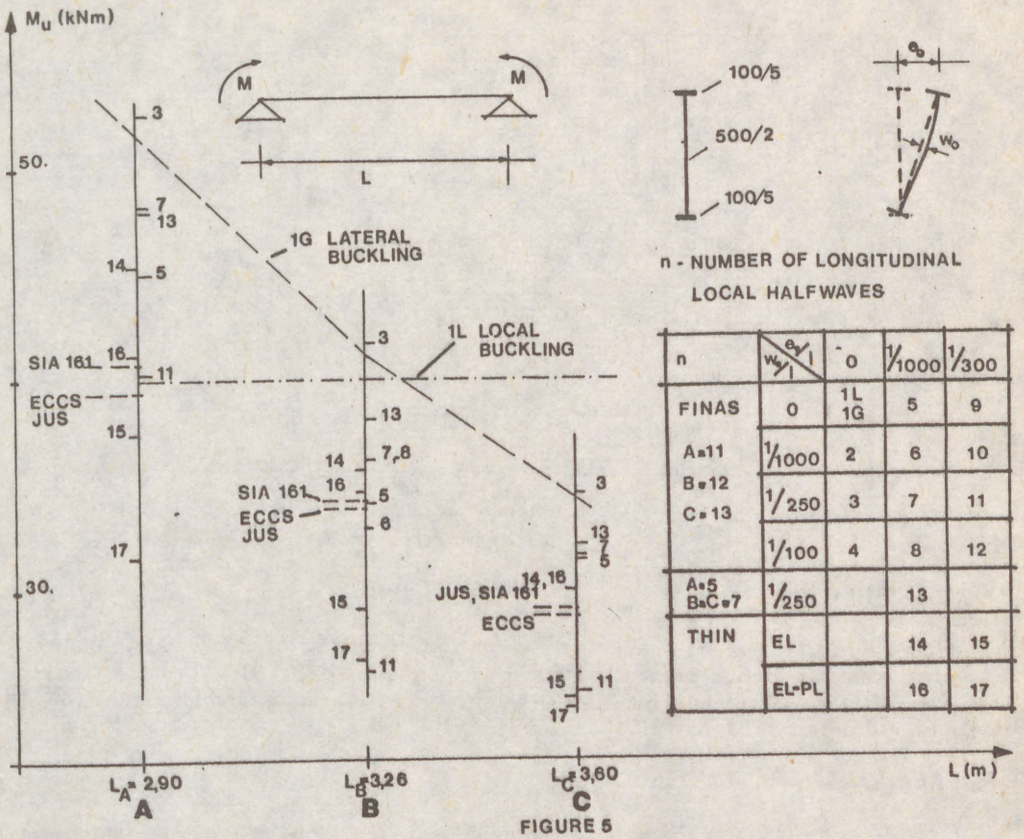

n - NUMBER OF LONGITUDINAL LOCAL HALFWAVES

n	w_0/l \ e_0/l	0	1/1000	1/300
FINAS	0	1L 1G	5	9
A=11 B=12 C=13	1/1000	2	6	10
	1/250	3	7	11
	1/100	4	8	12
A=5 B=C=7	1/250		13	
THIN	EL		14	15
	EL-PL		16	17

FIGURE 5

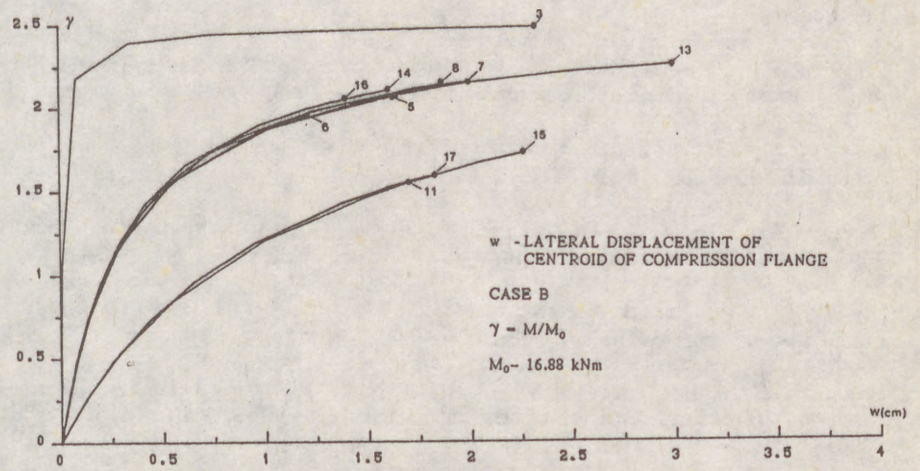

w - LATERAL DISPLACEMENT OF CENTROID OF COMPRESSION FLANGE

CASE B

$\gamma = M/M_0$

M_0= 16.88 kNm

FIGURE 6

(8)

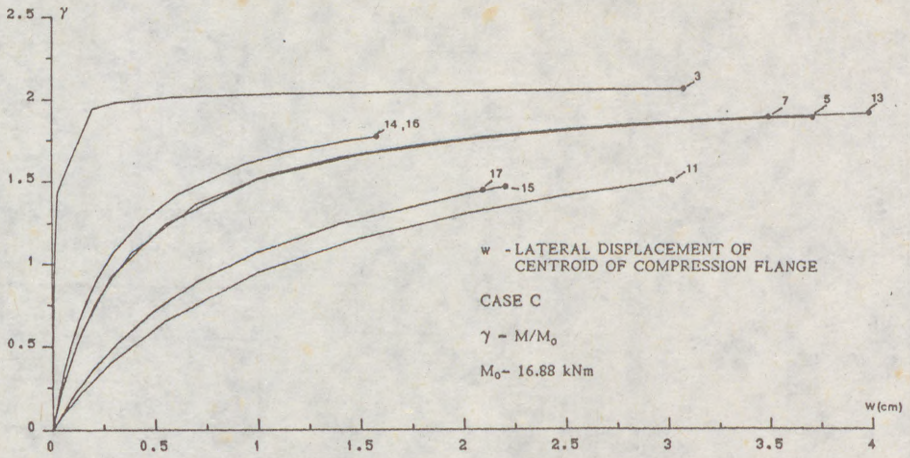

FIGURE 7

ACKNOWLEDGMENT

The author expresses his thanks to Research Community of Slovenia which partly financed the researches presented in this paper, and to Dr. Urs Trueb (Computer Centre Walder, Gumligen, Swiss) who enabled the free-of-charge use of the computer program FINAS.

REFERENCES

Beg, D., 1984, Numerical Analysis of Thin-Walled Structures according to the Second Order Theory, M. Sc. Thesis, University of Ljubljana, Department of Civil Engineering

Biljaard, P.P., Fisher, G.F., 1953, Column Strength of H-Sections and Square Tubes in Postbuckling Range of Component Plates, TN 2994, NACA, Washington, DC

Cherry, S., 1960, The Stability of Beams With Buckled Compression Flanges, The Structural Engineer, P. 227-285

Davids, A.J., Hancock, G.J., 1987, Nonlinear Elastic Response of Locally Buckled Thin-Walled Beam-Columns, Thin-Walled Structures, No. 5, p.211-226

De Wolf, J.T., Pekoz, T., Winter, G., 1974, Local and Overall Buckling of Cold-Formed Members, Journal of the Structural Division, Vol.106, No. ST7, p. 1557-1571

Hancock, G.J., Bradford, M.A., Trahair, N.S., 1980, Web Distortion and Flexural-Torsional Buckling, Journal of the Structural Division, Vol. 106, No. ST10, p. 2017-2036

Trueb, U., Stability Problems of Elasto-Plastic Plates and Shells by Finite Elements, A thesis submited for the degree of Doctor of Philosophy in the Faculty of Engineering of the University of London

(1)

CRAINICESCU, Magda (1)
SOARE, Mircea V. (2)
GEORGESCU, Dragoş (3)
MANOIU, Octavian (4)
GHITA, Nicolae (5)

ASPECTS CONCERNING STABILITY AND LOAD CARRYING CAPACITY OF A LARGE SCALE STEEL ROOF DECKING MODEL FOR SINGLE STOREY INDUSTRIAL BUILDINGS

INTERNATIONAL COLLOQUIUM
STABILITY OF STEEL STRUCTURES
BUDAPEST, HUNGARY, 1990
PRELIMINARY REPORT

Summary : The paper deals with aspects concerning stability and carrying capacity loss of a steel roof decking model - for single storey industrial buildings-subjected to in-plane or shear actions.

The carried out research aimed :

- to make evident the diaphragm action in the failure of a steel roof decking model, designed in acordance with the usual solutions provided by the type projects in force;
- to investigate the failure manner of the steel roof decking model, conceived in several variants with different fastening systems.

(1) Scientific Secretary, Building Research Institute-INCERC, Bucharest
(2) Professor of Strength of the Materials, Institute of Constructions - ICB, Bucharest
(3) Professor of Steel Constructions, Institute of Constructions - ICB, Bucharest
(4) Head of Design Group, Design Institute for Typified Constructions - IPCT, Bucharest
(5) Head of Division, Rolling Mill Designing Institute IPROLAM, Bucharest.

(2)

The experimental work devoted strictly to the model stability and carrying capacity loss was carried out in five stages (the overall research consisted in twelve stages).

1. Introduction

The experimental work aimed to investigate the mode of failure of a steel roof decking model for single storey industrial buildings.

The authors tested a large scale model of 6.00 x 12.00 m, which consisted in a roof framework, built-up with rafters (a), purlins (b), bracings (c) and corrugated steel sheets cladding (d) (table 1).

The model, designed in accordance with the usual solutions provided by the type projects in force, was conceived with two fastening systems :

- A – hexagon head screws in every corrugation as sheet/purlin fasteners and aluminium pop rivets as seam fasteners of adjacent sheets.
- B – self-cutting screws in every corrugation as sheet/purlin fasteners and hexagon head screws as seam fasteners of adjacent sheets.

The model was subjected to in-plane high intensity concentrated statical stepwise loading, applied at the purlins midspan.

With tests were analysed the model in-plane displacements of the rafter/purlin intersected points, for every loading step of the loading cycles.

In special cases (e.g. 1st experimental stage), the normal displacements to the model plane of certain additional points were analysed, too.

Five experimental stages, corresponding to five model making-up variants (table 1) are further on described and they belong to a broad experimental program performed in twelve stages.

The 1st stage aimed to investigate steel trusses behaviour in the post-critical range (the analysed truss was the model bare unclad framework).

The 2nd stage represented a supplement of the 1st stage.

The 3rd stage aimed to investigate the mode of failure of the completed model (framework with bracings and cladding) taking into account diaphragm action induced in the roof decking as a result of the interaction between corrugated steel sheeting and steel framework (A fastening system).

The 4th stage aimed to investigate the mode of failure of the clad model without bracings taking into account the diaphragm action (A fastening system).

The 5th stage, idem the 4th stage but with B fastening system.

(3)

2. Description of the experimental work

1st stage. Five loading-unloading cycles were performed. Due to the model conception, the bracings buckled in a normal plane to the model truss plane.

Within the first cycle, at a force H = 7.5 tf, the compression diagonal 1-2 (see table 1) buckled laterally (the calculated value of the critical load was H = 7.7 tf). At diagonal midspan corresponded a normal displacement to the truss plane $\Delta \approx 190$ mm (figure 1). The value of the remanent displacement was $\Delta = 60$ mm.

Within the next four cycles, carried out on the model displaced configuration, the truss ability of taking over additional in-plane loads was checked.

The truss proved considerable reserves of loading capacity, which ensured a (nonlinearly) elastic behaviour up to forces representing 45-50 % of the failure (buckling) load.

2nd stage. The buckled diagonal 1-2 was removed.

Two loading-unloading cycles were carried out up to a force H = 1.0tf.

The absence of the diagonal 1-2 led to a drastic reduction of the truss stiffness, so that, the forces H= 1,0 tf produced an average in-plane displacement at the purlins midspan $\Delta = 63.2$ mm (figure 2); in the previous stage - cycles 2 to 5 - at the same force, the value of the displacement was $\Delta = 1.7$ mm.

3rd stage. The loading was applied in steps of 2.0 tf up to a force H = 8.0 tf, then in steps of 1.0 tf up to the model failure. At the force H = 16.0 tf the bracing 1-2 buckled in a normal plane to the model plane. The average value of the in-plane displacements at purlins midspan was $\Delta = 25.2$ mm. Figure 7 shows the diagram H - Δ corresponding to this experimental stage. The high value of the failure force (representing 2,13 times the failure value reached in the 1st stage) is due to the diaphragm action as a result of the interaction sheeting/framework.

The 3rd stage emphasized the mode of failure of the completed model :

- load carrying capacity and/or stability loss of certain structural members in terms of their stiffness (in the present case a compression bracing);
- progressive shearing of the fasteners in zones including the failed structural members and, simultaneously, local buckling of the sheeting;
- emphasis and development of the sheeting buckling, consecutively to the increase of the number of sheared fasteners.

4th stage. All bracings were removed.

The loading was applied in steps of 1.0 tf up to a force H = 6.0 tf, then in steps of 0.5 tf up to the model failure.

(4)

At the force H = 7.5 tf some of the seam fasteners (pop rivets) located in the model tension zone were destroyied, occurring local buckling of the sheeting.

At the force H = 9.5 tf, the seam fasteners destruction was generalized and, consecutively, sheeting local buckling emphasized and developed along the seams (figure 3).The average value of the in-plane displacements at purlins midspan was Δ = 46.7 mm.

Figure 8 shows the diagram H - Δ corresponding to this experimental stage.

5th stage. The model defferentiated from that tested in the 4th stage through the fastening system (B).

The loading was applied in steps of 2.o tf up to a force H = 6.o tf, then in steps of 1.o tf up to the model failure.

At the force H $\approx$ 13.o tf, the purlins webs could not take any more the shear force acting in diaphragm; they worked plastically and,then, their upper part tore, at supports, in the vicinity of the stiffened cleats (figure 4). Consecutively, sheeting local buckling occurred at supports but no seam or sheet/purlin fastener degradation took place (figure 5). The average value of the in-plane displacement at purlins midspan was Δ = 62.9 mm.

The attempt of keeping the force at the constant value H = 13.o tf caused the purlins lateral buckling, sheeting buckling emphasis, sheeting tearing (only around the sheet/purlin fasteners), and, finally,the sheet tearing out (figure 6).

Figure 9 shows the diagrame H - Δ corresponding to this experimental stage.

3. Conclusions

The 1st and 2nd experimental stages proved that :

- the truss (the model bare unclad framework) working in the post-critical range - due to a compression bracing buckling - has, still, considerable reserves of load carrying capacity;

- with real cases of failure of a compression diagonal, this one will be kept - as such - in the structure until remedial work are performed, its removal reducing drastically the truss load carrying capacity reserves.

The 3rd, 4th and 5th experimental stages proved :

- the great load carrying capacity of the completed model: (3rd stage : the failure force H = 16.o tf, the corresponding in-plane displacement $\Delta \approx 25$ mm) as against the clad model without bracing (4th stage : the failure force H = 9.5 tf, the corresponding in-plane displacement Δ = 46.7 mm; 5th stage : the failure force H = 13.oo tf, the corresponding in-plane displacement Δ = 63.o mm);

(5)

- the dependence of the model failure force on the fastening system. Thus, the B system confers an additional stiffness to the model, respectively a value of the failure force with 37 % greater than the A system;
- corrugated steel sheeting contribution at the model stiffness and stability ensurance. Thus, the failure force of the completed model (H = 16 tf, 3rd stage) is approximately twice greater than that corresponding to the bare unclad framework (H = 7.5 tf, 2nd stage).

The experimental and theoretical research works were in good agreement.

References

1. x x x — European Recommendation for the Design of Light Gauge Steel Members. ECCS, TWG 7/1-1986.

2. BRYAN,E.R. — Constrado Monographs. The Stressed Skin Design of Steel Buildings. Crosby Lockwood Staples,London, 1973.

3. CRAINICESCU,M.M. SOARE,M.V. GHITA,N. IORDACHE,D. — Aspecte privind interacţiunea dintre elementele de închidere din tablă cutată de oţel (acoperiş) şi şarpantă la hale industriale parter şi clădiri social-cuturale. A V-a Conferenţă de Construcţii Metalice, Timişoara, 22-24 septembrie,1988

(6)

Table 1

Number	Type of tested model	Outline of tested model	Type of fastening system	Type of loading
1	Roof framework with bracings	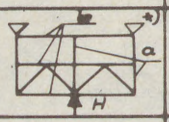	—	Statical stepwise loading
2	Roof framework with a removed bracing	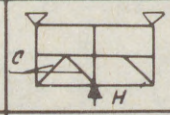	—	Statical stepwise loading
3	Roof framework with bracings and corrugated sheets cladding	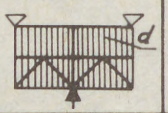	A	Statical stepwise loading, carried out up to the model failure
4	Roof framework with corrugated sheets cladding (all bracings removed)	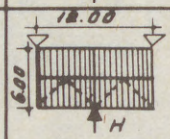	A	Statical stepwise loading, carried out up to the model failure
5	Roof framework with corrugated sheets cladding	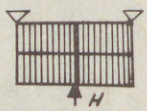	B	Statical stepwise loading, carried out up to the model failure

*) a - rafters
b - purlins
c - bracings
d - corrugated sheets cladding.

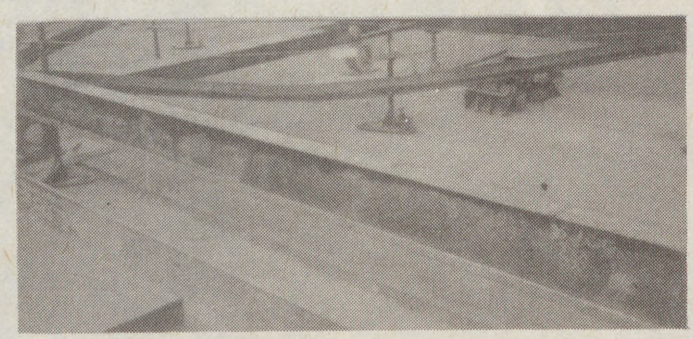

Fig.1. Laterally buckled compression diagonal

(7)

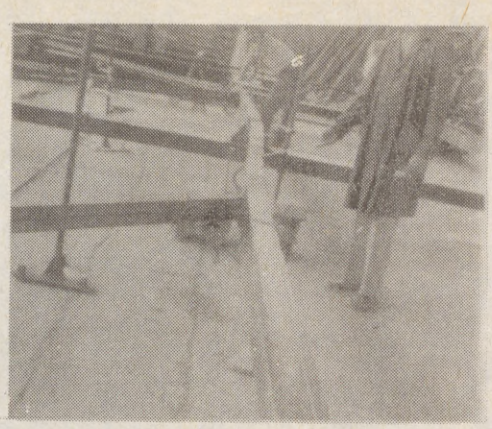

Fig.2. In-plane displacements at the purlin midspan caused by the buckled diagonal removal

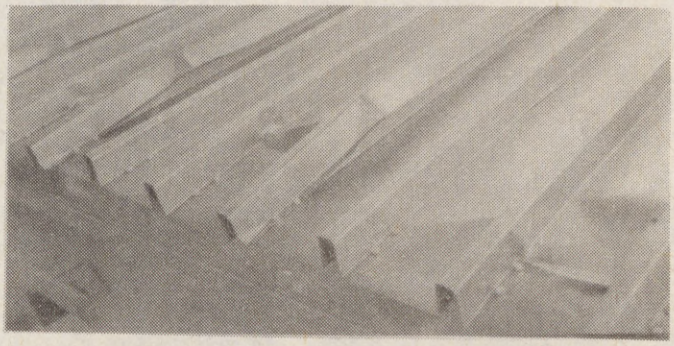

Fig.3. Sheets buckling developed along the seams

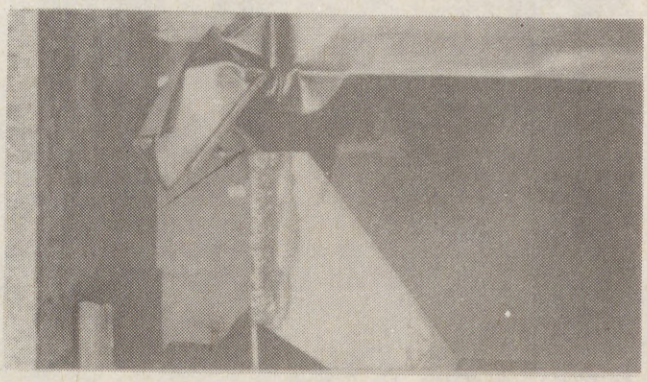

Fig.4. Purlin web torn in the vicinity of the stiffened cleats

(8)

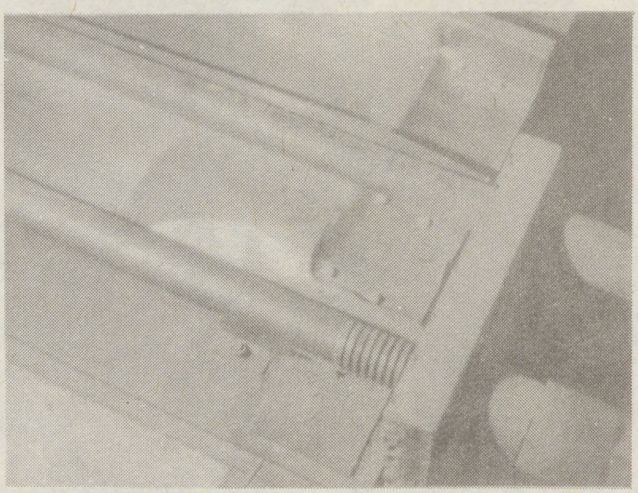

Fig.5. Sheeting local buckling occurred at supports with no fastener degradation

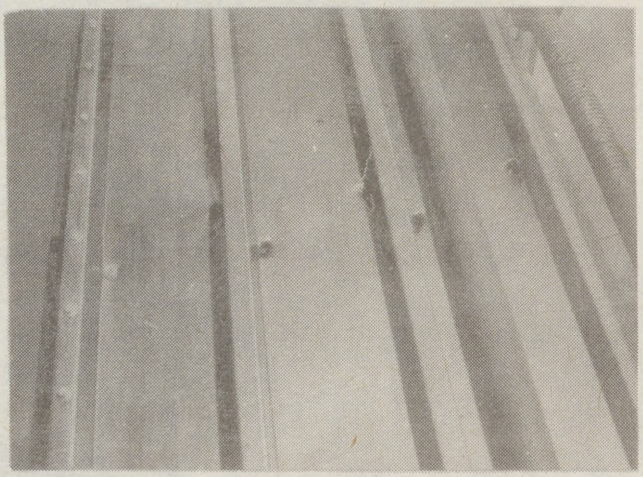

Fig.6. Sheeting tearing out (only at sheet/purlin fasteners)

(9)

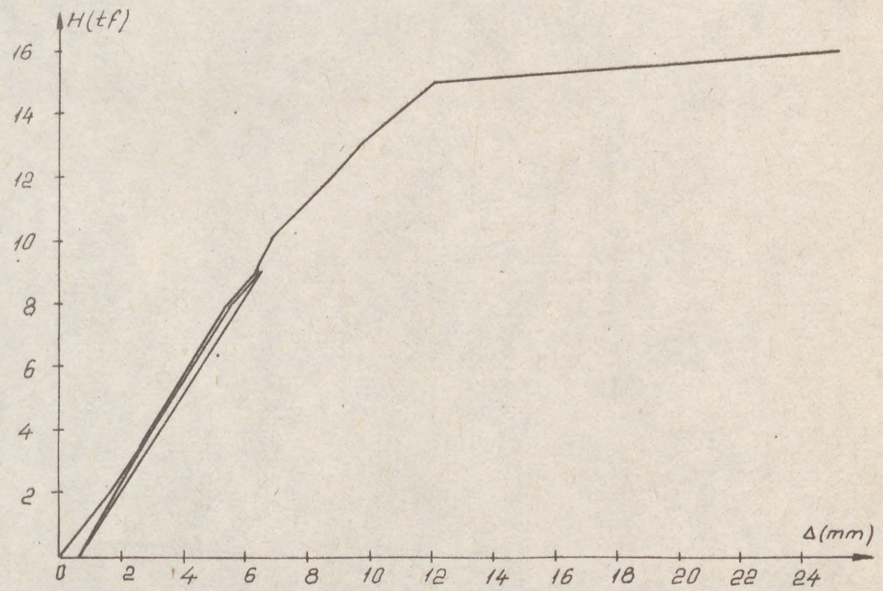

Fig.7. Diagram H – Δ corresponding to the 3rd experimental stage

(1o)

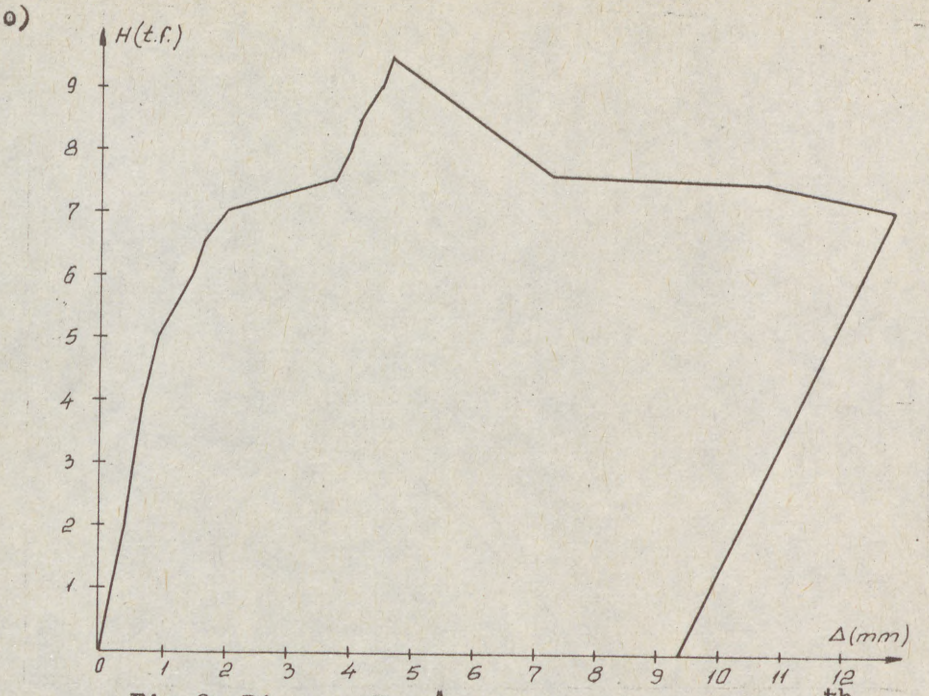

Fig.8. Diagram H – Δ corresponding to the 4th experimental stage

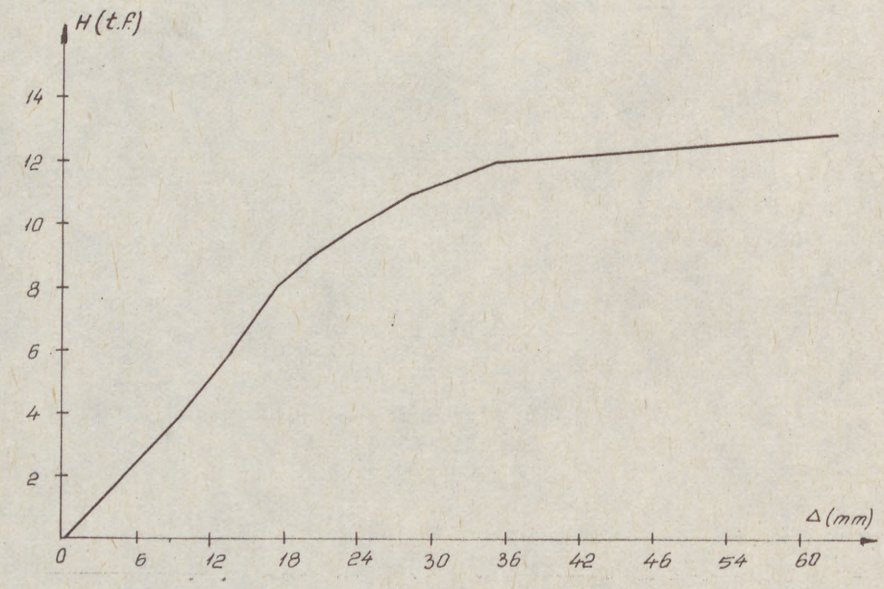

Fig.9. Diagram H – Δ corresponding to the 5th experimental stage

(1)
DE MARTINO, Attilio (1)
GHERSI, Aurelio (2)
MAZZOLANI, Federico M.(3)

CALIBRATION OF A BENDING MODEL FOR THIN-WALLED STEEL BOX-SECTIONS

INTERNATIONAL COLLOQUIUM
STABILITY OF STEEL STRUCTURES
BUDAPEST, HUNGARY, 1990
PRELIMINARY REPORT

Summary : *The results of a calibration procedure of a numerical model, based on the simulation of the moment-curvature relation for thin-walled box-sections, are presented.*

The simulation approach is provided by the use of a computer program built up by taking into account the main parameters and phenomena at the base of the bending behavior of thin-walled members.

INTRODUCTION : The contribution of the present paper has to be related to a general research program devoted to study the bending behavior of thin-walled sections through the analysis of the parameters which influence the shape of the moment-curvature diagram.

This problem is discussed in general in [De Martino et al., 1989] for all thin-walled sections and with particular reference to the case of box-sections, for which some experimental results [Ballio and Calado, 1986] are available to prove the reliability of the simulation procedure and then to get the calibration

---

1 Associate Professor of Structural Engineering, Università di Salerno, Italy
2 Assistant Professor, Università di Napoli, Italy
3 Professor of Structural Engineering, Università di Napoli, Italy

of the coefficients involved in the numerical models.
For box-sections, an appropriate distribution of residual stresses has been considered in order to take into account the particular forming process (in this case by weldings in the corners).
The influence of each parameter has been examined in [De Martino et al., 1989] on ideal box-sections with different values of flanges slenderness (b/t : 30, 40, 50 and 75).
The use of a computer program has allowed to describe the bending process of the section taking into account the local instability phenomena of compressed parts by means of different interpretative numerical models and various other parameters such as residual stresses, material law etc.
Now, it seems useful to point out that we have considered the main aspects influencing the basic bending phenomena, in stable and unstable range, which characterize the behavior of thin-walled profiles.
The numerical models of such phenomena are based on different interpretations which are characterized by the choice of appropriate parameters to be introduced in the formulae.
NUMERICAL MODELS : With the aim of a better interpretation of the calibration procedure steps, fig. 1 shows the influence of the different parameters considered in [De Martino et al., 1989] on the moment-curvature diagram of a given section.
In fig. 1a we can observe the influence of numerical models chosen to simulate the local instability of compressed flange compared to the base curve 0 obtained without the influence of any parameter (elasto-plastic material law only).
The main difference among the models depends on the interpretation of buckling phenomena.
In particular, they consider :
- stability depending from elastic-critical stresses (curve n° 1);
- stability depending from elastic-critical strains (curve n° 2);
- post-critical behavior interpreted by means of a sinusoidal strain distribution (curve n° 3);
- post-critical behavior interpreted as in [Kemp, 1985] and in [Lay and Galambos, 1967] (curve n° 4);
- post-critical behavior based on a formulation derived from the experimental values reported in [Ballio and Mazzolani, 1986] (curve n° 5).

(3)

In fig. 1b the authors analyze the influence of flange restrain conditions by considering a continuous plate (cases a and c) or half plate supported on one edge (cases b and d).
In the classical elastic formulation of critical stresses or strains, the flange fiber slenderness linearly depends upon the distance to the web.
It is possible, furthermore, to generalize this interpretation by assuming a non linear variation of the fiber length as in [Bianchi and Ceccoli, 1987]: this influence is shown in fig. 1c.
In order to take into account the stress distribution, different values of the restrain coefficient have been assumed in fig. 1d to analyze the consequence of the web stability.
In fig. 1e the influence of different distributions of residual stresses are examined.
Following some international codes the influence of the geometrical imperfection on the elastic critical stress and on the post-critical behavior is interpreted by means of a reduction of b_{eff} as suggested by Winter (fig. 1f).
Finally, the influence of the shape of the material law is shown in fig. 1g.
CALIBRATION PROCEDURE : The numerical model, which describes the bending process of the section taking into account the influence of the above mentioned parameters, has been applied to simulate the experimental results reported in [Ballio and Calado, 1986].
The comparison of results is obtained by following different steps: each step is used to select different influence parameters.
The tested specimens are four box-section cantilever beams, each one being obtained by welding four plates in the corners. The overall dimension of the tested profiles is always 300 x 200 mm.
The four sections are characterized by webs of same thickness and material, while, on the other hand, the flanges are composed by different materials and thicknesses, giving four different values of the ratio width to thickness for flanges, equal to 30, 37.5, 50 and 75 (sections a, b, c, and d).
In [Ballio and Calado, 1986] the results of the experimental tests are presented in the form of load versus displacement diagrams; for this reason it is necessary to transform, for each model, the moment-curvature relation into the F/v diagram.
Moreover, in figs. 2 to 5 the results are provided in dimensionless form by means of F/F_y-v/v_y curves, being:

- F_y the horizontal force which produces the first yielding in the section fibers;
- v_y the displacement corresponding to F_y.

The experimental values are plotted by square markers. Reference curve 0 shows the behavior of the same section considered as compact.

Fig. 2 shows, for the four sections (2a, 2b, 2c and 2d), the first step of the calibration procedure : the curve n° 1 is derived from the base curve 0 by considering the effect of the residual stresses (when assuming the values depending upon the forming process which is better interpreted by the model [a] of fig. 1e). For the material, looking to the round-house shape of the σ-ε curve, model [a] of fig. 1g has seemed to be the most appropriate to interpret the experimental results in the elastic range.

The results of the second step have been plotted in fig. 3: the curves n° 1,2 and 3 derive from curve n° 1, of the previous step (fig. 2), by keeping the instability model of curve n° 2 of fig. 1a. This step analyses the reduction of the critical value due to geometrical imperfections and to different variation laws for the fiber slenderness (circular, parabolic, linear of fig. 1c).

From the shown results of fig. 3 we observe that the curves n° 1 and 2 better agree with experimental behavior in plastic range.

Starting from the last conclusions, we have, furthermore, considered, in fig. 4, two types of stability models (the previous model and the Kemp's one), together with two coefficients for the compressed flange restrain conditions (K_{min} and K_{max}), obtaining six curves and in particular :

- curve n° 1, Kemp's stability model with circular law for fiber slenderness;
- curve n° 2, elastic strain stability model (curve n° 2 of fig. 1a) with circular law for f.s. and K_{max}= 5.3, 5.45, 5.66, 5.94 respectively for sections a, b, c and d;
- curve n° 3, elastic strain stability model (curve n° 2 of fig. 1a) with circular law for f.s. and K_{min}= 3.19, 3.37, 3.60, 3.93 respectively for sections a, b, c, d;
- curves n° 4, 5 and 6 correspond to the above mentioned curves 1, 2, 3 but using parabolic variation for fiber slenderness.

The values used for K coefficients are obtained by the following expressions :

- when considering the compressed flange as a continuous plate

$$K_{max} = 4 + \frac{2.97}{1+\beta}$$

- when considering the compressed flange as two counter-wise cantilevers

$$K_{min} = 4 \cdot \left(0.425 + \frac{0.852}{1+\beta}\right)$$

(5)

both the expression having :

$$\beta = \frac{b_w/t_w}{b_f/t_f}$$

It is easy to note that curve n° 3 gives in all cases the best agreement for this kind of section.

CONCLUSION : It seems reasonable to assume that the calibration of the analytical models, by means of the appropriate parameters, allows the computer program to describe the bending behavior of thin-walled box-section built up by welding.

This tool opens the way to perform a wide parametric analysis on this kind of section by a continuously varying range of plate slenderness.

From the calculation point of view, the use of curve n° 5 is suggested because it lays on the safety side in the full displacement range (see fig. 5).

REFERENCES

BALLIO,G., CALADO,L., 1986, "Sezioni inflesse in acciaio sottoposte a carichi ciclici. Sperimentazione e simulazione numerica.", Costruzioni Metalliche, n° 1

BALLIO,G., MAZZOLANI,F., 1987, Strutture in acciaio, Hoepli

BIANCHI,S.,CECCOLI, C., 1987, "Colonne di acciaio sottoposte a carichi ciclici. Simulazione numerica. e confronto con esperienze.", 3° Convegno Nazionale l'Ingegneria Sismica in Italia, Roma

DE MARTINO,A., GHERSI,A., MAZZOLANI,F., 1989, "Analisi dei parametri di influenza del comportamento flessionale delle sezioni a cassone in parete sottile", C.T.A. Giornate Italiane della Costruzione in Acciaio, Capri

ECCS, TC8, 1986, Behavior and Design of Steel Plated Structures, TWG 8.3

KEMP,A., 1985, "Interaction of plastic local and lateral buckling", Journal of Structural Engineering, vol. 111, n° 10

LAY,M., GALAMBOS,T., 1967, "Inelastic beams under moment gradient", Journal of the Structural Division, ASCE, vol. 93, n° ST.1, proc. paper 5110

VON KARMAN,T., SECHLER,E., DONNELL,L., 1932, "The strength of thin plates in compression", Applied Mechanics, APM-54-5

(6)

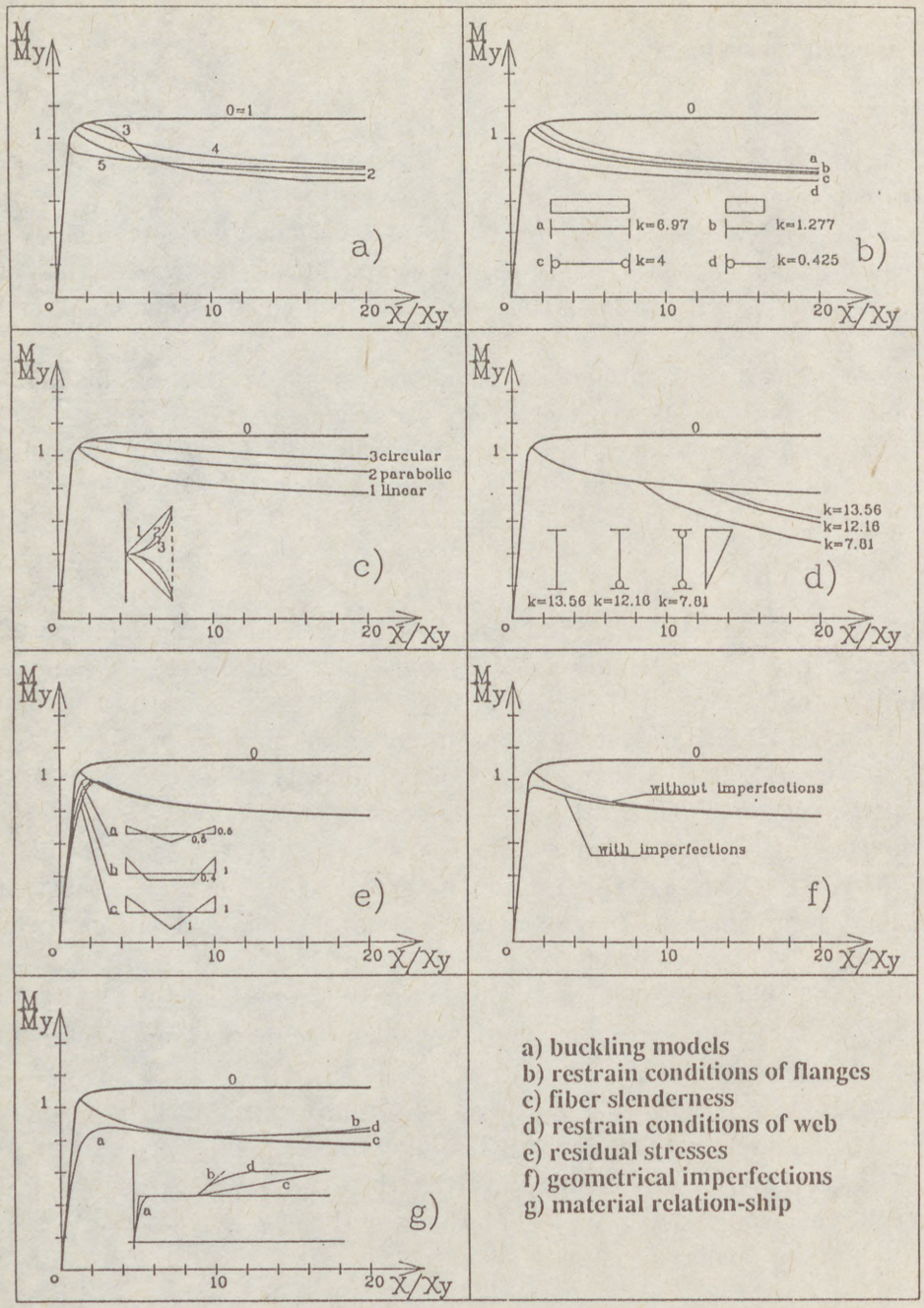

Fig. 1 Moment-curvature curves : the influence of behavioral parameters.

(7)

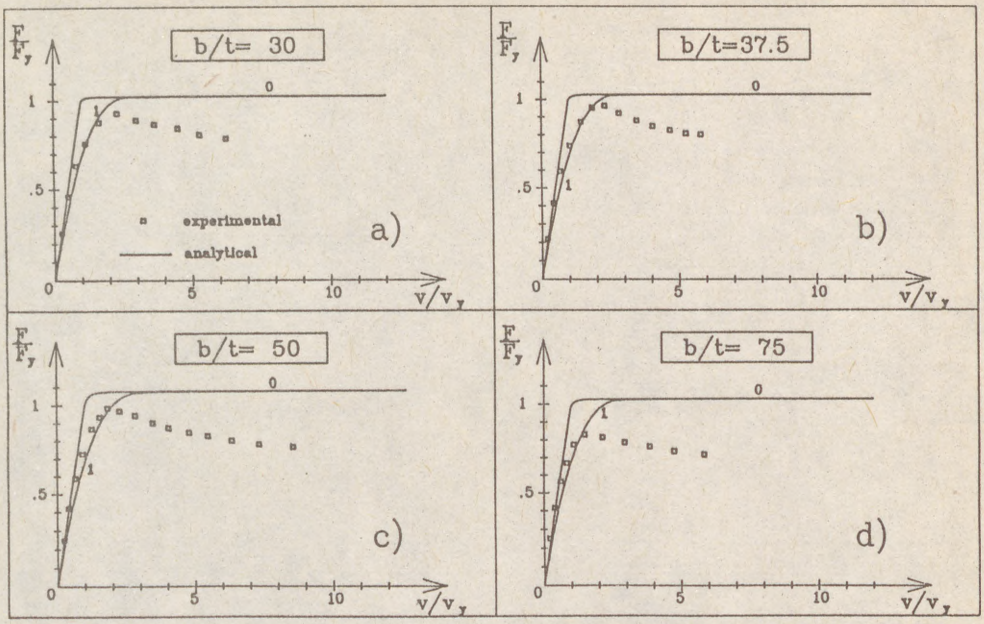

Fig. 2 Calibration procedure : residual stresses and material law.

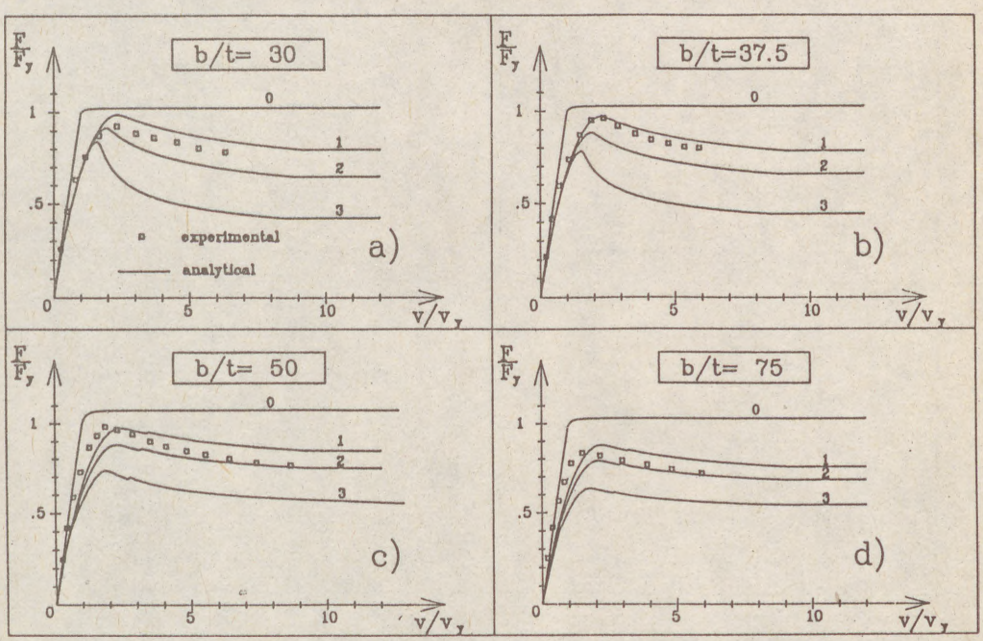

Fig. 3 Calibration procedure : compressed fiber slenderness variation law.

(8)

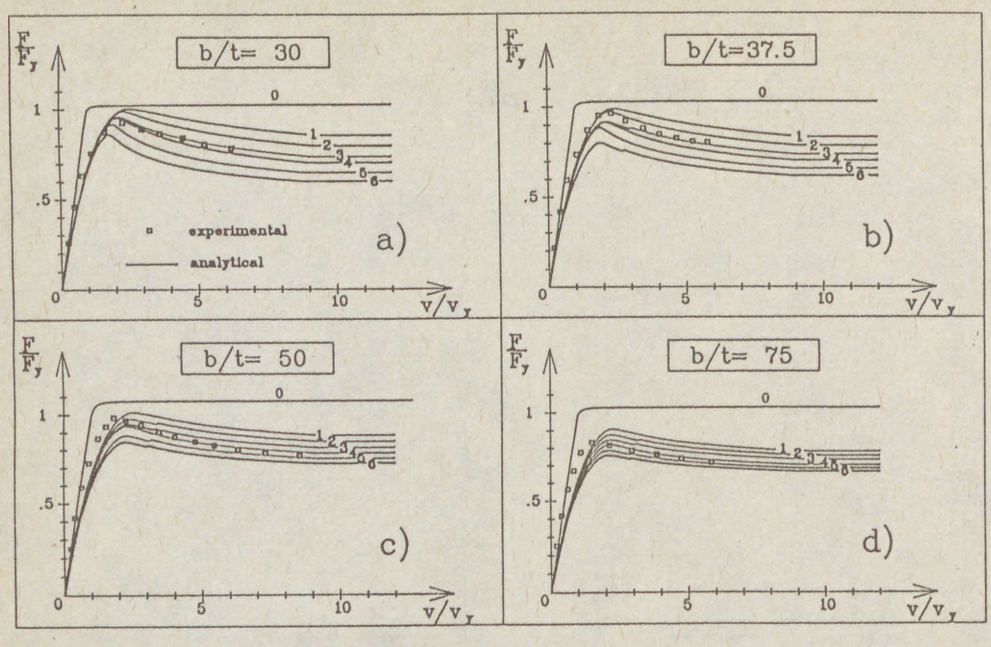

Fig. 4 Calibration procedure : instability models.

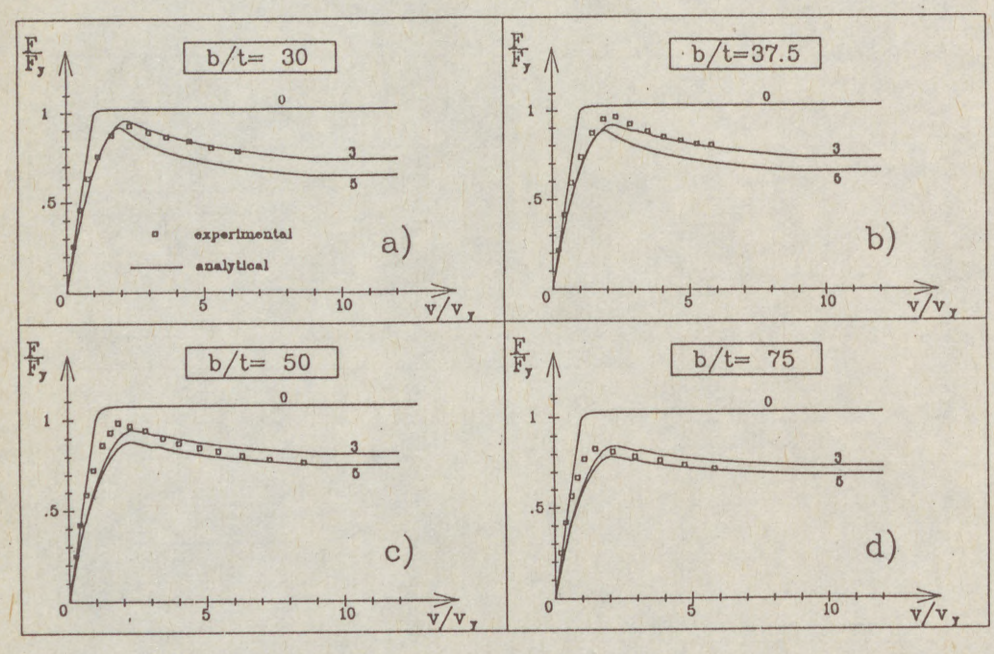

Fig. 5 Calibration procedure : selected behavioral curves.

(1)
DUBINA, Dan (1)
PACOSTE, Costin (2)

THE INTERACTION OF LOCAL AND OVERALL BUCKLING IN THIN-WALLED COLD-FORMED COMPRESSED MEMBERS

INTERNATIONAL COLLOQUIUM
STABILITY OF STEEL STRUCTURES
BUDAPEST, HUNGARY, 1990
PRELIMINARY REPORT

Summary: This paper presents a new concept and a new calculation formula for determining the yield stress of thin-walled cold-formed compressed members when local buckling and overall buckling interact. The numerical and experimental results put forth are compared with those obtained employing the interaction formulae in the ECCS recommendations and the AISI specifications.

1. INTRODUCTION

Dubina (1989), Dubina and Pacoste (1989 a), and Gioncu (1989) have shown that the interaction formula given in the ECCS recommendations (1987) for calculating overall buckling when it is associated with local buckling yields values which are too conservative in the case of both long members and members of average length. This fact has previously been reported by Batista in his Ph.D. thesis defended at the University of Liege under J.Rondal's supervision (Batista 1988), in which an improvement in the ECCS formula is put forth.

Fig. 1a and 1b present these results using two different modes of presentation. The symbols used are those standardized by ECCS.

The abovementioned situation has at least two causes.

1. The coefficient $Q = A_e/A$, denoting the reduction in the cross sectional area of the member, which is used in the interaction formula, is determined employing the concept of equivalent width - for this problem, see Dubina and Fleşeriu (1986),

(1) Lecturer of Structural Mechanics, Polytechnic Institute of Timisoara, the S.R. of Romania
(2) Researcher, ICCPDC Building Research Institute, Timisoara branch, the S.R. of Romania

(2)

Dubina (1988), Dubina and Pacoste (1989 a and 1989 b), and Rondal (1989). The equivalent width b_e is calculated assuming that the yield point, $\sigma_{max} = f_y$, has been reached in the corners of the section, while the equivalent cross sectional area is calculated assuming that all of the walls of the column have undergone buckling. Actually, in the case of slender columns, on account of the lateral displacements caused by the overall buckling of the column and the change in the location of the centre of gravity of the cross section following the local buckling of the walls, flexural moments occur which lead to increases in the compression load in some walls and decreases in the compression load in other walls. Consequently, the walls do not undergo buckling simultaneously, and in certain situations some walls may undergo no buckling whatsoever. Under these circumstances, if the equivalent cross sectional area A_e is used from the onset of column loading throughout the slenderness range of the column, $0 - \bar{\lambda}$, only the carrying capacity of the column will be affected. In the case of long columns, wall buckling may occur only when the column collapses due to column buckling.

It is therefore necessary either to use the coefficient Q in the interaction formula (which is to be differentiated over various slenderness ranges) or to consider interaction formulae differentiated over these ranges.

2. Thin-walled cold-formed sections do not fit adequately the ECCS local buckling curves developed for hot-rolled sections, which are characterized by marked mechanical imperfections (residual stresses). The only significant imperfections displayed by thin-walled sections are geometrical, because cold forming practically eliminates residual stresses. It is true that cold hardening causes great variations of the yield point in the corners of the sections, but the investigations carried out by Costa-Ferreira and Rondal (1986) show that this phenomenon has a beneficial effect. It is therefore obvious that the use of these curves for thin-walled cold-formed sections will yield, as it actually happens, results which are too conservative.

The authors are of the opinion that the order in which these two problems are to be solved should be identical to that in which they have been formulated.

The purpose of this paper is to reconsider the way column instability and local instability interact and to propose calculation formulae for various slenderness ranges.

2. COUPLING OF COLUMN INSTABILITY AND WALL INSTABILITY

Loughlan and Rhodes (1979) have suggested a way of evaluating the ultimate axial load N_u of lipped channel columns (compressed and bent C-section thin-walled columns), using for this purpose a semienergetic analysis method which takes into account the change in the location of the centre of gravity of the cross section of the column and the change in the location of the neutral axis while the phenomenon is under way. The interaction curve corresponding to this proposal is shown in Fig.

2. Qualitatively similar results have been reported by Ferneze-lyi (1986) for aluminium members.
Neither proposal takes into consideration the erosion of the critical load at the point where the two forms of instability - column instability and wall instability - couple and at the point where the two forms of instability branch (Fig. 3). From this point of view, Gioncu (1986 and 1989) considers that the interaction between column instability and local instability in thin-walled columns is of the "hard" type and is characterized by an up to 50% erosion of the critical branching load.
Starting from this idea and assuming that the coupling of the two forms of instability will occur only when the local buckling critical load has been reached in a wall $\bar{N}_p = 9$, the interaction curve can be plotted implementing the following algorithm (Fig. 4):

a. Determine the point $A(\bar{\lambda}_A, \bar{N}_w = 9) = \{(\bar{N}(\bar{\lambda}) \cap (\bar{N}_p(\bar{\lambda}_p))\}$;
b. Determine the point $B(\bar{\lambda}_B, \bar{N}_E = 9) = \{(\bar{N}_E(\bar{\lambda})) \cap (\bar{N}_p(\bar{\lambda}_p))\}$;
c. Determine the point $C(\bar{\lambda}_B, (1-\Psi)\,9)$.
d. Plot a connecting curve $\bar{N}^*(\bar{\lambda})$ as a second-order parabola tangent in A to the ECCS curve, $\bar{N} = \bar{N}(\lambda)$, which runs through C and intersects Euler's parabola, $\bar{N} = \bar{N}_E(\bar{\lambda})$ in E.

$$\bar{N}^*(\bar{\lambda}) = a(\alpha, 9, \Psi)\bar{\lambda}^2 + b(\alpha, 9, \Psi)\bar{\lambda} + c = 0$$

e. Check whether this curve has a monotonously decreasing slope - if it does not, plot the connecting curve $N^*(\lambda)$ as a third-order parabola which meets the conditions listed under d above and is tangent to the horizontal line when $\bar{\lambda} = \bar{\lambda}_E$. This yields:

$$\bar{N}^*(\bar{\lambda}) = a(\alpha, 9, \Psi)\bar{\lambda}^3 + b(\alpha, 9, \Psi)\bar{\lambda}^2 + c(\alpha, 9, \Psi)\bar{\lambda} + d(\alpha, 9, \Psi) = 0$$

f. Four $\bar{\lambda}$ intervals of column behaviour are obtained.

I. $0 < \bar{\lambda} \leq 0{,}2$: the case of short columns which collapse when wall buckling occurs, where $\bar{N} = \bar{N}_p(\bar{\lambda}) = Q$

II. $0{,}2 < \bar{\lambda} \leq \bar{\lambda}_A$: overall buckling with total local buckling. the behaviour of the column being defined by the curve $\bar{N} = \bar{N}(\lambda)$ according to the interaction formula in the ECCS recommendations.

III. $\bar{\lambda}_A < \bar{\lambda} \leq \lambda_E$: overall buckling accompanied by partial local buckling, the behaviour of the column being defined by the curve $\bar{N} = \bar{N}^*(\bar{\lambda})$ plotted using the algorithm described above

IV. $\bar{\lambda} < \bar{\lambda}_E$: overall buckling unaccompanied by local buckling, where $\bar{N} = \bar{N}_E(\bar{\lambda})$, because, as it has been shown, the ECCS curves are too conservatives as far as residual stresses are concerned.

Fig. 5 shows both the interaction curves obtained in this way for two cross sections, U 75x60x2 and C 155x54x47x1.5, and experimental results and the interaction curves called for by the

(4)

ECCS recommendations and the AISI specifications. The experimental results have been taken from Batista (1986). The $\bar{N} = \bar{N}(\lambda)$ curve has been plotted assuming that the sections illustrate the overall buckling curve b, with $\alpha = 0.339$, and the location of the point C has been determined assuming a moderate erosion of 30%, $\psi = 0.3$.
It is immediately apparent that these results are in close agreement with the experimental results.
It is to be noted that, since the coefficients Q and ς uniquely characterize the cross section of a column (Dubina and Pacoste 1989 a), the numerical determinations and the quantitative comparisons must involve dimensional section types.

3. CONCLUDING REMARKS

1. We consider that approaching the coupling of overall instability and local instability discriminately, over various column slenderness ranges, and taking into account the sensitivity of the cross section and the component walls to local buckling, is in agreement with the actual behaviour of thin-walled compressed members (and other thin-walled members). It is a fact that buckling intervenes progressively in the behaviour of the member.
2. The numerical model suggested for the quantitative evaluation of the interaction of overall buckling and local buckling is obviously liable to undergo improvement. In the first place, the model must be given a general form which should make it easy to implement in the design stage. In the second place, the experimental basis for its validation must be extended, particularly where the specification of the erosion factor Ψ is concerned, because this can vary from one cross section to another.
3. Ultimately, we believe that it is necessary for ECCS to coordinate a far-reaching effort - of the kind which has led to the development of the overall buckling curves for hot-rolled sections - with a view to developing the overall buckling curves for thin-walled cold-formed members. In the case of these members, priority must be given to geometrical imperfections, and when checking such members against these curves, it is advisable to take into consideration their sensitivity to local buckling, possibly differentiating stiffened members from unstiffened members in accordance with the way in which the coefficient Q is evaluated.
In this context, the results reported herein can be interpreted as a suggestion.

REFERENCES

AISI, 1986 - Specifications for the Design of Cold-Formed Steel Structural Members. American Iron and Steel Institute, August 19.

Batista, E. de Miranda, 1988. "Etude de la stabilite des profils a parois minces et sections ouverts de types U et C". These presentee a l'Universite de Liege.

(5)

Batista, E. de Miranda, 1988. "Essais de profils C et U en acier plies a frois". Universite de Liege, Rap. No. 157.

Costa-Ferreira, C.M., and Rondal, J., 1986. "Influences of Residual Stresses on the Stability of Compressed Angles". Proc. of the Int. Conf. on Steel Structures "Recent Research Advances", Padua, Sept. 28 - Oct. 1.

Dubina, D., 1988. "Recent Research and Design Formulae for the Effective Width of Stiffened and Unstiffened Elements". Proc. of the 5th Conf. on Metal Structures, Timisoara, Sept. 22 - 24, Vol. 1.

Dubina, D., 1989. "Considerații privind interactiunea dintre flambaj si voalare in studiul instabilitatii barelor cu pereti subtiri". St. Cerc. Mecanica Aplicata, Tom 48, No. 2, p. 157-178.

Dubina, D., and Fleseriu, E., 1986. "Equivalent Geometric Characteristics in Stability Analysis of the Thin-Walled Cold-Formed Members". Proc. of the 2nd Reg. Col. on Stability of Steel Structures, Hungary, Sept. 25 - 26, Vol. II, p. 227-235.

Dubina, D., and Pacoste, C., 1989 a. "Theoretical and Experimental Investigations Concerning the Interaction of Local and General Buckling of Thin-Walled Cold-Formed Compressed Members". Proc. of the 4th Int. Col. ICSSAS '89, Oct. 10 - 12.

Dubina, D., and Pacoste, C., 1989 b. "Theoretical and Experimental Investigations Concerning a New Formula for Determining the Effective Width of Thin-Walled Members". Proc. of the 4th Int. Col. on Stability of Metal Structures, New York, April 18 - 19.

ECCS, 1987 - European Recommendations for the Design of Light Gauge Steel Members. First Edition. European Convention for Constructional Steelwork.

Fernezelyi, S., 1986. "Ultimate Load of Thin-Walled Aluminium Members in Compression". Proc. of the 2nd Reg. Col. on Stability of Steel Structures, Hungary, Sept. 25 - 26, Vol. II, p. 237-245.

Gioncu, V., 1985. "Stable and Unstable Components of Critical Loads". Euromech 200, Metrafured, Hungary, p. 93.

Gioncu, V., 1989. "Coupled Instabilities in Bar Structures. Phenomenon, Theory, Practice". Proc. of the 4th Int. Col. on Stability of Metal Structures, New York, April 18 - 19.

Loughlan, J., and Rhodes, J., 1979. "Interactions of Lipped Channel Columns". Richards, T.H., and Stanley, P. (editors), Stability Problems in Engineering Structures and Components, Applied Sc. Publ. Ltd., London.

Rondal, J., 1989. "Transformation Model for the Design of Thin-Walled Steel Members". Conf. on Models for the Analysis of Steel Structures, Pardubice - Czechoslovakia, April 25 - 26.

(6)

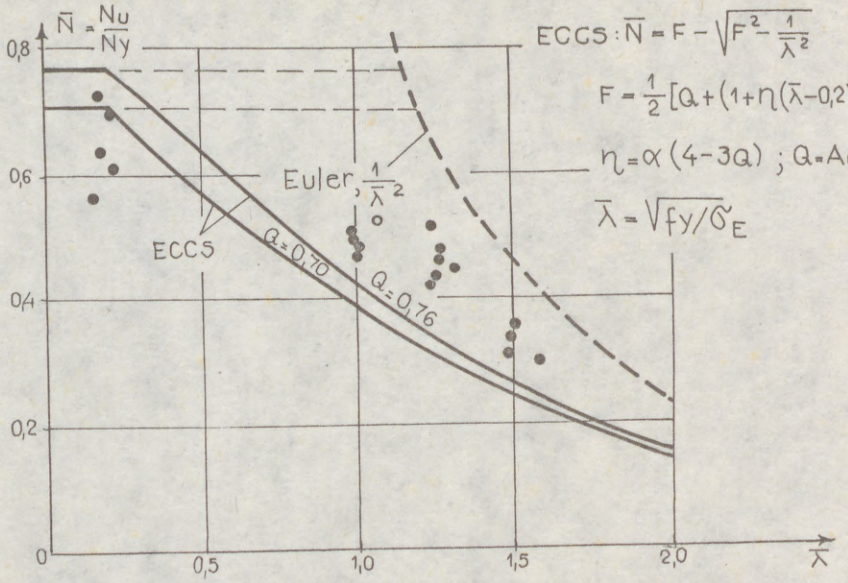
$\bar{N} = \frac{N_u}{N_y}$
ECCS: $\bar{N} = F - \sqrt{F^2 - \frac{1}{\bar{\lambda}^2}}$
$F = \frac{1}{2}[Q + (1 + \eta(\bar{\lambda} - 0{,}2))/\bar{\lambda}^2]$
$\eta = \alpha(4 - 3Q)$; $Q = Ae/A$
$\bar{\lambda} = \sqrt{f_y/\sigma_E}$
Euler, $\frac{1}{\bar{\lambda}^2}$
ECCS
Q=0,70
Q=0,76
0,8
0,6
0,4
0,2
0
0,5
1,0
1,5
2,0
$\bar{\lambda}$

a)

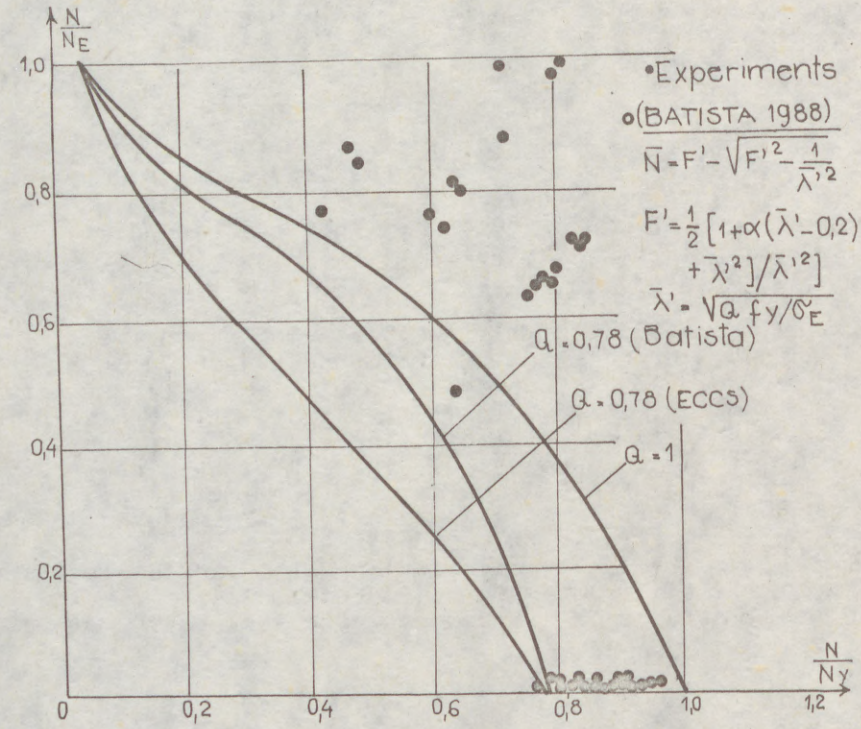
$\frac{N}{N_E}$
•Experiments
o(BATISTA 1988)
$\bar{N} = F' - \sqrt{F'^2 - \frac{1}{\bar{\lambda}'^2}}$
$F' = \frac{1}{2}[1 + \alpha(\bar{\lambda}' - 0{,}2) + \bar{\lambda}'^2]/\bar{\lambda}'^2$
$\bar{\lambda}' = \sqrt{Q}\, f_y/\sigma_E$
Q=0,78 (Batista)
Q=0,78 (ECCS)
Q=1
1,0
0,8
0,6
0,4
0,2
0
0,2
0,4
0,6
0,8
1,0
1,2
$\frac{N}{N_y}$

b

fig. 1

(7)

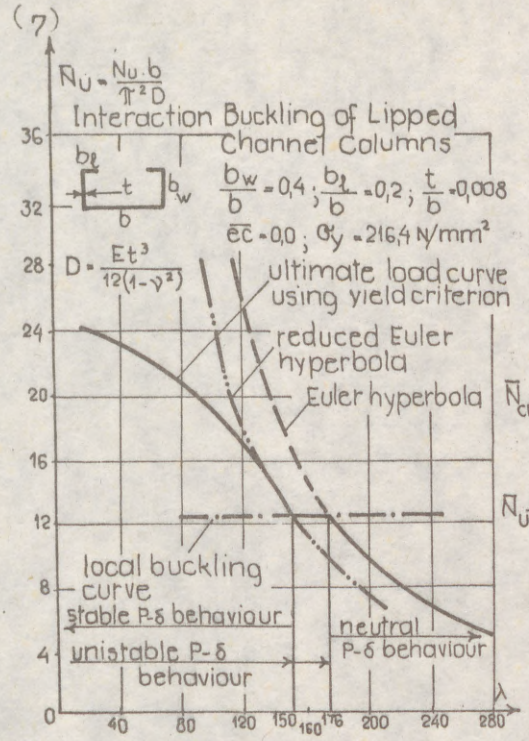

fig. 2

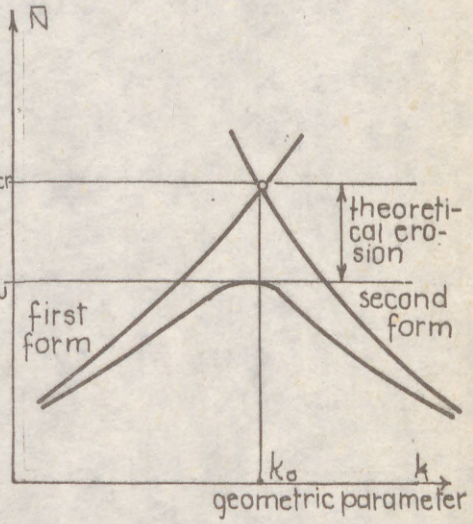

fig. 3

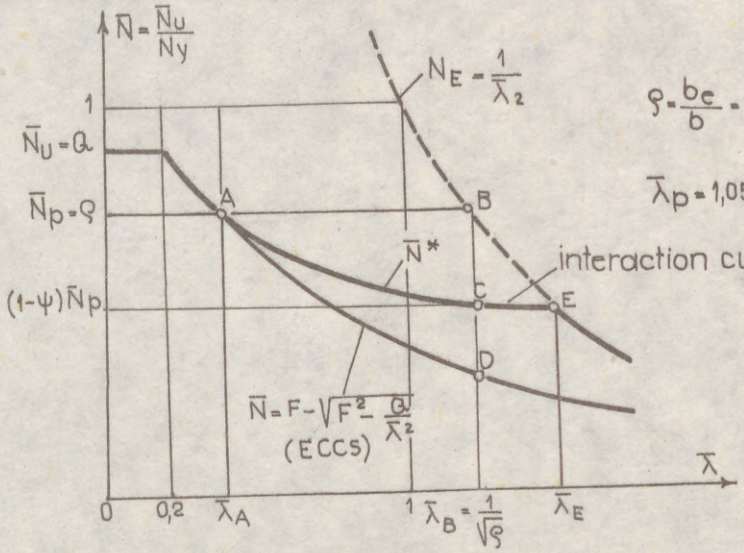

$$\varrho = \frac{b_e}{b} = \frac{1}{\bar{\lambda}_p}\left(1 - \frac{0{,}22}{\bar{\lambda}_p}\right)$$

$$\bar{\lambda}_p = 1{,}052 \frac{b}{t}\sqrt{\frac{f_y}{E k}}$$

fig. 4

(8)

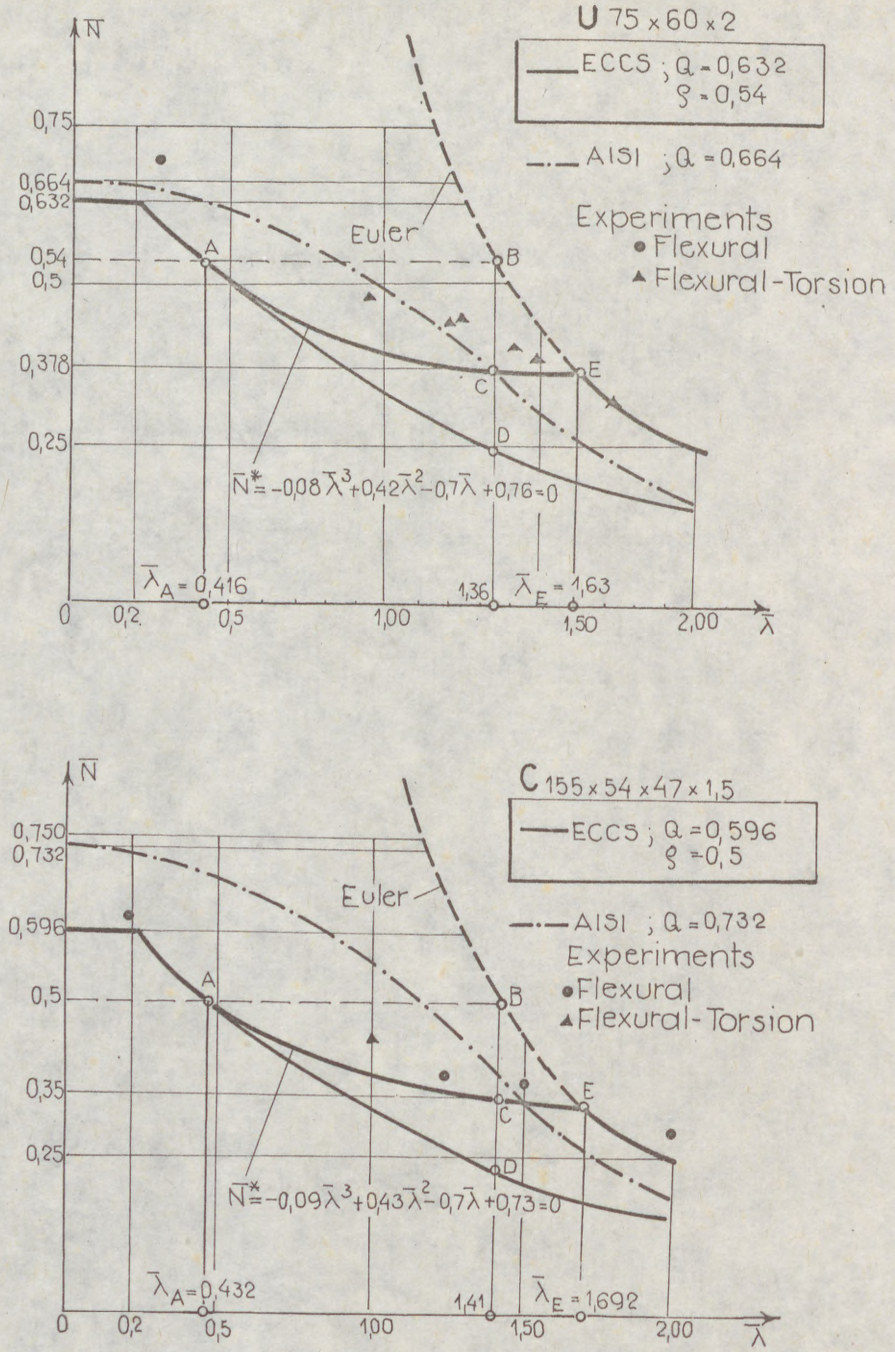
U 75 x 60 x 2
ECCS ; Q = 0,632
ς = 0,54
AISI ; Q = 0,664
Experiments
• Flexural
▲ Flexural-Torsion
Euler
N̄
0,75
0,664
0,632
0,54
0,5
0,378
0,25
A
B
C
D
E
N̄* = −0,08λ̄³ + 0,42λ̄² − 0,7λ̄ + 0,76 = 0
λ̄A = 0,416
λ̄E = 1,63
1,36
0
0,2
0,5
1,00
1,50
2,00
λ̄
C 155 x 54 x 47 x 1,5
ECCS ; Q = 0,596
ς = 0,5
AISI ; Q = 0,732
Experiments
• Flexural
▲ Flexural-Torsion
Euler
N̄
0,750
0,732
0,596
0,5
0,35
0,25
A
B
C
D
E
N̄* = −0,09λ̄³ + 0,43λ̄² − 0,7λ̄ + 0,73 = 0
λ̄A = 0,432
λ̄E = 1,692
1,41
0
0,2
0,5
1,00
1,50
2,00
λ̄

fig. 5

(1)
FARKAS, József (1)
JÁRMAI, Károly (2)

MINIMUM CROSS-SECTIONAL AREA DESIGN OF CENTRALLY COMPRESSED STRUTS OF SQUARE BOX SECTION WITH LONGITUDINAL STIFFENERS

INTERNATIONAL COLLOQUIUM
STABILITY OF STEEL STRUCTURES
BUDAPEST, HUNGARY, 1990
PRELIMINARY REPORT

Summary: An optimum design procedure is presented in which the four unknown dimensions of a square box section with longitudinal flat stiffeners are sought. The cross-sectional area should be minimized and constraints on overall and local buckling have to be fulfilled. The interaction of overall and local buckling is considered by a simple formula proposed by Nakai et al. The optimization is performed by the use of a computer program worked out on the basis of Rosenbrock's direct search method. The required cross-sectional areas for unstiffened and stiffened sections are given in graphical form and compared to each other. Steels of yield stress 235 and 355 MPa, respectively, are taken into account. The rounded dimensions of stiffened sections are given in tables.

1. Introduction

The best way for decreasing the weight of steel structures is the decrease of the thickness of their plate elements. This decrease may lead to interaction of overall and local buckling in compression members. The optimum design of centrally and eccentrically compressed struts of square hollow section without longitudinal stiffeners has been worked out by the first author (Farkas 1983, 1984). This optimization has been performed by the use of the Liège-method (Braham et al. 1980) which considers the interaction of overall and local buckling.

Box sections with longitudinal stiffeners have been treated by Nakai et al. (1986) with relatively simple formulae suitable for optimum design. The aim of the present paper is to apply this method to the minimum weight design of longitudinally stiffened box sections. Nakai et al. (1986) gave a calculation method for rectangular box sections subject to com-

(1) Professor of Metal Structures, DSc.
(2) Scientific research worker, CSc. Technical University, Miskolc, Hungary.

(2)

pression and bending, symmetrically stiffened with more equally spaced longitudinal ribs as shown in Fig. 1a. The yield stress of plate and stiffener elements may be different. This method considers the interaction of overall and local buckling as well as the interaction of local buckling of plate elements.

For the sake of simplicity we treat here the section shown in Fig. 1b. with square symmetry, considering only four ribs. The strut is simply supported at both ends and subject to pure compression. The yield stress of plate elements and stiffeners is equal, 235 and 355 MPa, respectively. In this case the interaction of local buckling of plate elements may be neglected but the interaction of overall and local buckling should be taken into account.

2. Objective function and constraints

The unknown dimensions b, t, h_s and t_s should be optimized (Fig. 1b) to minimize *the cross-sectional area*

$$A = 4(bt + h_s t_s) \tag{1}$$

or with non-dimensionalized unknowns

$$x_1 = 100b/L\,; \quad x_2 = 100t/L\,; \quad x_3 = 100h_s/L \quad \text{and} \quad x_4 = 100t_s/L$$

$$10^4 A/L^2 = 4(x_1 x_2 + x_3 x_4) \tag{2}$$

and to fulfil the design constraints as follows.

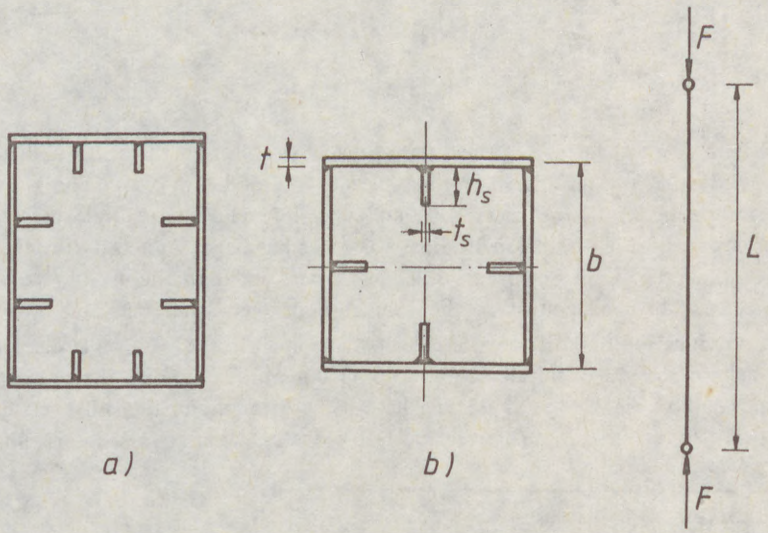

Fig. 1. Centrally compressed strut of a) rectangular and b) square box section with longitudinal stiffeners

Constraint on overall buckling for the *factored* compressive force

$$F \leqslant \min \begin{cases} k\sigma_y A & (3a) \\ k\sigma_y A\, k_{\text{int}} & (3b) \end{cases}$$

where σ_y is the yield stress. Note that the Japanese Specifications (1987) give for steels with yield stress 235 and 355 MPa allowable stresses 140 and 210 MPa, respectively. Furthermore, k is the overall buckling factor

$$k = 1.0 \qquad \text{when} \quad \bar{\lambda} \leqslant 0.2 \tag{4a}$$

$$k = 1 - 0.545\,(\bar{\lambda} - 0.2) \qquad \text{when} \quad 0.2 \leqslant \bar{\lambda} \leqslant 1.0 \tag{4b}$$

$$k = 1/(0.773 + \bar{\lambda}^2) \qquad \text{when} \quad \bar{\lambda} \geqslant 1.0 \tag{4c}$$

where

$$\bar{\lambda}^2 = A\sigma_y/F_e\,; \qquad F_e = \pi^2 EI/L^2 \tag{5}$$

or in transformed form using (2)

$$\bar{\lambda}^2 = \frac{10^8\, \sigma_y\, A/L^2}{10^8\, \pi^2\, EI/L^2} = \frac{10^4\, \sigma_y}{\pi^2\, E} \cdot \frac{10^4\, A/L^2}{10^8\, I/L^2} \tag{6}$$

$$I = \frac{2}{3} b^3 t + \frac{h_s^3\, t_s}{6} + 2h_s\, t_s \left(\frac{b}{2} - t - \frac{h_s}{2} \right)^2 \tag{7}$$

Considering (7), (6) may be written in the following form

$$\bar{\lambda}^2 = \frac{4 \times 10^4\, \sigma_y}{\pi^2\, E} \cdot \frac{x_1 x_2 + x_3 x_4}{\frac{2}{3} x_1^3 x_2 + \frac{1}{6} x_3^3 x_4 + 2x_3 x_4 \left(\frac{x_1}{2} - x_2 - \frac{x_3}{2} \right)^2} \tag{8}$$

Taking $E = 2.06 \times 10^5$ MPa, $\sigma_y = 235$ and 355 MPa we obtain

$$4 \times 10^4\, \sigma_y/(\pi^2\, E) = 4.62339 \quad \text{and} \quad 6.98428, \text{ resp.} \tag{8a}$$

The factor k_{int} expresses the interaction of overall and local buckling according to Nakai et al. (1986)

$$k_{\text{int}} = k_p + 0.2304\, \bar{\lambda}^2 \tag{9a}$$

where

$$k_p = 1.0 \qquad \text{when} \quad R \leqslant 0.31 \tag{9b}$$

$$k_p = 1.14 - 0.454\, R \qquad \text{when} \quad 0.31 \leqslant R \leqslant R_{\max} \tag{9c}$$

$$R = \frac{b}{nt} \sqrt{\frac{12(1-\mu^2)}{k_0\, \pi^2}} \sqrt{\frac{\sigma_y}{E}} \tag{10}$$

(4)

where n is the number of panels separated by stiffeners, in our case in Fig. 1b. $n = 2$. With values $k_0 = 4$, $\mu = 0.3$, and $E = 2.06 \times 10^5$ MPa we obtain for $\sigma_y = 235$ MPa

$$R = b/(112t) = x_1/(112x_2); \quad R_{\max} = 0.8 \tag{11a}$$

and for $\sigma_y = 355$ MPa

$$R = x_1/(88x_2) \tag{11b}$$

For a box section without stiffeners ($n = 1$) it is

$$\text{for } \sigma_y = 235 \text{ MPa} \qquad R = x_1/(56x_2); \qquad R_{\max} = 1.0 \tag{11c}$$

$$\text{and for } \sigma_y = 355 \text{ MPa} \qquad R = x_1/(44x_2) \tag{11d}$$

Limitation of the R-value i. e. allowable b/t-ratio of a stiffened or unstiffened plate restrained along two edges

$$R \leqslant R_{\max}. \tag{12}$$

Constraint of local buckling of plate elements

$$F \leqslant k_p A \sigma_y \tag{13}$$

where k_p is given by (9).

Constraints on buckling of longitudinal stiffeners according to Nakai et al. (1986) and the Japanese Specifications (1987):

$$\text{for } \sigma_y = 235 \text{ MPa} \qquad h_s/13.1 \leqslant t_s \tag{14a}$$

$$\text{for } \sigma_y = 355 \text{ MPa} \qquad h_s/10.7 \leqslant t_s \tag{14b}$$

$$I_L = \frac{h_s^3 t_s}{3} \geqslant \frac{bt^3}{11} \gamma_{L\,\mathrm{req}} \tag{15}$$

and

$$A_L = h_s t_s \geqslant \frac{bt}{10n} \tag{16}$$

1) when

$$\alpha = a/b \leqslant \alpha_0 = \sqrt[4]{1 + n\gamma_L} \tag{17}$$

and the moment of inertia of a transverse stiffener is

$$I_T \geqslant \frac{bt^3}{11} \cdot \frac{1 + \gamma_{L\,\mathrm{req}}}{4\alpha^3} \tag{18}$$

then, for

$$t \geqslant t_0 \qquad \gamma_{L\,\mathrm{req}} = 4\alpha^2 n \left(\frac{t_0}{t}\right)^2 (1 + n\delta_L) - \frac{(\alpha^2 + 1)^2}{n} \tag{19a}$$

(5)

for

$$t < t_0 \qquad \gamma_{L\,\mathrm{req}} = 4\alpha^2 n(1 + n\delta_L) - \frac{(\alpha^2 + 1)^2}{n} \tag{19b}$$

2) other than in 1)

$$\text{for } t \geqslant t_0 \quad \gamma_{L\,\mathrm{req}} = \frac{1}{n}\left[\left\{2n^2 \left(\frac{t_0}{t}\right)^2 (1 + n\delta_L) - 1\right\}^2 - 1\right] \tag{20a}$$

$$\text{for } t < t_0 \quad \gamma_{L\,\mathrm{req}} = \frac{1}{n}\left[\left\{2n^2 (1 + n\delta_L) - 1\right\}^2 - 1\right] \tag{20b}$$

where $\quad$ for $\sigma_y = 235$ MPa $\qquad t_0 = b/(28n)$ (21a)

$$\text{for } \sigma_y = 355 \text{ MPa} \qquad t_0 = b/(22n) \tag{21b}$$

a is the spacing of transverse stiffeners,

$$\delta_L = \frac{A_L}{bt} = \frac{h_s\, t_s}{bt} = \frac{x_3\, x_4}{x_1\, x_2}. \tag{22}$$

The spacing a is taken here so that $\alpha = \alpha_0$ and it is assumed that (18) is fulfilled, thus, formulae (19) are used. When the non-dimensionalized unknowns are applied, then x_1, x_2, x_3 and x_4 should be used instead of b, t, h_s and t_s, respectively, in (15)–(20).

Size constraints: $x_i^L \leqslant x_i \leqslant x_i^U$; $\quad i = 1, \ldots, 4$ (23)

The lower and upper limit values x_i^L and x_i^U resp., are taken according to the minimal and maximal values of unknowns as follows (in mm):

	min	max		Δ
		$\sigma_y = 235$	355 MPa	
b	50	1400	1400	10
t	2	20	25	2*
h_s	20	200	200	5
t_s	2	16	20	2

* between 22 and 25 $\Delta = 3$.

Δ is the step value considered in the discretization to obtain rounded optimal values.

3. Optimization and results

The optimal dimensions have been computed by the use of a program developed on the basis of the Rosenbrock's direct search method (Rosenbrock 1960, Jármai 1989). First the unrounded optimal values have been found and then the computation has been complemented by a discretization procedure to obtain rounded optimal values.

(6)

Fig. 2. shows the graphical representation of results. The lines have been determined using computed unrounded optimal values. It can be seen that the relationships $A/L^2 - F/L^2$ may be characterized in a log-log coordinate-system by straight lines. The rounded optimal values for stiffened box sections with yield stress 235 and 355 MPa, respectively, are given in Table 1 and 2.

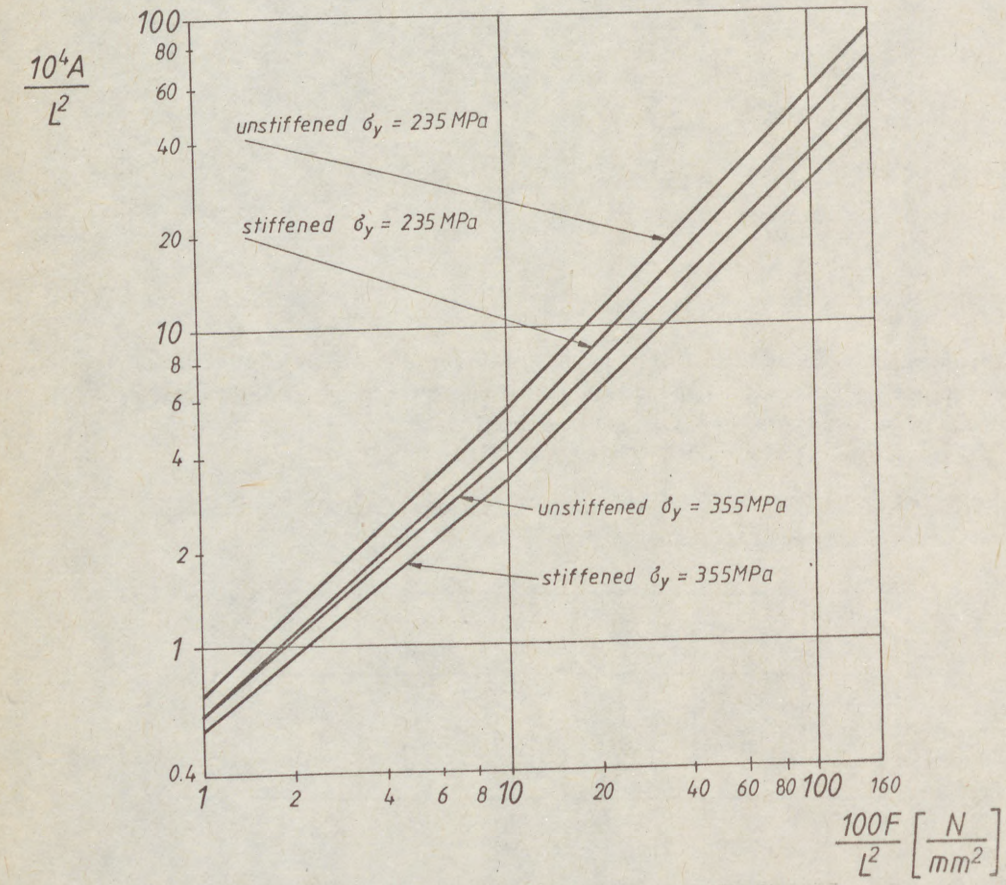

Fig. 2. Optimal cross-sectional areas A/L^2 versus F/L^2 for unstiffened and stiffened box sections with yield stresses 235 and 355 MPa respectively

4. Conclusions

The method proposed by Nakai et al. (1986) complemented by the formulae given in the Japanese Specifications (1987) is suitable for optimum design of compressed struts of

(7)

Table 1. Rounded optimal dimensions of box sections, yield stress 235 MPa

L [m]	$F \times 10^{-3}$ [kN]	b [mm]	t [mm]	h_s [mm]	t_s [mm]	A [mm^2]
10	21	1050	20	200	16	96 800
	16	870	20	130	10	77 120
	11	890	14	150	12	57 600
	6	460	14	40	12	31 680
	1	350	4	45	4	6 320
8	21	1050	20	200	16	96 800
	16	870	20	130	10	77 120
	11	890	14	150	12	57 600
	6	450	14	60	10	28 880
	1	320	4	40	4	5 840
6	21	1050	20	200	16	96 800
	16	870	20	130	10	77 120
	11	890	14	150	12	57 600
	6	400	16	45	10	28 640
	1	310	4	40	4	5 760
4	21	1050	20	200	16	96 800
	16	880	18	165	14	72 600
	11	840	14	130	14	56 560
	6	400	16	45	10	28 640
	1	240	4	40	6	4 800

Table 2. Rounded optimal dimensions of box sections, yield stress 355 MPa

L [m]	$F \times 10^{-3}$ [kN]	b [mm]	t [mm]	h_s [mm]	t_s [mm]	A [mm^2]
10	21	740	20	130	14	66 480
	16	640	18	120	12	51 840
	11	490	16	115	18	39 640
	6	430	12	75	8	23 040
	1	350	4	40	4	6 240
8	21	740	20	130	14	66 480
	16	640	18	120	12	51 840
	11	520	14	95	14	34 440
	6	430	12	75	8	23 040
	1	280	4	40	4	5 120
6	21	740	20	130	14	66 480
	16	420	25	150	16	51 600
	11	470	16	60	14	33 440
	6	410	12	60	12	22 560
	1	280	4	40	4	5 120
4	21	740	20	130	14	66 480
	16	410	22	165	18	47 960
	11	390	20	65	8	33 280
	6	310	12	110	12	20 160
	1	160	6	20	6	4 320

longitudinally stiffened box section. The method considers the interaction of overall and local buckling.

The comparison of the minimal cross-sectional areas required for unstiffened and stiffened struts shows that one can achieve approximately 15% savings in weight using flat stiffeners.

The calculations show that, for $10^2\ F/L^2 \geqslant 10$, the optima lay in overall plastic buckling zone, because the compressive stresses F/A are in these cases larger than $0.75\ \sigma_y$. Thus the use of higher-strength steel decreases very effectively the weight, the savings in weight may be 40% or more.

References

Braham, M. , Grimault, J. P., Massonnet, Ch., Mouty, J. and Rondal, J. (1980) Buckling of thin-walled hollow sections. Cases of axially loaded rectangular sections. *Acier-Stahl-Steel*, **45**, No. 1. 30–36.

Farkas, J. (1983) *Optimum square hollow sections for centrally and eccentrically compressed steel members.* 3rd Internat. Colloquium on Stability of Metal Structures, Paris. CTICM, Final Report, 121–125.

Farkas, J. (1984) *Optimum design of metal structures.* Budapest. Akadémiai Kiadó, Chichester, Ellis Horwood.

Japanese Specifications for Highway Bridges (1987). Part 2. Steel bridges. English edition. Japan Road Association.

Jármai, K. (1989) Single- and multicriteria optimization as a tool of decision support system. *Computers in Industry* **11**, 249–266.

Nakai, H., Kitada, T. and Miki, T. (1986) On a design criterion for checking ultimate strength of thin-walled steel frames. *Mem. Fac. Eng. Osaka Univ.* **27**, 245–269.

Rosenbrock, H. H. (1960) An automatic method for finding the greatest or least value of a function. *Computer J.* **3**, No. 3. 175–184.

(1)
HOLMSTRÖM, Lars (1)
SAMUELSON, Lars Å. (2)
ZUBACZEK, Jerzy (3)

OVERALL STABILITY OF THINWALLED MOBILE CRANE BOOMS OPERATING IN THE POSTBUCKLING RANGE

INTERNATIONAL COLLOQUIUM
STABILITY OF STEEL STRUCTURES
BUDAPEST, HUNGARY, 1990
PRELIMINARY REPORT

Summary:

Mobile telescopic cranes are built in thin plate design and in some cases buckling is allowed to occur under normal operating conditions. However, a number of national crane design codes, including the Swedish code, do not allow buckling of any kind. The present investigation was carried out in order to provide complementary design rules for postbuckling analysis. The two major design factors are static strength and global instability. The postbuckling strength analysis is readily done by use of available methods. Mobile crane booms are often long slender beams which have to be designed with due consideration to second order effects, even when buckling is not allowed. When a crane is designed for operation in the postbuckling range, the interaction of local plate buckling and global instability (tilting) has to be considered.

1 Introduction

Mobile crane booms have, in most cases, been developed under the assumption that buckling must be avoided. An American producer has designed cranes on the basis of thin plate technology as developed by the aircraft industry, where the load carrying capacity, even in the extreme postcritical range, has been utilized for a long time.

---

(1) Royal Institute of Technology, Dept.Mat. Techn., Stockholm.
(2) The Swedish Plant Inspectorate, Stockholm
(3) The Swedish Plant Inspectorate, Stockholm

(2)

2 Stiffness of typical boom sections

It was decided at an early stage in the investigation to use the effective width concept in the buckling analysis. A plate subjected to an inplane compressive force is fully effective only as long as the plate is perfectly flat. If the plate deflects out of its plane bending is introduced and the stiffness decreases. This results in a drop in stresses in the plate midplane and an increase along the edges where the lateral deflection is restricted. The stress distribution is shown in Fig. 1 together with the effective width idealization. In general, the effective width is a function of the load level. Various expressions for this function have been given in the litterature, see for instance Gerard, 1957. The objective of the present effort was, however, to provide fairly simple rules for the verification of the operational envelope of the crane. Thus, the design review is based on conservative estimates of the minimum effective width and the influence of buckling on the global stability (tilting) during operation. The following scheme is used in the design review:

The buckling stresses are calculated from the classical theory, Brush, Almroth, 1975, in the case of inplane compression and shear:

$$\sigma_{cr} = K_c \frac{\pi^2 D}{b^2 t}$$

$$\tau_{cr} = K_s \frac{\pi^2 D}{b^2 t} \quad \text{where}$$

$$D = \frac{Et^3}{12(1-\nu^2)}$$

E = Young's modulus, ν = Poisson's ratio, b = plate width and t = plate thickness

The values of the buckling coefficients are assumed for simply supported edges which leads to:

$K_c = 4$ and $K_s = 6$

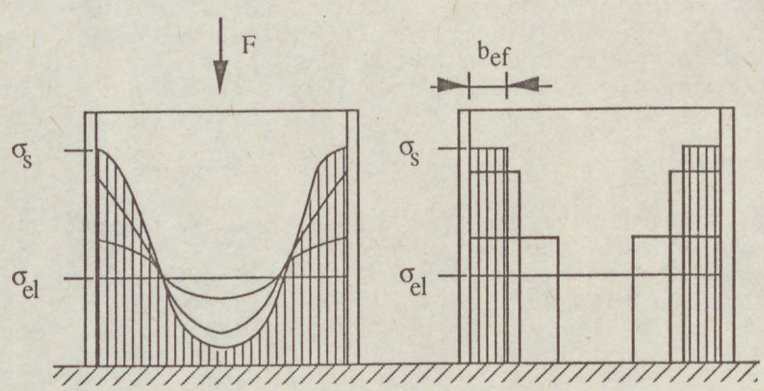

Fig. 1 Stress distribution in a thinwalled plate subjected to buckling b_{ef} = effective width

(3)
This assumption is on the safe side as will be demonstrated below. If, however, it is found that the required safety margins are not satisfied with this conservative model, the analysis is easily extended to include more accurate stiffness data. When buckling occurs, the inplane stiffness is assumed to decrease instantaneously to the values shown schematically in Fig. 2. Interaction between shear and compression buckling may occur in the webs. This is considered as follows: If the web has buckled due to shear, the carrying capacity for compression is assumed to be reduced to a value represented by the effective width of $b_{ef} = 20t$ and vice versa.

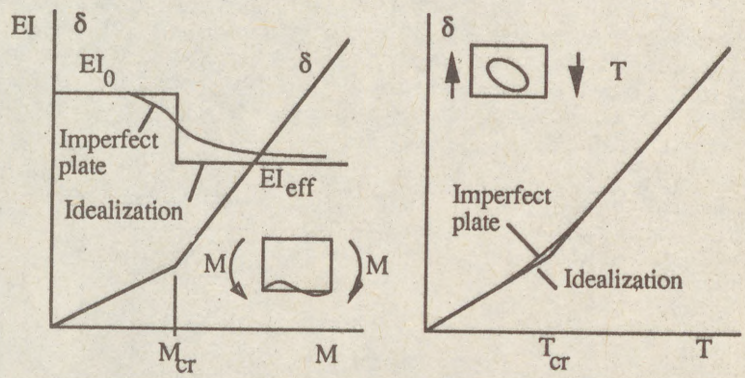

Fig. 2 Variation in stiffness and deflection of a box beam in the case of bending and shear

A specific boom configuration is shown in Fig.3. The main loading force is vertical causing buckling in some of the bottom panels and webs. The stiffness parameters to be evaluated are related to bending, torsion and shear and are calculated for the effective boom sections indicated in Fig. 3 The deflections of the boom are calculated iteratively using the stiffness data for the full cross section as a first estimate.

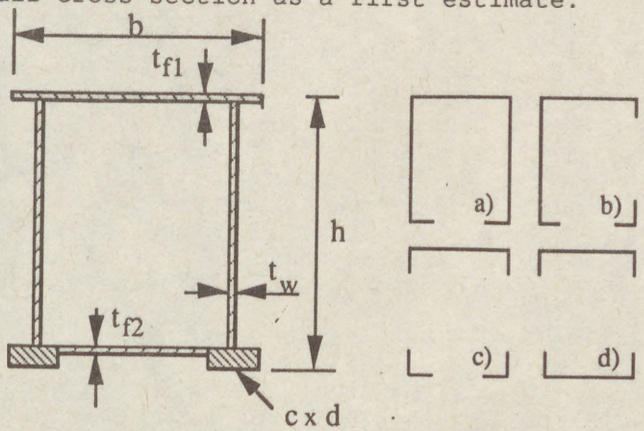

Fig. 3 A typical box beam section where the bottom flange and the webs may buckle

(4)

3 Experimental investigation

Although reports from numerous experimental investigations may be found in the literature, it was decided that a few simple tests on boom sections similar to those found in practice would contribute significantly to the understanding of the buckling behavior. An experimental study was, therefore, carried out by use of two thinwalled box beams subjected to three point bending. Test specimen No 1 was made of 0.2 mm Mylar plastic film and specimen No 2 of 0.6 mm sheet aluminum, see Fig.4. The buckling load of specimen No 1 was so low that the behavior during buckling could not be observed. On the other hand, the stiffness in the extreme postbuckling range could be accurately determined. Specimen No 2 was designed to buckle at a stress level of one third of the yield stress, which should be sufficient for observations of the beam stiffness in the vicinity of the buckling limit.

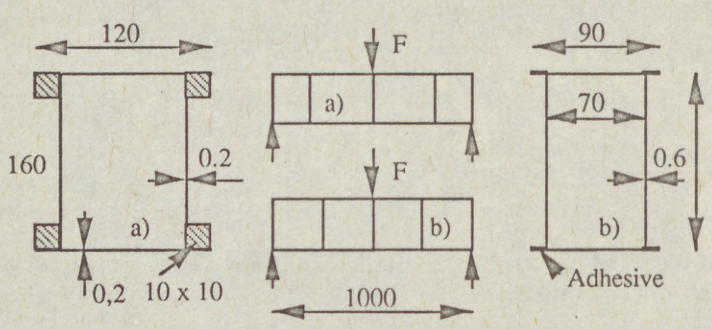

Fig. 4 Geometries of test specimens a) Mylar plastic beam and b) Aluminum beam. The beams had slightly different vertical stiffener arrangements as indicated

A few **results** of the tests with **specimen No 1** are shown in Fig.5 where measured midpoint deflections are given as functions of the load. Theoretical values based on various models for the beam stiffness are included. It is evident that a sufficiently accurate estimate of the tangent stiffness in the extreme post-buckling region is obtained with the calculation model proposed in Section 2. The deflections predicted by the nominal stiffness of the unbuckled beam is included for comparison. It is clear that the reduction in stiffness due to buckling is considerable.

The ultimate load was not determined since the material is not representative of those used in practice. Also, the bending stiffness of the longitudinal stiffeners did not match the plate thickness and a strength test would not be meaningful.

The results obtained with **specimen No 2** are shown in Fig. 6. Again the slope of the load vs deflection curve obtained by use of the approximate theory agrees very well with the experimental results at loads well above the buckling limit. Moreover, the theory of beam bending and shear predicts the deflections at low loads accurately as should be expected. In the intermediate

(5)
range $F_{cr} < F < 2F_{cr}$ there is a gradual decrease in stiffness which could be predicted by use of more elaborate effective width models or finite element analyses if required. It should also be noted that the assumption of simple supported edges is conservative.

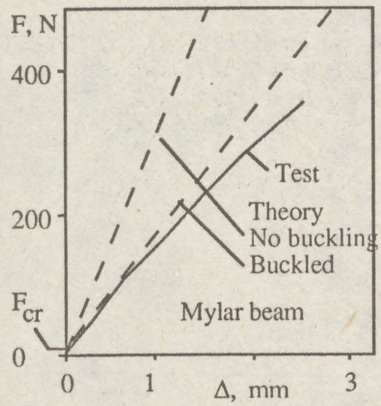

Fig. 5 Test results Mylar beam in 3-point bending

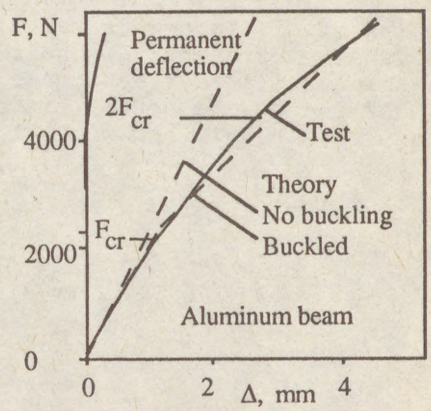

Fig. 6 Test results aluminum beam, 3-point bending

Buckles became clearly visible at a load level slightly higher than the theoretical buckling load. Interaction between the deflections of the compressed flange and the web was also evident and the twist of the flange was fairly large.

The beam was subjected to successively higher loads until the ultimate load was reached at 6250 N. At that load level the yield strength of the material is reached and the deflection measurements also showed a certain amount of permanent strain, see Fig. 6. Fracture occured through separation in the adhesive joint between the web and the upper plate.

4 Analysis of boom deflections and stresses

Based on the general theory of postbuckling and the experience gained from the tests, a simple strategy was worked out for the analysis of slender beams subjected to local plate buckling.

* First the deflections and stresses of the beam are calculated for the specific geometry and loading configuration. A typical example is given in Fig.7. In general it is necessary to consider the effect of second order terms in this analysis.

* Based on the results, the areas subjected to buckling are identified and new values of the stiffness parameters are calculated.

* A new calculation of the deflections and stresses is performed using the redefined stiffnesses.

(6)

* The result is inspected with respect to the assumed extension of the buckled regions. If there are indications that more areas would buckle due to the increased bending moment, the stiffness parameters are recalculated and a new iteration is performed.

* The calculations are repeated until steady state conditions are reached.

Examples of displacements calculated for the boom head under various assumed buckling conditions are shown in Fig. 7. In this case the vertical deflection is only marginally influenced by the buckling of the bottom plate but the lateral deflection depends very heavily on whether the webs are buckled or not.

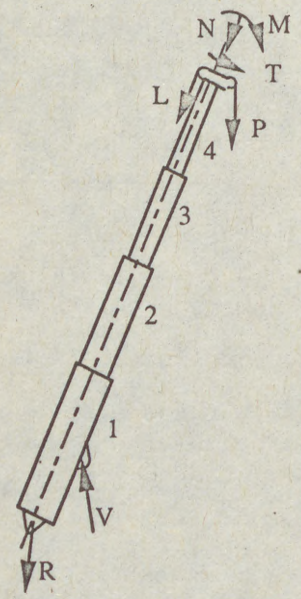

Part	a)		b)		c)	
1234	↓	→	↓	→	↓	→
0000	1.000	1.000	1.000	1.000	1.000	1.000
*						
1000	1.009	1.007	1.017	1.084	1.035	1.173
1100	1.068	1.042	1.103	1.520	1.169	2.454
1110	1.187	1.087	1.280	2.365	1.454	6.797
1111	1.264	1.108	1.393	2.841	1.636	9.938

*, 0 = full stiffness, 1 = bottom plate and/or web buckled

Fig. 7 Four section telescopic boom. Calculated deflections for fully effective boom sections (0) and when local buckling has ocurred (1)

5 Overall stability considerations

The loading of the crane must at all times be applied such as to ensure that instability can not occur. The effect of buckling of the plated structure must then be considered. An example is given in Fig. 8. A crane boom is assumed to be loaded by a vertical force causing stresses in the plates and webs equal to the buckling stresses. The deflection of the boom is then defined by the stiffness of the fully effective cross section. The crane boom is then rotated an angle $\Delta\alpha$ ($\alpha = \alpha_1 + \Delta\alpha$), see Fig 8, resulting in a bending moment increment of ΔM.

(7)
This increment is composed of two parts, ΔM_1 corresponding to the displacement which would result if the bending stiffness was invariant. ΔM_2 is the additional bending moment caused by the loss of bending and shear stiffness of the boom due to buckling. The deflections in the vertical plane thus must be controlled such as the margin against overturning is not surpassed. This is achieved in the load control system which measures the force in the hydraulic actuator and warns the operator against overloading.

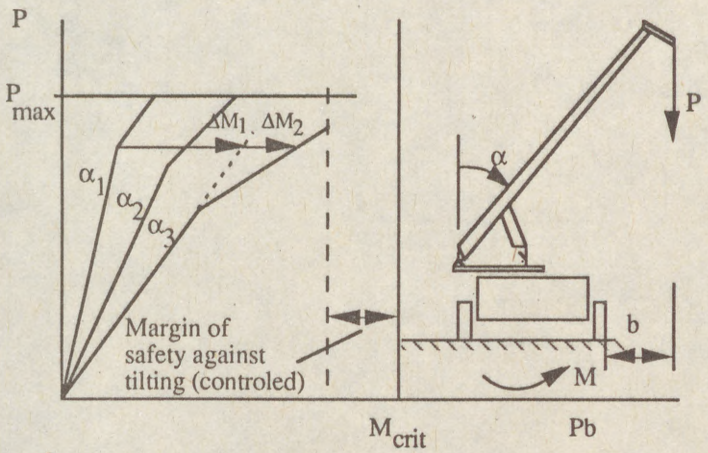

Fig. 8 Stability of crane carrying a vertical load P.

The effect of lateral deflections caused by a small horisontal load or a slight rotation of the base plate out of the horisontal plane are somewhat more difficult to estimate and control as shown in Fig. 9. A lateral, second order, deflection initiated at A causes an increase of the base moment M but does not influence the actuator force. Consequently, the margin of safety may be lower than indicated by the control system. The lateral deflections are composed of several parts: linear beam bending, including effect of buckling, torsion of beam due to skew loading and second order effects involving the vertical force P. A sketch of the behavior of a typical beam is included in Fig. 9.

The table given in Fig. 7 shows an example of the lateral deflections to be expected in a beam where the webs are buckled due to shear. Case b) indicates that the bending deflections may be expected to increase by a factor of 3 if all the webs on the compressed side are working in the postbuckling range. Case c) shows the behavior of a beam where both webs are buckled causing a further decrease in the bending stiffness. These conditions apply only for small deflections since the buckling deflections on the tension side will be reduced and the conditions of case b) will be approached. This leads to the conclusion that shear buckling of the webs may have an influence on the stability margin of the crane in cases similar to that of Fig, 9. Since the lateral deflections cause a moment which is not measurable

(8)

in the conventional way it is important that the effect of the postbuckling induced stiffness reduction is considered in the choice of stability margin and in the operation manual.

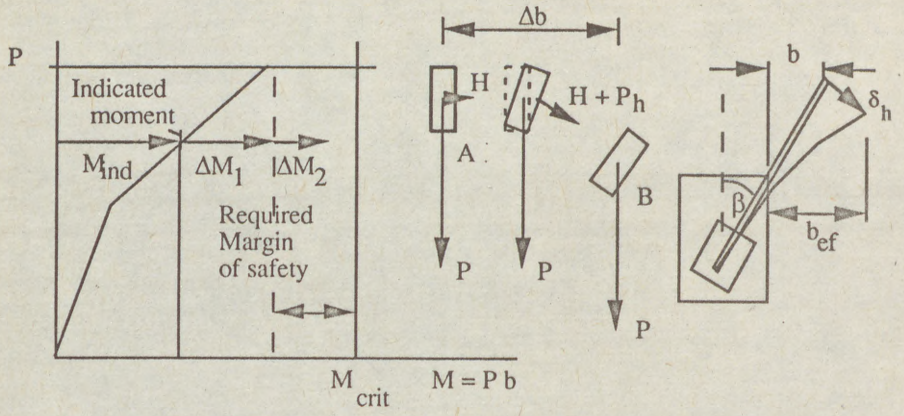

Fig. 9 Effect of web buckling on the overall stability limit of the crane in the case of lateral loading.

6 Discussion

Thinwalled mobile crane booms may be designed for operation in the postbuckling range. Most of the current design codes do not allow buckling and the present investigation was carried out in order to supply a procedure for evaluation of the strength and stiffness of such booms.

It was found that local buckling of bottom and web plates may have a significant influence on the displacements of the boom head and, thus, on the stability of the crane. A calculation procedure was worked out which considers the second order effects in an approximate but conservative way by use of the effective width concept. The results obtained in specific case studies are in acceptable agreement with the crane specifications.

Acknowledgements

The present investigation was funded by The National Board of Occupational Safety and Health.

References

Brush, D., Almroth, B., Buckling of bars, plates and shells. McGraw Hill, 1975.

Gerard, G., Becker, H., Handbook of structural stability, Part I Buckling of flat plates. NACA TN 3781, 1957.

Dubas, P., Gehri, E., Behaviour and design of steel plated structures. ECCS No 44, 1986.

(1)
JÁRMAI, Károly (*)

MULTICRITERIA OPTIMIZATION OF STIFFENED BOX GIRDERS VIA STABILITY CONSTRAINTS

INTERNATIONAL COLLOQUIUM
STABILITY OF STEEL STRUCTURES
BUDAPEST, HUNGARY, 1990
PRELIMINARY REPORT

Summary: A decision support system, contains seven various type multicriteria and six various singlecriterion optimization techniques, is applied to optimize welded, stiffened box girders. Using various slendernesses, the computer program determine a great number of optima. Increasing the limit slendernesses can be seen the effect on the volume and deflection of the girder. The great number of Pareto optima give the possibility of making better decisions at design.

1. Introduction

The increased availability of digital computing devices has been a significant contributing factor in the emergence of structural optimization as a discipline in its own right. The optimality criteria and the nonlinear programming methods have received considerable attention in this period of development.

Usually a scalar-valued objective function is optimized over a feasible design space and the result is then used as a guiding devise in striving for the best practicable structure. However,

(*) scientific research worker, Technical University for Heavy Industry, H-3515 Miskolc, Egyetemváros, Hungary

there often exist several structural design problems, which involve several, usually conflicting, objectives to be considered by the designer. A promising approach for solving this type of problem seems to be multiobjective nonlinear programming, where a vectorvalued objective function is examined. The problem is stated as:

Find the vector of design variables $\bar{x}$ which minimizes the vector of criterion or objective functions

$$f(\bar{x}) = (f_1(\bar{x}), f_2(\bar{x}), \ldots, f_k(\bar{x})) \qquad (1)$$

subject to $g_j(\bar{x}) \leq 0 \quad j = 1,2, \ldots, M$

and the objective functions $f_j(\bar{x})$ may be noncommensurable.

The multiobjective optimization arose in a natural fashion in mathematical economics; its use in engineering and structural design is relatively recent. A variety of techniques and applications of multiobjective optimization have been developed in the past several years.

A vector $\bar{x}^*$ is called Pareto-optimal for the problem of eqn (1) if there exists no feasible vector $\bar{x}$ which would decrease some objective function without causing a simultaneous increase in at least one objective function. Usually several Pareto optima exist for a vector optimization problem and additional information is needed to order the Pareto-optimal set.

This clearly makes it possible to bring in additional considerations not included in the optimization model, thus making the multiobjective approach a flexible technique for most design problems.

Several numerical methods have been suggested for solving a vector optimization problem. We have used seven of them (Jármai 1988). Each method in general, generates a different Pareto-optimal solution.

We used the

- min-max method,
- weighting min-max method,
- two types of global criterion method,
- weighting global criterion method,
- pure weighting method,
- normalized weighting method

(3)
as multiobjective optimization methods, and the
- flexible tolerance method of Himmelblau,
- direct-random search method of Weisman,
- hillclimb method of Rosenbrock,
- direct search-feasible direction of Pappas,
- complex method of Box,
- conjugate gradient method of Davidon-Flecther-Powell,

as singleobjective optimization methods.
The developed decision support system (DSS) contains these algorithms and the designer can change the method, solving the problem (Jármai 1989.a).

2. Limit slendernesses at welded, stiffened box girderds

Frieze (1980) determined the values of limit slendernesses for welded box girders, without longitudinal stiffeners. For steel Fe 360 for pure bending, the limit slendernesses of web and flanges are 145 and 30 respectively.

Longitudinally stiffened webs and flanges allow larger plate slendernesses and reduce the mass of structure. Very slender webs and flanges buckle simultaneously and it is difficult to consider the interaction in the design. Thus we made some experiments to determine limit slendernesses, when the interaction of web and flange buckling may be neclected (Jármai 1989.b).

We found, that up to limit slendernesses 200 and 60, at a stiffened box girder, the interaction may be neclected. The yield stress of the steel was 300 MPa.

According to Klöppel, Scheer (1960) the buckling coefficients due to pure bending and shear are $k_B = 110{,}8$, $k_\tau = 10$, respectively.

At speciment 200-60 if the concentrated load is 30 kN the computation according to the Hungarian standard MSZ 15024 (1985) is as follows:

F = 30 kN; $\sigma_B = 132.5$ MPa; $\tau_Q = 26.6$ MPa; $\sigma_r = 140.2$ MPa so the reduced buckling coefficient k_r is as follows:

$$k_r = \frac{\sigma_r}{\sqrt{\left(\frac{\sigma_B}{k_B}\right)^2 + \left(\frac{\tau_B}{k_\tau}\right)^2}} = 48.07 \qquad (2)$$

the slenderness ratio λ_o is

(4)

$$\lambda_o = \frac{3.3}{\sqrt{k_r}} \left(\frac{h}{t_w}\right) = 118.98 \qquad (3)$$

the equivalent slenderness is $\lambda_E = \pi \sqrt{\frac{E}{R_y}} = 82.3$

$$\bar{\lambda}_o = \frac{\lambda_o}{\lambda_E} = 1.45 \qquad (4)$$

so the decreasing factor φ_b is

$$\varphi_b = \frac{1}{\bar{\lambda}_o^2} = 0.48 \; . \qquad (5)$$

There is no buckling if

$$\sigma_r \leq 1.1 \; \varphi_b \; R_n \; ; \; 140.2 < 157.8 \text{ MPa} \; . \qquad (6)$$

So buckling of web does not occur. If the force is higher than F = 35 kN, buckling may occur, or the safety is too small according to the code.

3. Economic design of welded, stiffened box girders

The investigated structure is shown in Fig.1.

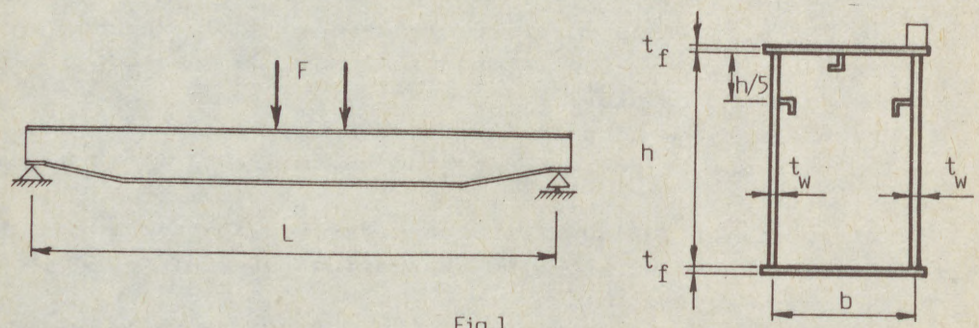

Fig.1.

Independent variables: height of web h = x(1), width of flanges b = x(2). The other dimensions of the beam, using limit slendernesses are as follows:

$$t_w = 0.2 \; \frac{h}{30} = \frac{h}{150} = \frac{x(1)}{150} \qquad (7)$$

$$t_f = \frac{b}{2} \cdot \frac{1}{30} = \frac{b}{60} = \frac{x(2)}{60} \qquad (8)$$

Objective functions:

- volume of the girder

$$V = (2 \; h t_w + 2 \; b t_f) \; L = \left(2x(1) \; \frac{x(1)}{150} + 2 \; x(2) \; . \; \frac{x(2)}{60}\right) . 3000 \qquad (9)$$

as the speciment beam length was L = 3000 mm.

(5)

V = F(1) ⇒ min

- deflection of the girder

$$w_{max} = \frac{FL^3}{48EI_x} \qquad (10)$$

$$I_x = 2\,\frac{h^3 t_w}{12} + \frac{h^2 b t_f}{2} = \frac{x(1)^3\,\frac{x(1)}{150}}{6} + \frac{x(1)^2\,x(2)\,.\,\frac{x(2)}{60}}{2}$$

w_{max} = F(2) ⇒ min

Contraints:

- stress constraint $\frac{FL}{4W_x} \le R_{adm}$ or $R_{adm} - \frac{FL}{4W_x} \ge 0$ (11)

where $W_x = 2\,\frac{h^2 t_w}{6} + hb\,t = \frac{x(1)^2\,\frac{x(1)}{150}}{3} +$

$+ x(1)\,.\,x(2)\,\frac{x(2)}{60}$; R_{adm} the admissible stress,

- size constraints.

For the independent variables $x_i^{min} \le x_i \le x_i^{max}$ (i = 1,2).
Four geometric constraints relating to the span length and the height of web:

$$L_{max} - x(2) \ge 0\ ; \qquad x(2) - L_{min} \ge 0 \qquad (12)$$

$$h_{max} - x(1) \ge 0\ ; \qquad x(1) - h_{min} \ge 0 \qquad (13)$$

3.1 Description of the problem in the coordinate system of variables

The concentrated load at the middle of the beam is 4800 N at span lenght 3 m, the maximum stress at midspan is 54 MPa. (as at the test beam were). So we choose an upper and lower limit both for the height and width of girder. They are 100÷400 mm, 100÷300 mm respectively.

Objective functions are as follows:

$$F(1) = \left(\frac{x(1)^2}{75} + \frac{x(2)^2}{30}\right)\,.\,3000 \qquad (14)$$

$$F(2) = \frac{4800}{48.2{,}06.10^5}\,\frac{LL^3}{\frac{x(1)^4}{900} + \frac{x(1)^2.x(2)^2}{120}} \qquad (15)$$

Inequality constraints are as follows:

(6)

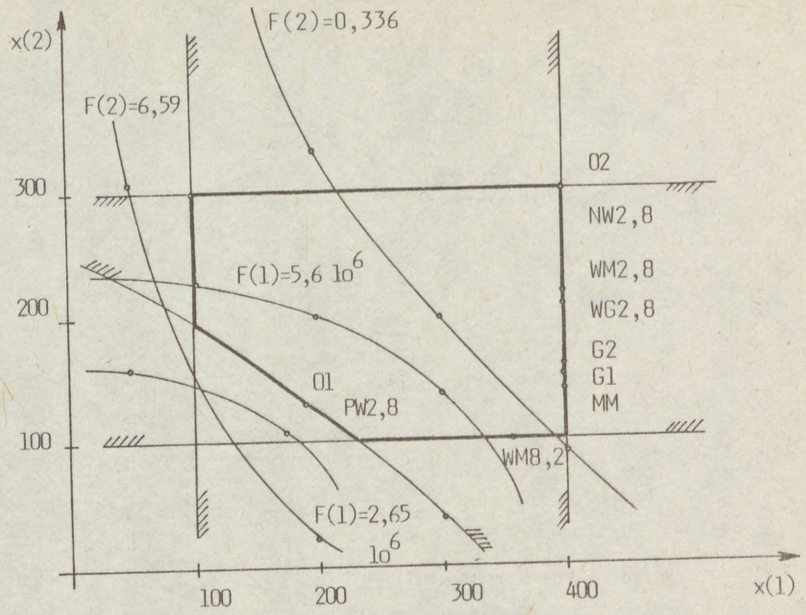
x(2)
F(2)=0,336
F(2)=6,59
O2
NW2,8
WM2,8
WG2,8
G2
G1
MM
F(1)=5,6 1o^6
O1
PW2,8
WM8,2
F(1)=2,65
1o^6
300
200
100
100
200
300
400
x(1)

Fig.2.

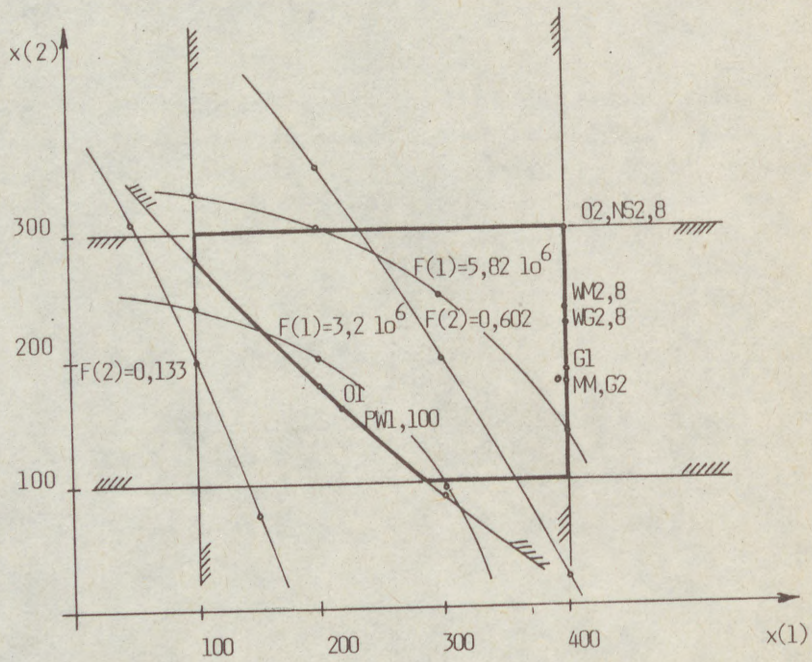
x(2)
O2,NS2,8
F(1)=5,82 1o^6
WM2,8
WG2,8
F(1)=3,2 1o^6
F(2)=0,602
G1
MM,G2
F(2)=0,133
O1
PW1,100
300
200
100
100
200
300
400
x(1)

Fig. 3.

(7)

$$G(1) = 54 - \frac{\frac{4800.3000}{4}}{\frac{x(1)^3}{450} + \frac{x(1).x(2)^2}{60}} \geq 0 \qquad (16)$$

$$G(2) = 400.-x(1) \geq 0 \qquad (17)$$

$$G(3) = x(1)-100. \geq 0 \qquad (18)$$

$$G(4) = 300.-x(2) \geq 0 \qquad (19)$$

$$G(5) = x(2)-100. \geq 0 \qquad (20)$$

Fig.2.3. show the F(i) and G(i) functions. O1 and O2 means the single-criterion optimum, WM is the weighting min-max, WG is the weighting global, PW is the pure weighting and NW is the normalized weighting method. Numbers mean the weighting coefficients, for example WM 2.8 means weighting min-max method where $w_1 = 0.2$, $w_2 = 0.8$, respectively.

Using the decision support system, we can get the various optima in the coordinate systems. The so called Pareto optima take place between the single-criterion optima.

Comparing the optima caused by various slendernesses (Table 1) it can be seen, that larger slendernesses cause decreasing in volume and increasing at deflection.

	x(1)	x(2)	F(1)(mm^3)	F(2) (mm)
slendernesses 150/30				
1.obj.	190	130	$0.3134.10^7$	$0.20065.10^1$
2.obj.	400	300	$0.154.10^8$	$0.8829.10^{-1}$
min-max weighting	400	140	$0.836.10^7$	$0.24014.10^0$
min-max w_1=0.2, w_2=0.8	400	220	$0.1127.10^8$	$0.1409.10^0$
slendernesses 200/60				
1.obj.	220	170	$0.2897.10^7$	$0.1684.10^1$
2.obj.	400	300	$0.93.10^7$	$0.16611.10^0$
min-max weighting	390	180	$0.6183.10^7$	$0.3292.10^0$
min-max w_1=0.2, w_2=0.8	400	240	$0.768.10^7$	$0.2194.10^0$

Table 1.

(8)

There is another possibility to reduce the volume of the beam: using higher strength steel.

References

Frieze, P.A. (1980): Behaviour and design of thin-walled rectangular hollow sections. Thin-walled structures. London, Granada, pp. 445-477.

Jármai, K. (1988): Design of economic steel structures. Candidate of Science Dissertation, Miskolc, Hungary,187 p (in Hungarian)

Jármai, K. (1989.a): Single- and multicriteria optimization as a tool of decision support system. Computers in Industry, Elsevier Science Publishers, Vol. 11. No.3. pp. 249-265.

Jármai, K. (1989.b): Design of economic, stiffened box girders, experiments for the local buckling interaction. Publ. of the Techn. Univ. 7 p. (under publication).

Klöppel,K., Scheer, J. (1960): Beulwerte ausgesteifter Rechteckplatten. Verlag von Wilhelm Erns & Sons. Berlin.

MSZ 15024 (1985): Design of steel constructions for buildings. Design requirements. Hungarian National Standard. (in Hungarian).

(1)
KUBICA, Ernest (1)
RYKALUK, Kazimierz (2)

PATHS OF LIMIT EQUILIBRIUM OF WELDED THIN-WALLED BOX COLUMN

INTERNATIONAL COLLOQUIUM
STABILITY OF STEEL STRUCTURES
BUDAPEST, HUNGARY, 1990
PRELIMINARY REPORT

Summary: The paths of the limit equilibrium of the welded column having deformable box cross-section were presented in the relationships: load--deflection and load-shortening. These curves are used for integral rigidities determining of a beam-column. The theoretical solution was verified by experiments taken on models.

The integral rigidities of each member should be known where the paths of the limit equilibrium of a frame structure are considered. There are axial rigidities-secant, tangent (Rykaluk 1986) and the flexural rigidity. Herein the paths of the limit equilibrium are determined for a welded box column with unstiffened walls in the following relationships: load (P) - uniform strain (S) and load (P) - column flexure (v). The first curve gives the axial rigidities, the second one gives the flexural rigidity.

For a box column eccentrically compressed (fig.1) the flexure v is calculated from the formula (Kubica 1989).

---

(1) Assistant Professor of Civil Engineering, Technical University of Wrocław, Poland
(2) Associate Professor of Civil Engineering, Technical University of Wrocław, Poland

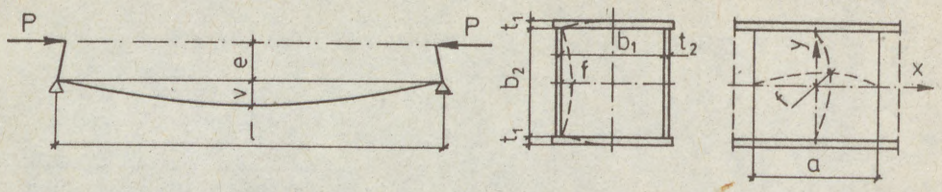

Fig.1

$$v = e \cdot \eta_p \left[(\cos \frac{kl}{2})^{-1} - 1 \right] , \qquad (1)$$

where: $k = (P/EI)^{0.5}$; $\eta_p = 1 + A_p(\sigma_{av}/f_y)^7$;

$$A_p = (\eta - 1)\varphi^7 \; ; \quad \eta = \frac{1 - \varphi}{m \varkappa_w} \left(\frac{1}{\varphi} - \bar{\lambda}^2 \right) ;$$

$$\bar{\lambda}^2 = \frac{Al^2 f_y}{\pi^2 EI} \; ; \quad \varkappa_w = 1 - \frac{1}{3} \frac{m\varphi_o}{1 - \varphi_o} + \frac{1}{27} \left(\frac{m\varphi_o}{1 - \varphi_o} \right)^2 ;$$

$\varphi = \sigma_{ult}/f_y$ - accordind with (Kubica and Rykaluk 1987),

φ_o - from the formula $\bar{\lambda}^2 = \frac{1}{\varphi_o} \left[1 - \frac{m\varphi_o}{3(1-\varphi_o)} \right]^3$;

σ_{ult} - limit axial stresses for a column,

$m = eA/W$;

A - cross sectional area of a column ;

W - section modulus of a column ;

f_y - yield-point stress.

Both the physical and the geometrical imperfections - total for the column and local for the walls are represented by the shape factor η_p and the required flexural rigidity EI_p with the relation to the axial sresses $\sigma_{av} = P/A$ is determinated by

$$EI_p = EI/\eta_p \; . \qquad (2)$$

In fig.2 the paths P-v are shown as a result of the equation (1). The results obtained by our own experiments carried on the columns 5 m long (Kubica and Rykaluk 1987) and by others (Klöppel and Schubert 1971) are signed by points.

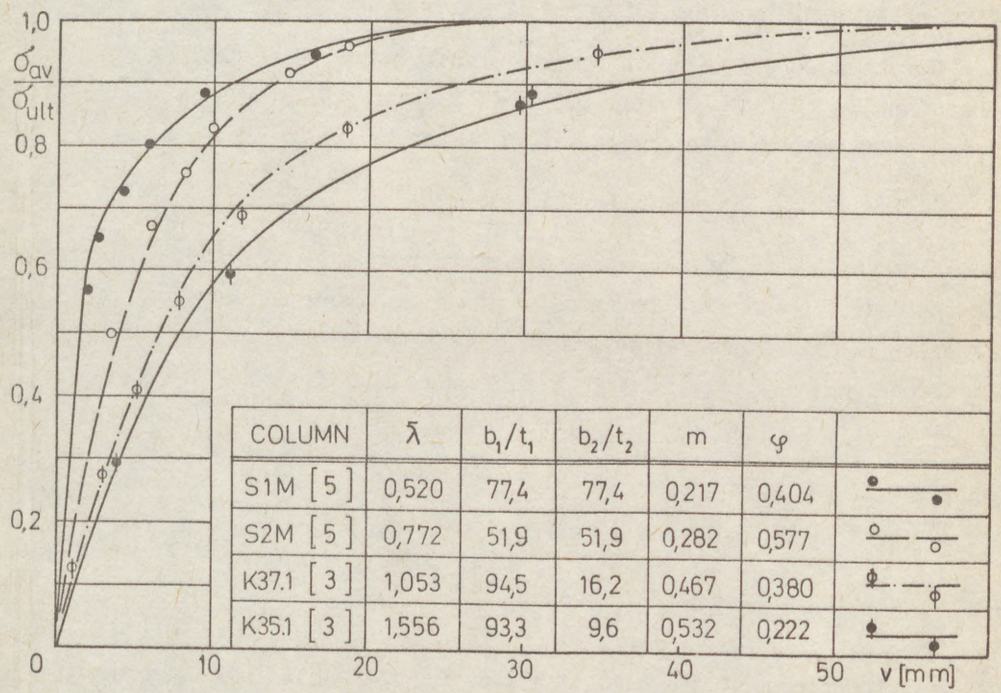

COLUMN	$\bar{\lambda}$	b_1/t_1	b_2/t_2	m	φ	
S1M [5]	0,520	77,4	77,4	0,217	0,404	
S2M [5]	0,772	51,9	51,9	0,282	0,577	
K37.1 [3]	1,053	94,5	16,2	0,467	0,380	
K35.1 [3]	1,556	93,3	9,6	0,532	0,222	

Fig.2

The axial column shortening S comes from the uniform compression of the material, initial deflection and local walls folding. The biggest theoretical problem is produced by the last effect. For solving this problem the equation of the limit equilibrium path of the thin-wall with imperfections given by Klöppel, Schmied and Schubert (1966) was used

$$0.23551\left(\frac{f_1}{t}\right)^3 + \frac{f_1}{t}\left[1 - \frac{\sigma_x}{\sigma_k} - 0.16239\,\frac{\sigma_{res}}{\sigma_k} - 0.23551\left(\frac{f_o}{t}\right)^2\right] - \frac{f_o}{t} = 0 \quad (3)$$

(4)

where:

f_1 - the flexure amplitude of the thin-wall corresponding with σ_x ,

f_o - the initial flexure amplitude of the thin-wall,

σ_{res} - residual edge stresses of the thin-wall,

$\sigma_k = \pi^2 Et^2 / 3(1 - \nu^2) b^2$,

b, t - the width and the thickness of the thin-wall.

The equation (3) is valid for the elastic range. When the membrane stress reaches σ_e the plasticization of the material starts in the external layer according to the criterion H-M-H

$$\sigma_x^2 + \sigma_y^2 - \sigma_x\sigma_y = f_y^2 ,$$

where the components σ_x, σ_y are the algebraic sums of membrane, flexural and residual stresses. In the range of the geometrical and physical non-linearity it is proposed to determine the limit equilibrium path by the incremental method. Thus obtained results were aproximated by a curve

$$f_2 = f_1 \xi ,$$

where:

f_1 - the flexure amplitude of the thin-wall surface calculated from (3),

$$\xi = [(\sigma^1_{ult} - \sigma_e)/(\sigma^1_{ult} - \sigma_{av})]^{1/16} ,$$

σ^1_{ult} - the stress in the limit state of the thin-wall with imperfections having a length measured between the break points.

Such an analitical solution was compared with that given by Djubek (1983), Kowal-Michalska and Grądzki (1986), and own experiments executed on models. The analitycal curve follows satisfactorily the experimental one (fig.3 and fig.4). The shortening of the part of the column equal to the sinusoid half-wave of the flexure length - a is:

$$S_a = \frac{\sigma_{av}}{E} + \frac{\pi^2}{8a^2}(f_1^2 - f_o^2) . \qquad (4)$$

The load-bearing capacity of such a stab-column depends on the load-bearing capacity of the thin-walls σ^1_{ult} , whereas the load-bearing of the column σ_{ult} is additionally governed by the slenderness and initial flexure. Within the field of the non-linear changes the column shortening

(5)

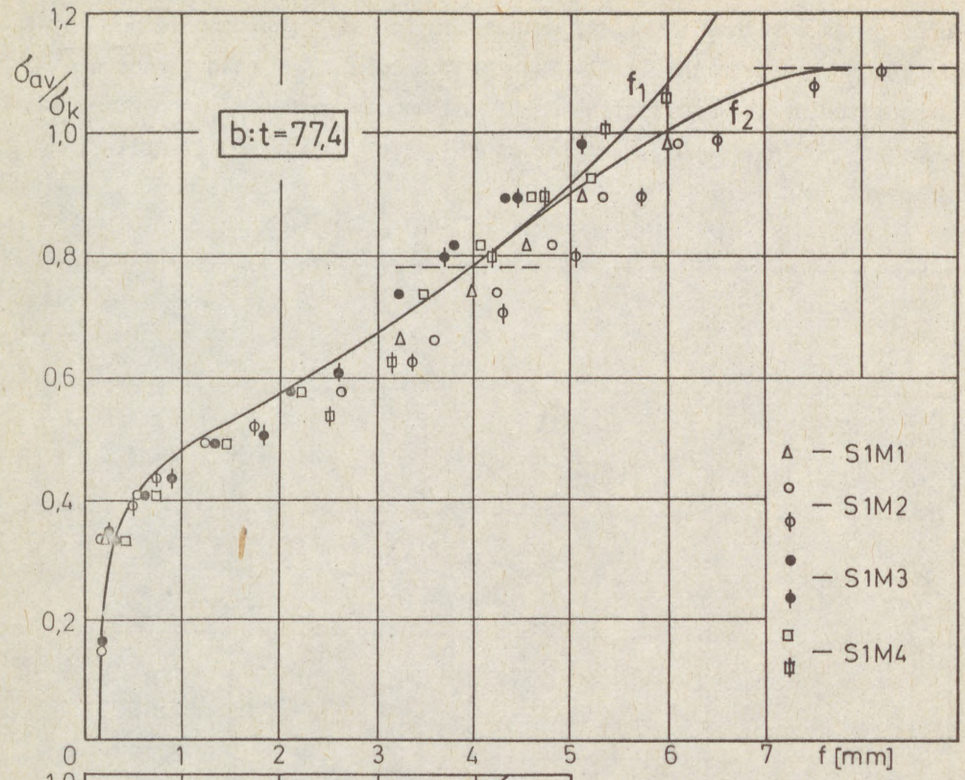
1,2
σ_{av}/σ_k
1,0
0,8
0,6
0,4
0,2
0
b:t=77,4
f_1
f_2
S1M1
S1M2
S1M3
S1M4
1
2
3
4
5
6
7
f [mm]

Fig. 3

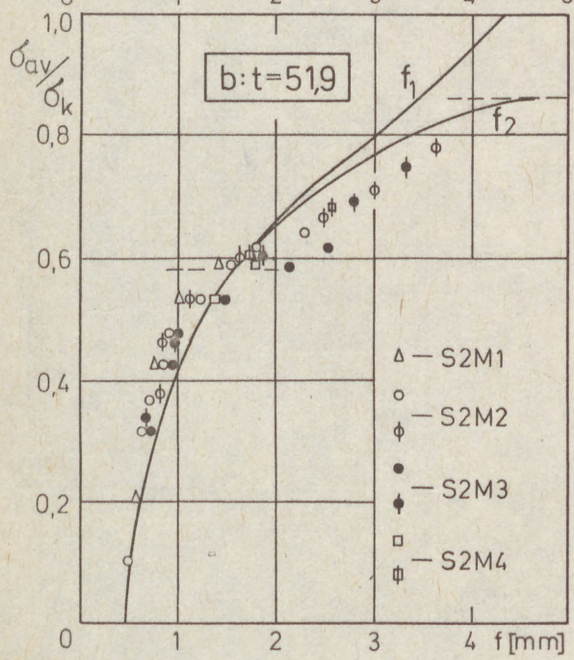
1,0
σ_{av}/σ_k
0,8
0,6
0,4
0,2
0
b:t=51,9
f_1
f_2
S2M1
S2M2
S2M3
S2M4
1
2
3
4
f [mm]

Fig. 4

(6)

produces a mean arithmetic value, determined for both the concave and the convex column side. In the limit state of the column the mean stresses σ_{ult} are associated by the limit stresses of the concave side $\sigma^1_{ult} = \sigma_p$ and the stresses $\sigma_o = 2\,\sigma_{ult} - \sigma^1_{ult}$ of the convex side (the Bernoulli criterion was assumed).

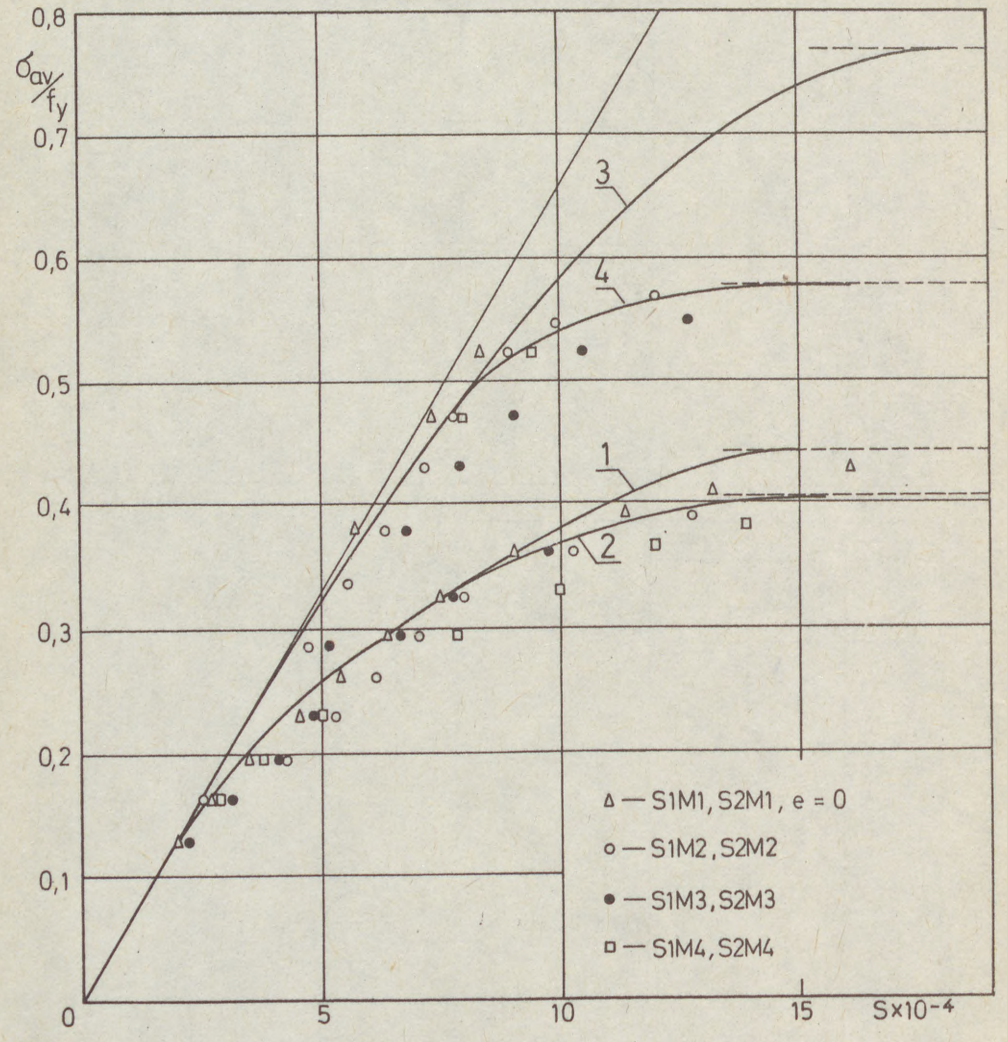

Fig.5

(7)

Assuming the concave side $f_1(\sigma_p)$ and convex side $f_1(\sigma_o)$ over the whole column length remains constant, where

$$f_1(\sigma_p) = f_1 \xi_p \; ; \quad f_1(\sigma_o) = f_1 \xi_o \; ; \quad n = \sigma^1_{ult}/\sigma_{ult} \; ,$$

$$\xi_o = [(\sigma^1_{ult} - \sigma_e)/(\sigma^1_{ult} - n\,\sigma_{av})]^{1/16} \; ;$$

$$\xi_p = [(\sigma^1_{ult} - \sigma_e)/(\sigma^1_{ult} - 2\,\sigma_{av} - n\,\sigma_{av})]^{1/16}$$

the relative shorting can be determined as follows.

$$S = \frac{\sigma_{av}}{E} + \frac{\pi^2}{16\,a^2}\,[f_1^2(\sigma_o) + f_1^2(\sigma_p) - 2f_o^2] + \frac{\pi^2\,v^2}{4\,l^2} \; . \qquad (5)$$

The relative shortenings S_a of the stab-column according to (4) and that for columns - S according to (5) where shown in fig.5. The curves 1 and 3 present the shortenings of the stab-columns of the columns S1M and S2M, whereas the curves 2 and 4 present the total shortening of these columns. Results of the own model experiments are signed by points.

References

1. Djubek, J. (1983), Elastoplastic slender web subjected to compression. Incremental method (in Slovac), Stavebnicky Casopis (Building Journal) 31, 373-393.
2. Klöppel, K., Schmid, K., Schubert, J. (1966), The non-linear theory of the load-bearing capacity of the thin-walled box columns under axial and non-axial compresion (in German), Der Stahlbau , H.11 , 321-337.
3. Klöppel, K., Schubert, J. (1971), Calculation of the load-bearing capacity of the thin-walled box columns under axial and non-axial compresion in the post-critical range (in German), TU Darmstadt, Volume 13, 1-127.

4. Kowal-Michalska, K., Grądzki, R. (1986), The post-buckling behaviour of thin-walled columns in the elastoplastic range, Rozprawy Inżynierskie (Engineering Transactions), 34, 4, 503-515.

5. Kubica,E., Rykaluk,K. (1987), The carying capacity of the eccentric compressive force of thin-walled box member with deformability cross section (in Russian), Stroitelnaja mechanika i rascet sooruženij, 6, 54-57.

6. Kubica,E. (1989), The flexures of the box columns with deformable cross-sections (in Polish), VIII-th International Scientific Technical Conference "Metal Structures", Gdańsk, Volume 2, 92-96.

7. Rykaluk, K. (1986), Elastic-plastic axial rigidity of a compressed member with imperfections (in Russian), Stability of Steel Structures, Tihany, Hungary, Volume 1, 117-124.

(1)
STUDNIČKA, Jiří (1)

WEB CRIPPLING OF WIDE DECK SECTION

INTERNATIONAL COLLOQUIUM
STABILITY OF STEEL STRUCTURES
BUDAPEST, HUNGARY, 1990
PRELIMINARY REPORT

Summary: Paper presents the results of extensive experimental investigation of web crippling load for multiple web deck sections which are used in building constructions in Czechoslovakia. One flange loading and two flange loading were tested, for both, end and interior reactions. Based on the test data, it can be concluded that satisfactory conformity was obtained with Canadian Standard formula for interior support. For end support slightly modified formula was developed.

1. Introduction

Cold-formed steel wide multiple web deck sections are used extensively in building constructions. Where these sections are supported by end or interior bearing plate, or are subjected to a concentrated load at some point of the span, failure of deck can occur by web crippling. Bending stress can be also present, but for some combinations of loading and deck profiles the contribution of the bending stress is small and may not contribute significally to failure. Research has shown (Baehre 1975) that there is negligible interaction between bending and crippling when $M < 0.33\ M_{ult}$. This opinion was adopted by other researchers (Ratliff 1975, Hetrakul and Yu 1980, Wing and Schuster 1986).

Ultimate web crippling load capacity is a function of number of parameters, namely, the web slenderness ratio H, the inside bend radius ra-

(1) Assoc.Prof., Czech Technical University Prague, Czechoslovakia

(2)
tio R , the bearing length ratio N , the angle of web inclination θ and the yield strength of steel F_y , Fig. 1.

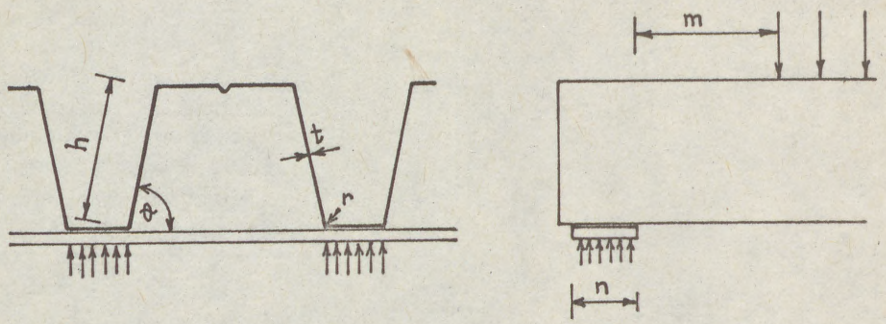

Fig. 1 Cross section of multiple web deck. $H = \frac{h}{t}$, $R = \frac{r}{t}$, $N = \frac{n}{t}$

Load capacity also depends on distance between the bearing edges of adjacent opposite concentrated loads or reactions. When this distance m is greater than 1,5 h one flange loading occurs, when it is equal or less, two flange loading occurs. When uniform loading works on beam, support areas are classified as one flange loading zones (Yu 1985). Finally, substantial difference is between end and interior reaction loadings, of course.

The objective of this study was to determine, by experimental way, the load resistence of multi-web deck sections subjected to end and interior reaction loading P , as shown in Fig. 2.

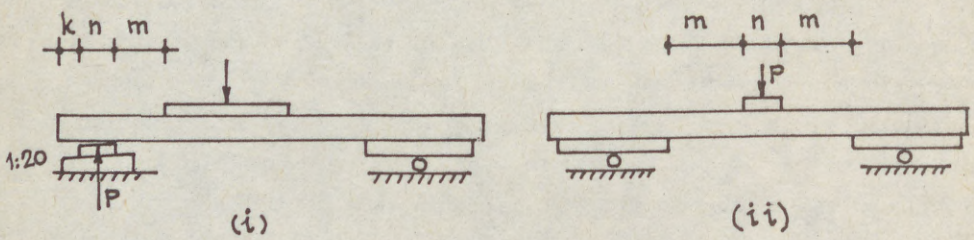

Fig. 2 Test setup for (i) end reaction, (ii) interior reaction

2. Test program

Test program was designed to encompass the most important parameter variations that influence the web crippling resistance of multi-web deck sections. Test speciments were obtained from Czechoslovak manufacturer VSŽ Košice. The both types of specimens are shown in Fig. 3. Spreading of webs was at some tests prevented by transverse tie rods which were bolted to the bottom flange of profiles, see Fig. 4.

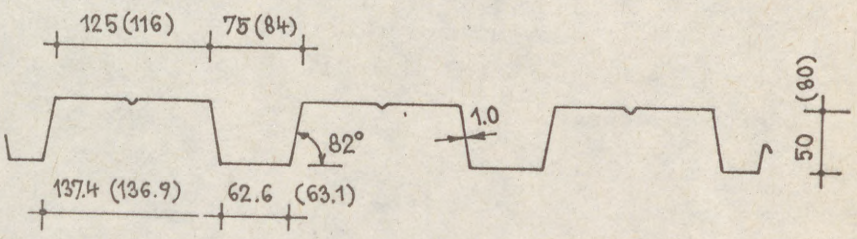

Fig. 3 Tested wide deck sections. VSŽ type 12 002 (type 12 102)

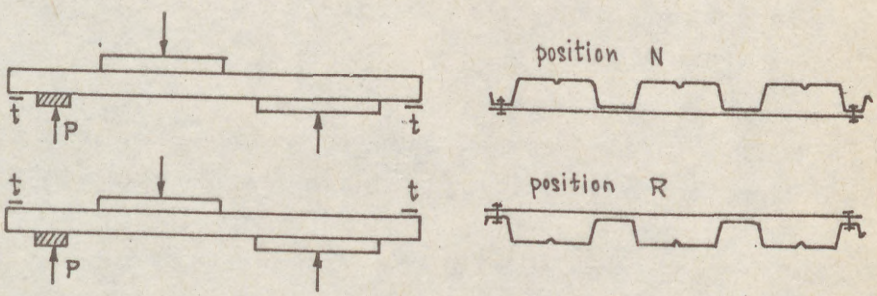

Fig. 4 End support test. Positions of profile. Tie rods t bolted to the flange

The specimens were simply supported at the ends and the load was applied at centre, as shown in Fig. 2. Relatively large end bearing plates were used for these tests to insure that failure would occur at the interior load position and vice versa for end load position. The

(4)

distance m from edge of the interior bearing plate to the interior edge of the exterior bearing plate was changed to catch the conditions for one flange and two flange loadings. But main changeable dimension was bearing width n , see Fig. 2. For tests at end support the inclined steel bearing plate was used following the ECCS Recommendations (1978). The deck specimens were tested in both positions N and R , see Fig. 4. The span of beam specimens was very small to be held the condition $M < 0.33\ M_{ult}$ mentioned above. The test load P_t was taken either as the largest load the specimen was able to sustain (after which a sudden decrease in load was experienced), or as the load which a residual deformation 1.0 mm brought about, whatever lesser.

3. Test results

3.1 Interior support

Altogether 40 specimens were tested. Next notices over test results can be done :

(i) test loads are not different substantially for N and R position of deck

(ii) test loads are almost linearly influenced by bearing width n

(iii) test loads for specimens with ties are somewhat greater than without ties.

3.2 End support

Test results for 76 specimens were obtained. The same three comments as for interior support can be concluded and next two can be added :

(iv) influence of distance m on test results is very small

(v) when distance k is greater, test load is greater too. But influence is not very significant.

4. Comparison of test loads and computed loads

The AISI Specification (1986) and Canadian code (1984) were used to compute the ultimate web crippling load P_c . Since method of permissible stress is used in AISI Specification, multiplying all equations by safety factor 1.85 was necessary. On the contrary Canadian code is completed in limit states terms, therefore no corrections must be done except missing resistance factor ϕ_s . Dimensions from Fig. 3 and measured yield strength F_y = 260 MPa were used for computation of P_c .

(5)

4.1 Interior support

Only one flange loading was used for interior support tests. Comparisson of test results P_t with ultimate computed web crippling loads P_c using AISI Specification and Canadian Code was done. Better conformity with Canadian code, which is using formula

$$P_c = 18t^2 F_y \sin\theta\,(1-0.1\sqrt{\frac{F_y}{230}})(1-0.075\sqrt{R})(1-\frac{H}{1000})(1+0.005\,N) \qquad (1)$$

was obtained. The solid line in Fig. 5 represents perfect correlation ($P_t = P_c$); the dashed lines are $\pm$ 20 % limits which are acceptable scatter

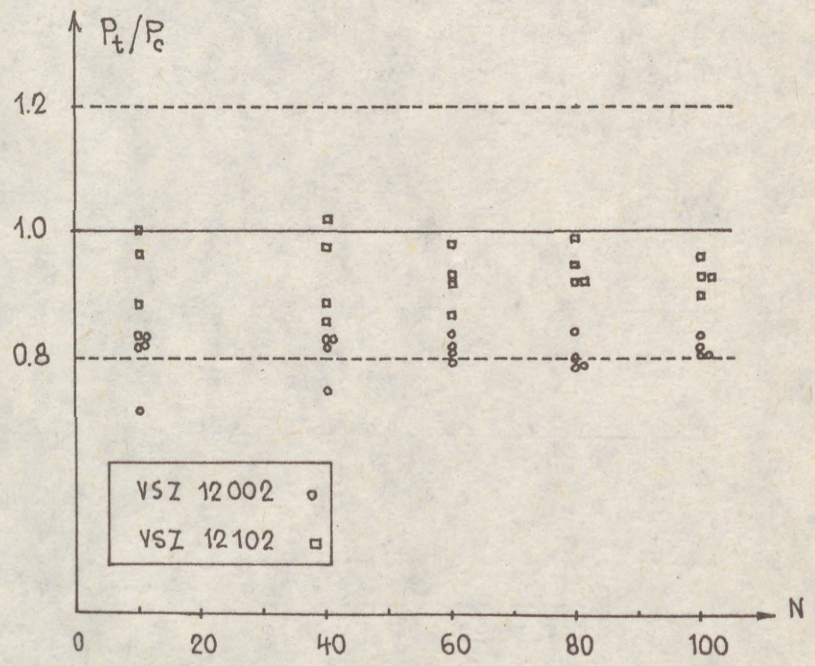

Fig. 5 Test load P_t vs. computed load P_c . Interior support

limits for tests of this type, based on previous research. One can see in Fig. 5 that almost all results are within these limits over full range of the bearing length. But mean value P_t/P_c (0.867) with coefficient of variation (0.073) is somewhat disturbing. A little small number of tests

(6)

makes impossible to carry out more firm conclusion.

4.2 End support

Both, one and two flange loadings, were used in this type of tests. Using the test results, new slightly modified formula was developed following Canadian standard for loading capacity of one web

$$P_c = 10\, t^2 F_y \sin\Theta\, (1-0.1\frac{F_y}{230})(1-0.1\sqrt{R})(1-\frac{H}{500})(1+\frac{K}{15H})(1+0.005\, N) \qquad (2)$$

in which $K = \frac{k}{t}$, see Fig. 2.

Eq. 2 predicts well the web crippling capacity for end reaction and for both, one and two flange loading, if $K \leq 3\,H$. The other limitations from CAN 3 - S 136 are let fully valid. Comparisson eq. 2 with test data in Fig. 6 shows very good correlation. It is indicated also by the values of the mean (1.018) and coefficient of variation (0.136) of ratio P_t/P_c.

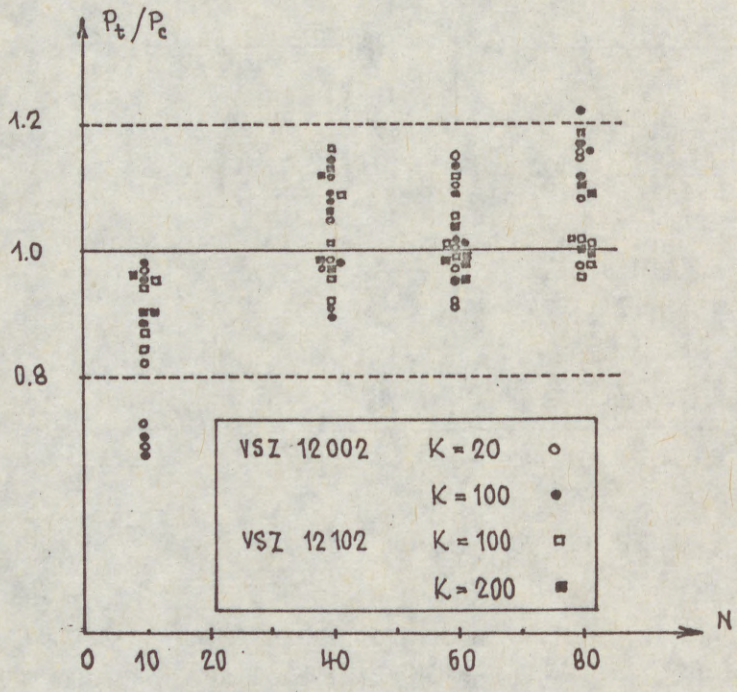

Fig. 6 Test load P_t vs. computed load P_c. End support

(7)

5. Conclusions

Based on the comparissons of the results of 40 interior support and 76 end support tests with different methods of computation, the following conclusions were made :

(i) The Canadian code predicts the web crippling capacities reasonably well for interior support.

(ii) The use of Eq. 2 resulted in a better prediction of the web crippling capacity for end support than any of the existing methods. Eq. 2 is fully valid for one flange loading and two flange loading.

(iii) Test with end support did not confirm the frequent opinion that the increasing of distance k from edge of the bearing plate to the end of multi-web deck can bring substantial increasing of web crippling capacity.

Notation

h clear distance between the flats of flanges measured in the plane of the web

k distance between end of deck and edge of bearing

m distance between edges of adjacent opposite concentrated loads

n bearing length

r inside bend radius

t web thickness

F_y tensile yield strength

$H = \frac{h}{t}$ web slenderness ratio

$K = \frac{k}{t}$ end ratio

M_{ult} ultimate bending moment

$N = \frac{n}{t}$ bearing length ratio

$R = \frac{r}{t}$ inside bend radius ratio

θ angle between plane of web and plane of bearing surface, $45^{\circ} \leq \theta \leq 90$

(8)

References

American Iron and Steel Institute (1986), Specification for the Design of Cold-Formed Steel Structural Members, Washington

Baehre,R. (1975) Sheet Metal Panels for Use in Building Construction, Current Research Project in Sweden, Proc. of the Third Spec. Conference on Cold-Formed Steel Structures, Univ. of Missouri-Rolla, Nov. 24 - 25

Canadian Standards Association (1984) CAN 3-S 136-M 84, Cold Formed Steel Structural Members, Toronto

European Recommendations for Steel Construction (1978) The Testing of Profiled Metal Sheets, Publ. No 20

Hetrakul,N. - Yu,W.W. (1980) Cold-Formed Steel I-Beams Subjected to Combined Bending and Web Crippling, in Thin Walled Structures ed. by J.Rhodes and A.C.Walker, Constrado

Ratliff,C.D. (1975) Interaction of Concentrated Loads and Bending in C-shaped Beams, Proc. of the Third Spec. Conference on Cold-Formed Steel Structures, Univ. of Missouri-Rolla, Nov. 24 - 25

Tsai,Y.-M.-Crisinel,M. (1988) Étude des formules de résistance à l'écrasement des âmes de profiles à parois minces, Construction Métallique, No 1

Veröci,B. (1986) Experiments on steel trapezoidal sheets, Proc. of Second Reg. Colloguium on Stability of Steel Structures, Tihany, Sept. 25 - 26

Wing,D.A.-Schuster,R.M. (1986) Web Crippling of Multi-Web Deck Sections Subjected to Interior One Flange Loading, Proc. of the Eight Spec. Conference on Cold-Formed Steel Structures, St.Louis, Nov. 11 - 12

Yu,W.W. (1985) Cold-Formed Steel Design, Wiley

(1)
VERŐCI, Béla *)

ON THE BASIC WIDTH OF PROFILED SHEET COMPRESSION PLATES

INTERNATIONAL COLLOQUIUM
STABILITY OF STEEL STRUCTURES
BUDAPEST, HUNGARY, 1990
PRELIMINARY REPORT

Summary: The effective width of cold formed members' plates is determined using the "basic width" of the plate considered. Present contribution studies the provisions of two modern specifications, i.e. the AISI Specification and EC3 - Annex A, regarding the above problem pointing out the differences between them in the particular case of large bending radii. The results of two tests, carried out at the Department of Steel Structures, TU Budapest, seem to verify the provisions of the American Specification.

NOTATION

b_{ef}, b	- effective width of compression plates
k_σ , k	- buckling coefficient (k=4.0 may be considered for profiled sheets)
t	- plate thickness
b_p, w	- notional width of plane plate element and flat width of element, respectively
f_y, F_y	- yield point of steel
E	- modulus of elasticity (Young's modulus), 206000 N/mm^2
W	- elastic section modulus belonging to the extreme fibre in compression

---

*) Senior Assistant Professor, Department of Steel Structures
Technical University of Budapest

(2)

Effective width calculation

In order to determine the load capacity of a uniformly compressed stiffened element, its effective width is calculated by the **EC3-Annex A** and the **AISI Specification** as follows:

EC3	AISI	
$b_{ef} = b_p$	$b = w$	when λ and $\lambda_p \leq 0.673$
$b_{ef} = \varrho\, b_p$	$b = \varrho\, w$	when λ and $\lambda_p > 0.673$

where

$\varrho = (1 - 0{,}22/\lambda_p)\,\lambda_p$	$\varrho = (1 - 0{,}22/\lambda\ )/\lambda$
$\lambda_p = 1.052\, b_p/t \sqrt{f_y/(Ek_\sigma)}$	$\lambda = 1.052/\sqrt{k}\ (w/t)\sqrt{f/E}$

The above forms of the effective width formulae belong to the case if the compressive stress is equal to f_y ($f=F_y$), i.e. the initial yielding is in compression in the element considered (this is the case of the tested panels).
One can say that the above formulae are the same. It is true but there is a difference in the manner how the two aforesaid codes define the notional width of plane plate element (b_p) and the flat width (w), i.e. the **basic width**, respectively.
Fig. 1 shows the definition of the basic width by the codes considered. Let us study the case when the bending radii of the sheet are great (by EC3: $r/t > 5$) and the calculation of the cross section properties shall be based, even by EC3, on the actual geometrical configuration of the cross section.
J. Rondal (Rondal, 1989) has studied the influence of the basic width definition on the calculation of the effective width and pointed out the $(b_{ef}/b_p)_{EC3}$ over $(b/w)_{AISI}$ ratio for different r/t ratios having had values about from 0.82 to 0.97.

Cross section properties of the tested panels

Fig. 2a and 2b show the cross section of the tested panels with sharp and rounded corner dimensions, respectively. One can realize that the bending radii are unusually large: 15 mm and 12 mm for the upper (in compression) and the bottom (in tension) flange, respectively. The dimensions, necessary for the calculations carried out by the **EC3**, are as follows:

- upper flange: $r_m = 15.5$ mm, $f = 9.61$ mm, $g = 2.64$ mm,
  $b_p = 51.72$ mm
- bottom flange: $r_m = 12.5$ mm, $f = 7.75$ mm, $g = 2.13$ mm,
  $b^* = b_p - 2f = 40.24$ mm

The flat width of the upper flange, used for the calculations carried out by the **AISI Specification**, is: $w = b - 2f = 32.5$ mm.
Table 1 shows the results of the effective width calculations. In the case of the EC3 results, b_{ef}^* means the plane part of the effective width between the ends of round corners.

(3)

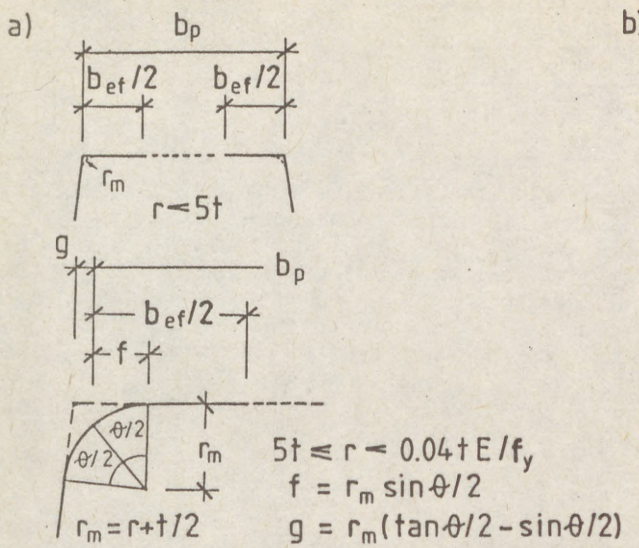
a)
b_p
$b_{ef}/2$
$b_{ef}/2$
r_m
$r \leq 5t$
g
b_p
$b_{ef}/2$
f
$\vartheta/2$
$\vartheta/2$
r_m
$r_m = r + t/2$
$5t \leq r \leq 0.04\, t\, E/f_y$
$f = r_m \sin\vartheta/2$
$g = r_m(\tan\vartheta/2 - \sin\vartheta/2)$

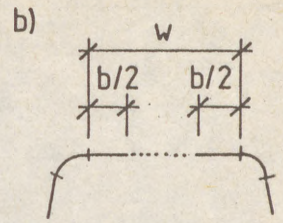
b)
w
b/2
b/2

Fig. 1

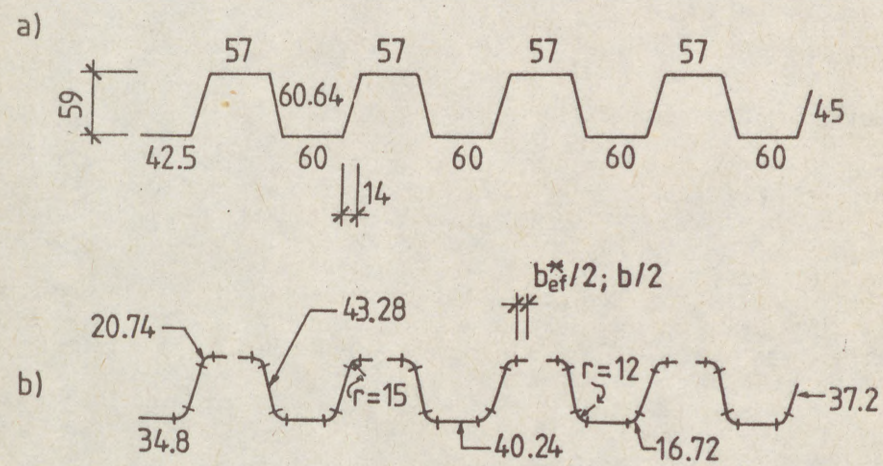
a)
57
57
57
57
59
60.64
45
42.5
60
60
60
60
14
b)
$b_{ef}^*/2$; b/2
20.74
43.28
r=15
r=12
37.2
34.8
40.24
16.72

Fig. 2

(4)

Table 1

t	EC3		AISI
mm	b_{ef} [mm]	b_{ef}^* [mm]	b [mm]
0.96	35.78	16.56	30.91
0.93	34.91	15.69	30.32

One can realize how much is affected the effective width by the definition of the basic width: the AISI Specification accounts the compression flange almost fully effective, but the EC3 provision ignores about a 16 mm wide part of it. It is not surprise that this difference appears also in the value of the section modulii belonging to the upper extreme fibre (first yielding takes place in compression). The above mentioned section modulii, calculated for the tested sheets by the two codes, can be found in Table 2.

Table 2

t	W [mm^3]	
mm	EC3	AISI
0.96	13472	16092
0.93	12903	15492

The W_{EC3}/W_{AISI} ratio is 0,837 and 0,833 for the two panels.

For comparison, author has calculated the 0.96 mm thick sheet section modulus assuming r/t = 5 value (upper limit for using sharp corner configuration by EC3) and has found the results, respectively by the EC3 and AISI provisions, as follows:

- basic width: 57 mm and 48.66 mm,
- section modulus: 13718 mm^3 and 14717 mm^3.

The aforesaid ratio is 0.932.

Test results and their comparison to calculated values

The above mentioned two tests have been carried out, among 8 ones, at the Laboratory of the Department of Steel Structures, Technical University of Budapest in the framework of a diploma thesis (Barna, 1987). During the experiments, regulations of the ECCS (ECCS, 1983) were followed. The arrangement of tests are shown in Fig.3.
The actual geometry of the panels had been shown in Fig.2b. The average value of the yield point, determined on specimens cut from the sheets considered, has been 354 N/mm^2 and the net thicknesses of the plates have been 0.96 mm and 0.93 mm for the 1.5 m and 3.0 m span sheet, respectively.
The force F was realized by a hydraulic jack with its distribution in longitudinal and transversal direction. Fig.4 shows the load-deflection diagram determined during the experiments.
The ultimate bending moments can be compared to the calculated values given in Table 3.

(5)

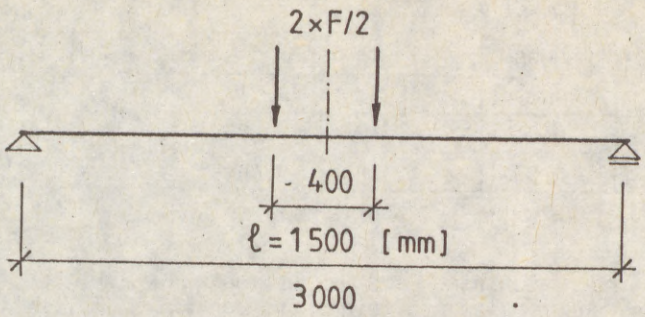
2×F/2
400
ℓ = 1500 [mm]
3000

Fig. 3

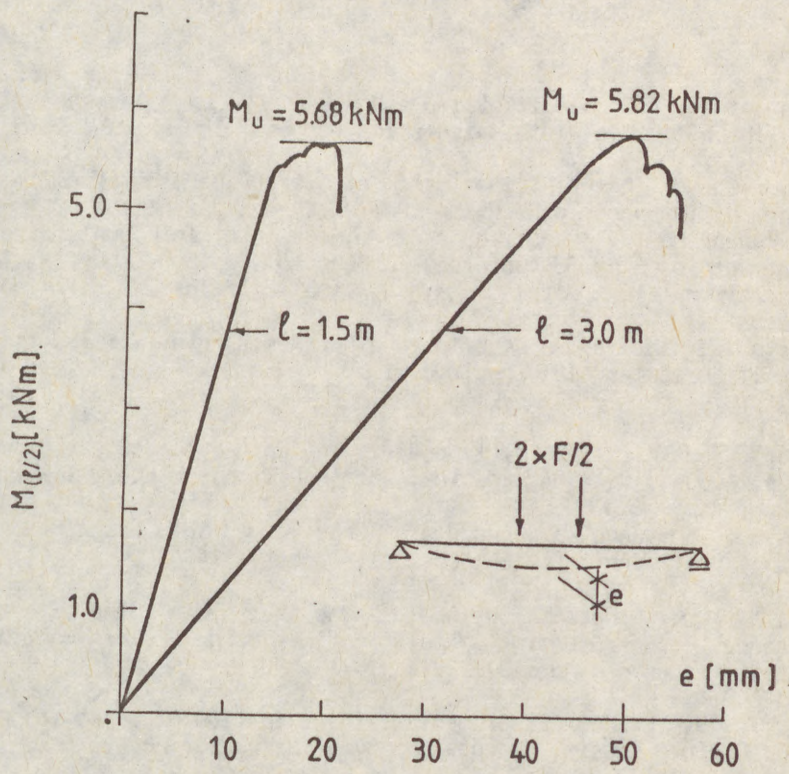
M_u = 5.68 kNm
M_u = 5.82 kNm
5.0
1.0
ℓ = 1.5 m
ℓ = 3.0 m
$M_{(\ell/2)}$ [kNm]
2×F/2
e
e [mm]
10
20
30
40
50
60

Fig. 4

(6)

Table 3

Span	Thick-ness	Theoretical ultimate bending moment [kNm]		Experimental [kNm]
m	mm	EC3	AISI	-
1.5	0.96	4.769	5.697	5.68
3.0	0.93	4.568	5.484	5.82

$M_{th}[kNm] = W \cdot f_y = W\,[mm^3] \cdot 354\,[N/mm^2] \cdot 10^{-6}$

Comparison of the calculated and experimental values of the ultimate bending moments shows that provisions of the AISI Specification approach better the test results than the EC3 ones which seem to be more conservative.
Going back to the title of the paper, the basic width definition of the AISI Specification is more realistic in the highlight of the above test results.

Conclusions

Provisions of the AISI Specification and the EC3-Annex A have been studied regarding the effective width calculation for profiled sheets' compression elements.
Author has found that in the case of large bending radii there is significant difference, caused by the different definition of the **basic width**, between the two codes. The section modulii of the panels, tested at the Department of Steel Structures, TU Budapest, have been by 16% less if the calculation is carried out by the EC3 instead of the AISI Specification.
The results of the above mentioned experiments have verified the basic width definition of the AISI Specification.

References

AISI (1986) Specification for the Design of Cold-Formed Steel Structural Members. August 19, 1986, Edition. American Iron and Steel Institute

EC3-Annex A.. Eurocode 3, Annex-A - Cold-Formed Thin-Gauge Members and Sheeting. Draft for technical comment, January,1989.

Rondal, 1989. J. Rondal: Models for the Analysis of Steel Structures. Conference "Transformation Models for the Design of Thin-Walled Steel Members". Pardubice, April, 1989.

Barna, 1987. B. Barna: Experimental Investigation of Steel Trapezoidal Sheets. Diploma thesis, Budapest, 1987. (Instructor: B. Verőci)

ECCS, 1987. European Recommendations for Steel Construction: The Design of Profiled Sheeting. ECCS Committee TC7, Working Group TWG 7.1, April, 1983.

Verőci, 1989. B. Verőci: On Load Carrying Capacity of "Dunaferr DV-1-HT" Profiled Sheets. Magyar Építőipar, 1989, No. 9, pp. 413-416 (in Hungarian)

TABLE OF CONTENTS

VOLUME I.

Session 1. "General Design Concepts"

Session 2. "Compression Members"

Session 3. "Built- Up Members"

Session 4. "Beams"

Session 5. "Beam-Columns"

VOLUME II.

Session 6. "Plate and Box Girders"

VOLUME III.

Session 8."Arches"

Session 9. "Triangulated Structures"

Session 10. "Tubular Structures"

Session 11. "Shells"

Session 12. "Cold Formed Members and Interactive Buckling"

VOLUME IV.

Session 13. "Composite Members"


Insignia Liberæ Regiæ Me
-ropolitanæ Civitatis Budensis

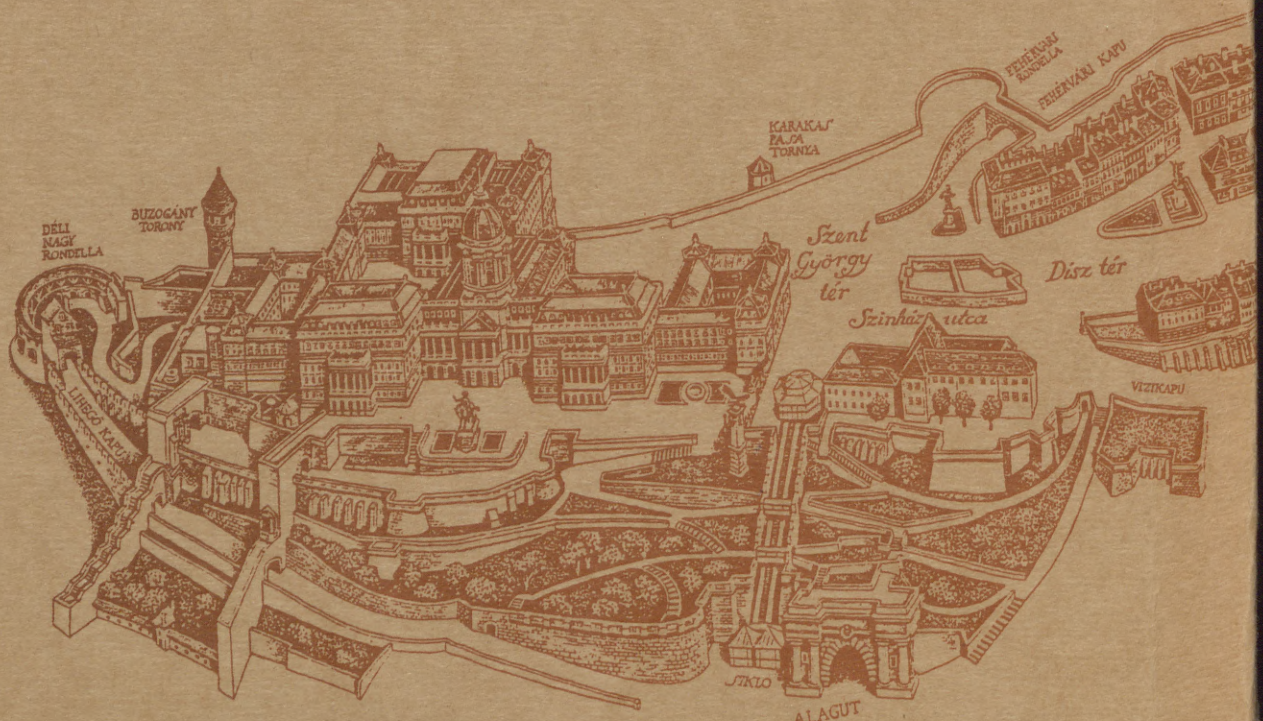
FEHÉRSÓS RONDELLA
FEHÉRVÁRI KAPU
KARAKAS PAŞA TORNYA
DÉLI NAGY RONDELLA
BUZOGÁNY TORONY
Szent György tér
Dísz tér
Színház utca
VÍZIKAPU
LIHEGŐ KAPU
JÁKLÓ
ALAGÚT

INTERNATIONAL COLLOQUIUM

STABILITY OF STEEL STRUCTUR

HUNGARY, BUDAPEST 19

PRELIMINARY REPORT

VOLUME III.